Dynamic Modelling and Performance Analysis of Energy Storage Systems for Frequency Regulation in Bulk Power Systems

by

Noela Sofía Guzmán Encalada

A thesis
presented to the University of Waterloo
in fulfillment of the
thesis requirement for the degree of
Doctor of Philosophy
in
Electrical and Computer Engineering

Waterloo, Ontario, Canada, 2021

Examining Committee Membership

The following served on the Examining Committee for this thesis. The decision of the Examining Committee is by majority vote.

Co-Supervisor:	Claudio Cañizares University Professor, Department of Electrical and Computer Engineering, University of Waterloo
Co-Supervisor:	Kankar Bhattacharya Professor, Department of Electrical and Computer Engineering, University of Waterloo
Internal Member:	Magdy Salama Professor, Department of Electrical and Computer Engineering, University of Waterloo
Internal Member:	Mehrdad Kazerani Professor, Department of Electrical and Computer Engineering, University of Waterloo
Internal-External Member:	Mehrdad Pirnia Lecturer, Department of Management Sciences, University of Waterloo
External Examiner:	Vijay Vittal Regents Professor, Department of Electrical, Computer, and Energy Engineering, Arizona State University

Author's Declaration

I hereby declare that I am the sole author of this thesis. This is a true copy of the thesis, including any required final revisions, as accepted by my examiners.

I understand that my thesis may be made electronically available to the public.

Abstract

Renewable Energy Sources (RESs) provide a feasible alternative to supply electrical loads without the unfavorable environmental impacts of fossil fuels. However, despite the significant environmental benefits of RESs, several operational challenges associated with their high levels of penetration in power systems need to be addressed. Extensive research has shown that Energy Storage Systems (ESSs) facilitate increased penetration levels of RESs by providing flexibility to the system, especially considering the technical maturity and decreasing cost of these technologies; hence, penetration of ESS, such as batteries and flywheels is likely to grow significantly in the coming years. Indeed, services that have been traditionally procured from synchronous generators such as Frequency Regulation (FR) are already being provided by ESSs. However, appropriate frequency control must be considered to take advantage of the fast response capability of ESS facilities, while coordinating their response with the bulk conventional generators currently used for FR. Some characteristics of the bulk power grids, regulation signals, and the State of Charge (SoC) management of the ESSs need be considered for the design of proper FR controls.

In this thesis, a FR model is proposed of a large interconnected power system including ESSs such as Battery Energy Storage Systems (BESSs) and Flywheel Energy Storage Systems (FESSs), considering all relevant stages in the frequency control process. The model, which considers Communication Delays (CDs) in the transmission of signals in the FR control loop, is developed from the viewpoint of an Independent System Operator (ISO), using the Ontario Power System (OPS) as case study. To this effect, empirically-based and generic SoC models for FESS and BESS considering the charging and discharging process characteristics are proposed. The system, ESSs, and SoC components are modelled in detail from a FR perspective and validated using real system and ESSs data, and a practical transient stability model of the North American Eastern Interconnection (NAEI) in Dynamic Security Assessment Tools (DSATools™) platform. The proposed model is validated with and considers all main stages of the FR control process, including CDs and the SoC management model of the ESS facilities, ensuring a realistic closed-loop response. Simulation studies show that the proposed model accurately represents the FR process of a large interconnected power system including ESSs, and can be used for accurate FR studies. The impact of CDs and SoC management of ESS facilities on the Area Control Error (ACE), and the computational efficiency of the proposed FR model are studied and discussed.

A novel $\mathcal{H}_2$ filter design is proposed to optimally split the FR signal between conventional and fast regulating ESS assets, considering typical CDs. The design approach includes filtering the FR signal by producing a slowly-varying component or Traditional

Regulation Signal ($RegA$) to be provided to the slow regulating resources (i.e., Traditional Generators (TGs)), while the remaining fast component or Dynamic Regulation Signal ($RegD$) is provided to the fast response ESS facilities (FESS and BESS) to take advantage of their fast response characteristics. The design of the $\mathcal{H}_2$ filter is formulated as an optimal control design problem, and the proposed filter is integrated into the previously validated FR model with ESSs to form an Integrated Model, which includes a Proposed Set-Point (PSP) calculation and an anti-windup strategy. The PSP allows FR capacity from ESSs to be comparable to TGs FR capacity while keeping the system stable, which is not the case in the current FR process for the OPS. The proposed anti-windup strategy is added to avoid saturation when both TGs and ESSs reach their limits, or TGs reach their limits while the ESS facilities are not able to follow the PSP signals because of their SoC limits. Thus, the proposed filter sends $RegA$ and $RegD$ signals considering the SoC of fast response resources and capacity limits of ESSs and TGs, and depend on the conditions of the system, working in a coordinated manner. The FR performance with the $\mathcal{H}_2$ filter signals, $RegA$ and $RegD$, is also compared with the existing FR process in the OPS, focusing on studying the impact of CDs and limited regulation capacity, and the effect of the PSP calculation and anti-windup strategy. The results show that the $\mathcal{H}_2$ filter design and signal splitting strategy improves the FR process performance significantly, in terms of reducing the ACE, and thus reduce the need for regulation capacity.

Finally, a detailed methodology is developed to obtain Marginal Rate of Technical Substitution (MRTS) curves for the Independent Electricity System Operator (IESO). The IESO's MRTS curves consider different ESSs and discharging times (i.e., 15 min for FESS, and 15 min, 1 h, 2 h, and 4h for BESS), scenarios (i.e., peak hours, non-peak hours, morning ramp hours, and evening ramp hours), and seasons. The criteria agreed upon with the IESO for the generation of heat maps and MRTS is also presented. Furthermore, the procedure to select the representative typical days per season to be used in the generation of the MRTS curves is explained in detail, and an example of how to interpret one of the MRTS curves is explained. Heat maps and MRTS curves are proposed as analysis tools to allow ISOs to select the desired performance metric, and the combination of $RegA$ and $RegD$ resources that would allow to achieve it while still reducing the total regulation capacity. Although this methodology is applied to the IESO, it could be applied to other ISOs with appropriate modifications.

Acknowledgements

First of all, I want to thank God for enlightening my path during these years, guiding me when I felt lost, and helping me to start over when I thought it was not possible.

I would like to express my sincere gratitude to my supervisors, Professor Claudio Canizares and Professor Kankar Bhattacharya, for giving me the opportunity to be part of their research group, it has been an honor to work under the supervision of such extraordinary professionals and human beings. Also, I want to thank them for being such excellent examples of hard work, commitment, and values; for their invaluable advice and suggestion during my research; for sharing their time and knowledge; and mainly for their support to overcome difficulties during my PhD program.

My sincere appreciation to my Ph.D. Committee members for their valuable comments and observations: Professor Magdy Salama, Mehrdad Kazerani from the Department of Electrical and Computer Engineering at University of Waterloo; Professor Mehrdad Pirnia, from the Department of Management Sciences at the University of Waterloo; and Professor Vijay Vittal, from the Department of Electrical, Computer, and Energy Engineering at Arizona State University.

I am deeply grateful to Professor John Simpson-Porco, from the Department of Electrical and Computer Engineering, University of Toronto, and Dr. Mariano Arriaga from the Energy and Power Innovation Centre at Mohawk College, Hamilton, Ontario, for their their insightful comments and suggestions during part of my research.

I thankfully acknowledge the funding support from Natural Sciences and Engineering Research Council (NSERC) Canada, Energy Storage Technology (NEST) Network, and NRStor Inc. for kindly providing the data needed to carry out this work, under the auspices of an experimental research program facilitated by Ontario's IESO. I want to express my gratitude to Daniel Sohm and Edward Arlitt from Advanced Technology Research, IESO, Ontario, for the opportunity to work with them and for their valuable advice at every stage of this research.

Many thanks to my past and current colleagues in the EMSOL lab, for providing such a pleasant work environment. Special thanks to my friends Carlos, Mariano, Dario, Mauricio, and Diego for the great memories and laughs, which made life more enjoyable.

I would like to thank my parents, Eloy and Angelita, for their unconditional support through all these years, their kind words, advice, motivation, and love, which kept me going despite many difficulties. I am also grateful to my cats Suzy and Mimi for being in my life when I needed them most.

Dedication

This is dedicated to my mom and dad, Angelita and Eloy.

Table of Contents

List of Figures

List of Tables

List of Abbreviations

RegA	Traditional Regulation Signal.
RegD	Dynamic Regulation Signal.
ACE	Area Control Error.
AGC	Automatic Generation Control.
ATR	Alternate Technologies for Regulation.
BA	Balancing Authority.
BAAL	Balancing Authority ACE Limit.
BESS	Battery Energy Storage System.
BF	Benefit Factor.
CAES	Compressed-Air Energy Storage.
CAISO	California Independent System Operator.
CD	Communication Delay.
CPS1	Control Performance Standard 1.
DSATools™	Dynamic Security Assessment Tools.
ESAG	Energy Storage Advisory Group.
ESS	Energy Storage System.
EV	Electric Vehicles.

FERC Federal Energy Regulatory Commission.
FESS Flywheel Energy Storage System.
FR Frequency Regulation.

GA Genetic Algorithm.
GP Generalized Plant.

IAM IESO-Administered Market.
IESO Independent Electricity System Operator.
ISO Independent System Operator.
ISO-NE Independent System Operator of New England.

LESR Limited Energy Storage Resources.
LFC Load Frequency Control.

MAE Mean Absolute Error.
MISO Midcontinent Independent System Operator.
MRTS Marginal Rate of Technical Substitution.

NAEI North American Eastern Interconnection.
NDA Non-Disclosure Agreement.
NERC North American Electric Reliability Corporation.
NN Neural Network.
NYISO New York Independent System Operator.

OPG Ontario Power Generation.
OPS Ontario Power System.

PFR Primary Frequency Response.
PI Proportional-Integral.
PID Proportional-Integral-Derivative.
PJM PJM Interconnection LLC.
PSP Proposed Set-Point.

REM Regulation Energy Management.
RES Renewable Energy Source.

RFP Request for Proposals.
RMSE Root-Mean Squared Error.
RTO Regional Transmission Organization.
RTU Remote Terminal Unit.

SCADA Supervisory Control and Data Acquisition System.
SD Standard Deviation.
SDP Storage Design Project.
SoC State of Charge.
SP Set-Point.

TG Traditional Generator.

UW University of Waterloo.

VSC Voltage Source Converter.

.

Nomenclature

Indices

0	Initial value.
ESS	ESS: FESS or BESS.
i	Elements in $W(z)$.
j	Elements in $Z(z)$.
k	Generators.
q	Average MRTS curve data point on segment v.
r	Isoquant data point on segment u.
t	Time.
u	Segments on a $RegD$ MW-interval on an isoquant.
v	Segments on a $RegD$ MW-interval on an average MRTS curve.

Parameters

a, b, c, d	Parameters used in the identification of ESS's SoC bands.
$\tilde{A}_u, \tilde{B}_u$	Matrix and vector, respectively, containing the inequality constraints of the isoquant approximation problem of segment u.
$\tilde{A}eq_u, \tilde{B}eq_u$	Matrix and vector, respectively, containing the equality constraints of the isoquant approximation problem of segment u.

$\hat{A}eq_v, \hat{B}eq_v$	Matrix and vector, respectively, containing the equality constraints for the average MRTS optimization problem of segment v.
AV_{ESS}	Status availability of the ESS.
B	Balancing Authority (BA) bias [MW/0.1Hz].
β	Frequency response of the system [MW/Hz].
β_{EI}	Eastern Interconnection frequency response [MW/0.1Hz].
β_{IESO}	Ontario power system frequency response [MW/0.1Hz].
$C(z)$	ESS charging transfer function.
c_f	Stage II gain.
$\tilde{C}_u$	Matrix containing the values of $x_{r,u}$ for segment u.
$\hat{C}_v$	Matrix containing the values of $x_{q,v}$ for segment v.
CD	Communication delay (z^{-4}) [s].
CD_{TG}	Communication delay for TGs [s].
CF	Correction Factor block.
CF_1^D, CF_2^D	Correction factor discharging input multipliers.
CF_{eq}, CF_1^C, CF_2^C	Correction factor charging input multipliers.
$CFout^C$	CF block charging output.
$CFout^D$	CF block discharging output.
D	Damping factor modelling variations respect to frequency D_f [MW/Hz] or speed D_ω $[\frac{Nm}{rad/s}]$
$D(z)$	ESS discharging transfer function.
$\tilde{d}_u$	Vector containing the values of $y_{r,u}$ for segment u.
$\hat{d}_v$	Vector containing the values of $y_{q,v}$ for segment v.

E_{ESS}	ESS energy capacity [MWh].
Eq	Equality condition parameter.
$F(z)$	Transfer function that allows closer fit between the model results and measured data for frequency.
f_s	Scheduled frequency [Hz].
Fsr	Falling slew rate[MW].
H	Inertia constant [MWs/MVA].
$Hv1, Hv2$	Highest value of $RegD$ for an isoquant and an average MRTS curve, respectively [MW].
I	Identity matrix.
IME	Interchange metering error [MW].
In^C	CF block charging input.
In^D	CF block discharging input.
IP	Inadvertent payback [MW].
K	Power-to-energy value [hr/s].
k_i	Integral controller gain.
K_I, K_{I1}, K_{I2}	Integral controller gains of the units providing secondary regulation.
k_p	Proportional controller gain.
ks_{dw}, kr_{dw}	Parameters representing SoC values for k_{dw} flip-flop.
ks_{up}, kr_{up}	Parameters representing SoC values for k_{up} flip-flop.
L	Total number of segments v in an average MRTS curve.
$\overline{L}_{off}$	Upper limit of the ESS's lower SoC band.
$\underline{L}_{on}$	Lower limit of the ESS's lower SoC band.
N_u	Total number of isoquant data points on segment u.

n_g	Total number of generators.
NI_s	Scheduled net interchanges [MW].
ω_0	Rated rotor angular speed [rad/s].
O_v	Total number of average MRTS curve data points on segment v.
Pc_{ESS}	ESS power capacity [MW].
R	Speed regulation or droop [Hz/MW].
RC	FR capacity limit [MW].
RC_{ESS}	ESSs FR capacity limit [MW].
RC_{TG}	TGs FR capacity limit [MW].
Rsr	Rising slew rate[MW].
T	Total number of segments u in an isoquant.
$TG(z)$	Transfer function representing the action of TGs contracted for FR.
$\underline{U}_{off}$	Lower limit of the ESS's upper SoC band.
$\overline{U}_{on}$	Upper limit of the ESS's upper SoC band.
$x_{q,v}, y_{q,v}$	Values of $RegD$ and MRTS, respectively, corresponding to the q average MRTS data point on segment v.
$x_{r,u}, y_{r,u}$	Values of $RegD$ and $RegA$, respectively, corresponding to the r isoquant data point on segment u.

Variables

A, B, C, D	State-space matrices of $GP(z)$ including $F_{W_i}(z)$ and $F_{Z_j}(z)$.
α_{ESS}	Factor indicating the capacity contribution of the ESS to RC_{ESS} [p.u.]
$\tilde{a}_u, \tilde{b}_u, \tilde{c}_u$	Coefficients of the quadratic function approximating a segment u on an isoquant.

$\hat{a}_v, \hat{b}_v$	Coefficients of the linear function representing each segment v on the average optimized MRTS curve.
ACE	Area Control Error [MW].
$ACE_{filtered}$	ACE filtered signal [MW].
B_p	Base-point [MW].
BP_{ESS}	ESS fixed base point [MW].
BPm_{ESS}	ESS moving base-point [MW].
Clp	Clamping signal.
δ	Rotor angle [rad].
f	Frequency [Hz].
Φ	Controller/Filter.
$F(IP)$	Function of inadvertent payback [MW].
Φ_W, Φ_Z	Weighting filters associated to the input W and output Z, respectively.
f_a	Actual frequency [Hz].
Δf_{ss}	Steady state frequency deviation [Hz].
$GP(z)$	Generalized Plant transfer function matrix.
$Hv1$	Highest value of $RegD$ for an isoquant [MW].
$Hv2$	Highest value of $RegD$ for the average optimized MRTS curve [MW].
ΔIs_1	Change in the value of the isoquant Is_1 [MW].
Is_1, Is_2, Is_3	Isoquants representing the output RMSE of ACE [MW].
k_{up}, k_{dw}	Outputs of the set-reset flip-flops.
$\overline{M}_{ESS}$	Maximum available capacity of the ESS [MW].
$\underline{M}_{ESS}$	Minimum available capacity of the ESS [MW].

MP_{RegD}, MP_{RegA}	Marginal product of $RegD$ and $RegA$, respectively.
$MRTS_{RegD,RegA}$	MRTS of $RegA$ for $RegD$.
$N(z)$	Lower linear fractional transformation of $F(z)$ around $GP(z)$.
NI_a	Actual net interchanges [MW].
ω_r	Rotor angular speed [rad/s].
P_D	Load of the system [MW].
P_{ESS}	Power output of the ESS [MW].
P_e	Real electric power [MW].
P_{GT}	Generation total dispatch [MW].
P_L	Load of the system [MW].
P_m	Mechanical power [MW].
P_{ref}	Power set-point [MW].
P_{TGr}	Output power of TG contracted for FR [MW].
$\tilde{p}_u$	Vector containing the coefficients $\tilde{a}_u, \tilde{b}_u, \tilde{c}_u$ in the isoquant approximation problem.
$\hat{p}_v$	Vector containing the coefficients $\hat{a}_v$ and $\hat{b}_v$ in the average MRTS optimization problem.
R_{dw}	Reset state of the k_{dw} flip-flop.
R_s	Regulation service provision [MW].
R_{up}	Reset state of the k_{up} flip-flop.
$RegA$	Traditional Regulation Signal [MW].
$RegA_L$	Traditional Regulation Signal limited [MW].
$RegD$	Dynamic Regulation Signal [MW].
$RegD_L$	Dynamic Regulation Signal limited [MW].

S_{dw}	Set state of the k_{dw} flip-flop.
S_p	Set-point [MW].
S_{up}	Set state of the k_{up} flip-flop.
SOC_{ESS}	ESS SoC [%].
SP_{ESS}	ESS SP signal [MW].
SR	Scheduled FR signal [MW].
SR_{ESS}	ESS regulation signal [MW].
T_e	Electrical torque [Nm].
T_m	Mechanical torque [Nm].
U	Control signals.
U_1	$RegA$ as control signal.
U_2	$RegD$ as control signal.
W	(Weighted) exogenous inputs/disturbance input vector
Y	Sensed outputs.
Y_1	ACE as sensed output.
Y_2	Cumulative ACE as sensed output.
Z	(Weighted) exogenous outputs/error output vector.

Chapter 1

Introduction

1.1 Motivation

Renewable Energy Sources (RESs) provide a feasible alternative to supply electrical loads in power systems, without the undesirable environmental impacts of fossil fuels. However, despite the significant environmental benefits of RESs, there are several operational challenges associated with high levels of penetration in power systems. Most of these challenges are linked to the inherent variability of RESs and the fact that these are not dispatchable, which leads to increased generation/load mismatches that particularly impact Frequency Regulation (FR). Research has shown that Energy Storage Systems (ESSs) facilitate increased penetration levels of RESs [1, 2], and can help to maintain grid stability and reliability [1, 3]; in addition, these ESS systems can be used to provide energy arbitrage and ancillary services such as FR, spinning reserve, voltage support, and supplemental reserves, to name a few, while being competitive and economically viable [4, 5]. However, the ESS power and energy capacities, State of Charge (SoC) management, and type of technology are limiting factors for these services.

In recent years, there has been a significant interest in ESS technologies because of their increasing technical maturity and lower cost trends. It is expected that by 2030, ESSs costs will reduce by up to 75% of current levels, rendering them comparable to the cost of traditional generation sources; for instance, the total installation cost of Li-ion and NaS batteries could decrease by up to 61% and 75%, respectively, while Flywheel Energy Storage Systems (FESSs) could reduce their installation cost up to 35% by 2030 [6, 7].

Policies around the world are being modified and new services are being created to facilitate participation of ESSs as fast FR service providers [3, 8, 9]. However, there is

a need to develop dynamic models for bulk power systems equipped with ESS. These models need to be tested and validated over long-term simulation time-horizon for robust performance.

Currently, in Ontario, two scheduled regulation signals are sent: one to traditional generators, and one to ESS facilities. The signal sent to traditional facilities, which are actually in charge of most of the FR service in Ontario, assumes that these cannot react to very fast frequency changes. However, while ESSs have the ability to respond to fast frequency excursions, the signal they receive in Ontario is not coordinated with the signal sent to traditional generators, which can cause over-compensation of the Area Control Error (ACE) once the capacity of ESS facilities contracted for FR becomes significant as compared to traditional resources. This can lead to increased ACE and hence increased regulation capacity requirement, thus reducing the potential benefit that fast resources could add to the FR control process. Therefore, an adequate optimized strategy to split the scheduled regulation signals into two coordinated signals: one to be sent to the slower response facilities (Traditional Regulation Signal ($RegA$)), and the other to fast response facilities (Dynamic Regulation Signal ($RegD$)), which is similar to what is done in some US jurisdictions and should improve the FR performance in Ontario.

Fast response ESS technologies can mitigate frequency variations when included in the FR control loop [10]. A critical factor that influences the FR service provided by ESSs is the SoC management of the facility. Any inappropriate management of SoC of the ESS facilities, such as imposing a neutrality condition when not needed or not having an idling state, can worsen the ACE signal. Therefore, accurate modelling and appropriate analysis of the SoC management in the existing ESS facilities can help improve FR performance. In addition, Communication Delays (CDs) in the signal transmission from/to the control center to/from the facilities contracted for FR, affect the FR process performance; with CDs not allowing ESSs to act as fast as they are able to, since CDs could be longer (e.g., several seconds) than the time response of the ESSs to a given signal (i.e., milliseconds to seconds). Hence, including CDs in system models for FR studies is essential in order to obtain realistic results pertaining to the benefits of adding ESS in the FR control loop. This requires having a model that allows long-term closed-loop frequency analysis to examine the impact on ACE when considering ESS in the FR process and splitting of the FR signal into two signals.

In February 2017, PJM Interconnection LLC (PJM) proposed the implementation of a Marginal Rate of Technical Substitution (MRTS) curve replacing a Benefit Factor (BF) curve used at the time, with the latter and its incorrect implementation through optimization, clearing and settlement process introducing flaws in PJM's regulation market regarding under- and over-payment of fast resources. However, this proposal was rejected

by the Federal Energy Regulatory Commission (FERC) because of its inconsistencies with Order 755 [11, 12, 13]. Although the Independent Electricity System Operator (IESO) is not under FERC jurisdiction, it is considering the participation of ESSs in the IESO-Administered Markets (IAMs) through the Storage Design Project (SDP) Long-term Design Vision, which suggests that with a correct implementation, the IESO can take advantage of the benefits of MRTS as a tool to determine the appropriate combination of regulation capacity from fast and slow resources. Hence, there is a need to develop the MRTS curves for Ontario and examine their performance in reducing the overall regulation capacity used, which can yield cost savings for the IESO.

In view of the aforementioned issue, the main objective of this research is to analyze the impact of fast FR in bulk power systems, using the Ontario Power System (OPS) as a case study, starting with developing a proper system model for a real power grid considering the main stages in the FR control process, and appropriate empirical-based models of ESSs for FR studies. These models are then used to design a filter to divide the FR signal and to investigate the split signal impact on ACE, considering CDs, and taking into account the SoC management model of the ESSs. The developed models and controls should be suitable for long-term FR studies. Finally, representative MRTS curves are developed for Ontario and are considered for analysis in the implementation of ESS facilities in IAMs.

1.2 Literature Review

The literature review presented in this section focuses mainly on frequency regulation with ESS and splitting the regulation signal. The issue of CDs in signal transmission in the FR control process is also discussed, and FR practices by various Independent System Operators (ISOs) in US and Canada are reviewed.

1.2.1 Frequency Regulation Practices in US and Canada

In 2018, the US FERC amended its regulation (Order 841) to facilitate the participation of ESS in energy, capacity, and ancillary service markets operated by ISOs and Regional Transmission Organizations (RTOs) [8]. In addition, FERC Order 755 recommends a performance-based payment for FR to incentivize the integration of fast response ESS technologies [14], which led to changes in market design in some of the US markets, and to the introduction of a two-part payment scheme for FR reserves: capacity and performance payment (mileage payment) [15, 16, 17]. In 2019, the SDP was initiated by the IESO to

clearly formalize the participation of ESS in IAMs for the interim period, and develop a vision for their participation in the IAMs over the long-term [18]. All these changes suggest that the role and importance of ESS will keep growing in Ontario and in jurisdictions worldwide; therefore, studies to analyze the impact of ESSs in the provision of power system ancillary services are needed.

Some ISOs are considering measures to support the integration of ESS within their administered markets [9], or have procured or already implemented ESS-based FR to exploit the unique characteristics and potential benefits of fast responding technologies such as Battery Energy Storage Systems (BESSs) and FESSs [3, 7, 14, 15, 19]. For instance, the California Independent System Operator (CAISO) includes ESS within a set of resources called non-generating resources, which can be non-Regulation Energy Management (REM) resources and be subject to the same conditions as traditional generators to meet a 60 minute continuous energy requirement, or be REM resources with an energy requirement of 15 minutes [20]. In the New York Independent System Operator (NYISO), the ESSs are called Limited Energy Storage Resources (LESR), and are assigned their regulation base point depending on their SoC every 5 minutes [16]. The IESO of Ontario has procured around 50 MW of ESSs capacity in recent years, and has actively encouraged the participation of ESS in the IAMs through several programs and pilot projects, which provide various services to the system and learning opportunities for all stakeholders [9, 21]. In March 2018, the first fully dispatchable BESS was integrated with the Ontario system, and later, in April 2018, the Energy Storage Advisory Group (ESAG) was established to support the IESO in developing policies and tools to integrate ESS facilities within the IAM. Additionally, recent legislative changes in Ontario related to net metering regulation [22], render RESs with ESS of any size as eligible for net metering. Hence, penetration of ESS technologies is likely to grow significantly in the coming years. Indeed, it is also envisaged that services besides FR such as reactive support and voltage control, which have traditionally been procured from synchronous generators and capacitor banks, will be provided by ESSs.

Over the last few years, some ISOs in USA have implemented strategies to split the FR signal into a slow signal $RegA$ and a fast signal $RegD$, which act on conventional and fast-responding assets, respectively [3, 15]. This is done to use the fast response capability of ESS beyond the traditional Automatic Generation Control (AGC) framework, with resources following the $RegD$ signal receiving extra payment [20]. For instance, PJM considers the participation of ESS in its FR market and offers two regulation signals: $RegA$ meant for traditional generators with limited ramp rate, and $RegD$ meant for high ramp rate capability units. The signal $RegD$ is derived from the same algorithm as $RegA$, but $RegD$ filters out low-frequency components, resulting in a fast cycling signal [15, 16]. The

Independent System Operator of New England (ISO-NE) includes ESS facilities in their Alternative Technology Regulation Resources; it uses two faster energy neutral signals (energy-neutral continuous and energy neutral trinary) meant for alternative technologies, and also sends a slower AGC signal to conventional facilities every four seconds [20, 23]; these signals behave similarly to PJM's *RegD* and *RegA*, respectively [20]. The Mid-continent Independent System Operator (MISO) also has an AGC-enhanced signal for fast ramping resources, specifically to allow ESSs to participate in the regulation reserve market and to improve the use of fast ramping facilities [17].

1.2.2 Frequency Regulation with Energy Storage

The fast response characteristic of ESSs, such as FESS and BESS, make them particularly suitable to provide fast FR services [4]. In [24], a combination of wind power and a BESS is proposed in a real-time cooperation scheme to take advantage of their complementary characteristics in joint energy and regulation markets. In the proposed scheme, the wind power is used to track the FR signal and the BESS compensates for insufficient and inaccurate power. The cooperation scheme is tested using historical market and *RegD* data from PJM. However, the proposed scheme is developed from the facility point of view, thus not making it suitable for FR studies from the ISO's perspective.

In [25], a hybrid scheme that includes a super capacitor and a BESS is proposed for FR provision from the system viewpoint. The objective is to combine both technologies so that their mutual disadvantages can be compensated; thus, the proposed scheme intends to increase the lifespan of the BESS by reducing cycling, given the initial fast response of the super capacitor. However, the hybrid scheme is only tested on a small single area system while the SoC of the BESS is not considered, which can impact the results significantly.

A robust optimization framework proposed in [26] is adopted for the provision of FR by Electric Vehicles (EV) in a performance-based compensation scheme. The proposed formulation takes into account uncertainty of the AGC signal and dynamic arrival and departure times of the EVs, and seeks to enhance their revenues considering US market rules. An aggregator coordinates the EVs to provide regulation services to the ISO. The framework allows the EVs to follow the AGC for most of the time. Actual AGC signals and prices from PJM are used in the simulation studies. However, as noted in the paper, the FR service provision is not guaranteed all the time, and hence the regulation by EVs need to be supported by a facility fully dedicated to the FR provision. Furthermore, the proposed scheme is developed from the perspective of EVs and does not examine the provision of FR from an ISO perspective.

An optimization framework considering a BESS for provision of FR and peak shaving applications is presented in [27]. BESS degradation, operational constraints, and uncertainties in FR signals and customer loads are considered. The joint optimization of using BESS for both FR and peak shaving for a commercial customer results in greater savings than the sum of savings from BESS used for individual applications. In [28], energy arbitrage and FR from BESS are considered simultaneously by co-optimizing the two services using a Markov decision process formulation. Since the two services are on different time scales, a dynamic programming approach that takes advantage of the nested structure and solves smaller sub-problems is used. However, both [27] and [28] are modelled from the BESS owners' perspective, and thus investigating their impact on the regulation control process is not feasible.

A coordination algorithm to dispatch FR services between slow and fast resources is presented in [29], from the facility's point of view. The purpose of the algorithm is to prioritize an FESS to follow the ACE signal while its SoC is within a desired band, and a conventional generator is dispatched if the SoC moves outside that band, to charge/discharge the FESS and bring the SoC within the desired range. An actual ACE signal is used, normalized to ± 25 MW. However, the FESS with SoC band control is based on a manufacturer provided model and no details are provided. Furthermore, although the FR regulation range is ± 25 MW, the algorithm is not tested for a FR signal beyond the ± 20 MW range, and the insensitivity of FESS to deep discharges is not taken advantage of.

An FR strategy using fuzzy-logic control based on ACE and the SoC of a BESS is presented in [30]. The ACE and SoC of the BESS are inputs to the fuzzy controller while the output power of the BESS is the output of the controller. The ACE and SoC of the BESS are both divided into four regulation zones, so that the BESS participates in secondary FR according to AGC instructions combined with the fuzzy controller to smooth the output of the BESS and assist thermal power units. The model is tested on a system formed by a thermal power unit and a BESS. However, the SoC model used is not presented, even though this is one of the inputs to the controller.

A BESS control strategy to improve the AGC performance is studied in [31]. The controller seeks to minimize the rate of non-compliance of a dynamic performance criteria by maintaining the AGC response within the FR response accuracy margins, which define the slowest and fastest response to an FR signal. An SoC control that levels out the SoC of the BESS is included in the strategy, and the BESS is only used during certain FR assistance periods to keep degradation and extreme SoC levels to a minimum. The strategy is evaluated using 400 h of the actual AGC signal of a Balancing Authority (BA) of the Spanish power system, whose AGC regulator is based on merit order. However, the impact of the BESS response to this control strategy on the system's frequency is neglected, since

there is no modification in the FR signal in response to the BESS for the cases analyzed. This is not an accurate representation of the FR process, since the response of the facilities to the FR signal modify the ACE.

The Load Frequency Control (LFC) of a two-area interconnected system, each area with one steam turbine and an FESS is considered in [32]. The FESS and the governors of the generators have Proportional-Integral-Derivative (PID) controllers, with their parameters optimized using a Genetic Algorithm (GA). The FESS directly controls its output to correct the system frequency, preventing sudden changes in the governor of the generator. It is noted that the PID controller of the FESS is more robust, faster, and more accurate than the generator's PID controller. However, the capacities of the conventional generator and the FESS are not provided. Also, the signal sent to the FESS does not include a bias factor nor the tie-line flow deviations, and the FESS model does not include the effect of SoC.

The AGC operation of a 1 MW/2 MWh BESS in a 10 MW grid connected wind park is examined in [33]. The actual BESS responses to historic *RegD* signals from PJM are obtained from the Modbus network. The BESS has five operating modes including maintenance, idling, and three AGC provision modes, a time response lower than one second, and an insignificant CD. Simulations show that the BESS is able to follow the set-point signal 64% of the time, that the error in following the signal is higher as the SoC increases, and that the efficiency of the BESS is 76% under the test conditions. It is concluded that BESS are fast response devices, able to provide AGC. However, the authors do not model the FR signal sent to the BESS or analyze the operation of the BESS with a different FR signal.

In [34], a BESS model including the battery bank model and the dc-to-dc converter model is presented and tested on a benchmark transmission system. However, the model is quite detailed and require information on the internal state variables which is not practical for long-term FR of bulk power systems. ESS models for frequency control are presented in [35, 36, 37]; however, these only consider primary frequency control provision and not secondary regulation.

1.2.3 Splitting the Regulation Signal

Initial attempts of ISOs to split the FR signal between conventional and fast assets, considering economic and operational factors such as market aspects, system stability, and performance [3, 15], have resulted in reduced FR procurement requirements [20]. However, only limited technical information on the ISOs' implemented strategies is publicly

available, with only block diagrams and no details on their design or tuning processes [38]. Thus, it is impractical to develop split signal strategies without detailed design data.

The coordination between conventional generators and BESSs at high wind penetration is reported in [39]. A droop with SoC feedback fitting conventional primary and secondary FR controls is presented. The BESSs tracks the high frequency components of frequency deviations, complementing the primary FR provided by conventional generators. In the secondary FR process, the SoC of BESSs is restored to a desired level with power from conventional generators which also provide secondary FR. The method controls the participation of the BESSs based on their SoC level, is theoretically demonstrated and validated through time and frequency domain analyses, and is tested in a future grid scenario of the power system in Jeju Island, in South Korea. However, this strategy may not be transferable to bulk power systems, since CDs in the FR process are not considered, which can have a significant impact on FR performance in large power systems, affecting primary FR provision and secondary frequency control.

In [40], an FR scheme is proposed wherein a BESS acts together with the conventional AGC signal, and an AGC control strategy based on the ACE signal is formulated. In the first AGC approach, an index that captures the capability of the BESS to respond to AGC signals in charging/discharging mode is proposed, using it instead of the SoC to decide the participation of BESS in the AGC. In the second strategy, the ACE signal is distributed to conventional generators and BESS, based on the capability index of the latter. The approaches are tested on a model of the Salvadorian power system, showing significant benefits in AGC performance with the inclusion of the BESS. However, the first AGC approach does not take advantage of the fast power response capability of BESS, since the signals received by the conventional generator and BESS are the same, only scaled to their capacity. On the other hand, the second AGC approach includes a filter and a Proportional-Integral (PI) controller in the FR path for conventional generators, and another in the FR signal path for the BESS, but no tuning details of the filter or PI controller are provided.

A method of scheduling ESS and conventional FR capacity in a day-ahead FR market based on compliance of the Control Performance Standard 1 (CPS1) is proposed in [41], from a system viewpoint. The regulation signal used is the ACE multiplied by participation factors, one for conventional units and one for ESS. Two piece-wise linear functions representing the relation between conventional and ESS resources and between ESS power and energy capacity are developed to establish a capacity relationship between ESS and conventional generators. These curves are then integrated in an optimization problem with the objective to allocate resources, while minimizing total capacity cost. The method, tested on the two-area IEEE Reliability Test System in PSS/E, is effective in scheduling

FR capacity of ESS and conventional facilities to meet CPS1 in the presence of stochastic load variations at minimum cost. However, the ESS model only accounts for power capacity limits and no SoC model is considered, which yields unrealistic ESS benefits in FR control.

Strategies to provide FR using ESS and thermal generation using two data sets of total generation are studied in [42]; power, ramp rate, and energy duration curves are used to determine the ESS capacity needed. A model to split the FR signal into two, one sent to the fast ESS units and the other to slower thermal generation units, is proposed. A high pass filter is used to extract the high frequency component, and a closed-loop to control the SoC including an integrator with saturation is proposed; the remaining component of the signal is sent to the thermal generation units. An undesirable ramping of the slow signal shows up when the second data set is used; analyses reveal that the level of "fuzz" or large changes are influenced by the control area size and the measurement frequency of the sample data, which play an important role in filter design. However, the study does not account for the closed-loop feedback effects of the filter outputs in FR control. Also, it does not investigate if the fast FR signal reduces the AGC capacity requirement, or the implications of this signal on the ACE. Finally, the ESS model is not validated, as it does not correspond to any specific technology, and therefore practical limitations arising from specific technologies are not properly modelled, such as ramp rate, SoC management, and service duration.

1.2.4 Communication Delays in Frequency Regulation

An H_∞-based delay-dependent non-linear sliding mode controller for FR with constant and time variant delays CDs is proposed in [43]. The delays are in the communication of the ACE signal from the control center to the facilities, and the communication of frequency and power in the interconnection signals from Remote Terminal Units (RTUs) to the control center. The Lyapunov-Krasovskii functional approach is used to study the delay dependent stability of the closed-loop system. The objective of the controller is to minimize the effect of CDs and load changes on frequency deviations and tie-line power exchanges. The controller is tested on a two-area closed-loop system for a random load disturbance and generation rate constraints with constant and time-variant CDs; each area is represented by one equivalent generator. However, variables such as load changes, power from other generators in the system, inadvertent payback, and scheduled frequency and tie-line power, which are present in real bulk power systems, are not considered as inputs in this controller. Furthermore, the maximum CD considered in the work is only 2 s, whereas

large power systems present higher CDs in practice; for instance, the average CD from the control center to conventional generators in the Ontario system is 34 s.

In [44], a robust decentralized design of a PI controller for AGC is presented, which considers CDs modelled as a low order norm-bounded multiplicative uncertainty. The stability and performance objectives of the AGC are accomplished with an H_2/H_∞ mixed control technique, through an iterative linear matrix inequalities algorithm, resulting in a sub-optimal solution. The results demonstrate that the conservative design of the controller is a good trade-off for all AGC objectives when load disturbances and CDs are present. However, the CD associated with the tie-line power measurements received at the control center, and included in ACE calculation, are not considered, which would otherwise increase the model complexity. Moreover, the ACE signal filter is not included, which is necessary to avoid fast fluctuations of the ACE signal which cause wear and tear of generators.

The authors in [45] present the practical application of a 2 MW/0.5 MWh BESS connected to the terminal of a coal-fired generator, which has the worst AGC performance out of four units in a power plant in Beijing. The BESS constraints related to SoC, state of health, and power limits are considered for the control of the BESS, which communicates with the generator to aid its response to AGC commands. The control system and configuration of the BESS are described in detail, as well as its coordinated control strategy. It is noted that coordinated operation of the BESS and the generator result in improved overall performance of the AGC response of the power plant and BESS, meeting the set requirements. However, the average 3 s delay introduced by this controller (signal measurement, execution of control, and communication) does not consider other significant CDs present in large systems that affect the performance of FR.

1.2.5 Discussion

Based on the preceding literature review, most of the research on FR with ESSs does not consider more than one type of ESS technology, and only a few papers consider the FR process. Furthermore, some studies include CDs in the FR process, but ESSs are not included, while only a few studies that consider ESS include a model of the SoC of the facility. However, CDs and proper models of the ESS SoC, which are not all simultaneously included in any of the aforementioned works, have the potential to impact the FR performance [43, 46]. Indeed, appropriate ESS models for FR studies are lacking, which are necessary for impact studies of ESSs on FR from the ISO's perspective.

Detailed and accurate models of the BESS have been reported, but their extensive level of detail make them unsuitable for FR studies of large interconnected power systems.

Other works present ESS models for primary FR, but do not include secondary regulation. Most of the works that present models for FR are focused on the control of the SoC or the regulation signal; however, a complete closed-loop and validated model considering all the main stages in the FR process from the ISO's perspective, including ESSs and CDs, is needed for long-term FR studies. Also, determining the actual and potential benefits of ESSs for FR in an interconnected power system requires a model that represents the system frequency dynamics and its limitations. To the best of the author's knowledge, there are no reported works that discuss the use and impact of ESSs on FR in real bulk power systems.

Finally, there is only limited information on splitting the regulation signals for FR with ESSs. Particularly, there is not much publicly available information on the strategies implemented by ISOs to split their regulation signals; only block diagrams and general descriptions of strategies are available. Splitting the FR signal into a slow and a fast component, while considering operational limits, is still a work in progress. Indeed, the actual benefits of ESSs can be only realized if there is an appropriate filtering strategy for the FR signal. Some splitting criteria has been reported in the literature, but most of these works do not consider the impact of the FR facilities on the ACE, thus not presenting a realistic view of splitting strategies for FR.

1.3 Research Objectives

Based on the literature review and the identified critical issues on FR with ESSs, FR signal splitting, and issues with CDs, the following are the main objectives of this thesis:

- Develop a comprehensive mathematical simulation model for FR of a large interconnected power system operating under normal conditions for FR simulations in short periods of time (i.e., seconds to a few hours), including empirically-based SoC models for FESS and BESS that consider their charging and discharging characteristics, and considering CDs in the FR model to analyze their impact on the ACE and SoC management of ESS for FR. The proposed FR model parameters are estimated and validated with OPS information and operational data provided by IESO. This model will be referred to as the Base Case Model throughout the thesis.

- Propose a novel $\mathcal{H}_2$-filter design procedure to optimally split the FR signal into fast and slow components, with the fast component sent to the ESSs and slow component sent to conventional generators to improve the FR performance in terms of minimizing

ACE variations, integrating the proposed $\mathcal{H}_2$-filter into the previously validated OPS FR simulation model that includes ESSs and CDs, to form an Integrated Model of the FR process.

- Demonstrate the impact of fast response ESSs on the FR process by applying the proposed Integrated Model to the OPS, accounting for and evaluating the effect of CDs and limited regulation capacity, comparing the performance of the Integrated Model with respect to the Base Case Model in terms of ACE reduction.

- Finally, propose a detailed methodology to generate the MRTS curves for the OPS for different ESS technologies with varying discharge times, load scenarios, and seasons, demonstrating the advantages of using MRTS curves in the context of the FR performance of the system, while considering both fast and slow response service providers.

1.4 Thesis Outline

The rest of this thesis is organized as follows: Chapter 2 presents a comprehensive review of the background topics relevant to this thesis, including the basics of FR in power systems. An overview of frequency control in Ontario, covering some of the latest developments on ESSs from a FR perspective, focusing on FESS and BESS, are also discussed.

Chapter 3 discusses the details of the Base Case Model developed. All the relevant stages in the frequency control process are considered, and the model is validated using data from the OPS and its two ESS facilities, based on a practical transient stability model of the North American Eastern Interconnection (NAEI). Model validation, impact of CDs, SoC management model of ESS facilities in the FR process, and computational efficiency of the proposed FR model are discussed in detail.

Chapter 4 presents the details of the $\mathcal{H}_2$-filter design and the Integrated Model, which is used to analyze the impact of ESSs facilities, CDs, and limited regulation capacity in the FR process for the OPS. Studies comparing the Integrated Model and the Base Case Model are presented and examined.

Chapter 5 presents the detailed methodology for developing the IESO's MRTS curves for different ESSs technologies, considering various discharging times, scenarios, and seasons. Finally, chapter 6 summarizes the thesis content, highlights the main conclusions and contributions from this research, and outlines the scope of possible future work.

Chapter 2

Background Review

This chapter provides a background review of the relevant topics and concepts related to the research presented in this thesis. The basics of FR in power systems and an overview of FR in Ontario are discussed. An overview of fast ESSs, including FESS and BESS, from a frequency control perspective is also presented.

2.1 Frequency Control in Power Systems

Frequency is a system-wide characteristic of power systems, which should be maintained within specified limits to ensure the stable and reliable operation of the system. Large frequency deviations can be caused by generators tripping or sudden changes in demand, which can result in system instability and blackouts, while small frequency deviations could damage frequency sensitive equipment such as thermal generators and transformers. Therefore, appropriate frequency control is essential to maintain the normal operation of a power grid.

FR in power systems refer to the dynamic control loop that maintains the system frequency at 50/60 Hz, given a predefined tolerance, by continuously balancing the power generation with the system load [47]. FR services are required in order to compensate for forecast errors, non-linear behaviour of demand between dispatches, and non-dispatchable generation/load resources. These uncertainties may exceed the contracted capacity of FR resources, which is automatically compensated by the grid inter-ties, thereby deviating the power interchanges from their scheduled values [48].

Each control area in an interconnected power system could be thought of as a large machine [48], where the "speed" of rotation is the frequency. The steady-state frequency is common throughout the whole control area. If the total generation within the control area exceeds the demand, the frequency increases beyond its nominal value. Conversely, if there is a generation deficit and the stored energy in not enough to eliminate the imbalance, the frequency decreases from its scheduled value. In either of these scenarios, the balance is initially restored by the instantaneous response of frequency dependent loads, and generators' governors that regulate their output. Normally, frequency deviations of less than 0.05 Hz are considered small [49], although this depends on the operating condition and the control area, with the control area frequency deviation depending on the relation between the magnitude of the imbalance and the size of the control area. These frequency deviations could be caused by congestion or equipment failure; thus, the frequency could be considered as a health indicator of the power system [48].

Table 2.1: Frequency Controls Timeframes [47, 50].

Control	**Typical timeframe**
Primary control (local generator's response)	10 to 60 s
Secondary control (control area level)	1 to 10 min
Tertiary control (system level)	10 to 30 min

2.1.1 Primary Frequency Control [47, 50]

Primary frequency control is also known as Primary Frequency Response (PFR), and is provided by sources already connected to the system. It is critical for maintaining the reliability of the interconnection after a disturbance by restoring the generation-load balance, and it is implemented through governor control and automatically assisted by the response of frequency dependent loads (mainly motors) [48]. This primary control has the objective of stabilizing the frequency of the system, generally at a different value of frequency than the scheduled one. The deviation of the frequency from its nominal value is caused by the power mismatch within the system. If PFR is not adequate, large frequency excursions could cause load interruption by triggering frequency protection relays, which may lead to blackouts.

The turbine-governor closed loop control is the main component for PFR [47]. The governor can have isochronous or speed-droop characteristics. The isochronous governor adjusts the valve of the steam turbine or gates of the hydraulic turbine based on a signal

originating from the difference between ω_r and its reference. However, if the generators involved in the FR process do not have exactly the same speed settings, they would fight each other to control the frequency based on their own settings; hence, isochronous control works well for an isolated generation-load system or a system in which only one generator is in charge of the FR. For a system with multiple generators in charge of the FR process, governors with speed-droop characteristic are preferred. These governors have proportional controllers with a gain of $1/R$, where R in Hz/MW is the speed regulation or droop of each generator and relates the frequency change Δf with respect to the change in power output ΔP as follows:

$$R = \frac{\Delta f}{\Delta P} \tag{2.1}$$

The essential variables in the operation of PFR are real power generated P_e, the mechanical power P_m, electrical torque T_e, mechanical torque T_m, and angular speed ω_r. In steady state, P_e is balanced by P_m, while dynamically ω_r depends on P_e and P_m through their corresponding torques T_e and T_m, respectively, as follows:

$$\frac{2H}{\omega_0^2} V A_{base} \frac{d(\Delta\omega_r)}{dt} = T_m - T_e - D_\omega \Delta\omega_r \tag{2.2}$$

$$\frac{d\delta}{dt} = \omega_r - \omega_0 = \Delta\omega_r \tag{2.3}$$

These represent the generator angle δ swing equation, which determines the rotor angular speed change $\Delta\omega_r$ during disturbances with respect to the synchronous speed ω_0, depending on the inertia constant H in MWs/MVA, and the load damping factor D, which models the variations in consumed power respect to frequency (D_f in MW/Hz) or speed (D_ω in $\frac{\text{Nm}}{\text{rad/s}}$). When a load change occurs, it is reflected as a change in T_e, thus causing a mismatch between T_m and T_e, that results in a change of $\Delta\omega_r$.

For a specific operating point, the system response Δf to a load change ΔP_L of the system illustrated in Figure 2.1 is determined by the frequency-sensitive load response to frequency changes[1], and by the kinetic energy stored in all mechanical systems at that moment. If there is no frequency deviation ($\Delta f = 0$), the errors sent to the governor-turbine closed loop controllers are driven by the error in the desired output power ΔP_{ref_k} only, where k is associated to each generator in the system. On the other hand, when a deviation in frequency takes place ($\Delta f \neq 0$), the governor-turbine closed loop controllers

[1]The electrical power change ΔP_e has two components, a non-frequency-sensitive load change ΔP_L, and a frequency-sensitive load change $D_f \Delta f$.

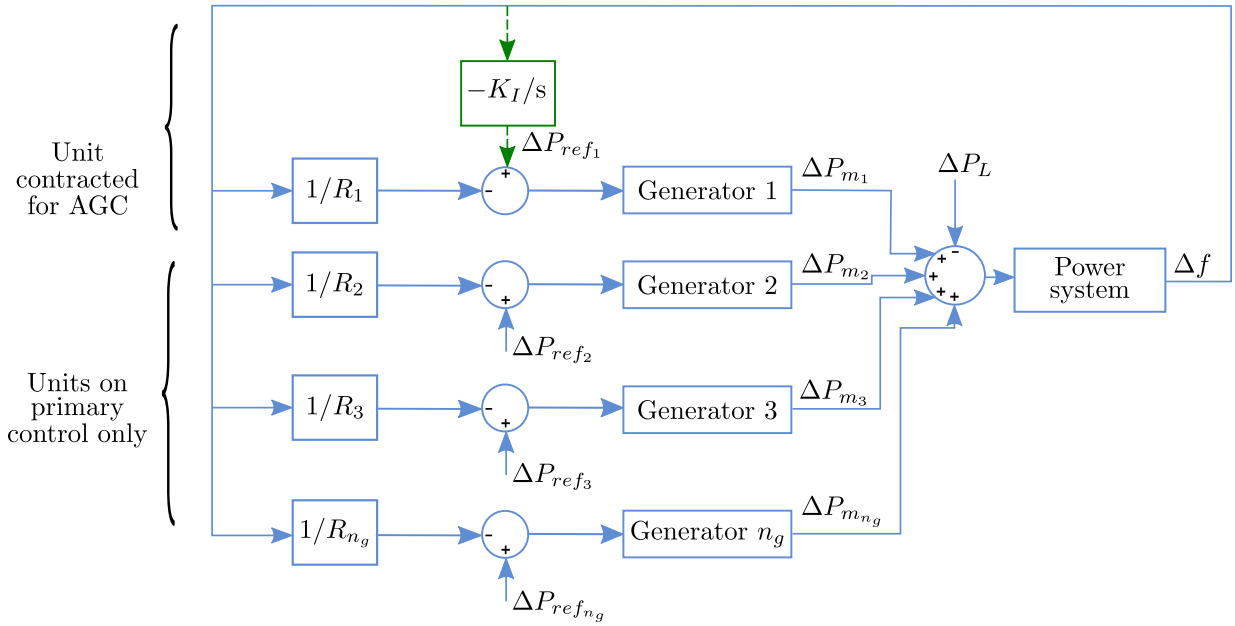

Figure 2.1: Block diagram of primary and secondary frequency control of an isolated power system [47, 50].

act on the error signal ($\Delta P_{ref_k} - \Delta f/R_k$), which try to eliminate the error by adjusting the mechanical power ΔP_{m_k}; the effect of the change of the generator output k on the frequency will depend on the generator's size compared to the system's size. The accumulated response of the generators, $\sum_k^{n_g} \Delta P_{m_k}$, seeks to eliminate the frequency deviation by matching ΔP_L. In Figure 2.1, Generator 1 is contracted to provide FR services, while Generator 2 to Generator n_g are on primary control only.

The composite frequency response characteristic of a power system depends on the sum of the droop characteristics of all generator speed governors $1/R_k$ and the load damping parameter D_f. Therefore, following a load change, the steady-state frequency deviation Δf_{ss} can be defined as follows:

$$\Delta f_{ss} = \frac{-\Delta P_L}{\sum_{k=1}^{n_g} 1/R_k + D_f} = \frac{-\Delta P_L}{\beta} \tag{2.4}$$

where n_g is the total number of generators in the system, and β is the frequency response of the system in MW/Hz, which for a real system is determined based on real historical events [51].

2.1.2 Secondary Frequency Control

There is a need to correct the generation-demand mismatch created by steady-state frequency deviations, which is provided by the dispatched generators in the control area and those that can be started up within a short time period. This action, known as secondary control, has the objective to restore the frequency to nominal values and to restore the primary control capability of the system, by modifying the power reference set-point of the generators that participate in this control. This can be manual or automatic centralized dispatch, is commonly referred to as AGC, and takes place after transients and governors' action have died down [48].

Isolated System AGC

It has the objective to restore the system frequency to its nominal value. An integral control acting on P_{ref} of the units contracted for AGC, as shown in Figure 2.1, ensures zero frequency error in steady state.

Interconnected System AGC

It seeks to maintain the scheduled interchange and frequency through governor control using measured power on the tie lines and frequency. The implementation of AGC relies on modifying the load reference set-point P_{ref}, of the generators contracted for this service, based on the signals from their respective control areas, as illustrated in Figure 2.2. The AGC's main objective is minimizing the frequency excursions and tie-lie errors as fast as possible to avoid stress on the controls and ensure system stability by adjusting the output of selected generators; this is referred to as load-frequency control. A secondary objective of the AGC is distributing the required change in generator's outputs among units to minimize operating costs [50]. Additionally, the cumulative frequency error and tie-line interchange power error should be relatively small to prevent bias in clocks and control systems, and inadvertent interchanges on the tie-lines.

Hydroelectric generators have traditionally provided AGC because they have less restrictive ramp limitations, and are thus able to respond relatively quickly to changes in the reference power signal. Other units traditionally used for this purpose are gas turbine facilities, even though they have more restrictive ramp limitations than hydro units, but less so than steam units.

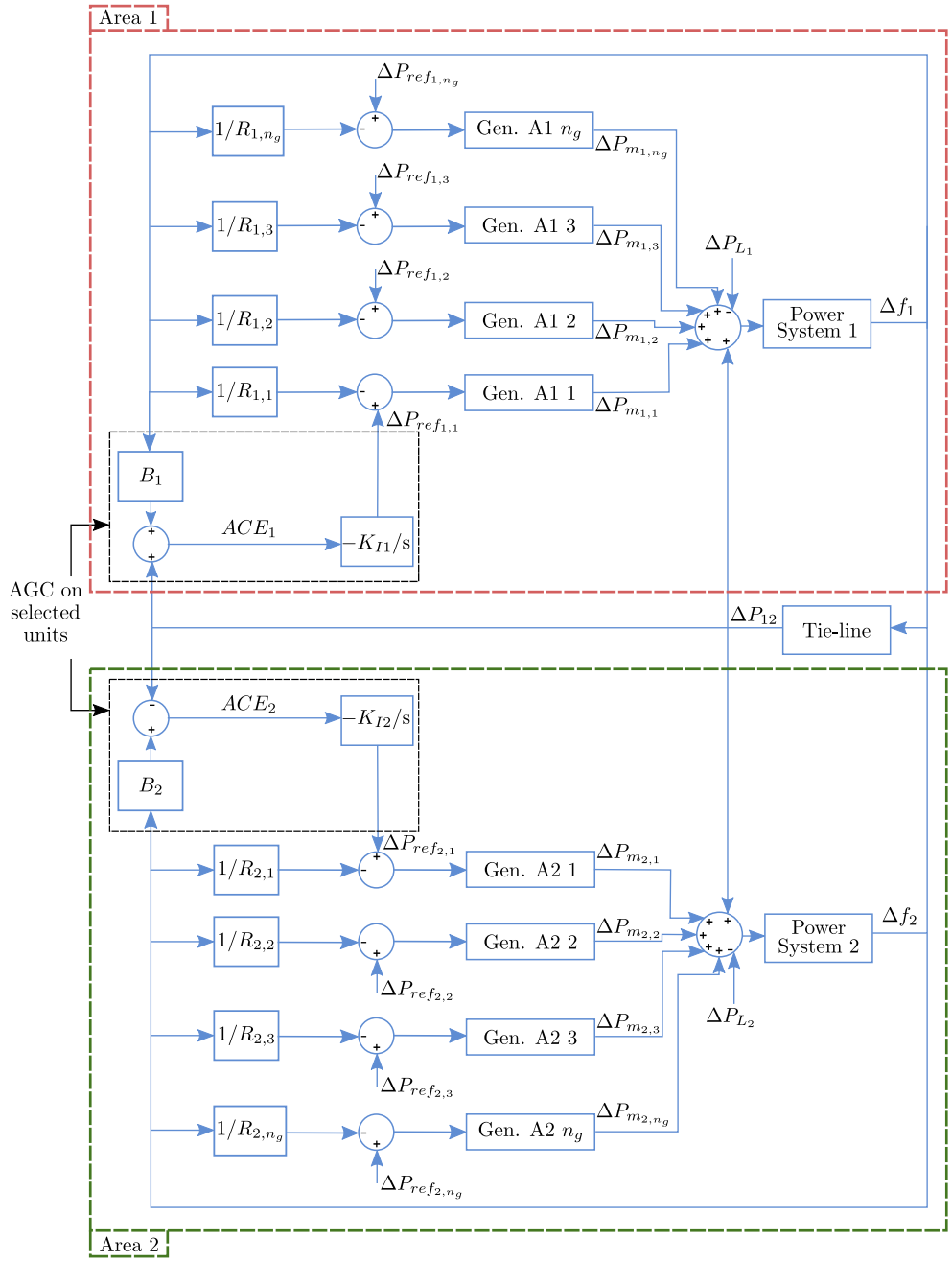

Figure 2.2: Block diagram of primary and secondary frequency control of a two-area power system [47, 50].

The generators contracted under AGC receive control signals sent by the ISO to the RTU or to the plant controller. The control signals must consider the technical characteristics of the units, such as ramp rates and maximum and minimum power, and can be sent as MW set-point commands to change the value of the generation or pulse commands to increase or decrease the output of the generator. The type of command depends on the ISO and the design of the units' governor system. Units without the capability to receive MW set-points will change their output power based on the pulse width, which changes the position of the unit's power control. Considering that the resulting change in MW may differ from the intended value, the next pass of the AGC controller will detect the error and apply further adjustments in all the generators participating in the AGC. Units with MW controllers with remote MW set-point capability can decide whether to receive raise/lower pulses or a direct MW set-point from the ISO. The latter is preferred because it eliminates the error that results in the conversion from a pulse width into a MW value. In both cases, the signal sent to the generators is filtered based on the units' capacities. The ISOs have to tune their filter parameters in agreement with the generating units that are part of the AGC, to reduce their wear and tear [52]. The AGC is an ancillary service contracted by ISOs to maintain the ACE within an acceptable range by controlling multiple generators.

Area Control Error

It is the instantaneous mismatch between the measured and scheduled interchange power in interconnected systems, considering the frequency bias effect, and the meter error correction. The ACE can be seen as a concept developed to extract the contribution of each control area to the interconnection frequency deviation. Hence, each control area monitors and seeks to keep the ACE within limits, while fairly balancing the responsibility among all control areas to maintain the interconnection frequency. This balance is achieved through computer-controlled adjustments of generators, communication with power plants, buying/selling power from/to other control areas, and possible emergency actions such as load shedding. Basically, if the ACE is positive, generation should decrease, while if ACE is negative, generation must increase to attain an ideal ACE value of zero. As part of the FR process, the control loop calculates the ACE, which extracts contributions of a control area to the interconnection frequency deviation, monitoring and keeping it within limits [47, 48]. The ACE is calculated as follows [50]:

$$ACE = (NI_a - NI_s) + 10B(f_a - f_s) - IME \tag{2.5}$$

where the first term, which comprises the measured net interchange NI_a and the scheduled net interchange NI_s, represents the interchange error; this assures that over long time

period the control area does not excessively depend on other interconnected areas for complying with the interchange obligations and meeting their demand. The net power interchange into a control area is positive, and negative otherwise.

The second term in (2.5) considers the bias B, the measured frequency f_a and scheduled frequency f_s. The intention of B is to provide frequency support without withdrawing it after the initial transient period or through the AGC action [53]. Alternative equations for ACE define this second term as negative, where B also negative. Considering that each control area has its own B, this term represents the area's bias obligation, which the North American Electric Reliability Corporation (NERC) sets as a negative number in MW/0.1 Hz and helps compensate frequency deviations. The bias should not be less than the control area's frequency response β, and has to be at least 1% of the predicted load or generation peak in accordance to BAL-003 [48].

The last term IME in (2.5) is the interchange meter error correction factor, whose purpose is to compensate for equipment errors. This generalized equation is used in an interconnected system where each ISO/BA is assigned FR responsibilities. The ACE provided by the ISO to the AGC of the dispatching units is defined in order to comply with NERC standards [48]. The resulting FR signal, based on the ACE, is sent to the assigned regulating assets at specified time intervals, which depending on the system complexity, technology used, and/or size can be 2 to 4 s for large grids.

2.2 Overview of Energy Storage Systems from Frequency Control Perspective

Electrical load variations can be seen on different time scales; thus, there are certain patterns which repeat from year to year, their behaviour[2] is different from one season to another, and some patterns can be observed monthly, weekends, weekdays, and even daily. While long-term load forecasts typically yield good accuracy, intra-hour load changes can be more challenging to predict. With the rapidly increasing penetration of RESs, the power system now experiences fast intra-dispatch interval power changes which are very difficult to predict and can significantly impact the FR performance [55]. These fast changes, which may occur every second, result in a mismatch between the generation and load, which the AGC tries to correct by appropriate frequency control. However, traditional generators are limited by their time response and ramp rate, and hence such fast changes in demand

[2]The load behaviour is influenced by factors such as economic outlook, weather scenarios, electricity price, energy conservation measures, and penetration of embedded generation [54].

cannot be properly tracked by these assets. When the mismatch occurs, the AGC sends a signal to generators to modify their power output; the generators respond to this signal a few seconds later because of CDs, thus causing the power imbalance to accumulate and the frequency deviation, and hence the ACE, to increase by the time the generator responds to the control signal. If a facility could correct the mismatch instantaneously when it occurs, the cumulative error can be reduced significantly, thereby reducing the frequency deviations and ACE as well. This can be realized by including fast response FR from ESS facilities in the FR control process, as PJM has been doing since 2012 [56].

The ESSs draw electrical energy from the power system, convert it to another form, and release it back to the system when needed. ESS technologies are able to store large amounts of energy and dispatch them when the grid requires, thereby improving the overall system operation by providing bulk energy services, customer energy management services, stacked services, and ancillary services. The latter services include spinning, non-spinning, and supplemental reserves, as well as voltage support, black start, and FR [4, 57]. The ESSs suitable for FR service are those with fast response characteristic, since they can accurately follow the FR signal.

ESS technologies include pumped storage hydro, BESS, FESS, Compressed-Air Energy Storage (CAES), super capacitors, hydrogen and thermal storage [4]. CAES and pumped storage hydro have high capacity (in GW) and are able to discharge for tens of hours. On the other hand, some batteries and flywheels are capable of discharging in the order of seconds to minutes only, and have lower energy storage capacity.

ESS grid-scale projects have been deployed to support FR services in different systems [3]. The maturity of BESS and FESS technology has opened the door to analyze and implement strategies that take advantage of their fast response characteristic. Various studies have examined the technical benefits and capacity limits of different fast regulating assets while complying with their performance standards (e.g., [19]). In general, the FR strategy of ISOs has evolved to allow more than one regulation signal depending on the asset ramp rate. For example, a traditional or slow changing FR signal is sent to conventional generators (e.g., hydro and gas turbines), while fast changing assets, such as FESS and BESS, are sent a faster changing FR signal that accounts for higher ramp rates of these technologies [3]. However, despite all the characteristics that make these ESS technologies suitable for FR provisions, both FESSs and BESSs have a limited energy storage capacity that impact the provision of FR services. The presented research focuses on these two specific ESS technologies, given their fast FR characteristics, and therefore brief descriptions of these are presented next [4, 58].

2.2.1 Flywheel Energy Storage Systems

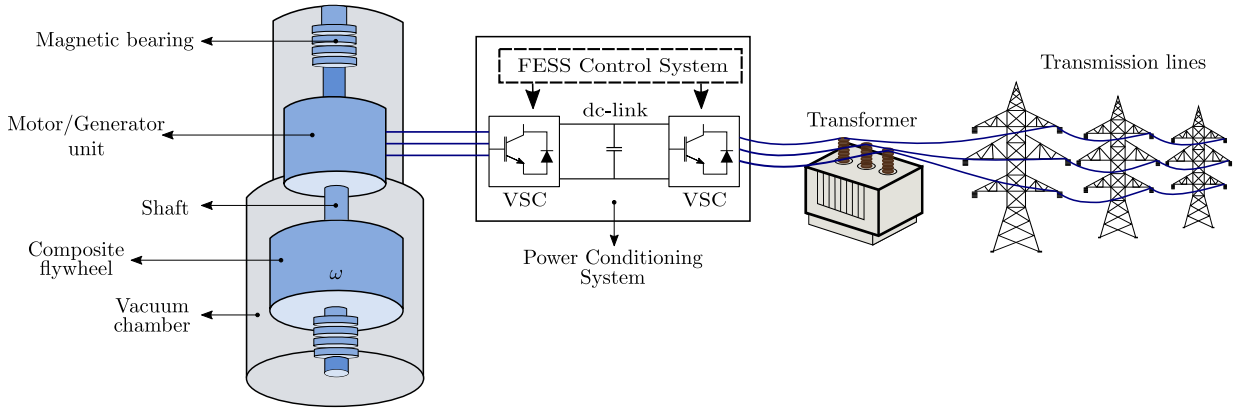

Figure 2.3: FESS configuration [59, 60].

This mechanical type of ESS technology, depicted in Figure 2.3, stores kinetic energy in the angular momentum of a spinning mass and responds in miliseconds to minutes, which make them a valuable option for power quality, UPS, and fast FR services. The FESS comprises a high mass rotor or flywheel, spinning at a high velocity to accrue rotational kinetic energy within the given constraints; a containment system of thick steel vessel surrounds and protects the rotor, motor-generator and other rotational components from external disturbances, and provides a high vacuum environment to minimize windage losses. A bearing assembly provides low loss support mechanism for the flywheel rotor, and a power conversion and control system operates the flywheel to store energy or generate electricity. The unit is interface to the grid using two bi-directional Voltage Source Converters (VSCs) connected by a dc-link. The VSC on the FESS side controls its active power and the voltage of the unit, and the VSC on the grid side controls the dc voltage and the FESS terminal voltage [60]. These ESSs operate in three modes: charging mode, driven by a motor while the converter operates as an inverter, and the speed of the spinning mass increases; stand-by mode when the speed is constant; and discharging mode where the converter operates as a rectifier and the motor operates as a generator. The energy stored depends on the size and speed of the rotor and the power rating depends on the motor-generator [4, 58].

FESSs have a very high cycle life (hundred of thousands of cycles), a long operational life (about 20 years), high round trip efficiency (up to 95%), high power density, insensitivity to deep discharges, fast response time (ms), discharge times of seconds to minutes, and are environmentally safe, reliable, and have modular characteristics [4, 61].

2.2.2 Battery Energy Storage Systems

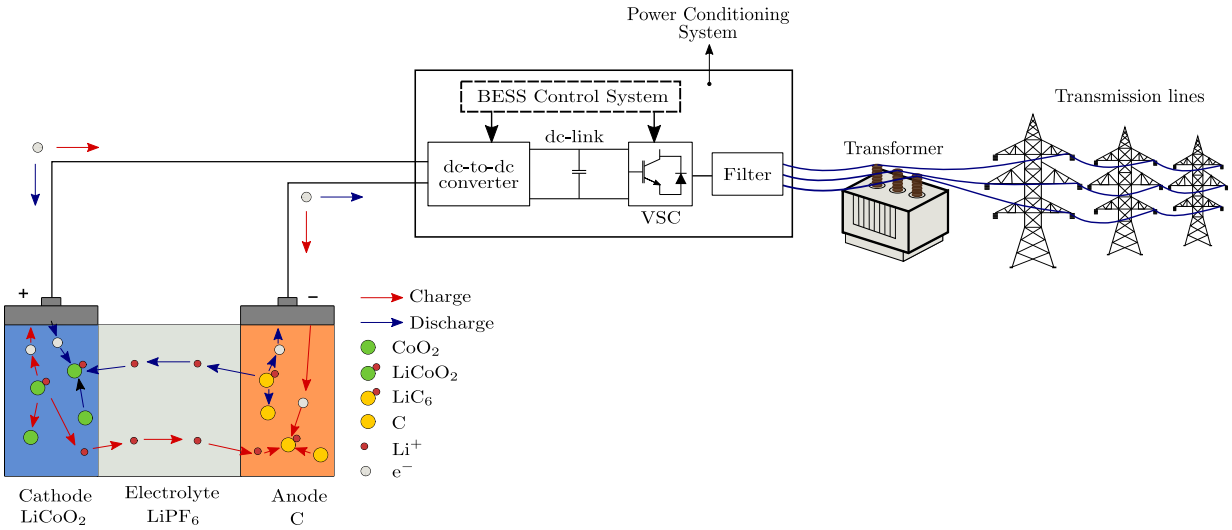

(a) Li-ion BESS

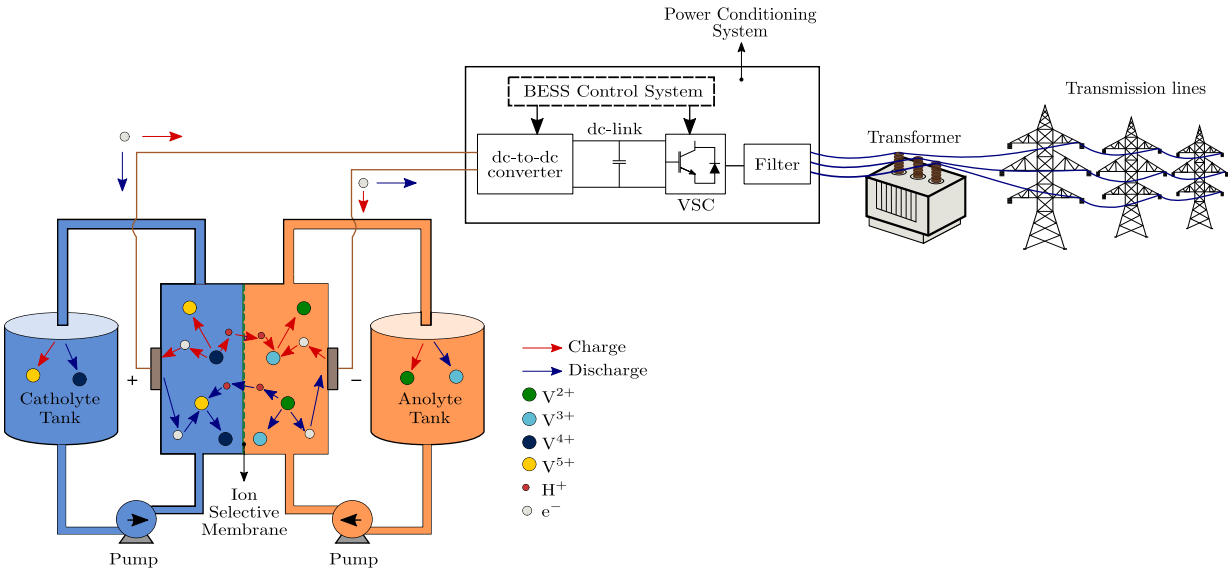

(b) Vanadium redox flow BESS

Figure 2.4: BESSs configurations [59, 62]

Batteries store electrical energy in the form of chemical energy, and are the next most commonly used storage technology after pumped storage hydro, in power systems. There are two types of batteries: flow and solid-state, which are both able to modify their output in less than one second, thus making them suitable for fast FR. In solid-state batteries, such as lead-acid, lithium-ion, nickel-cadmium or sodium-sulfur, the energy is stored in one or more cells. In the charging process, the chemical ions move from the positive to the negative electrode through the electrolyte, as shown in Figure 2.4a for a lithium-ion BESS. On the other hand, in the discharging process, the ions move in the opposite direction. The battery can be recharged by applying a voltage across the electrodes. In the case of flow batteries, such as vanadium redox, zinc bromine batter or and polysulfide bromide, the energy is stored in chemically reactive liquids separated from the actual battery cell and held in two tanks, as depicted in Figure 2.4b for a vanadium redox BESS. The reactive liquids are pumped from the tanks into the cell to cause a chemical reaction that delivers electrons to supply power; the inverse process happens when the batteries charge. In this case, electricity is injected into the cell, the chemical bond is broken and the reactive liquid is pumped into the respective tanks. The tanks are scalable, which make this type of batteries scalable [57].

BESSs are interfaced to the grid using dc-to-dc converters connected to a VSC through a dc-link, as shown in Figure 2.4. The dc-to-dc converters connect low-voltage battery arrays to the dc side of a VSC, which transforms the dc/ac power to ac/dc depending on the direction of power flow. A proper control of the converter switches allows the battery cells to be charged, absorbing power from the grid, or discharged, injecting power to the grid. Reactive control is possible by charging and discharging the capacitor in the dc link. A filter connected to the ac terminals of the VSC allows reducing the harmonics injected to the grid. The charging and discharging process can cause voltage variations in the dc-link, thus making the dc-to-dc converter necessary to add a third degree of freedom to the two degrees of freedom provided by the VSC, thus making possible to independently regulate the active and reactive power, and the dc-link voltage, and allowing four quadrant operation of the BESS [62].

Cost reduction trends, power/energy modularity, and industry competition have made BESS a feasible technology for ancillary services and other applications [61]. Depending on the chemistry of the battery, the round trip efficiency varies between 60% to 95%, discharge times vary from seconds to hours, response times are in the order of ms, and have lifetimes of up to 25 years [4, 61].

2.3 Frequency Control Practices and Market Entry of ESS in Ontario

The North American power system is divided into four major interconnections: Western, Texas, Eastern, and Quebec. Within the interconnections, the BAs provide frequency support and are in charge of balancing the generation and load by dispatching generators or controlling loads if possible; their net imbalances cause frequency deviations in the interconnection. The BAs provide operating services and are overseen by Reliability Coordinators.

The Ontario IESO serves as both the BA and Reliability Coordinator in Ontario, Canada. In order to maintain the system reliability, the IESO contracts four ancillary services: reactive power support and voltage control, reliability must-run, certified black start facilities, and FR. The FR service seeks to match the generation and load, including losses, to reduce the deviations in system frequency. Seven generation facilities (which are hydro and gas units) with AGC capability, two Alternate Technologies for Regulation (ATR) units, and two Phase I ESS facilities are contracted by the IESO to nominally provide ± 235.75 MW[3] of regulation capacity; however, typically ± 100 MW, with a ramp rate of 50 MW/min, is scheduled for regulation every hour[4] [49, 63, 64, 65].

Historically, the FR service has been provided by traditional facilities with AGC, which change their output in response to regulation signals. Since 2012, the IESO has allowed the participation of alternative technologies, such as aggregate loads, flywheels, and batteries as part of the ATR program, to evaluate their ability to provide FR as compared to the traditional ones [63]. The IESO procured 6 MW from two ESS facilities in 2012; the first is an FESS facility of 2 MW capacity, which is able to provide 0.5 MWh of energy, and the second is a Lithium-ion BESS of 4 MW/2.76 MWh capacity. These facilities provide FR services exclusively, receiving a regulation signal to reduce the system generation-load mismatch. ATR units were included in order to increase the FR capacity in Ontario system [63], and the main driving factors were [66]:

- Uncertainty in the forecast of variable generation (solar and wind) may lead to insufficient available resources to satisfy Ontario's demand, hence creating reliability concerns. Inaccuracies in the forecast affect the effectiveness of generator commitments in day-ahead market and export/import decisions in the hour-ahead dispatch. Hence, there is a need to increase the flexibility of supply resources, which can be achieved by adding fast response facilities to balance the power in the system.

[3] For the period January 1 to December 31, 2020, at a cost of $\$37,777,084$ [63].

[4] Currently, ESSs are not accounted for in the ± 100 MW regulation capacity.

- Demand fluctuations within a 5-minute dispatch interval can cause significant differences between the actual power generated and demanded because 5-minute dispatches assume a fixed demand during the interval.

- Autonomous behaviour of embedded distributed resources not subjected to IESO dispatch instructions, such as embedded generation and storage, may cause FR problems.

In 2014, there was a Grid Energy Storage Procurement of 50 MW for FR by the IESO, divided in two phases [7]. Phase I of the procurement targeted ESS capacity for ancillary services provision, and it was focused on increasing the reliability and grid efficiency, installing 28.8 MW of ESSs capacity for FR, and reactive support and voltage control services (Table 2.2). One of the requirements of Phase I was that the projects would be placed in different zones in Ontario to analyze their effectiveness in mitigating local constraints. These projects had the possibility to opt for the service to provide, i.e., FR, reactive support and voltage control, or both. Additionally, the IESO could dispatch them for their offered ancillary services and bulk energy services.

Table 2.2: Phase I Facilities of Ontario Grid Energy Storage Procurement [67].

Supplier	**Technology**	**Capacity**
Ellwood Energy Storage LP	Battery	4 MW
Sault Ste. Marie Energy Storage LP	Battery	7 MW
Powin Energy Ontario Storage II LP	Battery	2 MW
Powin Energy Ontario Storage II LP	Battery	2.4 MW
Powin Energy Ontario Storage II LP	Battery	2 MW
Powin Energy Ontario Storage II LP	Battery	2.4 MW
Hecate Energy Ontario Storage VII LP	Battery	2 MW
Guelph Energy Storage LP	Flywheel	5 MW
2562961 Ontario LTD	Hydrogen-gas	2 MW

In Phase II, 11.75 MW has been installed focusing on their capacity and arbitrage values. In energy arbitrage, the ESS would store energy when the prices are low, and reinject the energy into the grid when the prices are high. Table 2.3 presents the 6 facilities, providing a total of 11.75 MW through Phase II of the energy storage procurement.

In 2015, the IESO scheduled a minimum of ± 100 MW every hour for FR services, which was anticipated to increase because of the increasing penetration of intermittent generation. It only compensated for 53% of the demand forecast errors, which was expected to further

Table 2.3: Phase II Facilities of Ontario Grid Energy Storage Procurement [67].

Supplier	**Technology**	**Capacity**
Ameresco Newmarket Energy Storage Inc.	Battery	2 MW
Ameresco Newmarket Energy Storage Inc.	Battery	2 MW
Elmira Energy Storage, LP	Battery	2 MW
Parry Energy Storage, LP	Battery	2 MW
Baseload Power Corp.	Flow battery	2 MW
NRStor Goderich CAES L.P.	Compressed air	1.75 MW

decrease, resulting in increased dependency on the power from tie-lines [66]. To avoid this, the IESO had planned to increase its FR capability to ±150-200 MW by 2019, and up to 250-300 MW by 2020.[5] To reach this target, the 2017 Regulation Service Request for Proposals (RFP) for incremental regulation capacity seeked to increase the FR capacity while being open to different technologies [68].

The 2017 RFP sought to increase the FR capacity using different technologies, existent and new [68]. Two contracts, for a total of ±55 MW of FR capacity, were offered by the IESO through the RFP to two ESS facilities of 30 MW and 25 MW each. However, neither of the facilities attained commercial operation and no longer have a contract with the IESO [65].

In April 2018, the ESAG was created with the objective of supporting and assisting the IESO with evolving rules, processes, policies, and tools to facilitate the integration of ESS resources within the current structure of the IAM. The ESAG is in charge of identifying potential obstacles to fair competition for ESS from conventional resources, proposing mitigating strategies for those obstacles. It advises the IESO on ESS related issues, including those that potentially may affect ESS participation in the existing IAMs [69].

In December 2018, the IESO released a report which included recommendations for full participation of ESS facilities in wholesale electricity markets and associated services within Market Rules to facilitate competitive provision of services [9]. The SDP was initiated in October 2019 to ensure that communities and stakeholders understand how ESS will participate and operate in the IAM [70]. The SDP defines ESS participation for the current IAMs that maximizes the opportunity for them to compete within IESO's existing tool set [18].

In September 2020, the SDP Long-Term Design Vision laid the foundation for future ESS participation in post-Market Renewal [18]. In January 2021, an updated set of Market

[5] As of June 2021, the typical scheduled FR capacity of IESO is still ±100 MW.

Rules clarifying how ESS can participate directly within the existing IAMs came into effect. The requirements outlines every stage of market participation, operating guidelines, and apply to all ESS facilities in the IAM, including those embedded within a distribution system [70].

In the historical context of ESSs in Ontario, Sir Adam Beck Pumping Station (pumped hydro storage) of Ontario Power Generation (OPG) at Niagara has been delivering energy to the grid since 1958. It has 174 MW of pumped storage capacity and 300 MW of conventional hydro capacity. Besides, there are a number of storage facilities connected to the local distribution networks in the province, which are listed in Tables 2.2 and 2.3.

2.4 Summary

In this chapter, the relevant background topics related to this thesis were covered. An overview of frequency control in power system was first presented, including the most relevant characteristics of FR. Thereafter, an overview of ESSs devices from the frequency control perspective was presented, including details of FESS and BESS, which are the fast ESS technologies studied in this thesis. Finally, the frequency control practices and market entry of ESS in Ontario were discussed, covering some of the most recent changes introduced by the IESO.

Chapter 3

Frequency Regulation Model of Bulk Power Systems with Energy Storage

This chapter presents a model for FR studies of a large interconnected power system including ESSs such as BESSs and FESSs, considering all relevant stages in the frequency control process. The model takes into consideration the CDs in signal transmission in the FR control loop and ESSs, and their SoC management model, and represents the system, ESSs and SoC components in detail from a FR perspective. The model is validated using real system data from the OPS, ESSs data from two facilities in Ontario, and a practical transient stability model of the NAEI. The impact of CDs and SoC management of ESS facilities on the ACE and the computational efficiency of the proposed FR model, are also examined.

3.1 Frequency Regulation Model

To determine a baseline FR model of a real large interconnected power system as the one depicted in Figure 3.1, and estimate the model parameters for a physical system, for which operational information is available, power system analysis tools, such as the Dynamic Security Assessment Tools (DSATools™) used by the IESO [71], can be used, as these provide accurate results by properly modelling the system components. Large number of events, such as load changes and FR signal sent to Traditional Generators (TGs) and ESS facilities, with one second between events, limit the simulation time; for example, using DSATools™ to model and simulate load changes in the entire NAEI and the FR signal sent

to a group of generators in one area, limits the maximum simulation time to 102 seconds for the OPS under study, since the maximum number of switching events to represent load and generation changes allowed by this tool is reached. To make up for this limitation, multiple normal operating conditions were considered and simulated to develop the System model (Stage VII in Figure 3.1), so that the proposed FR model is appropriate for calculations such as the CPS1, which covers 12-month periods, or the Balancing Authority ACE Limit (BAAL), which requires calculations based on 30 consecutive clock minutes [72]. Therefore, the proposed FR model, developed from an ISO perspective, and depicted in Figure 3.1, can be used for accurate long-term studies, i.e., hours, days, weeks or even months, representing the main stages in the FR control process under normal operating conditions, CDs in the signal transfer, and SoC management of the ESS facilities, which ensures a realistic close-loop response.

The model presented here was developed with the help of the IESO, based on their recommendations and observations of the various signals provided, and through a trial and error approach, using real data. This was implemented in Simulink® [73], with the parameters within each block being determined using the Parameter Estimator application available in this software, since no parameter values were available. In this estimation process, the objective function is the sum of squared errors, the optimization solution is based on the gradient descent method and an interior-point algorithm, and real data is selected as the measured signal in each case. The real data corresponds to all the 28 signals presented in Figure 3.1.

The Supervisory Control and Data Acquisition System (SCADA) used by the IESO has a resolution of two seconds. However, the real data available does not necessarily have equal time spacing, because the SCADA Energy Management System uses a swinging door compression algorithm to compress the data before it is saved. This algorithm identifies linear segments within a signal trend and saves only the end points, to capture the behaviour of the complete signal, thus discarding the values in between to avoid storing excessive data [74]. Bearing this in mind, all the available data was re-sampled to one second resolution, assuming linear behaviour between each pair of neighboring points, after removing measurement errors based on recommendations provided by the IESO.

3.1.1 Bulk Power System

The model in Figure 3.1 is based on the IESO's approach to FR, but it is applicable to other North American ISOs, as discussed later in Section 3.1.3. It has seven stages that capture the most relevant aspects of the frequency control process of a large interconnected power

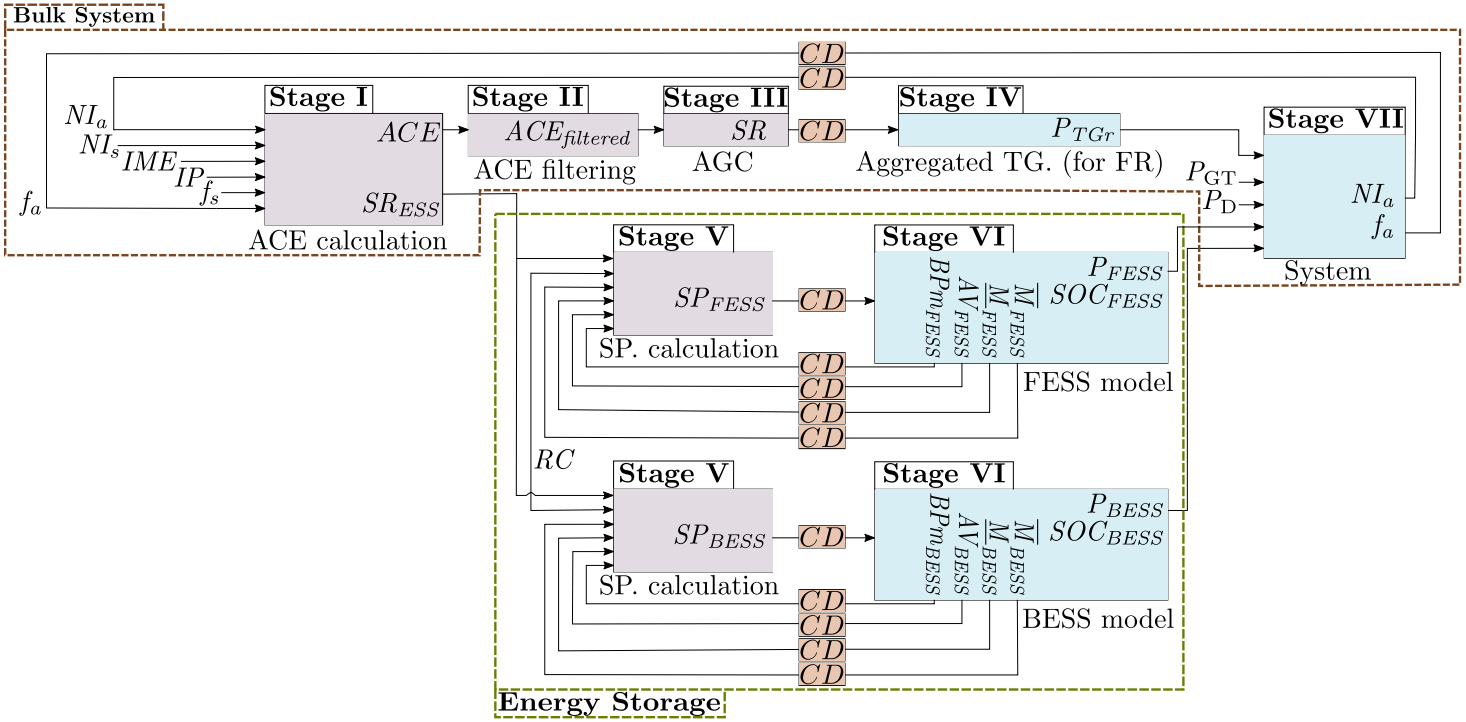

Figure 3.1: Frequency response model of a large interconnected power system with FESS and BESS. The stages in fuchsia correspond to calculations carried out at the control center, whereas the ones in light blue represent actual and relevant system components.

system. It includes CDs in the signals sent from/to the control center to/from the facilities contracted for regulation, which can significantly impact the FR process depending on the magnitude of the delay; for example, for the IESO, based on the available data, the average value of the one-way CD is about 4 s. However, this is not the case for all the facilities; the medium used to transmit the signals and the physical distance from the sending to the receiving point of the signal proportionally affect the delay. Based on the available data, an extra CD is included in the aggregated model of TG contracted for regulation. The aftereffect of CDs is an ACE signal that deviates from zero, and in the worst case scenario, the delayed FR signal could worsen the ACE. For example, it could happen that at time t, the system requires a positive regulation action from the FR assets; however, due to CD, the regulation coming from the facilities could be negative, as a result of calculations based on the state of the system at a time t - CD, thus increasing the ACE. Therefore, delays play an important role in the FR control process and hence should be modeled. It should be noted that the delays do not exists in the signals that are calculated, processed, and saved at the control center.

ACE Calculation

This is the first stage of the frequency control process. The inputs of this block are the actual power in the interconnection NI_a, and actual frequency f_a, which are the outputs of the system block; the scheduled power in the interconnection NI_s and scheduled frequency f_s change over time and are set by the ISO based on the system's needs; the inadvertent payback IP also changes over time and is set by the ISO; and the interchange metering error IME due to the difference between the revenue meter measurement and the measurements from the SCADA, which in this case is in manual mode set to -35 MW by the IESO. The block has two outputs: the ACE signal and the SR_{ESS} signal, calculated as follows:

$$ACE = (NI_a - NI_s) - 10B(f_a - f_s) - IME - IP - F(IP) \tag{3.1}$$

$$SR_{ESS} = (NI_a - NI_s) - 10B(f_a - f_s) - IME - F(IP) \tag{3.2}$$

where the BA bias B is equal to -248.2 MW/0.1Hz for the IESO, and the IP is the pay back of the inadvertent interchange accumulations, which is an input for the proposed model, and can be calculated by a method agreed upon by all regions in the interconnection [75]. One method is the energy "in-kind" payback, which can be bilateral or unilateral for the control areas involved, and considers that if inadvertent interchanges took place during peak hours, they should be paid back only during peak hours; similarly, inadvertent interchanges at non-peak hours should only be paid back during non-peak hours. Thus,

each control area should submit the monthly accumulated inadvertent interchange for peak and non-peak hours.

The $F(IP)$ function in (3.1) and (3.2) is introduced to represent the differences between the measured data and the model results, and is associated with the IP signal. This can be captured by a Neural Network (NN) with three signals as inputs: IP_t, IP_{t-10}, and $IP_t - IP_{t-10}$, and consists of 1 input layer with 3 neurons, 2 hidden layers with 48 and 1 neurons, respectively, and a 1-neuron output layer, with a tangent sigmoid as the activation function. The NN inputs are normalized between -1 and 1 before entering the training process, and the output is converted back to its real scale. One year data was used to obtain the NN model: 80% for training, 10% for testing, and 10% for validation. The resulting Mean Absolute Error (MAE) of this NN is 24.5 MW.

ACE Filtering

This corresponds to Stage II in the FR process and is presented in Figure 3.2. The input of this block is the ACE signal from Stage I, and includes a gain c_f and a first order Butterworth filter with a pre-warping frequency ω_0. The purpose of this filter is to get rid of fast signal changes, since TGs are not able to react to them.

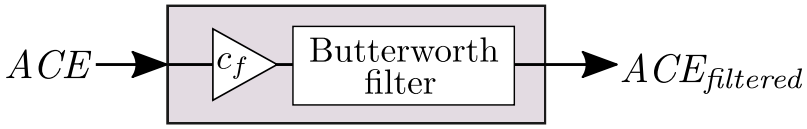

Figure 3.2: Stage II ACE filtering block.

AGC

It corresponds to Stage III in the FR control process, and is depicted on Figure 3.3. The input of this block is the filtered ACE signal from Stage II, and includes an initial negative gain, because the compensation provided by FR should be in the opposite direction to reduce the error. This signal goes into a discrete PI controller with parameters k_p and k_i, and clamping as anti-windup method. The output of the PI block goes through a rate limiter to ensure the generation changes are within limits defined by the ISO (e.g., $\pm$50 MW/min for the IESO), and feeds a saturation block to avoid exceeding the contracted regulation capacity $\pm RC$. The output of this block is the scheduled FR signal SR, sent to the TGs contracted for regulation.

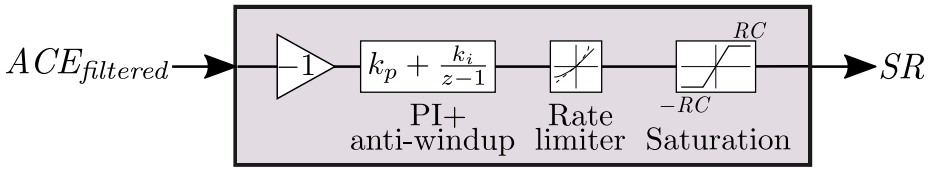

Figure 3.3: Stage III AGC.

Aggregated TG

It corresponds to Stage IV in the frequency control process, and is illustrated in Figure 3.4. Since the real signal available is the aggregated response of all the TGs to the *SR* signal, an aggregated model of these TGs is needed; the input of this block is the *SR* signal from Stage III plus the CD associated with the FR signal, as previously discussed. The delay in the signals is proportional to the physical distance from the control center to the facilities, which are typically located at different parts of the system. An extra CD CD_{TG} is included in this model (e.g., 30 s for the IESO) to represent the slower network used for signal transmission and measurements of the power response of the TGs to the FR signal. The third order transfer function $TG(z)$ represents the action of the TGs contracted for regulation, and can be readily estimated from actual measurements. The rate limiter, similar to that in Stage III, ensures the output of this model matches the real data by avoiding unrealistic power changes in the output of the TG group.

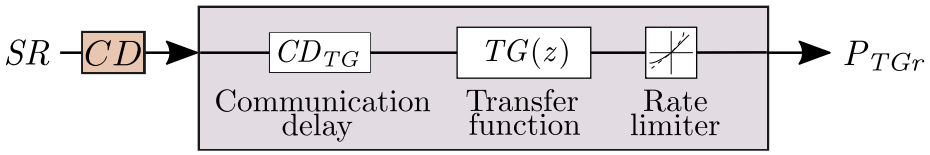

Figure 3.4: Stage IV Aggregated model of TG contracted for FR.

System Model

It represents the primary frequency response of the elements in the system and the power in the tie-lines, and corresponds to Stage VII in the FR control process. It has five inputs: the load of the system P_D; the generation total dispatch P_{GT}; and the outputs of the facilities contracted for regulation P_{TGr}, P_{FESS}, and P_{BESS}. This block calculates the

actual frequency f_a and power in the interconnection NI_a at time t, as follows:

$$f_{at} = f_{a0} + [-\Delta P_{Dt} + \Delta P_{GTt} + \Delta P_{TGrt} + \Delta P_{FESSt} + \Delta P_{BESSt}] \left[\frac{-1}{\beta_{EI}} \frac{1}{z-1} - F(z) \right] \quad (3.3)$$

$$NI_{at} = NI_{a0} + [-\Delta P_{Dt} + \Delta P_{GTt} + \Delta P_{TGrt} + \Delta P_{FESSt} + \Delta P_{BESSt}] \left[\frac{\beta_{EI} - \beta_{IESO}}{\beta_{EI}} \frac{1}{z-1} \right] \quad (3.4)$$

which include an OPS frequency response of 248.2 MW/0.1Hz, and an NAEI frequency response β_{EI} calculated from [76], using available data and a detailed transient stability model. In (3.3), the function $F(z)$ allows obtaining a closer fit between the model results and the measured data.

3.1.2 Energy Storage

Set-point Calculation

This is Stage V in the FR control process, and includes the calculation of the Set-Point (SP) signals SP_{FESS} and SP_{BESS} sent from the control center to the FESS and BESS facilities, respectively. The calculation of both SP signals is as follows, with the inputs changing for each facility:

$$SP_{ESS} = \begin{cases} \frac{1}{2}(\overline{M}_{ESS} - \underline{M}_{ESS}) \frac{min(SR_{ESS}, RC)}{RC} + BPm_{ESS} \\ \qquad \forall\ AV_{ESS} = 1, RC \neq 0\ ,\ SR_{ESS} \geq = 0 \\ \frac{1}{2}(\overline{M}_{ESS} - \underline{M}_{ESS}) \frac{max(SR_{ESS}, -RC)}{RC} + BPm_{ESS} \\ \qquad \forall\ AV_{ESS} = 1, RC \neq 0\ ,\ SR_{ESS} < 0 \end{cases} \quad (3.5)$$

where AV_{ESS} is the status availability of the facility, $\underline{M}_{ESS}$ and $\overline{M}_{ESS}$ are the minimum and maximum available capacity of the facility, respectively, and BPm_{ESS} is the moving base-point, which is modelled as the fixed base point of the facility BP_{ESS} moving between $\underline{M}_{ESS}$ and $\overline{M}_{ESS}$, and containing SoC information. Since these signals come from the ESS facilities, CDs are considered before they arrive at the control center, as shown in Figure 3.1. In addition, the FR capacity limit RC and the SR_{ESS} signal are required in

this calculation. The SP_{ESS} signal is in essence a scaled version of the SR_{ESS} signal that takes into account the SoC of the ESS facility reflected through the $\overline{M}_{ESS}$, $\underline{M}_{ESS}$, and BPm_{ESS} signals.

ESS Model

This is Stage VI in the frequency control process and includes the ESS models of the BESS and FESS facilities, as well as their SoC management model. Considering that similar operational data was available for the BESS and FESS facilities, similar ESS models were developed for both facilities, with different parameters and some specific features for each facility.

Figure 3.5 illustrates the base ESS model, representing both FESS and BESS, since similar input and output signals are used for both facilities at the control center. However, differences in these facilities are captured in the model by their different parameters in the Rate limiter, different transfer functions $C(z)$ and $D(z)$, differences in the CF block, and different values of $\overline{U}_{on}$, $\underline{U}_{off}$, $\underline{L}_{on}$,$\overline{L}_{off}$ for each ESS facility, which define the bands in SoC management. This model has two main parts: The first part, which is the output of the ESS facility in megawatts, depends on the sign of the regulation required from the facility ($SP_{ESS} - BP_{ESS}$), and the SoC parameters c and d. As shown in Figure 3.5, the output signal could be equal to BP_{ESS} or to the delayed SP signal coming from Stage V, and primarily considers the charging or discharging efficiencies of the ESS. The output signal goes through a ramp rate block with rising slew rate Rsr, and falling slew rate Fsr. The charging and discharging efficiencies of the ESS facilities are internally accounted for in their response to the set-point signal.

The second part of the model is the SoC management of the facility, and it is divided in two sections. In the first section, BPm_{ESS}, $\overline{M}_{ESS}$, and $\underline{M}_{ESS}$, and the four SoC parameters a, b, c, and d are calculated. Furthermore, three sections of the SoC are considered: a lower band from $\underline{L}_{on}$ to $\overline{L}_{off}$, a middle band from $\overline{L}_{off}$ to $\underline{U}_{off}$, and an upper band from $\underline{U}_{off}$ to $\overline{U}_{on}$. As illustrated in Figure 3.6a and Figure 3.6b and in the second block of Figure 3.5, the parameters a, b, c, and d are defined to identify the SoC operational band in which SOC_{ESS} is in, which defines the values of P_{ESS}, BPm_{ESS}, $\overline{M}_{ESS}$, and $\underline{M}_{ESS}$. As illustrated in Figure 3.5, the parameters c and d are part of the P_{ESS} calculation while a and b are part of the BPm_{ESS}, $\overline{M}_{ESS}$, and $\underline{M}_{ESS}$ calculations. After the SoC parameters are calculated and considering the power capacity and base-point of the facility designated for regulation, i.e., the Pc_{ESS} and BP_{ESS} signals, respectively, three states are formulated. State 1 considers the SoC in the middle band of Figure 3.6a and Figure 3.6b, where $a = 0$

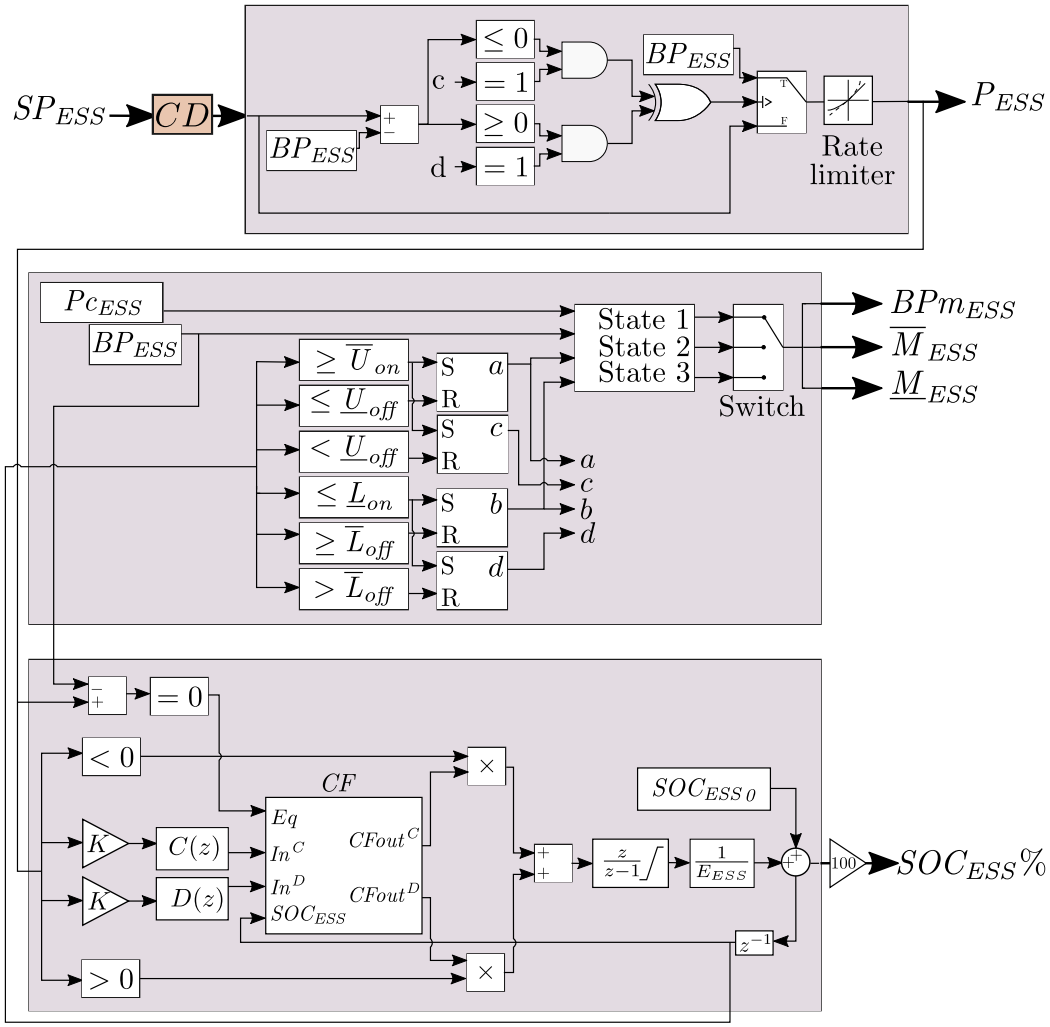

Figure 3.5: Stage VI base ESS model including SoC management.

and $b = 0$; the second state considers $a = 1$, and the third state considers $b = 1$. Observe that the difference between a and c is not very relevant for the proposed FESS model, since SOC_{FESS} would rarely be at $\underline{U}_{off}$ for more than one time step. However, for the BESS model, the difference between a and c can be significant, since its upper band is defined as $\bar{U}_{on} = \underline{U}_{off}$, with the facility remaining at this point, where $a = 0$ and $c = 1$, with an output BP_{BESS} until it is able to follow SP_{BESS} again. Likewise, b and d are similar for the proposed FESS model when the SOC_{FESS} reaches $\overline{L}_{off}$, whereas for the BESS model, the differences can be significant. Therefore, the signals BPm_{ESS}, $\overline{M}_{ESS}$, and

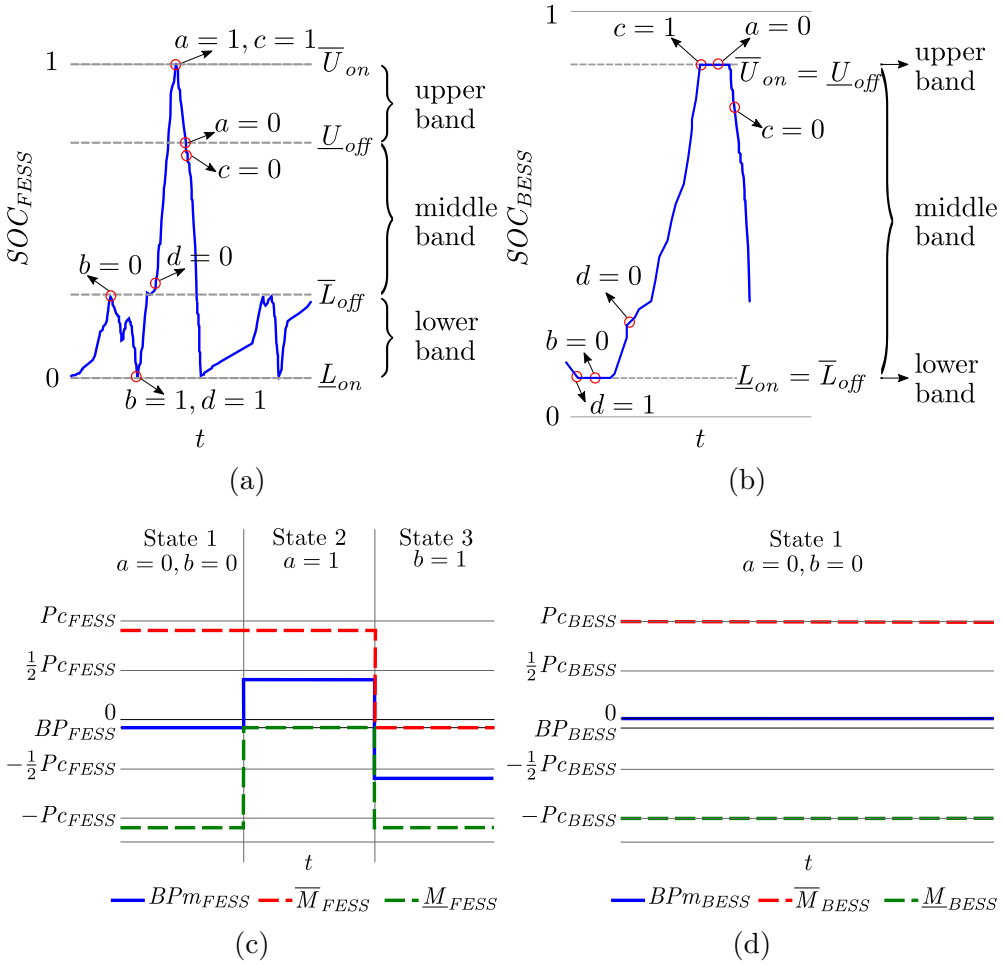

Figure 3.6: Relation of parameters a, b, c, and d in (a) and (b), and $\overline{M}_{ESS}$, $\underline{M}_{ESS}$, and BP_{ESS} in (c) and (d) to the SoC management of the ESS model.

$\underline{M}_{ESS}$, illustrated in Figure 3.6c and Figure 3.6d, can be defined as follows:

$$BPm_{ESS} = \begin{cases} BP_{ESS} & \forall \quad a=0, b=0 \\ BP_{ESS} + \frac{1}{2}Pc_{ESS} & \forall \quad a=1 \\ BP_{ESS} - \frac{1}{2}Pc_{ESS} & \forall \quad b=1 \end{cases} \tag{3.6}$$

$$\overline{M}_{ESS} = \begin{cases} BP_{ESS} + Pc_{ESS} & \forall \quad a=0, b=0 \\ BP_{ESS} + Pc_{ESS} & \forall \quad a=1 \\ BP_{ESS} & \forall \quad b=1 \end{cases} \tag{3.7}$$

$$\underline{M}_{ESS} = \begin{cases} BP_{ESS} - Pc_{ESS} & \forall \quad a = 0, b = 0 \\ BP_{ESS} & \forall \quad a = 1 \\ BP_{ESS} - Pc_{ESS} & \forall \quad b = 1 \end{cases} \tag{3.8}$$

In general, for the proposed base ESS model shown in Figure 3.5, if the output of the ESS causes the SoC to reach $\underline{L}_{on}$ $(b = 1)$ or $\overline{U}_{on}$ $(a = 1)$, the facility starts charging or discharging, respectively, irrespective of the system's needs, which are represented in the SR_{ESS} signal. This behavior continues until the SoC reaches values greater than or equal to $\overline{L}_{off}$ $(b = 0)$ or lower than or equal to $\underline{U}_{off}$ $(a = 0)$, during the charging/discharging operations, correspondingly. The rationale of dividing the range on which the SoC signal changes in three bands is to bring the SoC from a value where it can only act in one direction to a value that allows room for moving in both directions.

For the FESS, when the SoC reaches $\overline{U}_{on}$ or $\underline{L}_{on}$, the values of $\overline{M}_{FESS}$, $\underline{M}_{FESS}$, and BPm_{FESS} change as per (3.6)-(3.8), and if the SR_{ESS} signal indicates that the FESS should keep respectively charging or discharging, two things can take place until reaching $\underline{U}_{off}$ or $\overline{L}_{off}$, depending on the value of the SR_{ESS} signal. Thus, if $SOC_{FESS} = \overline{U}_{on}$ and $SR_{ESS} > -RC$, then the SP_{FESS} signal orders discharging as if the SR_{ESS} were shifted above the zero axis; otherwise, $SP_{FESS} = BPm_{FESS}$. On the other hand, if $SOC_{FESS} = \underline{L}_{on}$ and $SR_{ESS} < RC$, then the SP_{FESS} signal orders charging as if the SR_{ESS} were shifted below the zero axis; otherwise, $SP_{FESS} = BPm_{FESS}$. Since the FESS ignores the needs of the system in the aforementioned cases, this could negatively impact the ACE by increasing its value. An idling SoC, which would keep the facility from acting against the system's needs, could be implemented with a different SP calculation, as presented in Chapter 4.

For the BESS, the upper band defined as $\overline{U}_{on} = \underline{U}_{off}$ and a lower band defined as $\underline{L}_{on} = \overline{L}_{off}$ limit the 3 possible ESS states in Figure 3.5 to only State 1. Thus, after the SOC_{BESS} signal reaches $\overline{U}_{on}$ or $\underline{L}_{on}$ values, $\overline{M}_{BESS}$, $\underline{M}_{BESS}$, and BPm_{BESS} change as per (3.6)-(3.8), forcing the SP_{BESS} signal sent to the BESS to take into account the needs of system represented in the SR_{ESS} signal when possible. For the cases where the SoC is at $\overline{U}_{on}$ or $\underline{L}_{on}$ and the SR_{ESS} requires the BESS to keep charging or discharging respectively, P_{BESS} goes to zero, since following the SP_{BESS} is not possible.

The second section of the SoC management model is the SoC calculation itself, with the ESS output power P_{ESS}, and the base-point signal BP_{ESS} as inputs, as illustrated in the last block of Figure 3.5. The constant K is the power-to-energy value subject to the sampling-time resolution, which in this case is $K = -1/3600$ hr/s. Thus, $P_{ESS}K$ is the preliminary charge/discharge energy per sampling-time, which is equivalent to a simplified

Coulomb counting SoC method [77]. Additionally, the model assumes two second order transfer functions $C(z)$ and $D(z)$ to account for the different charging and discharging characteristics of the ESS facilities, respectively, such as variations in their charging and discharging efficiencies, as confirmed by the SoC response to the SP_{ESS} signals sent from the control center. The outputs of these blocks In^C and In^D, correspondingly, are inputs of the correction factor CF block in Figure 3.5, which compensates for different charge/discharge energy rates observed in the data provided after $\overline{U}_{on}$ and $\underline{L}_{on}$ are reached, as the charging/discharging slows or speeds up after reaching these limits. The CF block has a charging ($CFout^C$) and discharging ($CFout^D$) output, which for the FESS can be defined as follows:

$$CFout^C = \begin{cases} In^C & \forall\ k_{up} = 0,\ k_{dw} = 0 \\ In^C CF_{eq} & \forall\ Eq = 1,\ (k_{up} = 1 \vee k_{dw} = 1) \\ In^C CF_1^C & \forall\ Eq = 0,\ k_{up} = 1 \\ In^C CF_2^C & \forall\ Eq = 0,\ k_{up} = 0,\ k_{dw} = 1 \end{cases} \tag{3.9}$$

$$CFout^D = \begin{cases} In^D & \forall\ k_{up} = 0,\ k_{dw} = 0 \\ In^D CF_1^D & \forall\ k_{dw} = 1 \\ In^D CF_2^D & \forall\ k_{up} = 1,\ k_{dw} = 0 \end{cases} \tag{3.10}$$

where CF_{eq}, CF_1^C, and CF_2^C are estimated parameters that multiply In^C, according to the conditions shown in (3.9). The input Eq takes the value of 1 when the P_{FESS} is equal to BPm_{FESS}. Furthermore, CF_1^D and CF_2^D are estimated parameters, which multiply In^D, according to the conditions in (3.10). The variables k_{up} and k_{dw} are the outputs of set-reset flip-flops defined as follows:

$$k_{up_t} = S_{up_t} + k_{up_{t-1}}(\neg R_{up_t}) \tag{3.11}$$

$$k_{dwt} = S_{dwt} + k_{dwt-1}(\neg R_{dwt}) \tag{3.12}$$

where

$$S_{up_t} = 1\ \forall\ SOC_{ESS} \geq ks_{up} \tag{3.13}$$

$$R_{up_t} = 1\ \forall\ SOC_{ESS} \leq kr_{up} \tag{3.14}$$

$$S_{dwt} = 1\ \forall\ SOC_{ESS} \leq ks_{dw} \tag{3.15}$$

$$R_{dwt} = 1\ \forall\ SOC_{ESS} \geq kr_{dw} \tag{3.16}$$

and ks_{up} and kr_{up} are estimated parameters that represent the values of the SoC that cause the set S_{up_t} and reset R_{up_t} signals of the flip-flop k_{up_t} to become 1. Likewise, ks_{dw}

and kr_{dw} are estimated parameters associated with the SoC values that activates the set (S_{dwt}) and reset (R_{dwt}) signals of the flip-flop k_{dwt}, correspondingly.

For the case of BESS, the *CF* block can be defined as follows:

$$CFout^C = \begin{cases} In^C & \forall\ k_{up} = 0,\ k_{dw} = 0 \\ In^C \left[\frac{1}{1+SOC_{BESS}}\right] CF_1^C & \forall\ k_{up} = 1 \\ In^C \left[1 + SOC_{BESS}\right] CF_2^C & \forall\ k_{up} = 0,\ k_{dw} = 1 \end{cases} \tag{3.17}$$

$$CFout^D = \begin{cases} In^D & \forall\ k_{up} = 0,\ k_{dw} = 0 \\ In^D \left[1 + SOC_{BESS}\right] CF_1^D & \forall\ k_{dw} = 1 \\ In^D \left[\frac{1}{1+SOC_{BESS}}\right] CF_2^D & \forall\ k_{up} = 1,\ k_{dw} = 0 \end{cases} \tag{3.18}$$

where CF_1^C, CF_2^C, and CF_1^D, CF_2^D are estimated parameters that multiply a function of the SoC, and the inputs In^C and In^D, respectively. The variables k_{up} and k_{dw} in (3.17) and (3.18) are the same as in (3.11) and (3.12).

The transfer functions $C(z)$ and $D(z)$ both have a parallel comparison block (binary variables) to operate in either mode, which are related to the value of P_{ESS}; these binary variables are multiplied by $CFout^C$ and $CFout^D$, as shown in Figure 3.5. Finally, the estimated corrected energy for the sampling interval is integrated and divided by the ESS energy capacity E_{ESS} and added to the initial SoC value to obtain the estimated SoC output at time t. This value is later multiplied by 100% to obtain $SOC_{ESS}\%$ at time t. The SoC empirical model proposed in here is derived by analyzing operational data for an actual FESS and a BESS used for FR by the IESO. Note that the SoC model does not consider degradation or cell failure which will impact the output; further data would be required to model such effects.

Currently, the base-point signal BP_{ESS} for the IESO is zero or a value close to zero, set in each ESS facility. However, the control center may replace the BP_{ESS} with the dispatch from the energy market for facilities that are able to simultaneously participate in both markets. In such a situation, the regulation required from the ESS facilities would be in addition to the base-point signal ($SP_{ESS} - BP_{ESS}$), as currently is the case for TGs.

3.1.3 Model Genericity

Some stages of the proposed model shown in Figure 3.1 are specific to the FR control process of the IESO, which is similar in general to FR approaches used by other North

American utilities to meet NERC requirements, while others can be partially modified for their use in other bulk power systems, and a few can be directly used in any system after estimating the appropriate parameters. Thus, for the ACE calculation block in Stage I, equation (3.1) could be readily used, while the NN that defines $F(IP)$ should be re-trained or eliminated in case there is no mismatch between the measured data and the model results. In addition, equation (3.2) could also be maintained or replaced by new calculations, depending on the FR signal the ISO wishes to send to the ESS facilities. The ACE filtering block (Stage II), and SP calculation block (Stage V) are specific to the IESO, and thus should be modified to fit other system's approaches. On the other hand, the AGC (Stage III), Aggregated model of TG contracted for FR (Stage IV), and System (Stage VII) blocks can be readily applied to other systems after estimating new parameters. Finally, the proposed FESS and BESS models (Stage VI) are generic, since these ESS facilities, whose real data was used to validate them from the FR perspective, are typical. Thus the proposed models can be readily adapted to represent similar ESSs in other systems.

3.2 Validation of Proposed Frequency Regulation Model on Ontario Power System

All the stages in the proposed FR model shown in Figure 3.1 were validated using information provided by the IESO, which included a DSATools™ model of the NAEI, OPS data, and data from a 2 MW/0.5 MWh FESS, and a 4 MW/2.76 MWh BESS used for FR by the IESO. All the parameter values of the proposed model presented in Table 3.1 were determined using the Parameter Estimator tool in Simulink® for the large interconnected OPS with ESS. In 2020, this system had a peak demand of 24.4 GW [78], and a typical FR scheduled capacity of ±100 MW [63].

Parameter estimation was carried out sequentially for each stage of Figure 3.1, except for Stage VI, for which three steps were used. The first step considers the first block in Figure 3.5 with SP_{ESS} and P_{ESS} as input and output, respectively. The second step considers the first section of the SoC management model with Pc_{ESS}, BP_{ESS}, and $SOC_{ESS}/100$ as inputs, and BPm_{ESS}, $\overline{M}_{ESS}$, and $\underline{M}_{ESS}$ as the outputs to be fitted. The third step considers the second section of the SoC management model with the signals P_{ESS} and BP_{ESS} as inputs and $SOC_{ESS}\%$ as the output to be fitted. For Stages I to V, and Stage VII, and the three blocks considered in Stage VI, the Parameter Estimation tool used is fed with the real input signals to fit the output of each stage or block to the real output signals. All the parameters to be estimated are considered as variables in this process, and each is assigned a smallest and largest allowable value which depends on the variable and its position in

Table 3.1: Model Parameters.

Stage II: ACE filtering			
Parameter	Value	Parameter	Value
c_f	0.974	ω_0 [rad/s]	0.097
Stage III: AGC			
Parameter	Value	Parameter	Value
k_i	0.022	k_p	0.42
Stage IV: Aggregated model of TG contracted for FR			
Parameter	Value		
$TG(z)$	$\frac{3.45z^2+1.58}{3.78z^3+1.47z^2}$		
Stage VI: ESS models			
FESS Model		BESS Model	
Parameter	Value	Parameter	Value
Rsr[MW]	0.6	Rsr[MW]	1.28
Fsr[MW]	-0.6	Fsr[MW]	-1.28
$\overline{U}_{on}$	1	$\overline{U}_{on}$	0.885
$\underline{U}_{off}$	0.75	$\underline{U}_{off}$	0.885
$\overline{L}_{off}$	0.25	$\overline{L}_{off}$	0.125
$\underline{L}_{on}$	0	$\underline{L}_{on}$	0.125
K	$-1/3600$	K	$-1/3600$
$C(z)$	$\frac{4.23z^2+1.06z+2.8}{z^2+0.57z+0.42}$	$C(z)$	$\frac{0.16z^2+4.11z+7.52}{z^2+0.93z+0.54}$
$D(z)$	$\frac{5.57z^2+6.72z+3.02}{z^2+0.72z+0.81}$	$D(z)$	$\frac{2.88z^2+3.78z+4.57}{z^2+0.48z+0.55}$
CF_1^C	1.22	CF_1^C	0.014
CF_2^C	0.99	CF_2^C	0.50
CF_1^D	1.19	CF_1^D	0.51
CF_2^D	1.10	CF_2^D	0.64
CF_{eq}	0.35	CF_{eq}	$-$
ks_{up}	1	ks_{up}	0.885
kr_{up}	0.55	kr_{up}	0.884
ks_{dw}	0	ks_{dw}	0.125
kr_{dw}	0.60	kr_{dw}	0.144
Stage VII: System model			
Parameter	Value		
$F(z)$	$\frac{0.51z^5-1.97z^4+2.31z^3+2.93z^2-1.18z-2.73}{z^5-0.45z^4-0.77z^3-0.23z^2+0.6z-0.12}e^{-5}$		

the model. Since a trial-and-error approach was used to determine the proposed model, several orders for all the transfer functions involved were tested, with those presented in

Table 3.1 providing the least error in the fitting process.

3.2.1 Test Grid Validation

The first step in the validation process of the proposed FR model is the validation of frequency response of the DSATools™ model against real data. The DSATools™ model is a reduced representation of the NAEI (all pink lines in Figure 3.7), with a detailed representation of the OPS (shaded area), and a combination of detailed and equivalent aggregated models, depending on their impact and electrical distances of the rest. For the OPS, the f_a signal is measured at one of the Oakville buses, and thus a similar bus was selected in the DSATools™ system in the validation process. The DSATools™ model includes 7,840 ac buses, 2,071 generators, 3,082 loads, 12,272 lines, 2,858 adjustable transformers, 1,378 fixed shunts, 672 switchable shuts, 741 three winding transformers, 16 dc buses, 12 line commuted converters, and 10 dc lines. Adequate generator, compensator, stabilizer, excitation system, and turbine-governor dynamic models are included, and appropriate dynamic models of solar and wind generation are also represented. The areas considered in the DSATools™ model are ISO-NE, NYISO, IESO, Hydro Québec, New Brunswick System Operator, PJM, Manitoba Hydro, MISO, and five aggregated areas representing the rest of the NAEI.

The DSATools™ model for the NAEI has been provided to the University of Waterloo (UW) within the scope of two Non-Disclosure Agreements (NDAs) between UW and IESO. The model is generic and used for several studies; for FR studies, the IESO deactivates the governors of some generators or modifies their actions to replicate the real operational behaviour of facilities in the grid. However, DSATools™ model provided to UW did not include these modifications, since they are confidential information of the participants.

The frequency response for NAEI in 2017, according to [51], had a mean of 2,257 MW/0.1 Hz, with a minimum value of 1,043 MW/0.1 Hz, a maximum of 4,536 MW/0.1 Hz, and a standard deviation of 823 MW/0.1 Hz. Nuclear and large coal-fired generators do not contribute to reduce the frequency excursions, and some other generators have their governor control loop bypassed; hence, their mechanical set-point is fixed. As reported in [80], the governor dead-band settings in the NAEI, for the first to the third quartile, vary from 0 to 100 mHz, depending on the generator capacity. Accordingly, NERC advises [81] that generators with nameplate rating greater than 75 MVA should ensure that their governor dead-band does not exceed ±36 mHz, with the exception of nuclear generators. However, the actual settings of governors is confidential information, and not available. In addition, in the DSATools™ model, not all the governor models include a dead-band, and

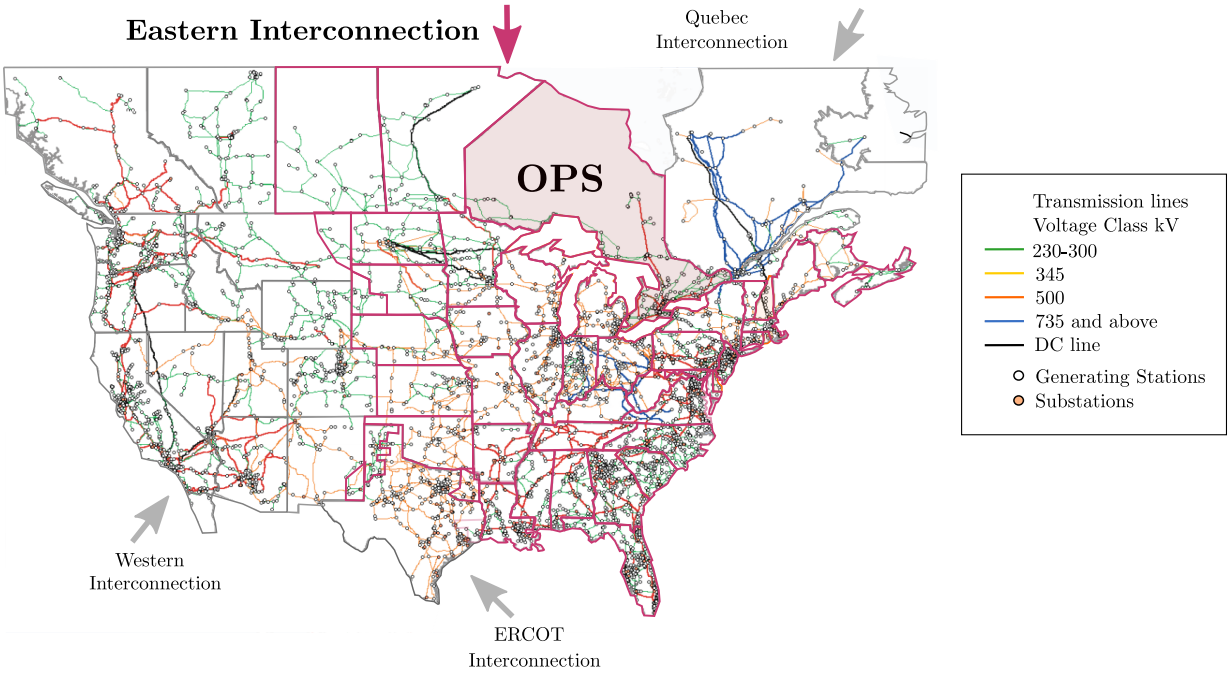

Figure 3.7: DSATools™ model [16, 79].

most of those that do, have their dead-band set at zero. Hence, directly using the provided model would likely yield a greater level of governor response than in a real system. Thus, the generator dynamic data was modified in this thesis based on recommendations from the IESO to approach the real frequency response of the model, disabling the governor models of all the nuclear stations and some gas turbines and generators in the external area of the OPS model.

For validation purposes, seven cases capturing the frequency response of the OPS were selected based on regulation signal changes, as follows:

1. Unchanged FR signal, equal to lower regulation capacity limit.
2. Unchanged FR signal, equal to upper regulation capacity limit.
3. Highest number of changes in the FR signal.
4. High magnitude changes when the FR signal is positive.
5. High magnitude changes when the FR signal is negative.
6. Large number of high magnitude changes when FR signal is positive.

7. Large number of high magnitude changes when FR signal is negative.

These cases correspond to various normal and typical operating conditions with different generators and loads involved, which is the main purpose and application of the proposed model, and thus it does not include major transmission system contingencies, i.e., abnormal operating conditions. The load changes for the NAEI were determined based on the measured frequency profile and load changes in the OPS; a frequency response value of -2760 MW/0.1 Hz for the NAEI; and the initial powers of the load, generation, and the interconnection for each scenario. The difference between the total expected load change for the NAEI and the total change in the loads in the OPS was proportionally distributed to all the loads in the rest of the interconnection. Furthermore, three hydroelectric generators in the OPS, with enough capacity to follow the regulation signal, were selected for the provision of FR; the regulation signal was equally divided and sent to these generators. Because of the large number of changes per second (3,082 load changes plus 3 changes in the set-points of TGs providing FR), the maximum possible simulation time allowed by the DSATools™ software is 102 seconds for the system under study. Since the simulation period is less than two minutes and the dispatch changes every 5 minutes, it was assumed that the generator active powers were fixed for each scenario.

The Root-Mean Squared Error (RMSE) and MAE of ACE for the seven cases on March 20, 2018 are presented in Table 3.2 and Figure 3.8, which can be considered acceptable. At the time this validation was carried out, only two days of data were available, March 20, 2018 and June 12, 2018, and thus seven cases for each day, using the criteria previously mentioned were selected; the RMSE and MAE of ACE for the cases on June 12 were similar to those for March 20, 2018. Even though more days of data could be used for validation, not much difference in the results is expected from a FR perspective, since the cases considered already covered several normal operating conditions. Therefore, this validated DSATools™ model was used next to validate the system block of the proposed FR model.

Table 3.2: Validation of the frequency response of the DSATools™ model.

	RMSE [Hz]	MAE [Hz]		RMSE [Hz]	MAE [Hz]
Case 1	0.00101	0.00082	**Case 5**	0.00279	0.00225
Case 2	0.00103	0.00084	**Case 6**	0.00183	0.00139
Case 3	0.00186	0.00129	**Case 7**	0.00470	0.00359
Case 4	0.00592	0.00512			

The difference between the measured data and DSATools™ model results could be due

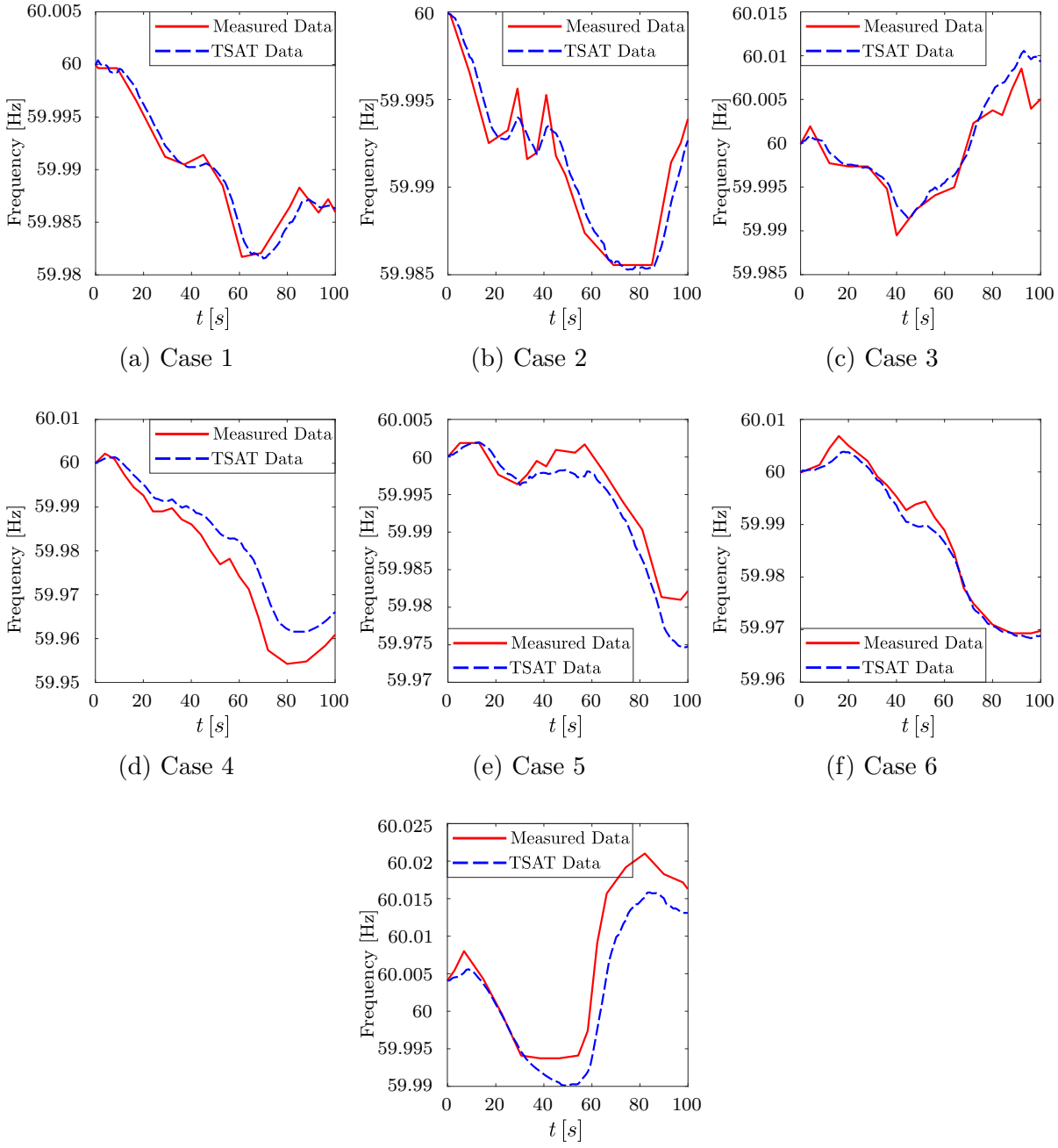

(a) Case 1 (b) Case 2 (c) Case 3

(d) Case 4 (e) Case 5 (f) Case 6

(g) Case 7

Figure 3.8: Frequency response validation of the DSATools™ model.

to the following reasons:

- The value of frequency response used to determine the power changes in the interconnection was assumed to be fixed for all the scenarios. However, with changes in loads, dispatched generators, and connected renewable generators, this value may change depending on the scenario.
- Since the load models are voltage dependent, and their parameters remain fixed during the simulation, while in the actual system these vary, the modelled load powers may not be the same as in the actual system.
- The dynamic file was modified to obtain a more realistic response from the system. However, these modifications may not be an exact representation of the day selected for simulations.

These yield, in Figure 3.8 for Cases 4, 5, and 7, a consistent unidirectional error between the measured data and the DSATools™ model results, which keeps accumulating over time.

3.2.2 Frequency Regulation Model Validation

All the stages in the proposed FR model are validated here. The data made available by the IESO corresponds to all the signals associated with the proposed FR model (Figure 3.1), which has two sections: the bulk system, which includes Stages I to IV, and Stage VII, and the ESS section, which includes Stage V and VI. For the validation of Stage I to Stage IV, one year of data (April-2018 to March-2019) was used. Figure 3.9 shows histograms comparing the measured data and the model results for the ACE, $ACE_{filtered}$, SR_{ESS}, SR, and P_{TGr} signals in MW.

After the validation of the frequency response of the DSATools™ model in Section 3.2.1, the Stage VII Simulink® model is validated against the DSATools™ model. Since the measured data of load changes in the neighboring interconnected areas is not available with the same resolution, and considering each BA is mainly responsible for compensating the load changes within its own area, load variations occurring only in the BA of interest are considered here. The same cases used for the validation of the DSATools™ model were used here, with the difference of no load changes considered in the other BAs within the NAEI. The RMSE and MAE of ACE for the seven cases are presented in Table 3.3. The validation results for f_a and NI_a are presented in Figure 3.10 and Figure 3.11, correspondingly, for all seven cases and are associated with the minimum and maximum NI_s values of 523 and

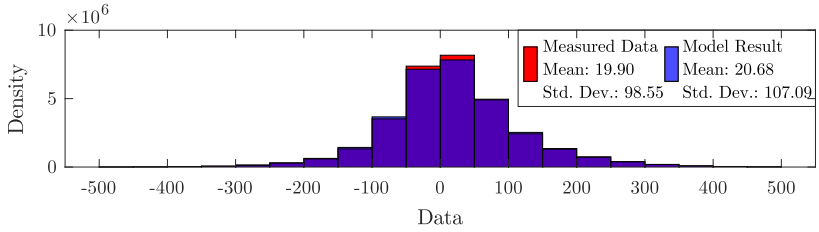

(a) ACE

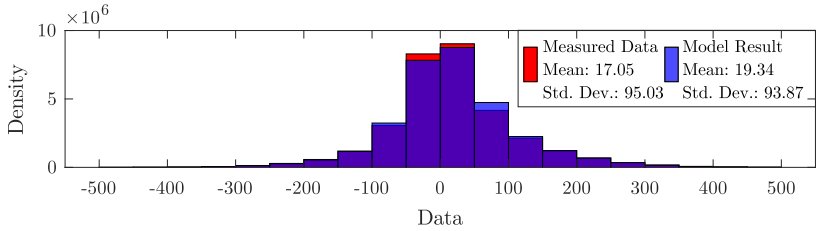

(b) $ACE_{filtered}$

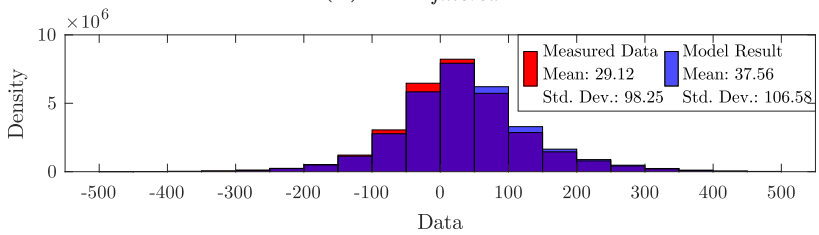

(c) SR_{ESS}

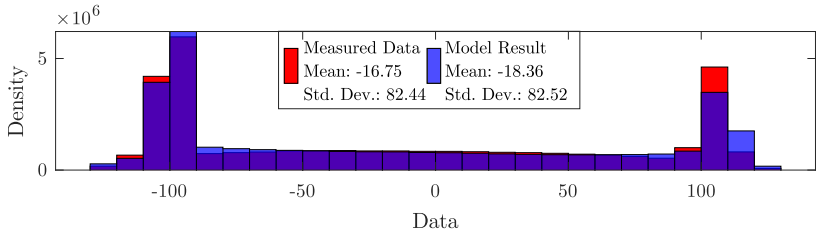

(d) SR

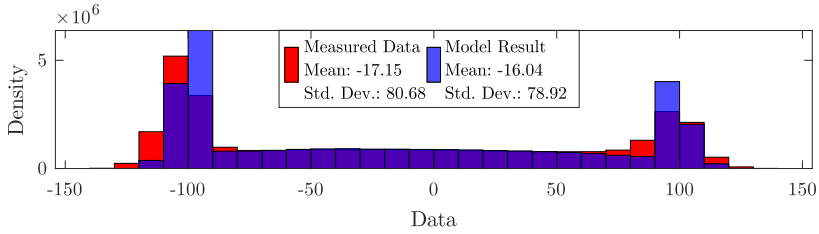

(e) P_{TGr}

Figure 3.9: Histograms of the measured data and model results for Stages I to IV.

731 MW, respectively. The results presented in Table 3.3, Figure 3.10, and Figure 3.11 can be considered acceptable, since the model results are close to the DSATools™ results, thus concluding that the model in Stage VII properly captures the system's primary frequency response, as well as the power in the tie-lines.

Table 3.3: Estimation errors for f_a and NI_a.

	Frequency		NI_a (523 − 731 MW)	
	RMSE [Hz]	MAE [Hz]	RMSE [MW]	MAE [MW]
Case 1	$2.7329e^{-04}$	$2.4423e^{-04}$	4.4963	4.0506
Case 2	$0.9063e^{-04}$	$0.8111e^{-04}$	5.1326	4.1198
Case 3	$1.8753e^{-04}$	$1.5642e^{-04}$	3.9204	3.2470
Case 4	$3.2162e^{-04}$	$2.5331e^{-04}$	15.953	14.161
Case 5	$1.9111e^{-04}$	$1.4437e^{-04}$	5.1016	3.8430
Case 6	$1.0038e^{-04}$	$0.7776e^{-04}$	4.0183	3.3039
Case 7	$0.3653e^{-04}$	$3.0986e^{-04}$	5.3813	4.1019

The ESS section of the proposed FR model is validated next. Thus, both Stage V and Stage VI of the FR control process are validated for the FESS and BESS using one day of data for each facility. The target signals are SP_{ESS} from Stage V, and BPm_{ESS}, $\overline{M}_{ESS}$, $\underline{M}_{ESS}$, P_{ESS} and SOC_{ESS} from Stage VI. Simulation results comparing the measured data and the model results for the signals in these two stages are presented in Figure 3.12 and Figure 3.13 for FESS and BESS, respectively. In these figures, it can be observed that the signals from the proposed FR model closely follow the measurement data from the ESS facilities. For visualization purposes, only a time span of six hours is presented in these figures, while Table 3.4 presents the MAE and RMSE of the FESS and BESS models for a period of one day, for all the signals in the SP calculation and ESS model blocks. Data for others days was also used to validate the FESS and BESS models, obtaining similar results to those presented in Table 3.4.

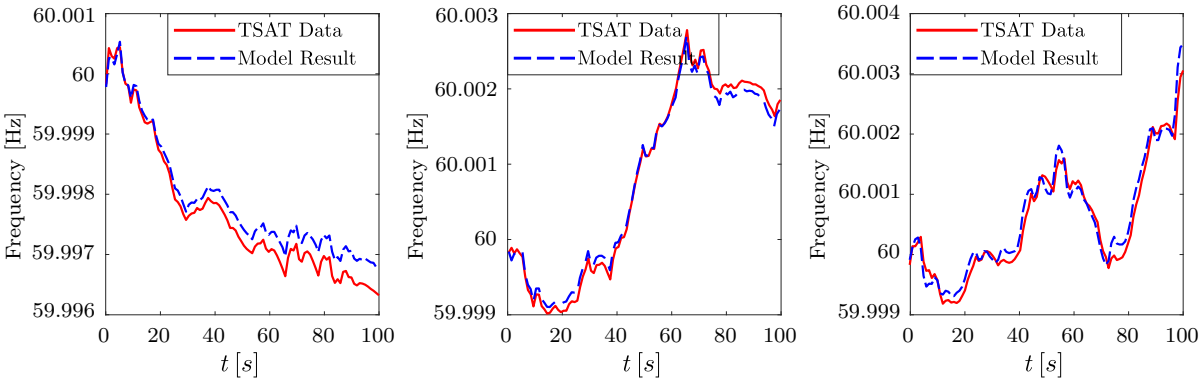

(a) f_a for Case 1. (b) f_a for Case 2. (c) f_a for Case 3.

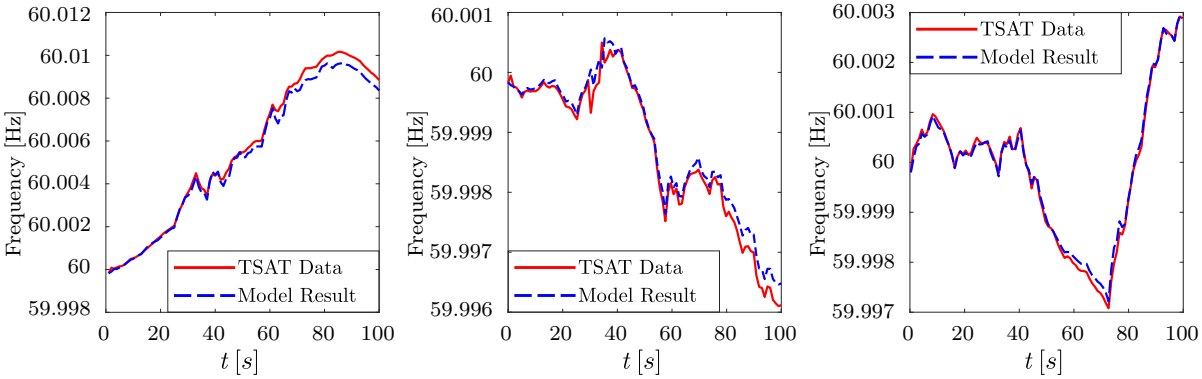

(d) f_a for Case 4. (e) f_a for Case 5. (f) f_a for Case 6.

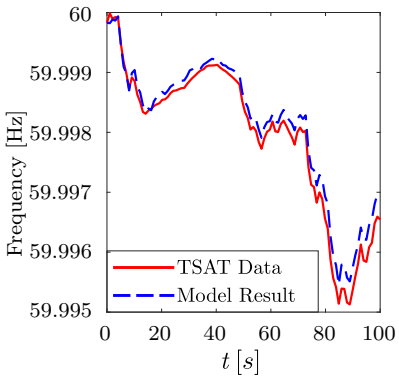

(g) f_a for Case 7.

Figure 3.10: Validation of f_a results of Stage VII.

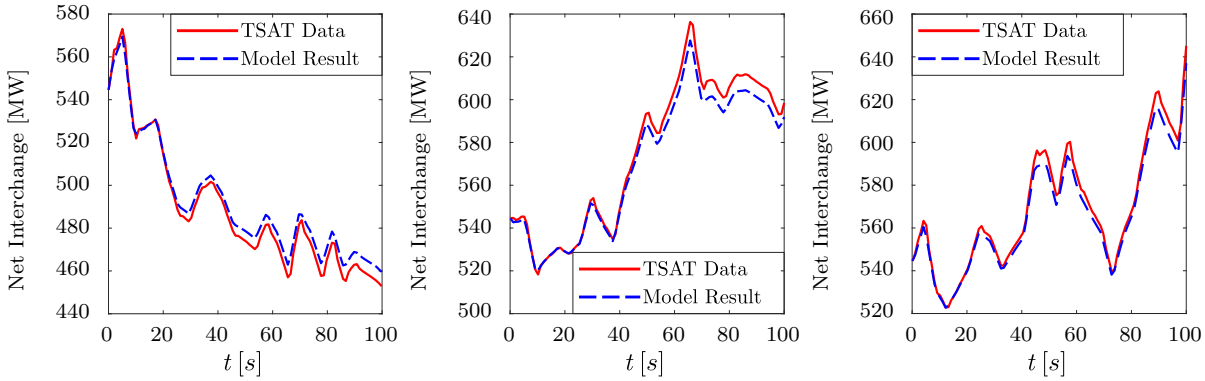

(a) NI_a for Case 1. (b) NI_a for Case 2. (c) NI_a for Case 3.

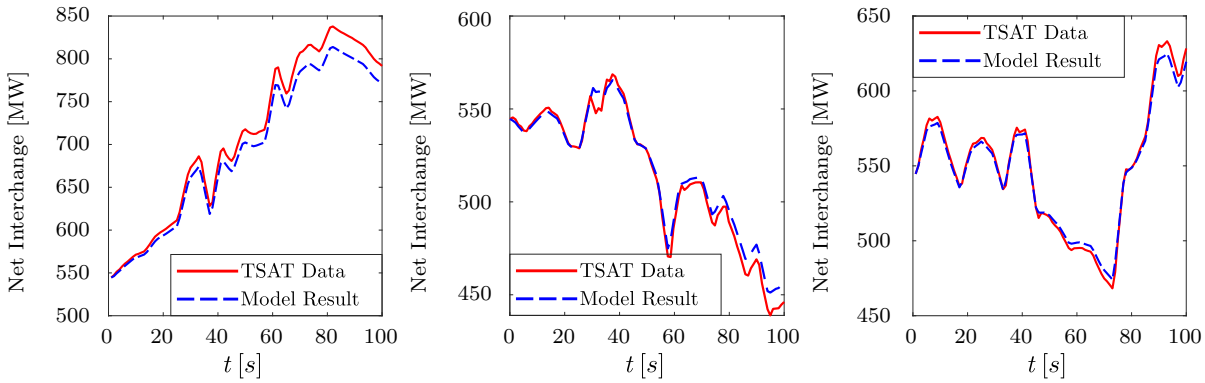

(d) NI_a for Case 4. (e) NI_a for Case 5. (f) NI_a for Case 6.

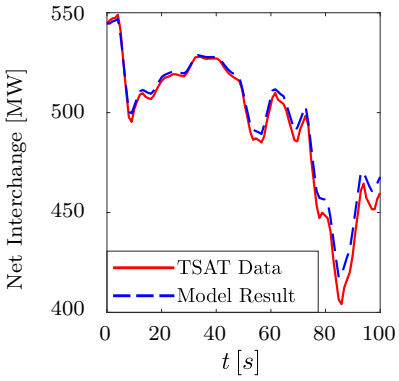

(g) NI_a for Case 7.

Figure 3.11: Validation of NI_a results of Stage VII.

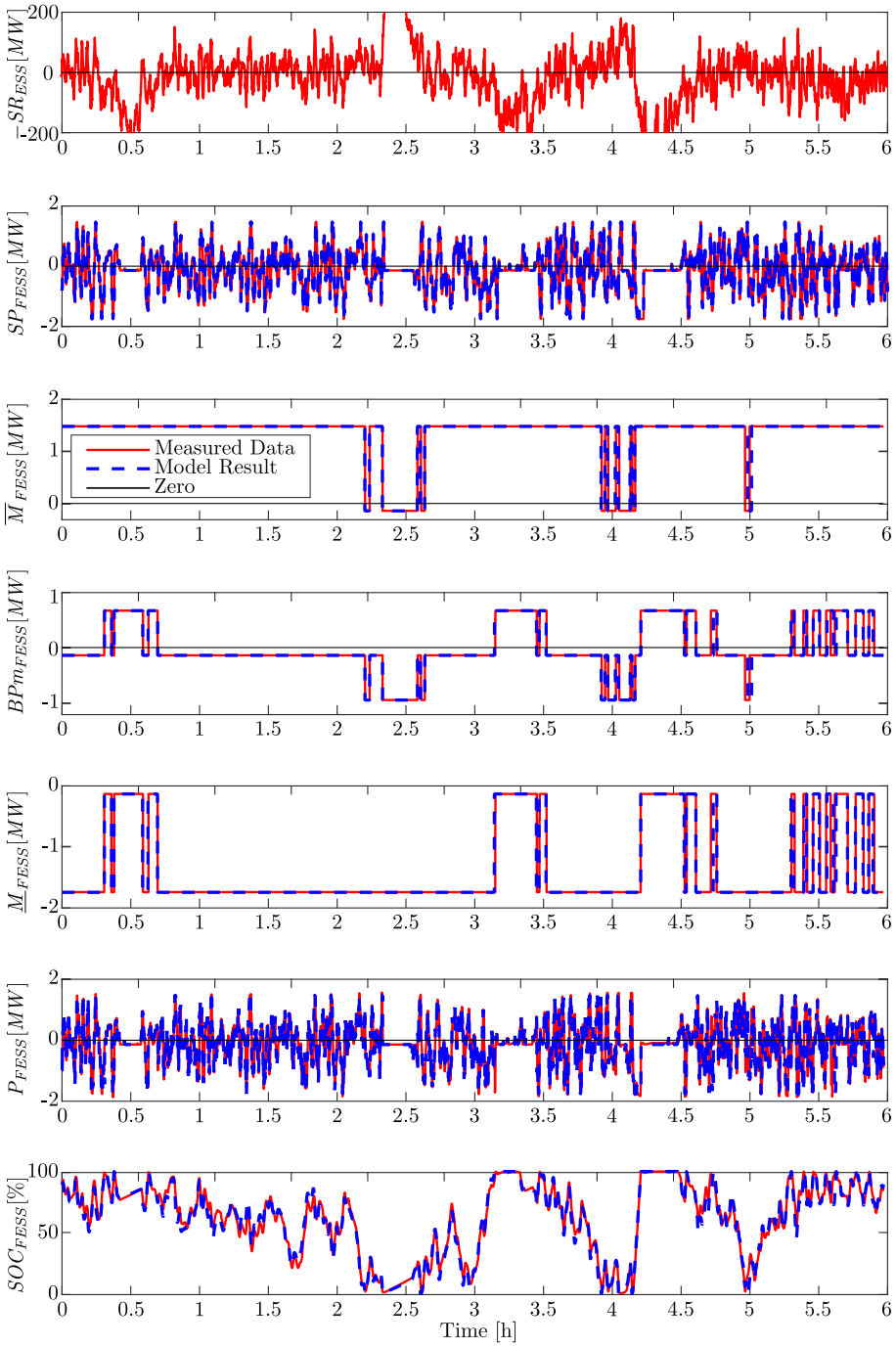

Figure 3.12: FESS validation results for February 26, 2020.

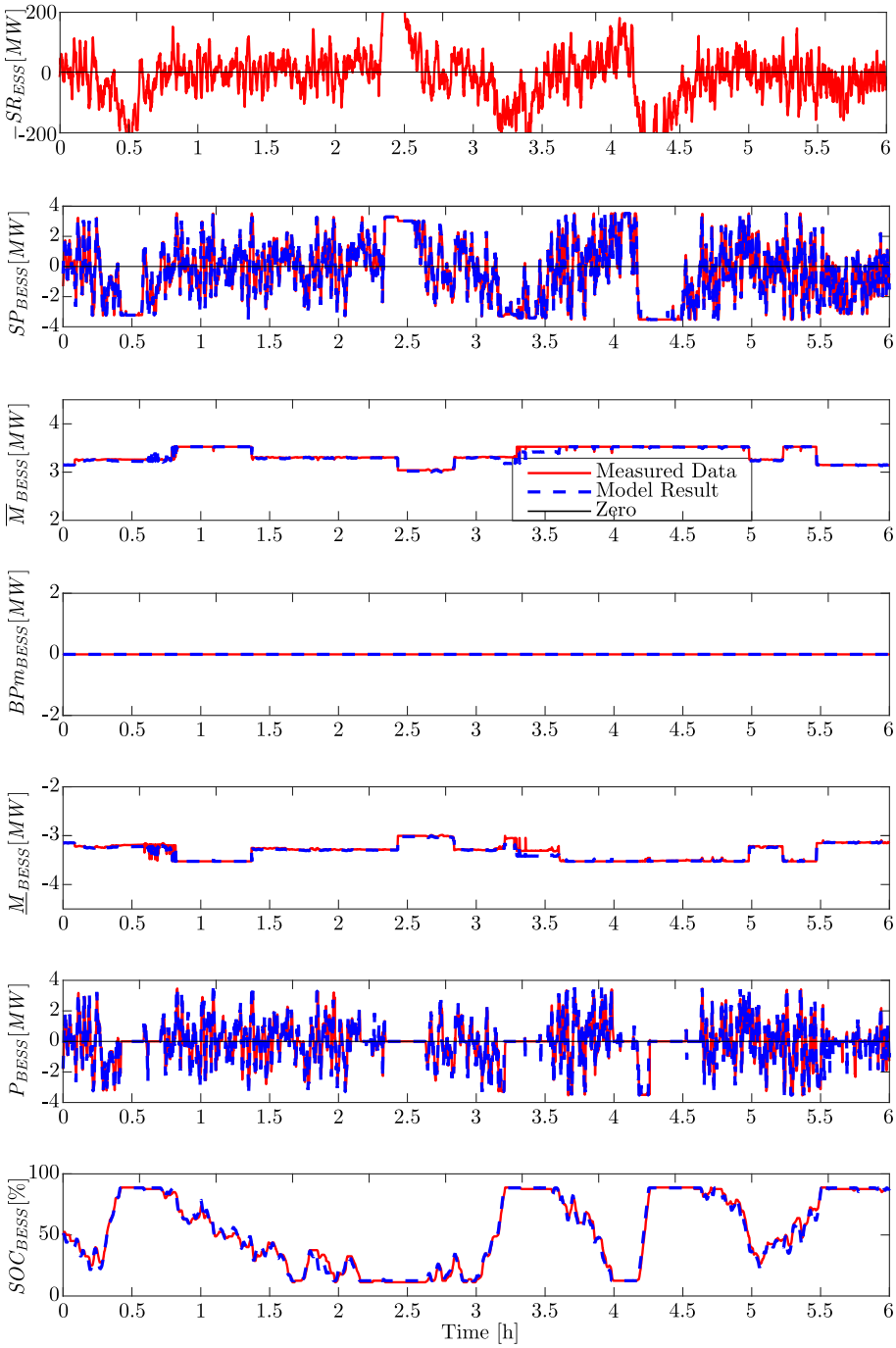

Figure 3.13: BESS validation results for February 26, 2020.

Table 3.4: Estimation errors for FESS and BESS models for February 26, 2020

		SP_{ESS} [MW]	$\overline{M}_{ESS}$ [MW]	BPm_{ESS} [MW]	$\underline{M}_{ESS}$ [MW]	P_{ESS} [MW]	SOC_{ESS} [%]
FESS	MAE	0.252	0.041	0.064	0.098	0.204	5.072
(± 2MW)	RMSE	0.425	0.248	0.226	0.390	0.372	7.450
BESS	MAE	0.432	0.018	0.000	0.018	0.330	2.648
(±4MW)	RMSE	0.655	0.044	0.000	0.044	0.611	4.243

3.3 Simulation Studies

The proposed FR model is used here to analyze the impact of CDs and to demonstrate the effect of the SoC model in the FR process. Also, the computational efficiency of the proposed FR model is discussed.

3.3.1 Communication Delays

In order to determine the impact of CDs in the FR process, simulations with the existing multiple delays, half the values of these delays, and no delays were considered. The impact is measured as a reduction in the ACE. Table 3.5 presents the RMSE and MAE with respect to the ideal ACE, i.e., 0 MW. As expected, the smaller the delay, the better the ACE performance. Note that reducing the CDs to half their current values has approximately the same effect on the ACE as increasing 30 MW of ESS capacity for FR with the current delay, based on the results discussed next.

Table 3.5: Impact of CDs for 100-day period.

Cases	RMSE [MW]	MAE [MW]
Current delay	87.55	56.91
Half of current delay	84.14	52.50
No delay	80.64	47.12

3.3.2 State of Charge Management

To demonstrate the effect of the SoC model in the FR control process, the ESS capacity used for FR was increased to 30 MW, comprising a ±15 MW/30 MWh BESS and a ±15 MW/3.75 MWh FESS. In the results presented in Table 3.6, it can be observed that ignoring the SoC leads to unrealistic ACE reductions, since without the SoC model, the ESS resources are assumed to have unlimited energy. Indeed, for the IESO case, considering ±30 MW of fast FR without the SoC model yields a better ACE than increasing the ESS FR capacity to ±80 MW (±40 MW/80 MWh BESS, ±40 MW/10 MWh FESS) with the SoC model, which could lead to under-procuring fast frequency response resources. Finally, the case of half of existing delays and 30 MW of ESS for FR, including the SoC model, was considered to demonstrate how a combination of reduced CDs and increased fast FR capacity can realistically reduce the ACE.

Table 3.6: Impact of SoC model on FR for 100-day period.

Cases	RMSE [MW]	MAE [MW]
Current ESS (SoC model)	87.55	56.91
30 MW ESS (SoC model)	83.89	52.81
30 MW ESS (no SoC model)	76.98	47.41
30 MW ESS (SoC model, 1/2 CDs)	81.12	49.09
80 MW ESS (SoC model)	80.37	49.34

3.3.3 Computational Efficiency

One of the main advantages of the proposed FR model is that it allows long simulation times while still considering the main stages of the FR process under normal operating conditions, which is the main application of the model. In order to demonstrate the computational efficiency of the proposed FR model, a computer with a processor Intel(R) Core(TM) i9-9900K CPU @3.60 Hz, 32 GB RAM, 64-bit operating system, x64-based processor was used to run several cases with different simulation times.

Table 3.7 presents the Simulation Time for each study and the corresponding average computation times for 5 simulation runs (Comp. Time), with a 1 s resolution for both the full FR model in Simulink® and the DSATools™ model, with the latter only allowing 102 s simulations due to the maximum number of switching events allowed, as previously explained. Note the speed up in the range of 2 to 3 orders of magnitude provided by the proposed model.

Table 3.7: Computational efficiency of the proposed FR model.

DSATools™ Model	
Simulation Time	Comp. Time
102 s	268.80 s
Full FR Model in Simulink®	
Simulation Time	Comp. Time
102 s	1.09 s
86400 s (1 day)	30.55 s
604800 s (1 week)	200.01 s
2592000 s (1 month)	845.74 s
31536000 s (1 year)	10252.98 s

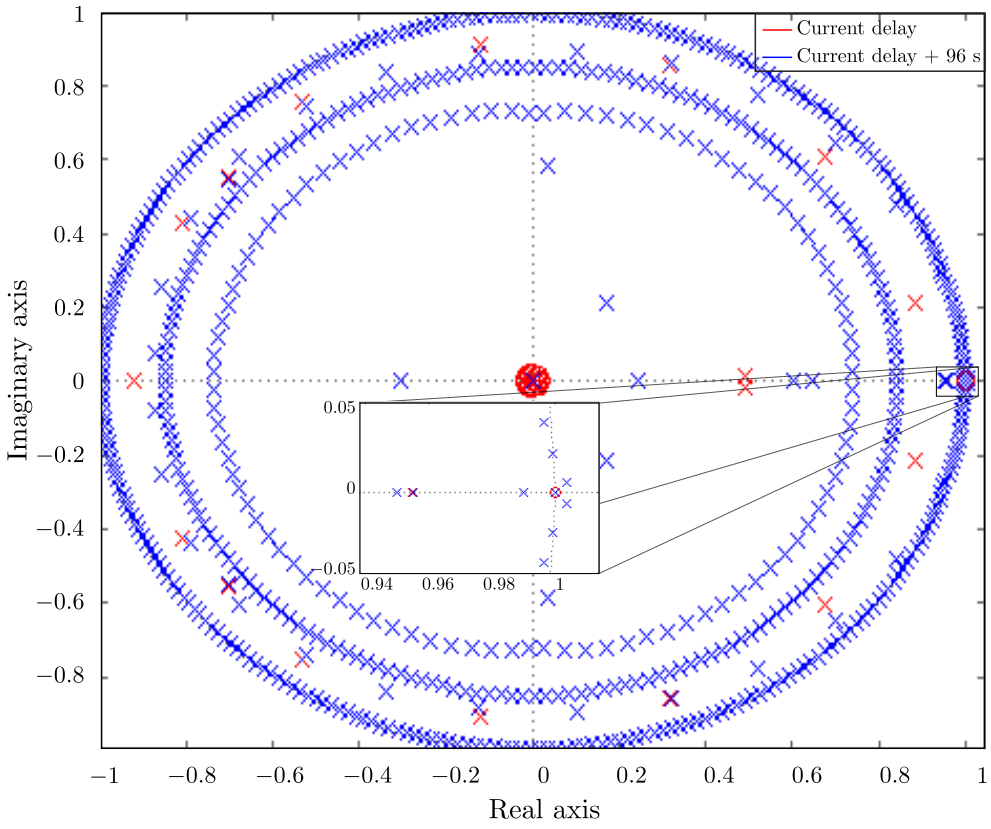

Figure 3.14: Eigenvalues of the FR model with different communication delays.

3.3.4 Stability Analysis

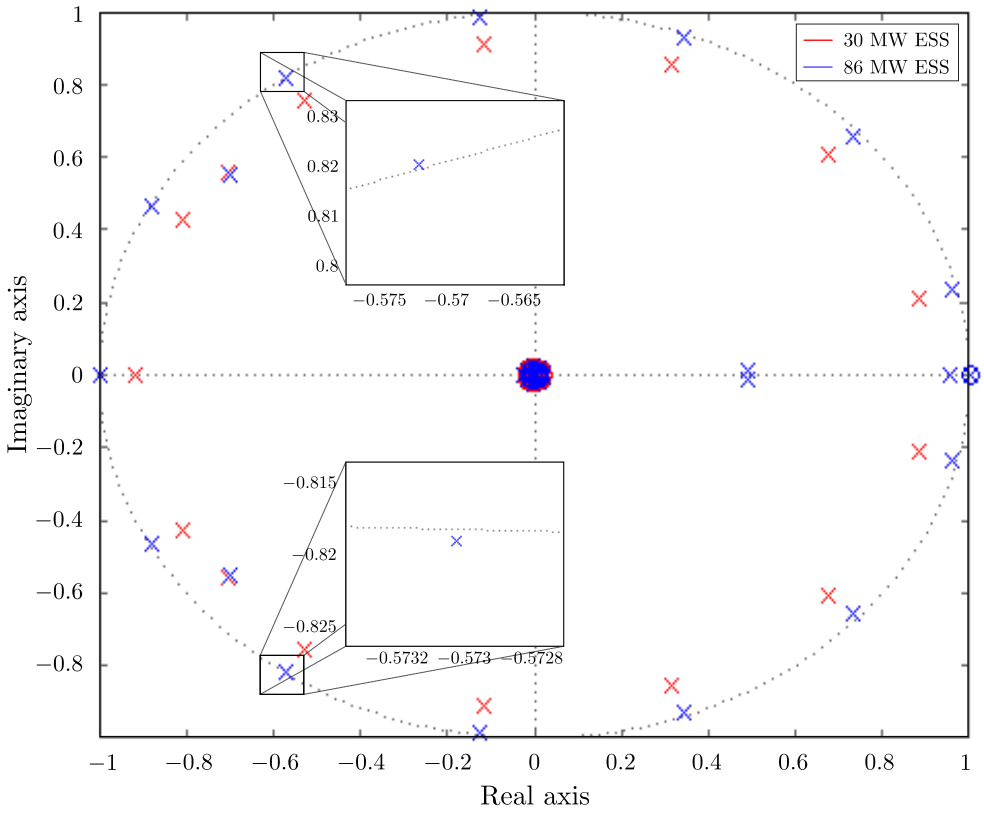

Figure 3.15: Eigenvalues of the FR model with different ESS capacity.

Given the complex nonlinear characteristics of the detailed FR model, eigenvalue analyses are used here to demonstrate the system stability for varying communication delays and ESS capacities, and hence evaluate the robustness of the system. To analyze the impact of increasing communication delays, a total ESS capacity of 30 MW which included a ±15 MW/30 MWh BESS and a ±15 MW/3.75 MWh FESS, were used, since these yielded reasonable FR performance for existing communication delays (CD = 4 s and CD_{TG} = 30 s). In this case, the system is marginally stable, presenting two poles on the real axis, both at (1, 0), associated with $F(z)$ in Stage VII. As communication delays are increased, the system performance deteriorates in terms of ACE, as expected, and finally becomes unstable for a 96 s increase in all the delays, i.e. for CD = 100 s and CD_{TG} = 126 s, as highlighted in Figure 3.14. This shows that the stability of the system is quite robust

for practical ranges of communication delays and only becomes unstable at significantly extreme values.

To analyze the impact of added ESS capacity on the stability of the proposed model, for the current communication delays, the capacities of the FESS and BESS facilities were increased simultaneously by the same values. As illustrated in Fig. 3.15, the system remains stable until the total capacity of the ESS reaches 86 MW, ±43 MW/86 MWh BESS and a ±43 MW/10.75 MWh FESS, when the system becomes unstable. This indicates that for the existing FR approach for ESS, the system is sensitive to ESS capacity increases, as also demonstrated in Chapter 4 where a new fast regulation approach for ESS is proposed that addresses this issue.

3.4 Summary

This chapter presented a validated model for long-term FR studies of a real interconnected power system including ESS facilities. The proposed FR model was designed to closely represent the frequency behaviour of a bulk interconnected power system, with the ESS model allowing an accurate representation of the SoC management and charging/discharging characteristics of FESS and BESS. Simulation results showed that reducing the CDs can potentially reduce the ACE without requiring any increase in FR capacity, and that neglecting the SoC model of ESSs in the frequency control process yields unrealistic improvements in the ACE. In addition, the proposed FR model allowed long-term simulations that can reduce the computation time significantly as compared to a more detailed dynamic model, while still capturing the required FR response of the system. Finally, it was shown that the stability of existing FR system is robust with respect to communication delays, but sensitive to ESS capacities.

Chapter 4

Regulation Signal Design and Fast Frequency Control with Energy Storage Systems

This chapter presents a novel $\mathcal{H}_2$ filter design procedure to optimally split the FR signal between conventional generators and fast regulating ESS assets, considering typical CDs. The filter is then integrated into the previously validated FR model including BESS and FESS, discussed in Chapter 3. This Integrated Model is used to analyze the impact of the ESSs, CDs, and limited regulation capacity on the FR process in the OPS. The proposed methodology to split the FR signal is also compared with the existing FR process in Ontario.

4.1 Design of $\mathcal{H}_2$ FR Filter

4.1.1 Filter Design

The design approach used here is to filter the FR signal by producing a slowly-varying component or *RegA* to be provided to the slow regulating resources, while the remaining fast component or *RegD* is provided to the fast regulating facilities, as in the PJM electricity market [15]. This is done to take advantage of the fast changing power output characteristic of ESSs in the FR control loop. Hence, it is assumed here, as per general practices, that fast response ESS technologies, i.e., FESS and BESS, receive the *RegD*

signal due to their fast response characteristics. Slower types of ESS technologies such as compressed-air and thermal ESSs can also be added to the FR control loop, receiving the $RegA$ signal due their prolonged discharging and slower power output characteristics.

The design of the filter is formulated as an optimal control design problem, based on the general control configuration shown in Figure 4.1, consisting of a Generalized Plant (GP) transfer function $GP(z)$, which includes weights, interconnected with a controller $\Phi(z)$, with the latter processing the available measurements Y to produce the control signal U. The signal W models exogenous inputs/disturbances, and the signal Z contains controlled variables that the designer wishes to keep small [82]. The blocks can be represented by the following transfer matrix relationship:

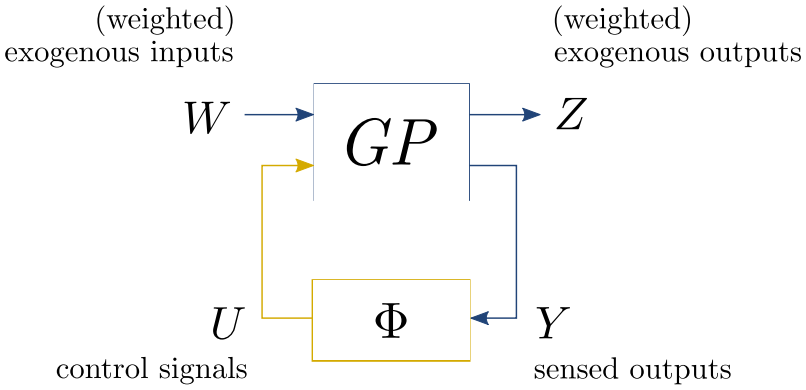

Figure 4.1: General control problem formulation.

$$\begin{bmatrix} Z \\ Y \end{bmatrix} = \begin{bmatrix} GP_{11}(z) & GP_{12}(z) \\ GP_{21}(z) & GP_{22}(z) \end{bmatrix} \begin{bmatrix} W \\ U \end{bmatrix} \tag{4.1}$$

$$U = \Phi(z)Y \tag{4.2}$$

The control problem is then to design $\Phi(z)$ such that the $\mathcal{H}_2$ norm of the closed-loop transfer function from W to Z, given by $GP_{11}(z) + GP_{12}(z)\Phi(z)(I - GP_{22}(z)\Phi(z))^{-1}GP_{21}(z)$, is minimized in the $\mathcal{H}_2$ sense (e.g., see [82] for a formal definition of the $\mathcal{H}_2$ norm). Effectively, this procedure minimizes the sensitivity transfer function from W to Z, thereby suppressing the effect of the exogenous disturbances W on the 60 controlled variables Z. This control problem is solvable via routine computational methods [82], which are implemented in Matlab [83].

The design of the proposed filter for FR can be cast into the aforementioned general framework, as shown in Figure 4.2, where the signals Y_1 and Y_2 correspond to ACE and

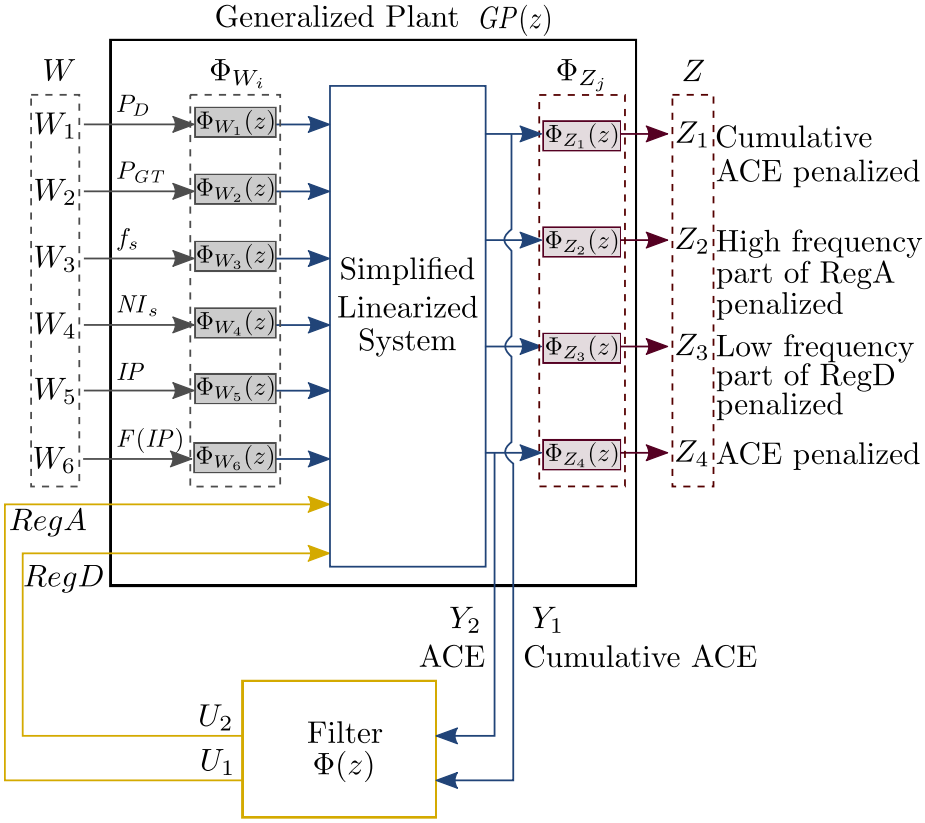

Figure 4.2: Optimal control configuration.

cumulative ACE signals, which are the plant measurement outputs provided to the controller; U_1 and U_2 correspond to $RegA$ and $RegD$, which are the control inputs the filter produces (the outputs of the filter). The generalized plant $GP(z)$ illustrated in Figure 4.3 is constructed from the simplified nonlinear version of the Base Case FR Model depicted in Figure 3.1 through the following steps: First, all signal loops that would enter the new filter $\Phi(z)$ are broken by removing the ACE filtering and AGC blocks. Next, nonlinearities such as limiters are removed, and all ESS systems are approximated as ideal set-point followers; this is done to obtain a simplified linear time-invariant model. Finally, the exogenous inputs W and performance outputs Z are identified, and associated weighting filters $\Phi_{W_i}(z)$ and $\Phi_{Z_j}(z)$ are added, where i and j are associated with each element in W and Z, respectively. The exogenous disturbance vector W corresponds to the inputs $[P_D\ P_{GT}\ f_s\ NI_s\ IP\ F(IP)]^\mathsf{T}$. The vector signal $Z = [Z_1\ Z_2\ Z_3\ Z_4]^\mathsf{T}$ contains the error outputs to be kept small, which corresponds to cumulative ACE, high frequency component of $RegA$, low frequency component of $RegD$, and ACE signals, which are penalized

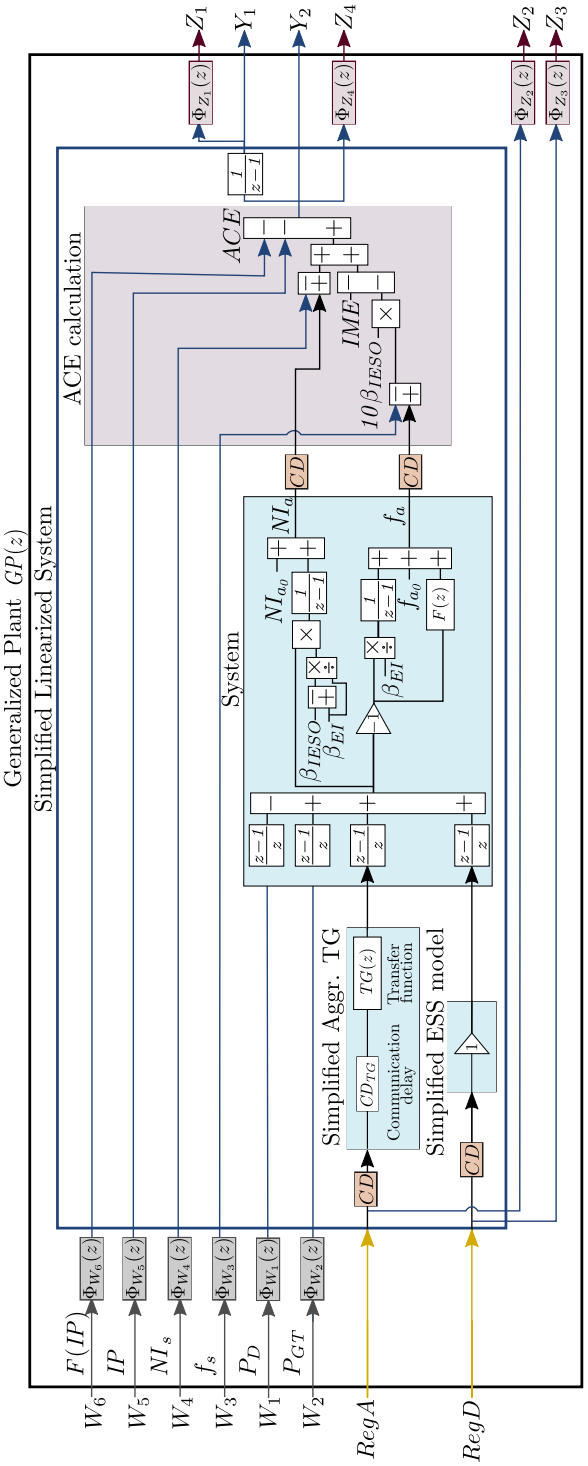

Figure 4.3: Linearized System and Generalized Plant $GP(z)$

by the $\Phi_{Z_1}(z)$ to $\Phi_{Z_4}(z)$ filters. The state-space representation of $GP(z)$ is obtained by implementing the model in Figure 4.3 in Simulink® and by using the Matlab function `linearize`, which yields the matrices A, B, C, and D corresponding to the state space representation at time zero of the transfer function $GP(z)$ in (4.1). The dimensions of the state-space matrices for the case with delays are $A_{50\times50}$, $B_{50\times8}$, $C_{6\times50}$, and $D_{6\times8}$, while for the case without delays are $A_{12\times12}$, $B_{12\times8}$, $C_{6\times12}$, and $D_{6\times8}$.

The various filters $\Phi_{W_i}(z)$ and $\Phi_{Z_j}(z)$ in Figure 4.2 are not physically present, but are design variables of the optimal control problem. These filters specify the magnitude of the disturbance/error signals, and allow to shape the closed-loop response by weighting the importance of disturbances and error variables over desired frequency ranges.

The filters $\Phi_{W_i}(z)$ are selected as constant gains here, based on the largest change observed in the real data provided by the IESO for each input i. The filters $\Phi_{Z_1}(z)$ and $\Phi_{Z_4}(z)$ are selected as constant gains. The $RegD$ signal should contain relatively little low-frequency content, while the $RegA$ signal should contain relatively little high-frequency content, and hence, $\Phi_{Z_2}(z)$ and $\Phi_{Z_3}(z)$ include a constant gain multiplying a high-pass and low-pass filter, respectively. The high-pass filter penalizes the high frequency content in $RegA$, while leaving the low frequency behaviour unchanged. Conversely, the low-pass filter discourages high frequency content in $RegD$, which encourage ESS facilities to provide a fast power response. The high- and low-pass filters can be determined based on the analysis of the discrete Fourier transform of the measured ACE signal. Furthermore, all the constant gains present in the filters $\Phi_{Z_j}(z)$ can be determined using a recurrent process, which included a GA technique described next to solve the required optimization problem.

The first GA step is to set the initial individual, which corresponds to the set of constant gains in $\Phi_{Z_j}(z)$; these gains together with the $\Phi_{W_i}(z)$ filters selected are then inserted in $GP(z)$. The filter $\Phi(z)$ is generated using the Matlab function `h2syn` that computes a stabilizing $\mathcal{H}_2$-optimal controller $\Phi(z)$ for the plant $GP(z)$ [83]. Next, $\Phi(z)$ is added to the Base Case Model to arrive at an Integrated Model, described below, and the RMSE of the ACE signal for a one day period is calculated. The GA determines the next individual, and the process continues until the stopping criteria is met and the individual that yields the lowest RMSE of ACE is selected.

The solution to the optimal control problem illustrated in Figure 4.2 requires that one appropriately selects the weighting filters Φ_{W_i} and Φ_{Z_j}. The computation of the filter $\Phi(z)$ that minimizes the norm of the transfer function from W to Z (while guaranteeing stability of the linear system) can then be systematically solved via standard methods in either $\mathcal{H}_2$ or $\mathcal{H}_\infty$ frameworks, as explained in [82]. In this study, the $\mathcal{H}_2$ synthesis procedure produced

better results compared to the $\mathcal{H}_\infty$ synthesis, as measured by smaller RMSE and MAE of the ACE signal for the simulation studies presented in Section 4.2, and hence only the results for the $\mathcal{H}_2$ filter design are described next.

4.1.2 Filter Integration

The Integrated Model shown in Figure 4.4 corresponds to the Base Case FR Model in Figure 3.1 with some modifications and the addition of the proposed $\mathcal{H}_2$ filter. The modifications, presented in green, include a Proposed Set-Point (PSP) calculation replacing the SP calculation block, and the substitution of the ACE filtered and AGC blocks by the designed filter. The $\mathcal{H}_2$ filter is implemented using its state-space representation, which has two input signals: ACE and cumulative ACE, and two outputs: $RegA$ and $RegD$, which go through a limiter block. Thus, $RegA_L$ corresponds to $RegA$ limited between $\pm RC_{TG}$, which is the FR capacity of TGs, and $RegD_L$ is $RegD$ limited between $\pm RC_{ESS}$, which is the FR capacity of fast response resources. The RC_{ESS} is obtained by adding the FESS and BESS FR capacity limits RC_{FESS} and RC_{BESS}, respectively.

Since the Integrated Model considers limited FR capacity and the SoC model of the facilities, six cases are possible, depending on whether the TGs are limited or not, and depending on whether the ESS is limited by its capacity, its SoC, or neither. Within these six cases, two extreme cases can arise: both TGs and ESSs reach their limits, or TGs reach their limit while the ESS facilities are not able to follow the SP signals because of their SoC limits. If these two extreme cases arise and the load-generation mismatch increases, the filter will receive increasing ACE and cumulative ACE signals, hence increasing the requirement from the regulation resources through $RegA$ and $RegD$. However, since the facilities are not able to follow their SP signals, the error will keep accumulating, and the requirement from the facilities will continue increasing. This saturation in the filter is an issue that can be corrected by implementing the following conditional integration

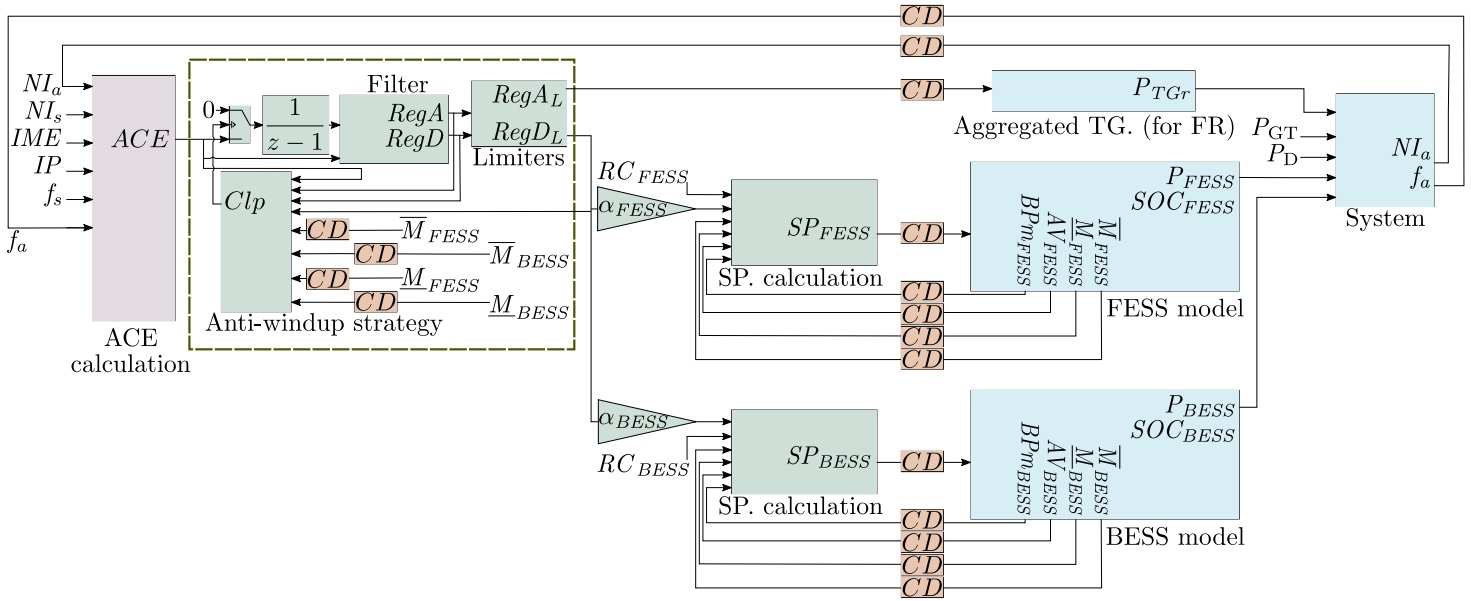

Figure 4.4: Filter integration into the Base Case Model of Figure 3.1 (Integrated Model).

anti-windup strategy:

$$Clp = \begin{cases} 1 & \forall \{[(RegD_L < 0 \wedge \underline{M}_{FESS} = BP_{FESS}) \vee \\ & (RegD_L \geq 0 \wedge \overline{M}_{FESS} = BP_{FESS})] \wedge \\ & [(RegD_L < 0 \wedge \underline{M}_{BESS} = BP_{BESS}) \vee \\ & (RegD_L \geq 0 \wedge \overline{M}_{BESS} = BP_{BESS})] \wedge \\ & (RegA > RC_{TG} \vee RegA < -RC_{TG}) \wedge \\ & [sgn(-RegA) = sgn(ACE)] \wedge \\ & [sgn(-RegD) = sgn(ACE)]\} \vee \\ & \{(RegA > RC_{TG} \vee RegA < -RC_{TG}) \wedge \\ & (RegD > RC_{ESS} \vee RegD < -RC_{ESS}) \wedge \\ & [sgn(-RegA) = sgn(ACE)] \wedge \\ & [sgn(-RegD) = sgn(ACE)]\} \\ 0 & \text{otherwise} \end{cases} \tag{4.3}$$

where Clp can be equal to 1 or 0, depending on the stated logic conditions, which consider the values and signs of $RegD_L$, $RegA$, the upper and lower limits of BESS and FESS, and the sign of the ACE signal. This signal controls the input switch to the cumulative discrete block in Figure 4.4, so that when $Clp = 1$, the switch is set to its upper position, forcing the first filter input to 0 to avoid saturation; otherwise, when $Clp = 0$, the switch is set to its lower position, so that the corresponding filter input is the cumulative value of the ACE signal.

In addition, BP_{FESS} and BP_{BESS} should be set in the control center; currently these values are close to 0 for the IESO, but can be different if the ESS facilities are also considered for energy arbitrage. The last four inputs of the anti-windup block contain SoC information for the ESS facilities, and since they come from these facilities, a CD is considered.

The proposed filter sends $RegA$ and $RegD$ signals considering the SoC of fast resources and capacity limits of ESSs and TGs, and depend on the conditions of the system, working in a coordinated manner. The hard energy neutrality condition or the soft neutrality condition on the $RegD$ signal, like those implemented in PJM [56], are not included here, to avoid issues such as over procuring fast response resources or having the ESS facilities work against the system FR needs to achieve the hard neutrality condition. The fast response ESS facilities are expected to follow closely a signal; however, if the signal sent to them worsens the ACE, it would eliminate the potential benefits of the ESS. Therefore, the control of the regulation signal is extremely important.The controller proposed here

acts to bring the ACE back to zero through an optimal coordinated control between fast and slow resources, thus optimizing the use of those resources while considering system limitations. Furthermore, since the ESS are exclusively being used for FR, there is no need to force this signal to meet an energy neutral condition, from the ISO perspective.

The SP calculation in Section 3.1.1 is modified here so that the FR capacity from FESS and BESS can be significant as compared to the TGs FR capacity, which is not the case in Section 3.1.1, where these are assumed to be small. The ESS facilities are considered to have different capacity limits here; thus, the FR signal $RegD_L$ sent to FESS and BESS is multiplied by a factor α_{FESS} or α_{BESS} for FESS or BESS, respectively ($\alpha_{FESS} + \alpha_{BESS} = 1$), which indicate their respective capacity contributions to the total ESS capacity required for FR. Accordingly, the SP calculation in (3.5) and Figure 3.1 is modified in the PSP blocks as follows:

$SP_{ESS} =$

$$\begin{cases} 0 & \forall\ (AV_{ESS} = 1,\ \alpha_{ESS}RegD_L \geq 0,\ \overline{M}_{ESS} = BP_{ESS}) \vee \\ & \quad (AV_{ESS} = 1,\ \alpha_{ESS}RegD_L < 0,\ \underline{M}_{ESS} = BP_{ESS}) \\ \alpha_{ESS}RegD_L & \forall\ (AV_{ESS} = 1,\ RC_{ESS} \neq 0,\ \underline{M}_{ESS} \neq BP_{ESS},\ \overline{M}_{ESS} \neq BP_{ESS}) \vee \\ & \quad (AV_{ESS} = 1,\ RC_{ESS} \neq 0,\ \alpha_{ESS}RegD_L \geq 0,\ \overline{M}_{ESS} \neq BP_{ESS}) \vee \\ & \quad (AV_{ESS} = 1,\ RC_{ESS} \neq 0,\ \alpha_{ESS}RegD_L < 0,\ \underline{M}_{ESS} \neq BP_{ESS}) \end{cases} \quad (4.4)$$

In this calculation, the ESS SP signal SP_{ESS} for either FESS or BESS is equal to 0 or $\alpha_{ESS}RegD_L$ depending on the values of AV_{ESS}, $\alpha_{ESS}RegD_L$, RC_{ESS}, and the facility's SoC, included in the signals $\overline{M}_{ESS}$ and $\underline{M}_{ESS}$. If the $\alpha_{ESS}RegD_L$ signal indicates that the facility should charge or discharge, but this is not possible from the SoC management perspective, the SP is set to 0. Otherwise, SP_{ESS} is equal to $\alpha_{ESS}RegD_L$. An idle state of the ESS, which has not been considered in Section 3.1.2, is enforced through this PSP calculation.

The proposed filter produces two different signals, $RegA$ and $RegD$, with similar characteristics to the current PJM FR approach. However, the proposed strategy has the following main advantages over the current PJM signals. First, the proposed $RegA$ and $RegD$ are the result of an optimal control design problem which incorporates the aggregated dynamics of traditional FR resources, along with approximate CDs and an aggregated model of the bulk power system; incorporating dynamic effects directly in the design stage leads to improved closed-loop response. Second, the PJM neutrality condition, which caused over procuring issues in PJM, is not included here.

Since the proposed approach takes advantage of the ESS high ramp rates, the $\mathcal{H}_2$ fil-

ter, anti-windup method, and PSP calculation could be implemented in ISOs that have adopted FERC Order 755, such as MISO, CAISO, ISO-NE, NYISO, and others, to take advantage of the fast regulation resources that are currently part of their regulation markets, and to coordinate traditional and fast resources. These ISOs have already modified their market structure to include ESS fast power responses, calculating the mileage and including a performance factor, which can be obtained from the *RegD* signal of the proposed filter. In addition, the proposed integrated model can be used to determine different regulation capacities for both conventional and fast response resources, and a conversion factor between regulation products, as in PJM [19].

4.2 Simulation Results

This section presents the simulation results of the proposed Integrated and Base Case Models for the OPS, for comparison purposes. For the cases considering limited FR capacity, the assumed scheduled capacity is ±100 MW and ±50 MW from TGs and ESS, respectively, since currently, the IESO schedules a minimum of ±100 MW from TGs and ±7.05 MW from ESS. This assumed ESS regulation capacity includes a 25 MW/6.25 MWh FESS and a 25 MW/50 MWh BESS (currently these are 2 MW/0.5 MWh for FESS, and 4 MW/2.76 MWh for BESS). The values of α_{FESS} and α_{BESS} are both 0.5, because both FESS and BESS are assumed to have the same capacity. The FESS and BESS models can be dispatched for energy with $BP_{ESS} > 0$; in the present studies, $BP_{ESS} = 0$ and thus the total available capacity is used for regulation, as this is the current practice at the IESO. For visualization purposes, a window of 8000 seconds is considered for all the simulation studies.

The values chosen for the $\Phi_{W_i}(z)$ filters for the OPS studies are the following, based on the highest change on the corresponding input:

$$\begin{aligned} &\Phi_{W_1}(z) = 1000 \text{ MW}, \ \Phi_{W_2}(z) = 1000 \text{ MW}, \\ &\Phi_{W_3}(z) = -\frac{1000 \text{ MW}}{B}, \ \Phi_{W_4}(z) = 1000 \text{ MW}, \\ &\Phi_{W_5}(z) = 100 \text{ MW}, \ \Phi_{W_6}(z) = 100 \text{ MW} \end{aligned} \tag{4.5}$$

where B, i.e., the BA bias, is $2,482$ MW/Hz.

The optimal values of the GA process for the $\Phi_{Z_j}(z)$ obtained for the OPS are as

follows:

$$\begin{aligned}\Phi_{Z_1}(z) &= 384.97,\ \Phi_{Z_2}(z) = 9567.88\frac{0.99z - 0.99}{z - 0.99},\\ \Phi_{Z_3}(z) &= 77967.58\frac{0.0016z + 0.0016}{z - 0.99},\ \Phi_{Z_4}(z) = 751.5\end{aligned} \tag{4.6}$$

The matrices A, B, C, and D defined in Section 4.1.1 can be found in [84]. These matrices are used to obtain the controllers $\Phi(z)$ for all the cases presented in this section.

It is important to mention that the real data used for the simulations in this section correspond to the following signals of April 1st, 2019: f_s, NI_s, IME, IP, P_{GT}, and P_D. This data has been provided by the IESO and has been re-sampled to 1 s resolution.

4.2.1 Impact of Communication Delays

When CDs are ignored, the FR signals are calculated at the control center at time t, and sent to the FR facilities, which are immediately received by them, and their responses sent back instantly to the control center. The TGs and ESS facilities act on these FR signals, reducing the ACE. However, CDs exist in the FR process and thus the ACE is not corrected instantly; hence, the error keeps accumulating and more regulation resources are needed to correct it. Ignoring CDs in real systems can potentially lead to errors in determining the FR capacity needed and the impact of regulating resources in reducing the ACE.

Figure 4.5 and Figure 4.6 presents the Base Case and Integrated Model results considering limited FR capacity without and with CDs of $\tau = 4s$ for most signals, and $\tau = 30s$ for the TG regulation signal, as it is currently the case in Ontario; for the case of the system without CDs, the delays were ignored in the filter design process, while for the case with CDs, these were considered. Note the significant reduction in ACE in Figure 4.5 due to the absence of CDs. The proposed filter, included in the Integrated Model, takes into account CDs in the design process and in the system to send appropriate FR signals. Observe that P_{FESS} and P_{BESS}, which are the response of FESS and BESS to $RegD$, move faster in the Integrated Model than the Base Case, while the P_{TGr} signal in both models is similar. Also, the SOC_{FESS}% and SOC_{BESS}% respond differently to the same $RegD$ signal, since the FESS and BESS facilities have different SoC management and energy capacity.

Table 4.1 presents the RMSE and MAE of the ACE signal measured with respect to the ideal ACE (i.e., 0 MW), and the mean and Standard Deviation (SD) of the same signal for the Base Case and Integrated Models without and with CDs. The MAE of the

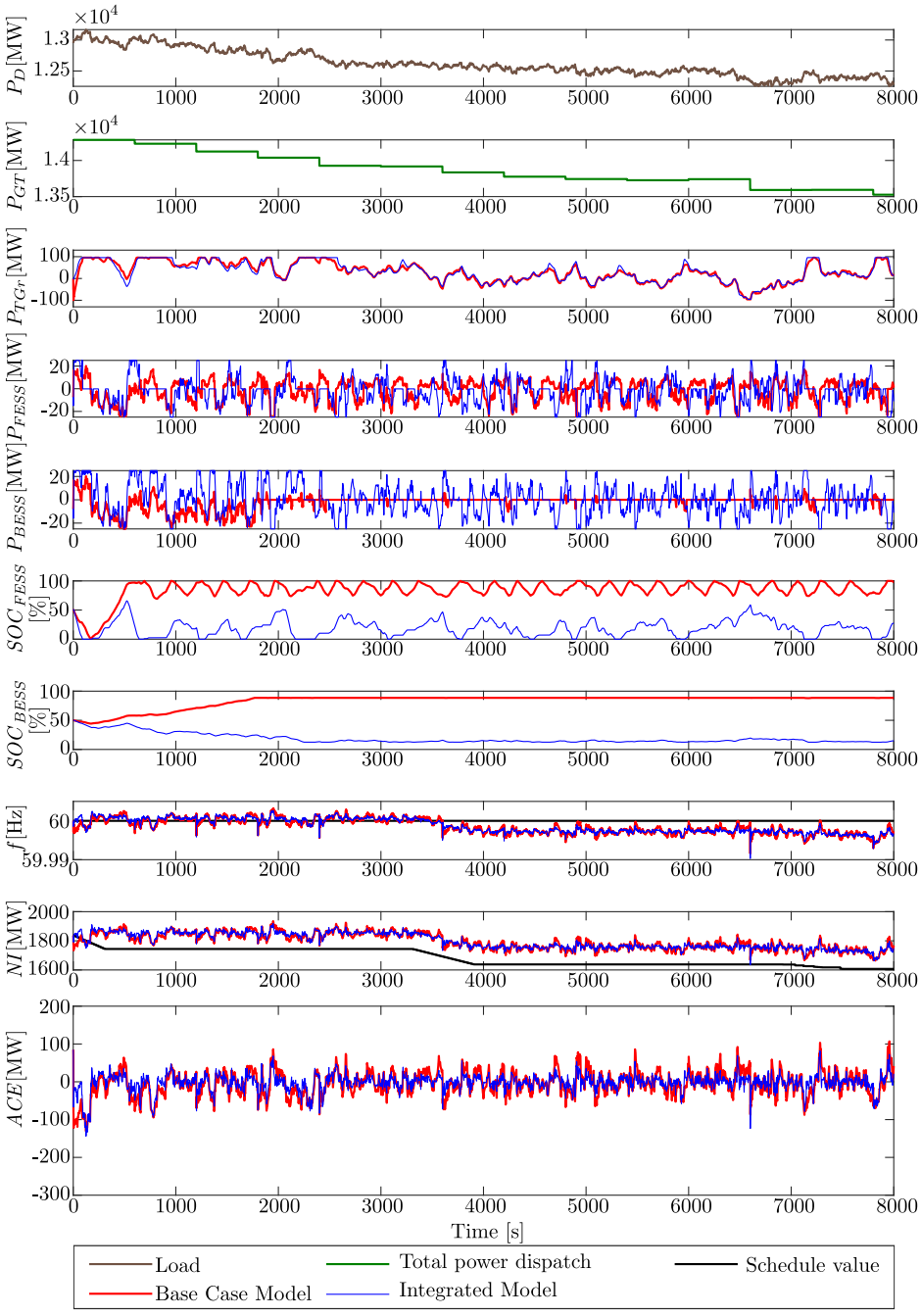

Figure 4.5: Base Case Model and Integrated Model comparison for limited FR capacity and without considering CDs.

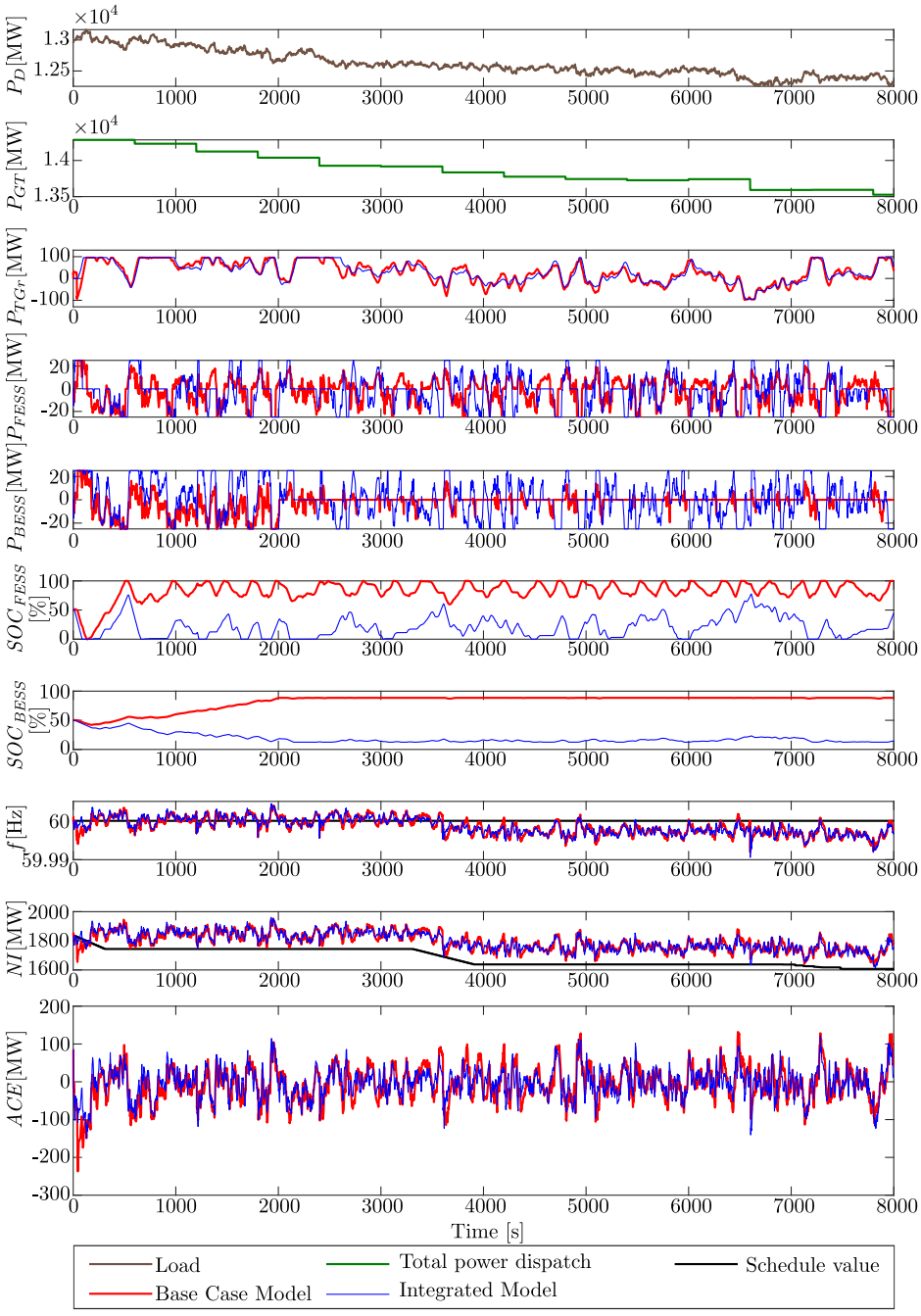

Figure 4.6: Base Case Model and Integrated Model comparison for limited FR capacity and considering CDs.

Integrated Model is 58% and 82% of the error of the Base Case Model without and with CDs, respectively. In addition, the RMSE, mean, and SD are closer to zero for the cases with the Integrated Model, specially for the case without CDs. These results highlight the importance of CDs in the FR process. Certainly, by eliminating or at least reducing CDs, the ACE can be improved by up to 42% without adding extra FR capacity.

Table 4.1: Impact of CDs on the FR process.

Case	RMSE [MW]	MAE [MW]	Mean [MW]	SD [MW]
No CDs				
Base Case Model limited FR cap.	32.57	25.16	-4.60	32.24
Integrated Model limited FR cap.	21.79	14.52	-2.22	21.68
With CDs				
Base Case Model limited FR cap.	46.35	36.45	-6.15	45.94
Integrated Model limited FR cap.	38.45	29.73	-3.18	38.32

4.2.2 Impact of Limited Regulation Capacity

Figure 4.5 and Figure 4.7 present the results of the Base Case and Integrated Models considering limited and unlimited FR capacity, respectively, and no CDs; likewise, Figure 4.6 and Figure 4.8 present the two cases considering CDs in the FR process. For limited FR capacity without and with CDs, it can be observed in Figure 4.5 and Figure 4.6 that the system frequency is close to 60 Hz between 0 to 3,550 s as compared to the rest of the interval of analysis; however, beyond this time interval the frequency is consistently below 60 Hz except for a few momentary spikes, due to a change in the value of NI_s. Observe, that at all times the frequency is within the normal frequency range (i.e., 60 Hz $\pm$ 0.02 Hz [85]).

When considering unlimited FR capacity, both power and energy capacity are assumed unlimited in TGs and ESSs, and thus the SoC model of the ESS facilities are ignored. Hence, the SOC_{FESS}% and SOC_{BESS}% signals in Figure 4.7 and Figure 4.8 remain at their initial values of 50% assumed for this study, and do not change. In this case, note in these figures that the Base Case becomes unstable, without and with CDs. This happens because $RegA$ and $RegD$ are generated independent of each other, resulting in an uncoordinated operation of the FR resources. A similar FR signal is sent to the AGC block,

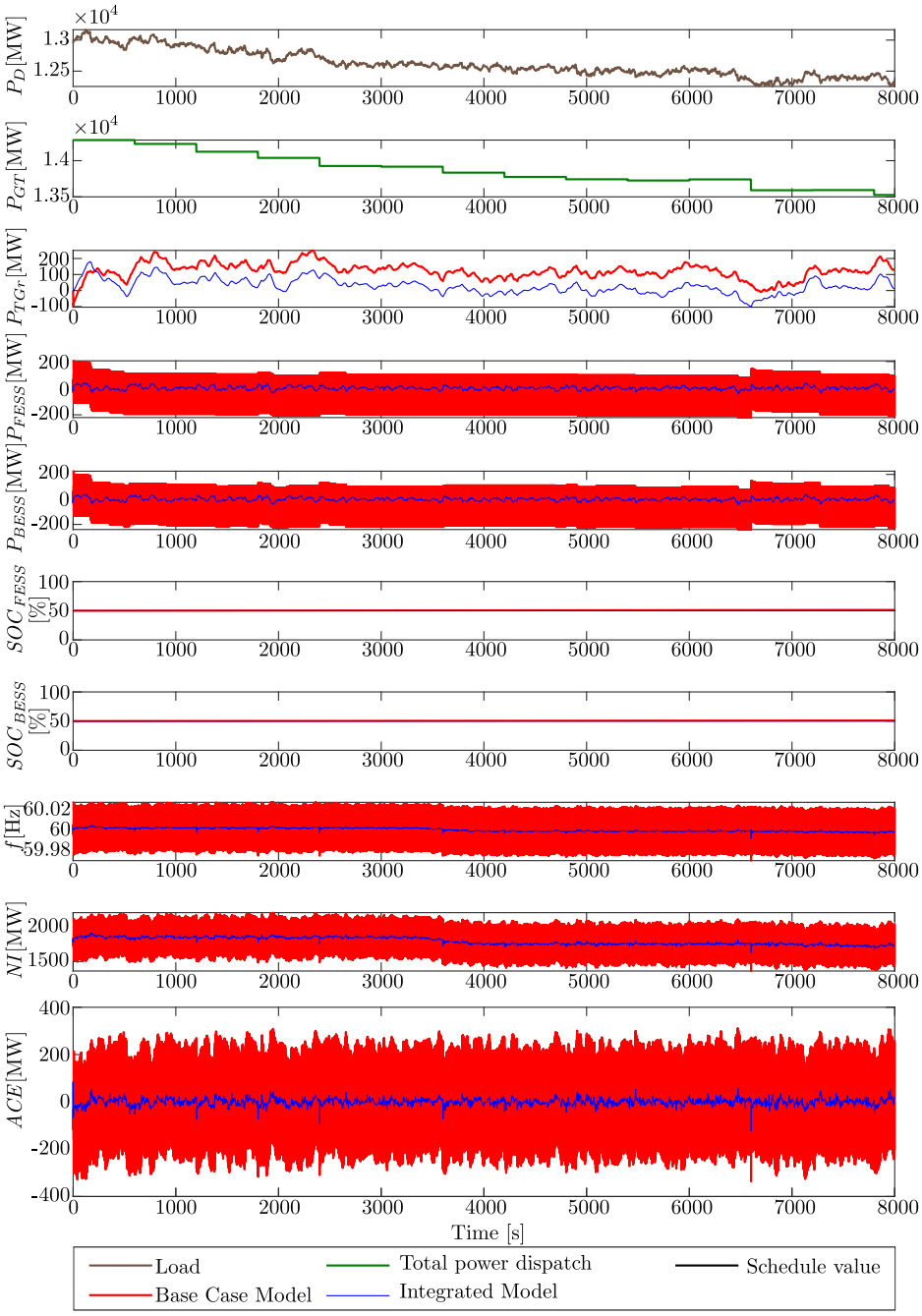

Figure 4.7: Base Case Model and Integrated Model comparison for unlimited FR capacity and without considering CDs.

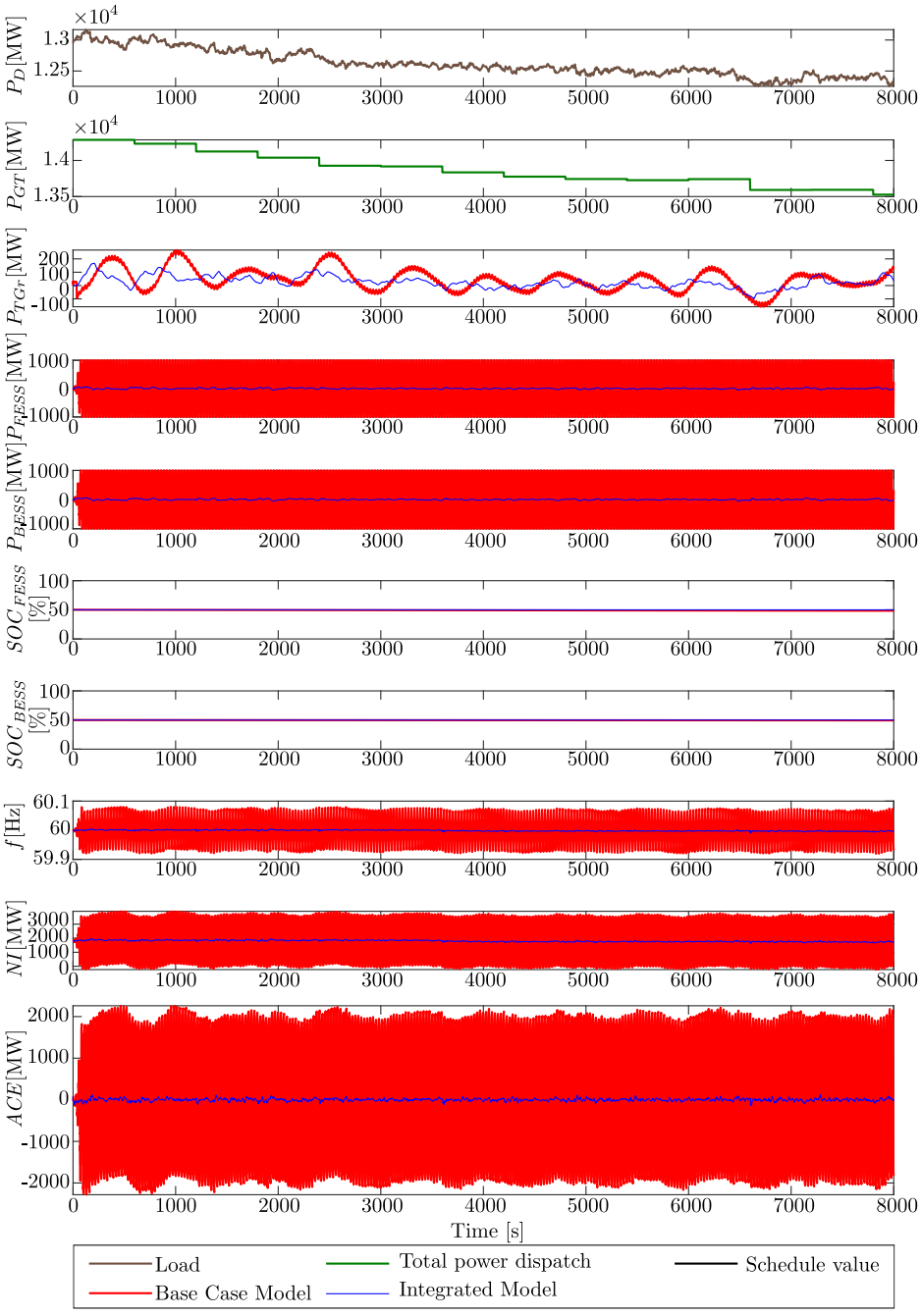

Figure 4.8: Base Case Model and Integrated Model comparison for unlimited FR capacity and considering CDs.

where the $RegA$ is calculated, and sent to the SP calculation blocks, where SP_{FESS} and SP_{BESS} are calculated, which are basically the same signal scaled to each facility's capacity; however, since unlimited capacity is considered, the entire $RegD$ is sent to both FESS and BESS. Hence, at every time interval, three times the FR requirement is requested from the regulation facilitates (TGs, FESS, and BESS); such overcompensation creates a regulation requirement in the opposite direction of the error on top of the generation-load mismatches for the next time interval. This keeps happening at every time interval making the system unstable. The situation is worse when CDs are considered, since the ACE keeps accumulating due to overcompensation of regulation resources and also due to the delays in the response from facilities contracted for FR.

Table 4.2: Impact of regulation capacity limit on the FR process.

Case	RMSE [MW]	MAE [MW]	Mean [MW]	SD [MW]
No CDs				
Base Case Model unltd. FR cap.	231.45	229.36	-1.28	231.46
Integrated Model unltd. FR cap.	13.53	10.39	-0.01	13.53
Base Case Model ltd. FR cap.	32.57	25.16	-4.60	32.24
Integrated Model ltd. FR cap.	21.79	14.52	-2.22	21.68
With CDs				
Base Case Model unltd. FR cap.	1632	1505	-1.40	1632
Integrated Model unltd. FR cap.	31.33	24.35	-0.06	31.32
Base Case Model ltd. FR cap.	46.35	36.45	-6.15	45.94
Integrated Model ltd. FR cap.	38.45	29.73	-3.18	38.32

Table 4.2 presents the RMSE, MAE, mean, and SD of the ACE signal related to all cases with limited and unlimited FR capacity and without and with CDs. The Integrated Model yields better results compared to the Base Case Model under the same conditions, in all the cases. In addition, as expected, when unlimited FR resource capacity is considered in the Integrated Model, the RMSE, MAE, mean, and SD of the ACE are close to zero compared to the cases with limited FR resources. The ideal case presented in this table corresponds to the Integrated Model considering unlimited FR capacity and no CDs. However, the ACE is not zero in this case because the TGs have a time response characteristic that causes some accumulation of the ACE, but the MAE is reduced by 72% compared to the Base Case Model using limited FR capacity and considering CDs. Even though the ideal case may not be achievable due to impossibility to eliminate all CDs, this result provides an idea of the maximum improvement in the FR process, measured as a reduction in the

ACE profile.

Considering unlimited capacity in the Integrated Model and analyzing the maximum regulation requirement allows for overall power sizing of traditional and fast regulation requirements to achieve optimal ACE reduction. Thus, when analyzing the case with CDs, the maximum regulation capacities from TGs, FESS, and BESS are ±167 MW, ±61 MW, and ±61 MW, respectively, while for the case without CDs the maximum required capacities are ±180 MW, ±42 MW, and ±42 MW, respectively. These capacities are for a time interval of 8000 s, but longer time periods could be analyzed following the same procedure.

Table 4.3: Impact of TG capacity on FR for the proposed $\mathcal{H}_2$ filter.

Case	RMSE [MW]	MAE [MW]	Mean [MW]	SD [MW]
Base Case Model with limited FR capacity and CDs				
100 MW TGs, 50 MW ESSs	46.35	36.45	-6.15	45.94
Integrated Model with limited FR capacity and CDs				
100 MW TGs, 50 MW ESSs	38.45	29.73	-3.18	38.32
90 MW TGs, 50 MW ESSs	38.73	29.96	-3.86	38.53
80 MW TGs, 50 MW ESSs	39.65	30.42	-4.71	39.37
70 MW TGs, 50 MW ESSs	40.52	30.71	-5.61	40.13
60 MW TGs, 50 MW ESSs	41.50	31.28	-7.30	40.86
50 MW TGs, 50 MW ESSs	42.47	31.68	-9.16	41.48

The proposed filter has the potential to impact the FR capacity required by the system, as a comparison of the results shows for the Base Case Model and Integrated Model with limited capacity and CDs, which reflect the existing system FR limitations. Thus, varying FR capacities for TGs were considered, while keeping the ESSs' capacities fixed at 50 MW, as shown in Table 4.3. Note that when the total FR capacity is reduced by 30 MW of the Integrated Model, i.e., for 70 MW of TG capacity, the RMSE, MAE, Mean, and SD for the ACE are closer to zero compared to the Base Case Model. Observe also that, even by reducing 50 MW of FR TG capacity in the Integrated Model, most of the results in Table 4.3 are closer to zero than the ones obtained for the Base Case Model.

The IESO spent $\$51,197,491$ in FR for the period of January 1, 2019, to December 31, 2019, scheduling typically ±100 MW of TG at all times [63]; thus, the approximate cost of 1 MW of scheduled FR capacity would be $\$511,975$. Assuming that similar and possible better system FR can be accomplished with the planned ±150 MW total FR capacity of

slow and fast resources considered in Table 4.3, for the same period and at the same cost per MW, the total FR costs would be $\$76,796,250$. Therefore, by implementing the proposed filter, which would allow to reduce the FR capacity by at least 30 MW, as it improves the system FR with respect to the Base Case Model, the total potential savings for the IESO would be $\$15,359,250$. This potential savings only relates to the operational costs of the system without considering further potential savings due to additional infrastructure requirements or economic benefits of lower ACE values. In spite of the broad assumptions made on this calculation, the likely cost savings demonstrate the possible economic benefits, besides the technical ones, of the proposed filter.

4.2.3 Effect of Proposed ESS Set-point Calculation

Table 4.4: Impact of PSP calculation in the FR process.

Case	RMSE [MW]	MAE [MW]	Mean [MW]	SD [MW]
Base Case Model SP calculation	46.35	36.45	-6.15	45.94
Integrated Model SP calculation	44.00	34.06	-3.71	43.85
Integrated Model PSP calculation	38.45	29.73	-3.18	38.32

The effect of the PSP calculation using the Integrated Model is presented in Figure 4.9, and considers CDs and limited FR capacity. The RMSE, MAE, mean, and SD of the ACE for the Base Case, which uses the SP calculation, and the Integrated Model with the SP and PSP calculation, are presented in Table 4.4. Although, the SP calculation in the Integrated Model provides smaller errors as compared to the Base Case, the PSP calculation in the Integrated Model yields better results and allows taking advantage of the coordinated control provided by the proposed $\mathcal{H}_2$ filter strategy.

4.2.4 Effect of Proposed Anti-windup Strategy

Figure 4.10 presents a comparison of the Integrated Model without and with the proposed anti-windup strategy explained in Section 4.1.2. Although, the Integrated Model ignoring or including the anti-windup strategy yields better ACE than the Base Case, as shown in Table 4.5, the anti-windup strategy reduces the ACE further by avoiding saturation when all the facilities reach their limits, or when the TGs are at their capacity limits

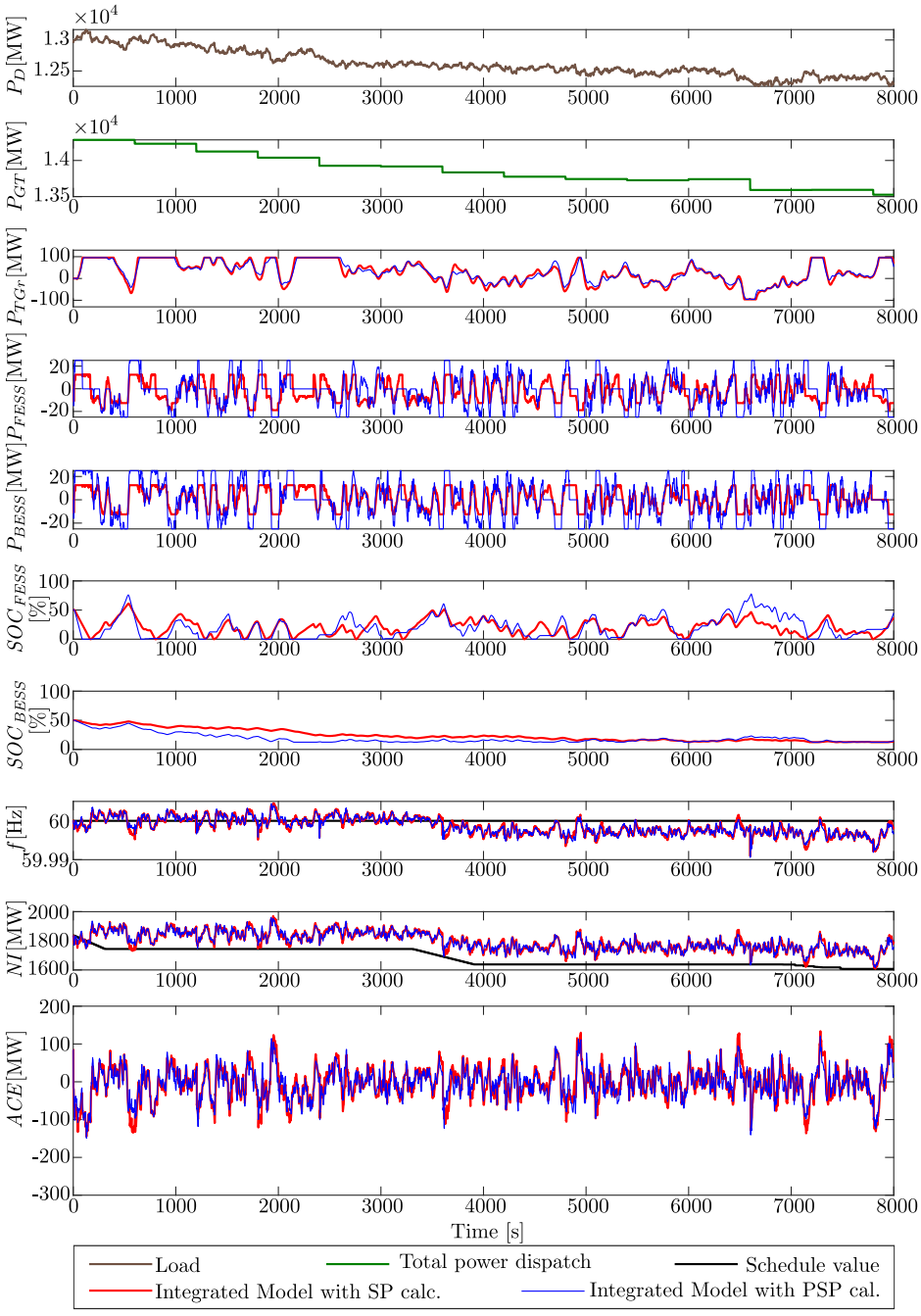

Figure 4.9: Integrated Model with SP and PSP calculation comparison for limited FR capacity and considering CDs.

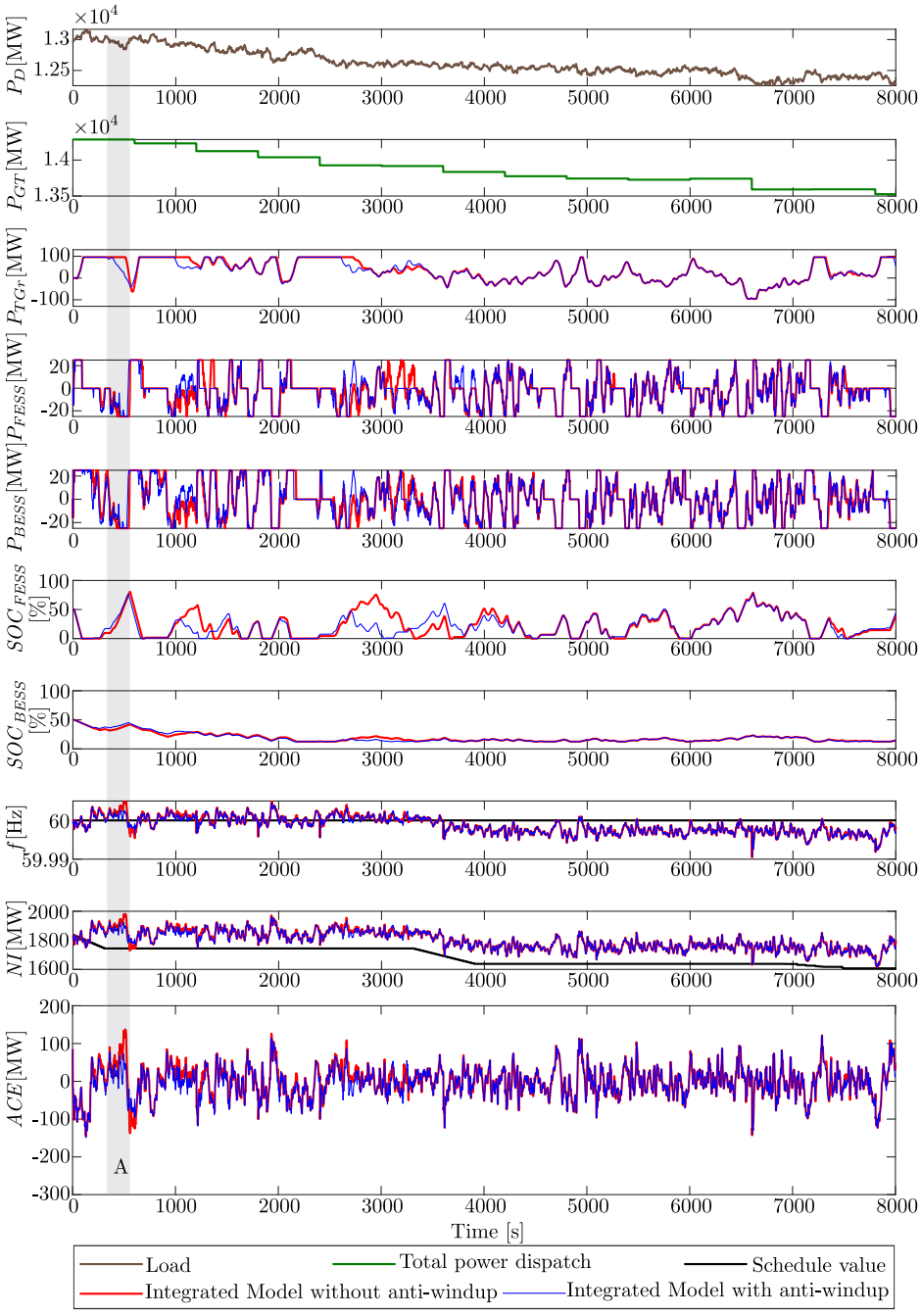

Figure 4.10: Integrated Model with and without anti-windup strategy comparison for limited FR capacity and considering CDs.

Table 4.5: Impact of anti-windup strategy on the FR process.

Case	RMSE [MW]	MAE [MW]	Mean [MW]	SD [MW]
Base Case Model	46.35	36.45	-6.15	45.94
Integrated M. without anti-windup	40.88	31.45	-0.28	40.88
Integrated M. with anti-windup	38.45	29.73	-3.18	38.32

and the ESS cannot follow *RegD* due to their SoC. An example of the effect of the anti-windup strategy when saturation occurs is highlighted in the shaded area A in Figure 4.10, where the saturation condition and the lack of anti-windup strategy yields a larger ACE as compared to the case with anti-windup. Since saturation cases can occur several times during the day, the presence of the anti-windup strategy is essential to take full advantage of the proposed $\mathcal{H}_2$ filter.

The standard filter design method used in this thesis guarantees local stability and robustness of the overall system [82]. Thus, the Integrated Model was designed to be locally stable, which is confirmed by the results of the simulations depicted in Figure 4.5 to Figure 4.10. In particular, Figure 4.7 and Figure 4.8 show that the overall nonlinear system that includes the designed filter is stable and robust, since it stabilizes the system under the conditions that cause instability in the Base Case Model.

4.3 Summary

This chapter presented an optimized $\mathcal{H}_2$ filter strategy to split the FR signal into a slow *RegA* signal sent to TGs, and a fast *RegD* signal sent to ESSs, to take advantage of the fast response characteristics of FESS and BESS. The proposed $\mathcal{H}_2$ filter strategy was implemented on the Base Case FR Model of the OPS presented in Chapter 3. The quantification of the impact of the proposed filter strategy on the FR performance was measured in terms of the reduction in ACE. Simulation results for the OPS showed that, in all cases, the proposed filter yielded better results as compared to the existing FR process. It was noted that CDs negatively affected the FR process and a 60% reduction in the MAE of ACE was achieved by adding the proposed filter strategy and eliminating the CDs, with the same FR capacity; the proposed filter produced FR signals that worked in a coordinated manner avoiding instability in the system. Furthermore, it was shown that the proposed Integrated Model could be used for sizing of FR facilities by assuming unlimited ESS capacity. A PSP calculation method and anti-windup strategy were also proposed to take full advantage of the novel $\mathcal{H}_2$ filter strategy, demonstrating their relevance for the

FR process. Overall, it is shown from the ISO perspective that the participation of ESS and the proposed filtering strategy can improve the performance of the regulation process and reduce the overall capacity requirement for FR services.

Chapter 5

Marginal Rate of Technical Substitution of Traditional with Dynamic Regulation Signals

This chapter presents a detailed methodology to develop IESO's MRTS curves, which can be used to optimally determine the appropriate substitution of *RegA* capacity with *RegD*, considering different ESS technologies and discharging times, scenarios, and seasons. Different comparisons of the MRTS curves are carried out, and the criteria used to obtain 16 average optimized MRTS curves, four per season, is presented. Finally, the 16 MRTS curves obtained for the IESO and their parameters are presented.

5.1 Definitions

The IESO is considering implementation of fast FR services using ESS in the IAM [18]. To this effect, it is important to determine the benefits of including fast resources to the FR service provisions, and analyzing the trade-offs among resources with similar performance characteristics. This can be accomplished with the aid of MRTS curves based on [19] and [38]. The methodology proposed in this work is generic and can be applied to any other ISOs with appropriate modifications.

The MRTS measures the reduction in one of the inputs vis-a-vis the increase in another input that is just sufficient to maintain a constant level of output [86]. In this thesis, the MRTS curve represents the *RegA* capacity that must be substituted by one more unit of

$RegD$ while maintaining the same output level or performance metric selected, such as RMSE of the ACE. Indeed, these MRTS curves help determining the $RegA$ capacity (in MWs) provided by conventional generators that can be replaced with $RegD$ capacity from ESSs, so as to reduce the total regulation capacity used, which is envisaged to decrease the cost of procuring FR services for the ISOs.

An isoquant is a curve in the input space that shows all possible combinations of inputs which produce the same level of output, and a family of isoquants is an isoquant map, as shown in Figure 5.1, where Is_1, Is_2, and Is_3 are isoquants which together form an isoquant map. The higher the position of an isoquant, with respect to another, the higher it its level of output [86, 87]. For example, Is_3 has a higher output value than Is_2 and Is_1, while Is_2 has higher output than Is_1.

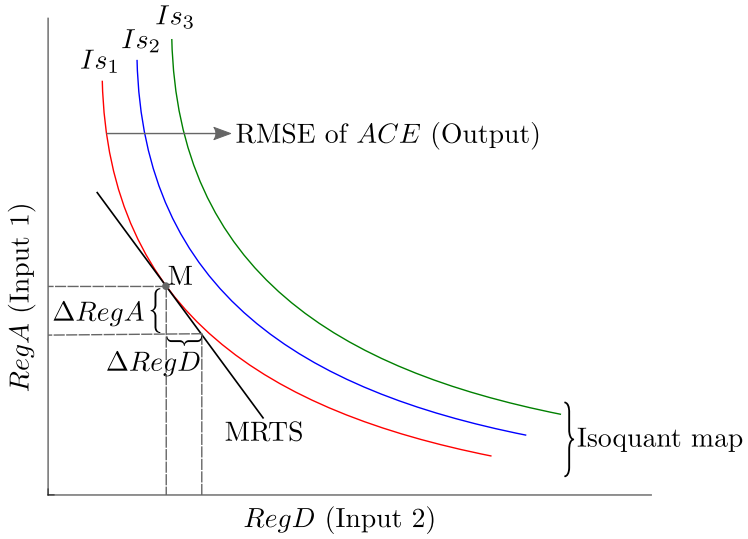

Figure 5.1: Isoquant map.

In Figure 5.1, the MRTS of $RegA$ (Input 1) for $RegD$ (Input 2), at any point on the isoquant, is denoted by $MRTS_{RegD,RegA}$, and can be defined as the negative of the slope of the isoquant at that point. Also, defining the marginal product of $RegD$ as $MP_{RegD} = \frac{\partial Is_1}{\partial RegD}$ and the marginal product of $RegA$ as $MP_{RegA} = \frac{\partial Is_1}{\partial RegA}$, for any point on an isoquant Is_1 (e.g., M) in Figure 5.1, maintains the output RMSE of ACE unchanged, i.e., $\Delta Is_1 = 0$. Hence, by linearizing Is_1, it follows that [87],

$$\begin{aligned} \Delta Is_1 &\approx MP_{RegD}\Delta RegD + MP_{RegA}\Delta RegA = 0 \\ &\implies MP_{RegD}\Delta RegD = -MP_{RegA}\Delta RegA \end{aligned} \tag{5.1}$$

Thus, solving for the slope of the isoquant $\frac{\Delta RegA}{\Delta RegD}$:

$$\left.\frac{\Delta RegA}{\Delta RegD}\right|_{\Delta Is_1=0} = -\frac{MP_{RegD}}{MP_{RegA}} \tag{5.2}$$

And, since $MRTS_{RegD,RegA}$ is the negative of the slope of the isoquant curve, the following definition can be obtained:

$$MRTS_{RegD,RegA} = -\left.\frac{\Delta RegA}{\Delta RegD}\right|_{\Delta Is_1=0} = \frac{MP_{RegD}}{MP_{RegA}} \tag{5.3}$$

5.2 Criteria for Generating MRTS Curves for IESO

In 2017, PJM proposed the use of MRTS curves to replace the BF curve being used, which measured the relative value of fast *RegD* versus the slower *RegA* resources, and was implemented in the regulation market [56]. Most of the flaws in the regulation market of PJM could be attributed to improper implementation of the BF curve between *RegA* and *RegD* resources, which causes both under- and over-payment for *RegD* resources, and over-procurement of *RegD* during some hours [11, 12]. The MRTS curves can be considered an improved version of the BF curve, but these have not been implemented, as they were rejected by FERC [13], because of settlement related inconsistencies with FERC Order No.755 [14]. Since the IESO is not under FERC jurisdiction, it can take advantage of the proposed MRTS curves and learn from PJM experiences.

The IESO has been considering introduction of fast resources in its FR process since 2012. Hence, it is essential to determine the benefit of adding fast resources to the FR process and analyzing the alternate trade-off resources that yield the same performance. The former can be achieved by using heat maps, while the latter can be addressed by using MRTS curves.

In the work presented in this Chapter, the following criteria for creation of heat maps and MRTS curves have been agreed upon with the IESO:

- The range of total regulation capacity (*RegA*+*RegD*) considered is between 40 and 300 MW.
- Incremental steps of 5 MW of fast and slow regulation capacity are considered when determining the *RegA*-*RegD* pairs of equivalent control.

- The performance metric selected for generation of heat maps is the RMSE of ACE.
- The RMSE of ACE obtained for a 100 MW *RegA* and 0 MW *RegD* is used to generate the isoquant curve, which is consistent with the current regulation service scheduled by the IESO [63].
- The following three features are considered in the MRTS curve generation for different ESS technologies and discharging times, scenarios, and seasons:
  - The FESS and BESS are considered for the studies, one at a time, since their SoC management are different. An FESS with discharging time of 15 min and a BESSs with discharging times of 15 min, 1 h, 2 h and 4 h have been selected for this study.
  - The scenarios considered for each representative day are Peak hours, Non-peak hours, Morning ramp hours, and Evening ramp hours (Table 5.1).
  - One representative typical day is selected per season, which is a non-holiday weekday.

  Thus, 16 MRTS curves are generated per ESS technology and discharging time, with a total of 80 MRTS curves.
- A multi-segment approach is used when generating the MRTS curves.

Table 5.1: Scenarios considered for the generation of the IESO's MRTS curves.

Scenarios	Summer	Fall	Winter	Spring
Peak hours	6 am to 10 pm			
Non-peak hours	10 pm to 6 am			
Morning ramp	5 am to 8 am			
Evening ramp	6 pm to 9 pm	8 pm to 11 pm		

Although this thesis does not focus on electricity markets, it is worth mentioning that the IESO can use the MRTS curves together with pricing data to determine the optimal combination of *RegD* and *RegA* resources to meet the system regulation requirement, while maintaining the same level of FR performance at minimum cost. Thus, when solving for the optimum combination of resources, *RegD* would substitute *RegA* when *RegD* is cheaper. The *RegD* resources determined using MRTS curves can be assigned a base payment and a mileage payment component, to provide a fair compensation for the service actually provided by fast resources. The value of *RegD* capacities should also be kept in mind by the IESO when planning for potential increments in regulation capacity.

5.2.1 Seasonal Representative Typical Days

The data considered was provided by the IESO and corresponds to March 1, 2019 to February 28, 2020, re-sampled to 1 s resolution. The following is the methodology used to select the representative typical days per season that will be used to generate the MRTS curves:

1. Consider the load curve data for all the days within each season.
2. Find the mean of the load curves for each season.
3. Calculate the MAE between the load curve of each day and the mean load curve for a season.
4. Select the day with the lowest MAE with respect to the mean load curve.
5. Verify that the selected days are weekdays and not holidays; if a holiday or weekend, select a day with the next lowest MAE.

Figure 5.2 presents an example of this methodology applied to the Fall season. The daily load curves for all days in Fall are shown, and the mean load curve is highlighted in red in the middle of the green shaded area, corresponding to one standard deviation. The black line, close to the mean load curve, corresponds to the day with the lowest MAE with respect to the mean; thus, this is selected as the representative typical day for Fall, which corresponds to September 9, 2019. Table 5.2 presents the selected representative typical days for all seasons after repeating this methodology to each season.

Table 5.2: Selected representative days for generating the MRTS curves

Day	Month	Season	Year
3 (Wednesday)	4 (April)	Spring	2019
15 (Thursday)	8 (August)	Summer	2019
24 (Tuesday)	9 (September)	Fall	2019
4 (Tuesday)	2 (February)	Winter	2020

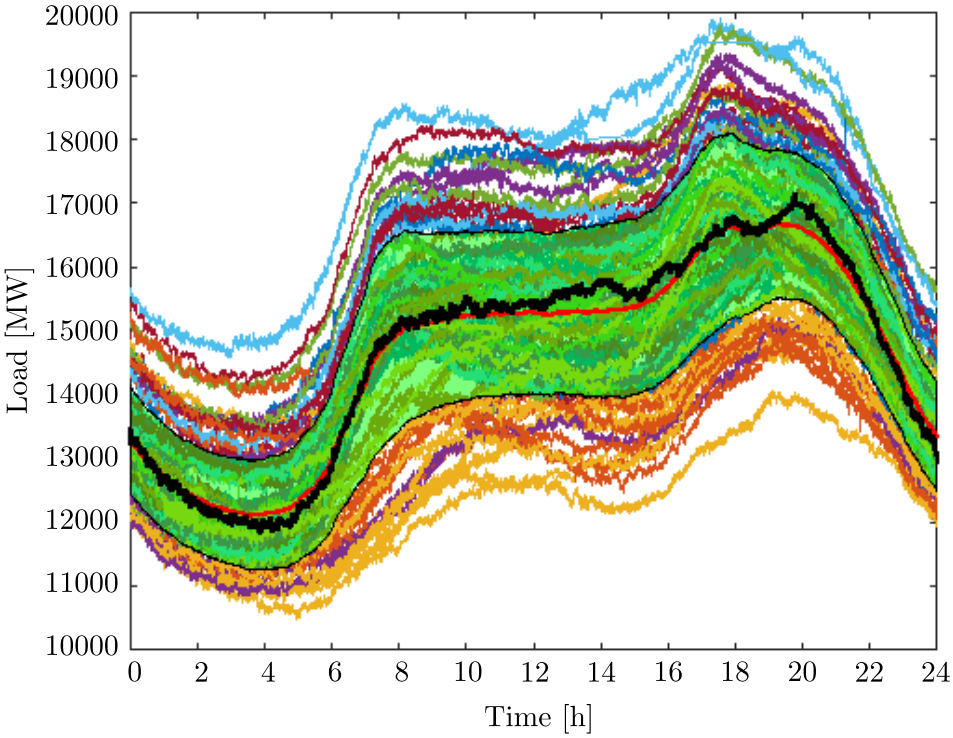

Figure 5.2: Example of the selection of a representative typical day in Fall.

5.3 Methodology for Generation of MRTS Curves

A method is proposed here drawing on the concepts from [19] and [38] to develop the MRTS curves for the OPS. Thus, the first step is to run the Integrated Model presented in Chapter 4 with CDs and one ESS technology at a time, varying the regulation capacity of fast and slow regulation resources for each scenario and season, for a total of 80 cases. As mentioned in Section 5.2, the capacity of *RegA* and *RegD* resources is increased in steps of 5 MW, for a total regulation capacity varying in the range of 40 MW to 300 MW. The initial state of the system corresponds to a point where the regulation resources are sufficient for the interval of analysis, thus allowing *RegD* and *RegA* trading. The initial ACE for all the simulations within the same case is selected as the initial ACE for the corresponding representative typical day at 100 MW regulation requirement, i.e., *RegA*=100 MW and *RegD*= 0 MW. The RMSE of the ACE for the interval of analysis is the performance metric and thus, for each simulation which considers one day of data with 1 s resolution,

is calculated, saved and used to generate heat maps.

5.3.1 Heat Maps

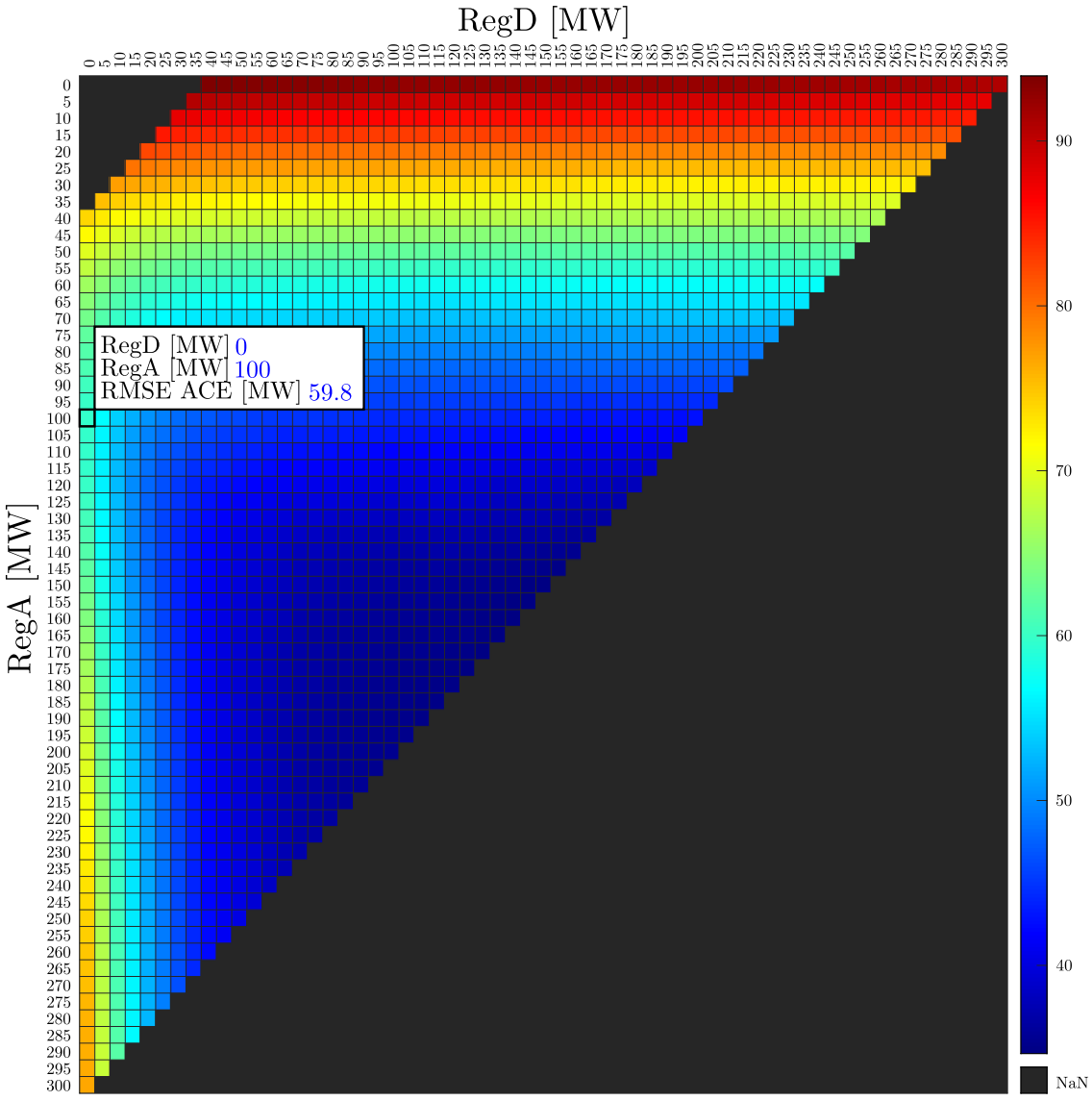

Figure 5.3: Example of heat map for Fall season, Peak hours scenario, and 4 h BESS.

Heat maps allow visualizing the value of the performance metric in color, on a two-

dimensional plot of *RegA* versus *RegD*. These heat maps contain information on *RegA* and *RegD* capacity, and the value of RMSE of the ACE, as illustrated in Figure 5.3 for one particular case; the rest of the heat maps for all cases analyzed in this work are presented in Appendix A. These heat maps allow evaluating the impact of different combinations of *RegA* and *RegD* capacities on the RMSE of the ACE, with the darkest blue indicating a mix of fast and slow resources that yields the lowest RMSE of the ACE, and with the darkest red indicating the opposite. The black areas indicate *RegA* and *RegD* capacity values not considered, as per the criteria stated in Section 5.2. Note that the ideal combination of *RegA* and *RegD* capacities, which yields the lowest RMSE of the ACE, may not be feasible because of high cost of procurement. A comprehensive analysis of all heat maps for different ESS technologies and discharging times, scenarios and seasons, allows looking at the big picture and selecting the optimal combination of regulation resources that results in the most benefit to the system, taking into account the procurement cost and capacity limits of *RegA* and *RegD* resources.

In the heat maps, as the one presented in Figure 5.3, it can be observed that for a given regulation capacity, when *RegD* capacity is increased, it results in an improvement in the performance metric; however, beyond a certain value, the performance deteriorates, which translates to reduced returns from using more *RegD* resources. The performance deterioration beyond a certain value of *RegD* is explained by the fact that these resources are typically energy limited (such as FESS and BESS) and thus will reach their SoC limits, resulting in increased ACE; hence, energy limited *RegD* resources need to be complemented with *RegA* resources [19]. Heat maps can be a powerful analysis tool for ISOs looking to expand their regulation capacity, and once the selection of performance metric and combination of regulation resources is determined, the MRTS curves can be created, as discussed next.

5.3.2 MRTS Curves

After generating the heat maps for all cases, the incremental step in the meshgrid data corresponding to *RegA* and *RegD* capacity is decreased from 5 MW to 0.02 MW, using interpolation of two-dimensional data in meshgrid format to obtain interpolated values of RMSE of the ACE; the purpose of this exercise is to increase the number of data points to generate a more accurate isoquant map. The isoquant map can then be generated from the interpolated data, with an example of this being presented in Figure 5.4, where the isoquant corresponding to the value of RMSE of ACE of 59.7966 MW (obtained for *RegA* = 100 MW and *RegD* = 0 MW, as highlighted in Figure 5.3) is selected and illustrated in Figure 5.5. The isoquant determines the *RegA*-*RegD* pairs of equivalent control, i.e.,

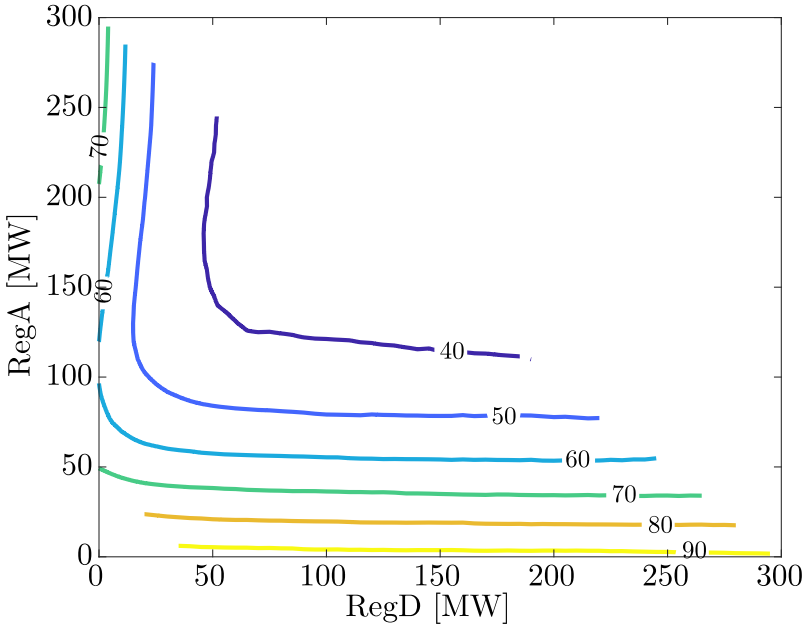

Figure 5.4: Example of an isoquant map for different values of RMSE of ACE.

equivalent RMSE of ACE. When an isoquant has two parts, as shown in Figure 5.5, only the part that allows analyzing the impact of reducing $RegA$ resources and replacing them by $RegD$ resources on RMSE of ACE is considered; this part of the curve is enclosed in a dotted square in Figure 5.5.

As agreed with the IESO and mentioned in Section 5.2, a multi-segment approach is used to generate the MRTS curves, which is a better approximation than a single-segment approach. Thus, 6 $RegD$ MW-intervals are considered with cuts at 5, 10, 25, 50 and 75 MW on the $RegD$ axis, producing the following intervals: [0 5], [5 10], [10 25], [25 50], [50 75], and [75 $Hv1$], where $Hv1$ is the highest value of $RegD$ for the isoquant. Each segment of the isoquant corresponding to a different $RegD$ MW-interval is denoted by a different color in Figure 5.6. For some isoquants, the value of $Hv1$ may be less than 75 MW, which will reduce the total number of $RegD$ MW-intervals. The single-segment approach was not considered to avoid the same issues that PJM had in its implementation, wherein the BF curve resulted in over-procurement of fast regulation resources [11, 12].

Each segment of the isoquant shown in Figure 5.6, can be approximated by a quadratic function. In order to determine the coefficients of the function, a constrained linear least-squares problem can be formulated for each segment u as follows:

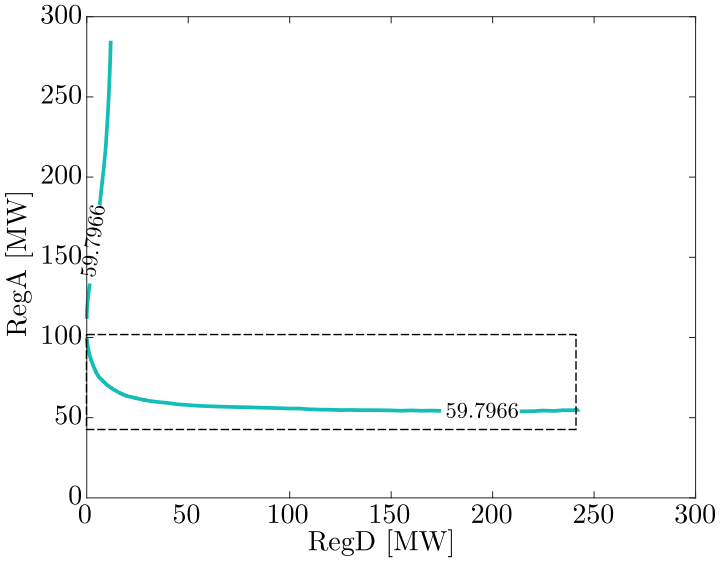

Figure 5.5: Isoquant line corresponding to 59.7966 MW RMSE of ACE in Figure 5.4.

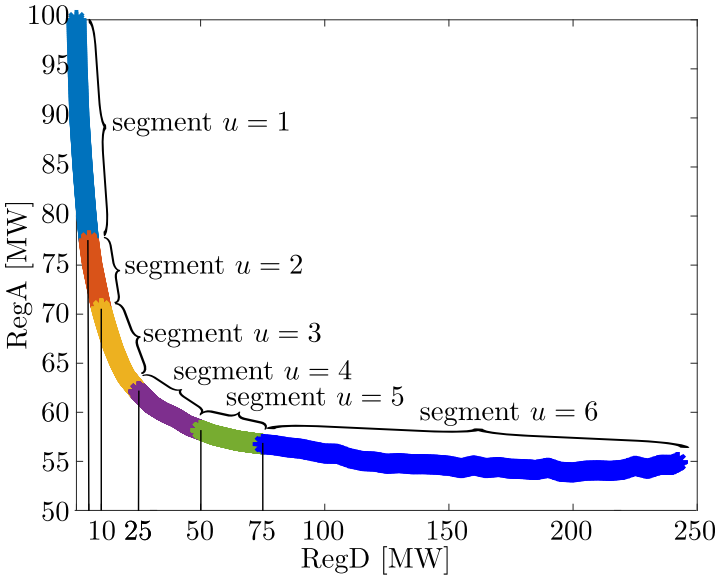

Figure 5.6: Example of an isoquant line divided in six segments.

$$\min_{\tilde{p}_1} \quad \frac{1}{2}\|\tilde{C}_1\tilde{p}_1 - \tilde{d}_1\|_2^2 \tag{5.4a}$$

$$\text{s.t.} \quad \tilde{A}eq_1\tilde{p}_1 = \tilde{B}eq_1 \tag{5.4b}$$

$$\min_{\tilde{p}_u} \quad \frac{1}{2}\|\tilde{C}_u\tilde{p}_u - \tilde{d}_u\|_2^2 \quad \forall\ (u>1) \wedge (u<T) \tag{5.5a}$$

$$\text{s.t.} \quad \tilde{A}eq_u\tilde{p}_u = \tilde{B}eq_u \quad \forall\ (u>1) \wedge (u<T), \tag{5.5b}$$

$$\tilde{A}_u\tilde{p}_u \leq \tilde{B}_u \quad \forall\ (u>1) \wedge (u<T) \tag{5.5c}$$

$$\min_{\tilde{p}_T} \quad \frac{1}{2}\|\tilde{C}_T\tilde{p}_T - \tilde{d}_T\|_2^2 \tag{5.6a}$$

$$\text{s.t.} \quad \tilde{A}eq_T\tilde{p}_T = \tilde{B}eq_T, \tag{5.6b}$$

$$\tilde{A}_T\tilde{p}_T \leq \tilde{B}_T \tag{5.6c}$$

where

$$\tilde{C}_u = \begin{bmatrix} x_{2,u}^2 & x_{2,u} & 1 \\ \vdots & \vdots & \vdots \\ x_{r,u}^2 & x_{r,u} & 1 \\ \vdots & \vdots & \vdots \\ x_{N_u-1,u}^2 & x_{N_u-1,u} & 1 \end{bmatrix} \quad \forall\ u \tag{5.7}$$

$$\tilde{p}_u = \begin{bmatrix} \tilde{a}_u \\ \tilde{b}_u \\ \tilde{c}_u \end{bmatrix} \quad \forall\ u \tag{5.8}$$

$$\tilde{d}_u = \begin{bmatrix} y_{2,u} \\ \vdots \\ y_{r,u} \\ \vdots \\ y_{N_u-1,u} \end{bmatrix} \quad \forall\ u \tag{5.9}$$

$$\tilde{A}eq_1 = \begin{bmatrix} x_{N_1,1}^2 & x_{N_1,1} & 1 \\ x_{1,2}^2 & x_{1,2} & 1 \\ x_{1,1}^2 & x_{1,1} & 1 \end{bmatrix} \tag{5.10}$$

$$\tilde{A}eq_u = \begin{bmatrix} x_{N_u,u}^2 & x_{N_u,u} & 1 \\ x_{1,u+1}^2 & x_{1,u+1} & 1 \\ 2x_{1,u} & 1 & 0 \end{bmatrix} \quad \forall\ (u>1) \wedge (u<T) \tag{5.11}$$

$$\tilde{A}eq_T = \begin{bmatrix} x_{N_T,T}^2 & x_{N_T,T} & 1 \\ 2x_{1,T} & 1 & 0 \end{bmatrix} \tag{5.12}$$

$$\tilde{B}eq_1 = \begin{bmatrix} y_{N_1,1} \\ y_{1,2} \\ y_{1,1} \end{bmatrix} \tag{5.13}$$

$$\tilde{B}eq_u = \begin{bmatrix} y_{N_u,u} \\ y_{1,u+1} \\ 2\tilde{a}_{u-1}x_{1,u} + \tilde{b}_{u-1} \end{bmatrix} \quad \forall\ (u > 1) \wedge (u < T) \tag{5.14}$$

$$\tilde{B}eq_T = \begin{bmatrix} y_{N_T,T} \\ 2\tilde{a}_{T-1}x_{1,T} + \tilde{b}_{T-1} \end{bmatrix} \tag{5.15}$$

$$\tilde{A}_u = \begin{bmatrix} 2x_{1,u} & 1 & 0 \\ 2x_{N_u,u} & 1 & 0 \\ 2x_{N_u,u} - 2x_{1,u} & 0 & 0 \end{bmatrix} \quad \forall\ u > 1 \tag{5.16}$$

$$\tilde{B}_u = \begin{bmatrix} 2\tilde{a}_{u-1}x_{1_u} + \tilde{b}_{u-1} \\ 2\tilde{a}_{u-1}x_{1_u} + \tilde{b}_{u-1} \\ 0 \end{bmatrix} \quad \forall\ u > 1 \tag{5.17}$$

In this formulation each isoquant data point is defined in the *RegD-RegA* space, given by $(x_{r,u}, y_{r,u})$, where u is the segment in a *RegD* MW-interval in the isoquant, r is the isoquant data point in a segment u, and $x_{r,u}$ and $y_{r,u}$ are the values of *RegD* and *RegA*, respectively, corresponding to the r isoquant point in segment u. The parameters T and N_u are the total number of segments in the isoquant of analysis and the total number of isoquant data points in the segment u, respectively. The matrix $\tilde{C}_u$ in (5.7) contains the values of $x_{r,u}$ to the power 2, 1 and 0 in its first, second, and third column, respectively. The vector $\tilde{p}_u$ in (5.8) contains the coefficients $\tilde{a}_u$, $\tilde{b}_u$, and $\tilde{c}_u$ of the quadratic function approximating the segment u in the isoquant. Finally, the vector $\tilde{d}_u$ in (5.9) contains the values $y_{r,u}$ for the segment u of analysis.

The first equality constraints of (5.4b), (5.5b), and (5.6b) fix the last isoquant point ($r = N_u$) in segment u. The second equality constraints in (5.4b) and (5.5b) ensure that the segments approximating the isoquant are connected, by considering the first point ($r = 1$) of the segment $u+1$. The third equality constraint in (5.4b) fixes the first isoquant point for the segment $u = 1$. The last equality constraints in (5.5b) and (5.6b) ensure that the derivative of the quadratic function approximating the segment u evaluated at its first point is equal to the derivative of the quadratic function approximating the segment $u-1$ evaluated at its last point, which is equal to the first point of the segment u. This is to ensure that the segments on the MRTS curve, which are formed by the negative of their

first derivatives of the quadratic functions approximating each segment of the isoquant, are connected to each other.

The first two inequality constraints in (5.5c) and (5.6c) ensure that the derivative of the quadratic function approximating the segment u, evaluated at its first ($r = 1$) and last point ($r = N_u$), are lower or equal to the derivative of the quadratic function approximating the segment $u-1$ evaluated at its last point, which is equal to the first point of the segment u. The third inequality constraints in (5.5c) and (5.6c) ensure that the derivative of the quadratic function approximating the segment u, evaluated at its last point minus the same derivative evaluated at its first point, be lower or equal to zero, which ensures that the segments of the MRTS have a negative slope, as desired. Figure 5.7 presents an example of the approximate quadratic curves and their equations.

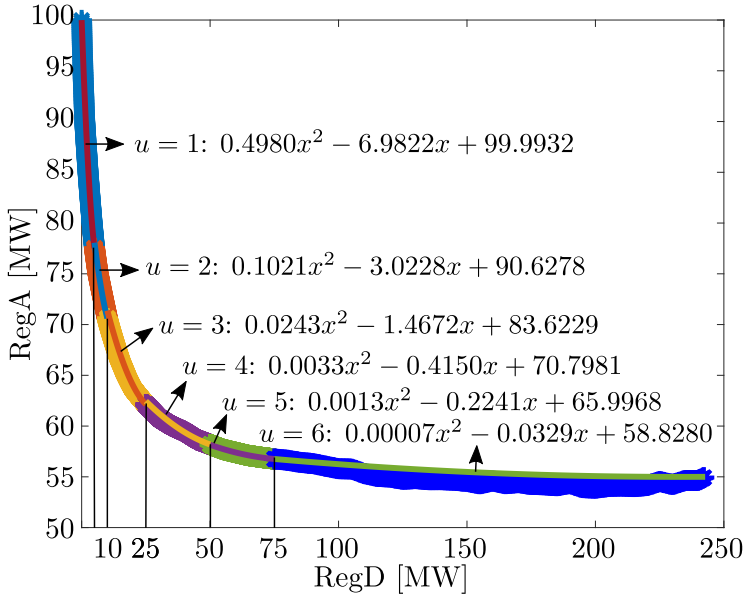

Figure 5.7: Example of approximate quadratic functions for each segment of the isoquant of interest.

Each MRTS curve is formed by the negative of the derivatives of the quadratic functions approximating the segments in the isoquant of interest, as shown for example in Figure 5.8. The parameters for all the linear functions corresponding to the MRTS curves for the cases studied in this chapter are presented in Appendix B. The formulation in (5.4) to (5.6) is applied to each segment u in the isoquant curve for all the 80 cases considered in this work, for different ESS technologies and discharging times, scenarios, and seasons. However, having 80 MRTS curves is not practical in a real system. Thus, several comparisons were

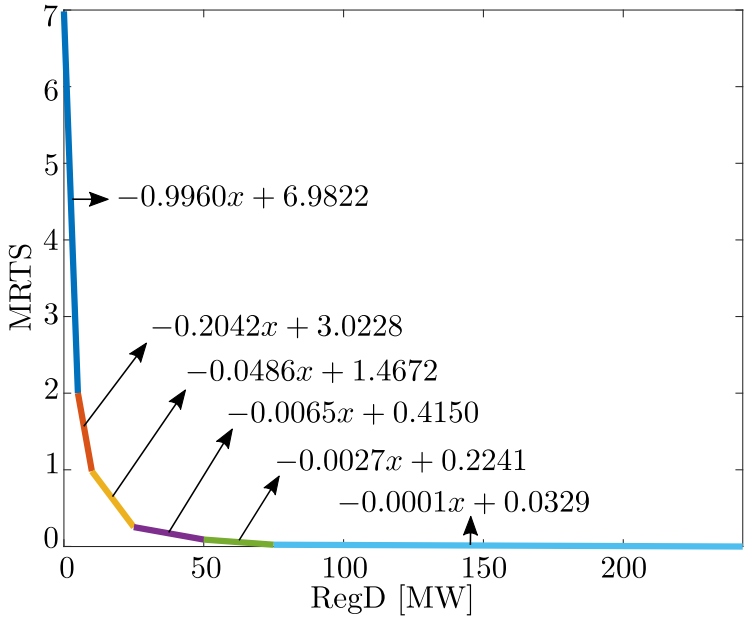

Figure 5.8: Example of MRTS curve formed by the negative of the derivatives of the approximate quadratic functions.

then carried out to determine similarities among the MRTS curves that allow establishing a criterion to reduce the number of curves. The comparisons are presented in Appendix C corresponding to Peak vs Non-peak hour scenarios per season for different ESS technologies and discharging times, Morning vs Evening ramp scenarios per season for different ESS technologies and discharging times, and different ESS technologies and discharging times per season for all the scenarios. An example of these comparisons is presented in Figure 5.9.

Comparing the MRTS curves, it is observed that the MRTS for different ESS technologies and discharging times, for the same scenario and season, have the highest similarities. Hence, average MRTS curves are obtained from each scenario and season resulting in a total of 16 average MRTS curves. To obtain these average curves, the average of each segment of all the MRTS curves that belong to the same scenario and season (different ESS technologies and discharging times) is calculated, as presented in Figures 5.10 to 5.13. However, the average segments are not necessarily connected to each other, and the maximum value of $RegD$ capacity considered may not be the same for all the curves, resulting in a discontinuity at the last segment, as shown in Figure 5.11d. To correct these issues, the average for each segment is used in the formulation of the following constrained linear least-squares problem:

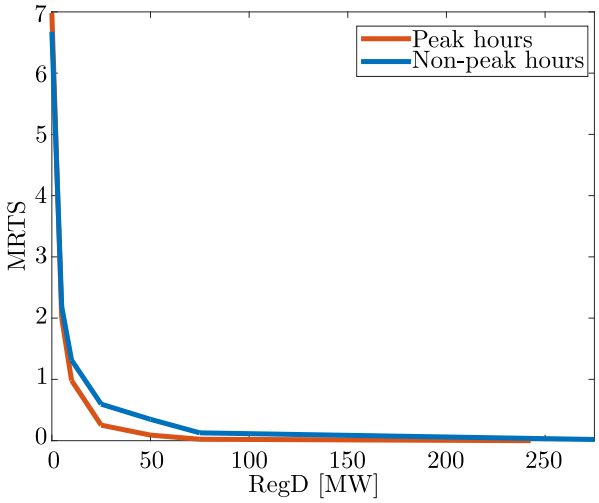

(a) Peak vs Non-peak scenarios (4 h BESS)

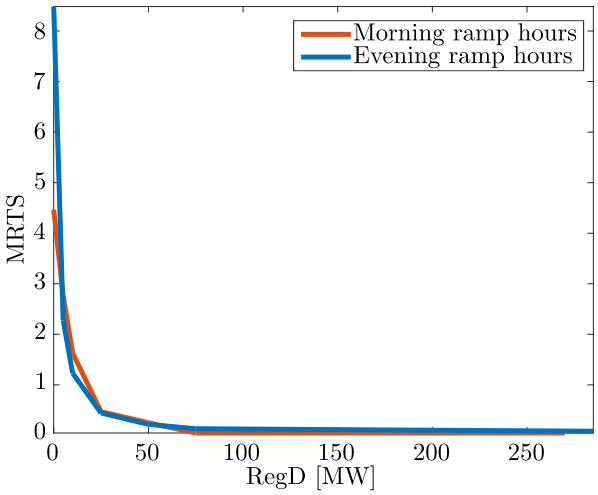

(b) Morning vs Evening ramp scenarios (4 h BESS)

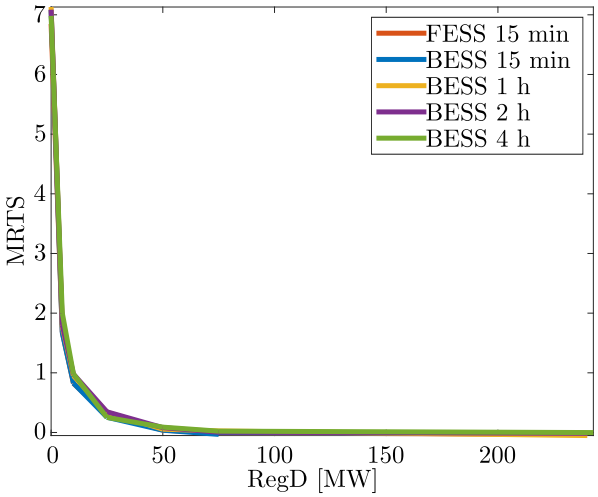

(c) Different ESS technologies and discharging times (Peak hours)

Figure 5.9: Example of criteria for comparing Fall MRTS curves.

$$\min_{\hat{p}_1} \quad \frac{1}{2}\|\hat{C}_1\hat{p}_1 - \hat{d}_1\|_2^2 \tag{5.18a}$$

$$\text{s.t.} \quad \hat{A}eq_1\hat{p}_1 = \hat{B}eq_1 \tag{5.18b}$$

$$\min_{\hat{p}_v} \quad \frac{1}{2}\|\hat{C}_v\hat{p}_v - \hat{d}_v\|_2^2 \quad \forall\ (v>1) \wedge (v<L) \tag{5.19a}$$

$$\text{s.t.} \quad \hat{A}eq_v\hat{p}_v = \hat{B}eq_v \quad \forall\ (v>1) \wedge (v<L) \tag{5.19b}$$

where

$$\hat{C}_v = \begin{bmatrix} x_{2,v} & 1 \\ \vdots & \vdots \\ x_{q,v} & 1 \\ \vdots & \vdots \\ x_{O_v-1,v} & 1 \end{bmatrix} \quad \forall\ v \tag{5.20}$$

$$\hat{p}_v = \begin{bmatrix} \hat{a}_v \\ \hat{b}_v \end{bmatrix} \quad \forall\ v \tag{5.21}$$

$$\hat{d}_v = \begin{bmatrix} y_{2,v} \\ \vdots \\ y_{q,v} \\ \vdots \\ y_{O_v-1,v} \end{bmatrix} \quad \forall\ v \tag{5.22}$$

$$\hat{A}eq_v = \begin{bmatrix} x_{O_v,v} & 1 \\ x_{1,v} & 1 \end{bmatrix} \quad \forall\ v \tag{5.23}$$

$$\hat{B}eq_1 = \begin{bmatrix} y_{O_1,1} \\ y_{1,1} \end{bmatrix} \tag{5.24}$$

$$\hat{B}eq_v = \begin{bmatrix} y_{O_v,v} \\ \hat{a}_{v-1}x_{1,v} + \hat{b}_{v-1} \end{bmatrix} \quad \forall\ (v>1) \wedge (v<L) \tag{5.25}$$

and v is the segment on the average MRTS curve, q is associated with each average MRTS curve data point in segment v, and $x_{q,v}$ and $y_{q,v}$ are the values of $RegD$ and MRTS, respectively, corresponding to the q average MRTS curve point in segment v. The parameters L and O_v denote the total number of segments v in the average MRTS curve of analysis and the total number of average MRTS curve data points in the segment v, respectively. The matrix $\hat{C}_v$ in (5.20) contains the values of $x_{q,v}$ to the power 1 and 0, in its first and second column, respectively. The vector $\hat{p}_v$ in (5.21) contains the coefficients $\hat{a}_v$, and $\hat{b}_v$ of the linear function approximating the segment v in the average MRTS curve, and the

vector $\hat{d}_v$ in (5.22) contains the values $y_{q,v}$ for the segment v of analysis.

The first equality constraints in (5.18b) and (5.19b) fix the last average MRTS curve point ($q = m_v$) for the segment v. The second equality constraint in (5.18b) ensures that the first average MRTS curve data point ($q = 1$) of segment v is a fixed value. The second equality constraint in (5.19b) ensures that all the segments within the average MRTS curves are connected, by making the linear function approximating the segment v evaluated at its first point equal to the value of the linear function approximating the segment $v - 1$ evaluated at its last point, which is equal to the first point of the segment v.

Figure 5.10 to Figure 5.13 presents the 80 MRTS curves grouped by scenarios, for all seasons, and their average MRTS curves, as well as the average optimized MRTS curves. The parameters of the linear equation for each segment of the 16 average optimized MRTS curves are presented in Table 5.3. In this table, the 6 segments of the average optimized MRTS curve correspond to the intervals [0 5], [5 10], [10 25], [25 50], [50 75], and [75 $Hv2$], where $Hv2$ is the highest value of $RegD$ for the average optimized MRTS curve. Figure 5.14 presents the final average optimized MRTS curves grouped per season for all the scenarios.

The MRTS curves help determine the MW capacity of $RegA$ that can be replaced by MW capacity of $RegD$ resources to produce the same performance metric, while decreasing the total regulation capacity used. Observe in Figure 5.14 that the average optimized MRTS curves have different starting points on the y-axis, which means that for different seasons and scenarios, different amounts of $RegA$ capacity can be replaced by one MW of $RegD$. Considering that FR provided by fast resources is likely to be more expensive, it is reasonable to consider MRTS = 1, on the y-axis of the MRTS curves, as the minimum value at which it would make sense to replace $RegA$ resources. Indeed, MRTS = 1 on the y-axis indicates that substituting $RegA$ by $RegD$ would yield the same system performance. An example of how to use the MRTS curves is presented in Figure 5.15, where 17.65 MW of $RegD$ capacity can replace 33.6 MW of $RegA$ capacity, while still maintaining the same RMSE of ACE and thereby reducing the required FR capacity from 100 MW to 84.05 MW. The 33.6 MW of $RegA$ capacity is the area under the curve, calculated using data from Table 5.3.

The IESO is at an early stage of implementation of fast FR using ESS resources in the IAM [18], and thus can take advantage of the heat maps as an analysis tool and combine them with the use of the MRTS curves to determine the appropriate value of FR capacity that the system needs, and the combination of fast and slow resources that can yield the same performance of the system, while avoiding over-procurement of FR resources. Therefore, the MRTS curves can be used to dispatch $RegA$ and $RegD$ resources at the least cost solution if price data is available.

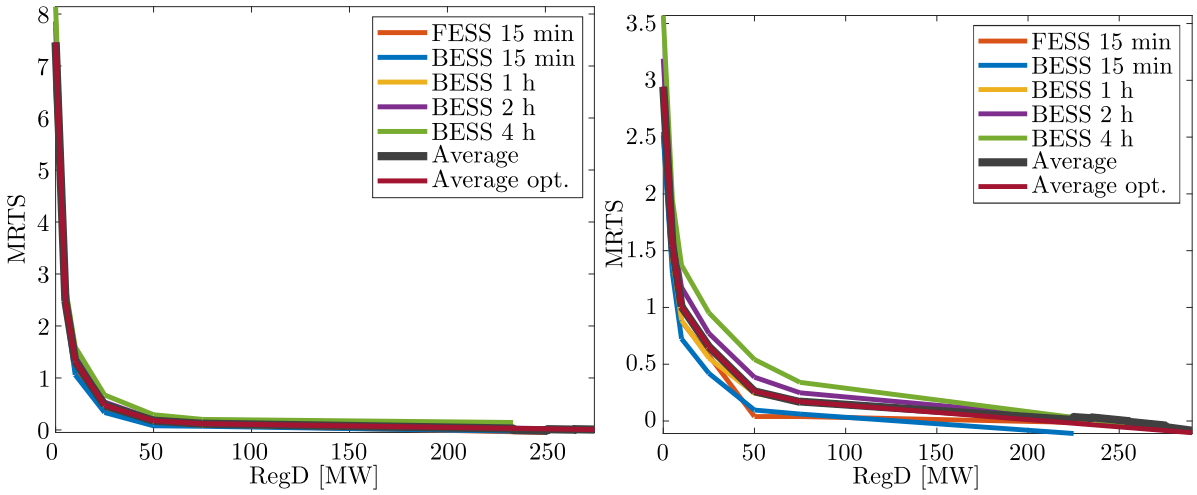

(a) Peak hours

(b) Non-peak hours

(c) Morning ramp hours

(d) Evening ramp hours

Figure 5.10: Average MRTS curves for Spring.

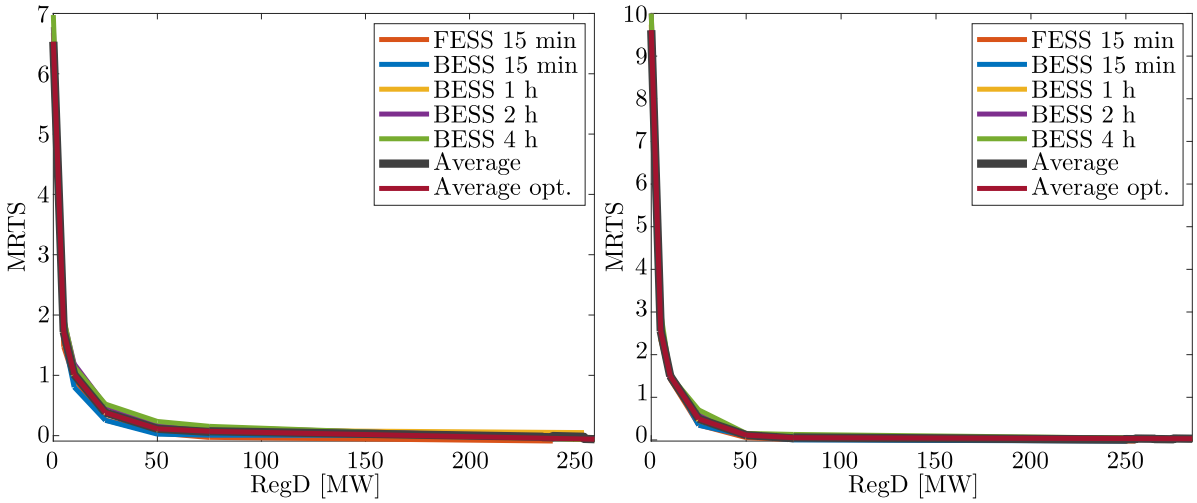

(a) Peak hours

(b) Non-peak hours

(c) Morning ramp hours

(d) Evening ramp hours

Figure 5.11: Average MRTS curves for Summer.

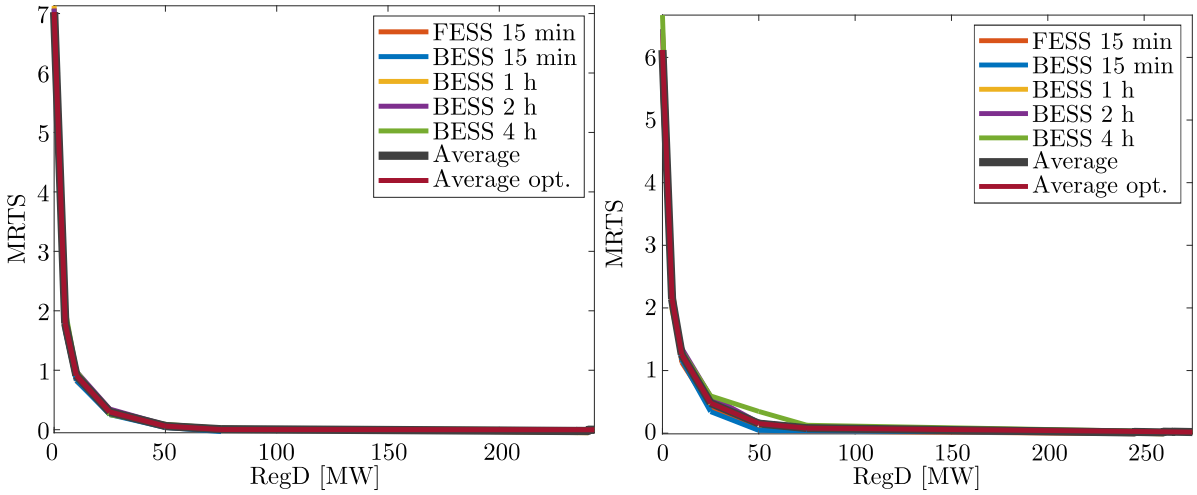

(a) Peak hours

(b) Non-peak hours

(c) Morning ramp hours

(d) Evening ramp hours

Figure 5.12: Average MRTS curves for Fall.

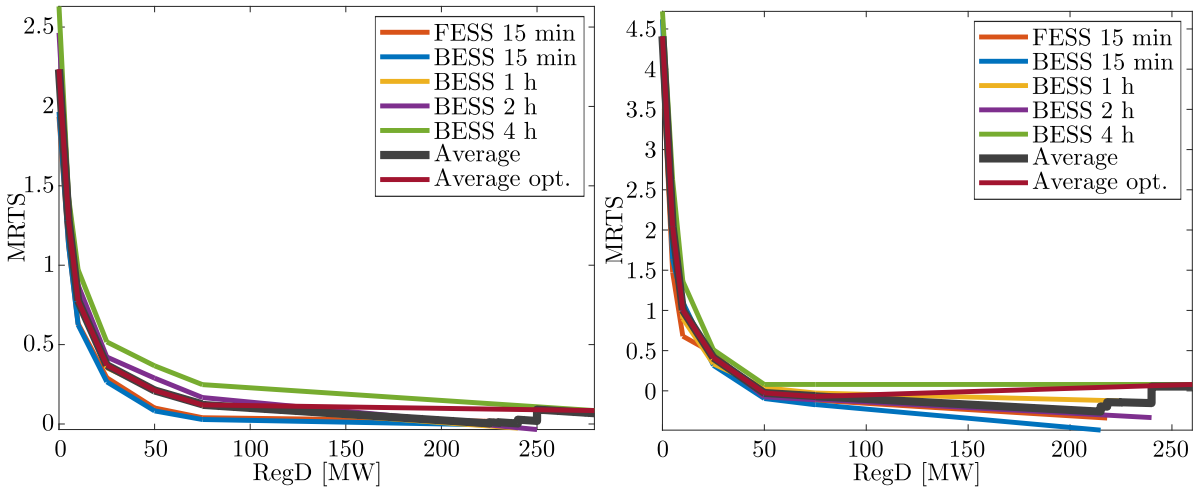

(a) Peak hours

(b) Non-peak hours

(c) Morning ramp hours

(d) Evening ramp hours

Figure 5.13: Average MRTS curves for Winter.

Table 5.3: Parameters of average optimized MRTS curves.

Scenarios	Segments	Spring		Summer		Fall		Winter	
	v	$2\hat{a}$	$\hat{b}$	$2\hat{a}$	$\hat{b}$	$2\hat{a}$	$\hat{b}$	$2\hat{a}$	$\hat{b}$
Peak hours	1	-0.9948	7.4573	-0.9621	6.5317	-1.0477	7.025	-0.1901	2.2347
	2	-0.2326	3.6458	-0.1411	2.4266	-0.175	2.6615	-0.1015	1.7921
	3	-0.0563	1.883	-0.0422	1.4375	-0.0409	1.3209	-0.0271	1.0478
	4	-0.0119	0.7736	-0.0108	0.653	-0.0095	0.5358	-0.0063	0.5286
	5	-0.0023	0.2955	-0.0017	0.1959	-0.0023	0.1764	-0.0036	0.3933
	6	-0.0006	0.1624	-0.0007	0.1251	0	0.0046	-0.0002	0.1334
Non-peak hours	1	-0.2796	2.9446	-1.4117	9.6077	-0.7961	6.1186	-0.4735	4.4091
	2	-0.1078	2.0858	-0.2105	3.6014	-0.1764	3.0202	-0.2075	3.0788
	3	-0.0235	1.2426	-0.0668	2.1649	-0.0517	1.7735	-0.0395	1.3985
	4	-0.0158	1.0495	-0.0153	0.8766	-0.0131	0.8082	-0.0175	0.8505
	5	-0.0036	0.4428	-0.0024	0.2331	-0.0029	0.2996	-0.0018	0.0623
	6	-0.0013	0.2667	-0.0001	0.0613	-0.0003	0.1039	0.0008	-0.1313
Morning ramp hours	1	-1.383	8.9788	-1.4773	9.7516	-0.3826	4.4678	-0.3955	4.1596
	2	-0.2133	3.1305	-0.1939	3.3346	-0.2162	3.636	-0.1687	3.0258
	3	-0.0367	1.3643	-0.0513	1.9079	-0.072	2.1935	-0.0442	1.7811
	4	-0.0028	0.5182	-0.0213	1.1577	-0.0102	0.6504	-0.0075	0.8631
	5	-0.0033	0.543	-0.0007	0.1306	-0.0043	0.3525	-0.0093	0.9522
	6	-0.001	0.3684	-0.0002	0.0937	0.0001	0.0244	-0.0009	0.3225
Evening ramp hours	1	-1.1646	7.7037	-0.5701	4.3952	-0.7214	5.7682	-1.0458	7.4031
	2	-0.1251	2.5063	-0.1038	2.0638	-0.199	3.1561	-0.1746	3.0471
	3	-0.0665	1.9203	-0.0716	1.7421	-0.0364	1.5304	-0.0546	1.8473
	4	-0.002	0.3076	-0.0057	0.0932	-0.0189	1.091	-0.0128	0.8026
	5	-0.0081	0.6109	-0.0038	0.0001	-0.0034	0.3162	-0.001	0.2112
	6	0.0002	-0.0106	-0.0005	0.2471	0.0001	0.0566	-0.0014	0.2418

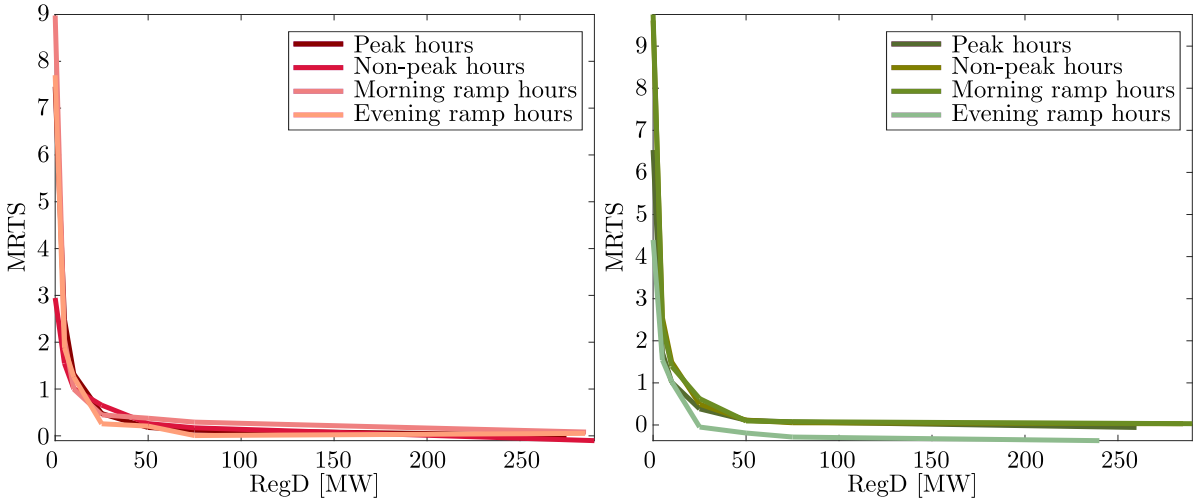

(a) Spring

(b) Summer

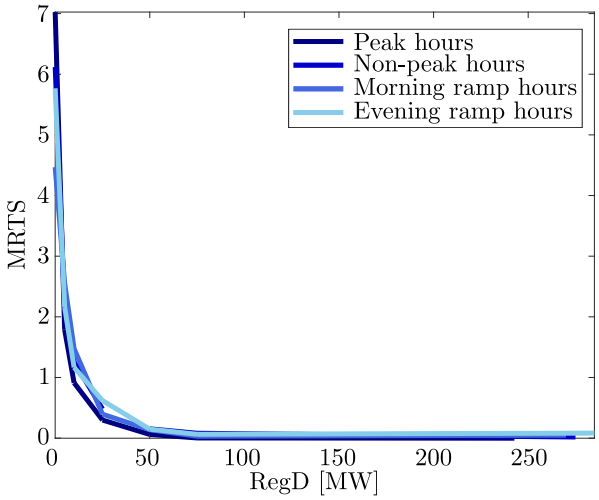

(c) Fall

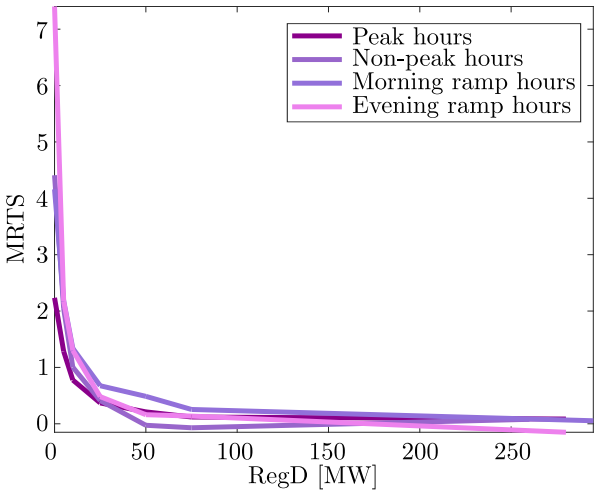

(d) Winter

Figure 5.14: Average optimized MRTS curves per season for all scenarios.

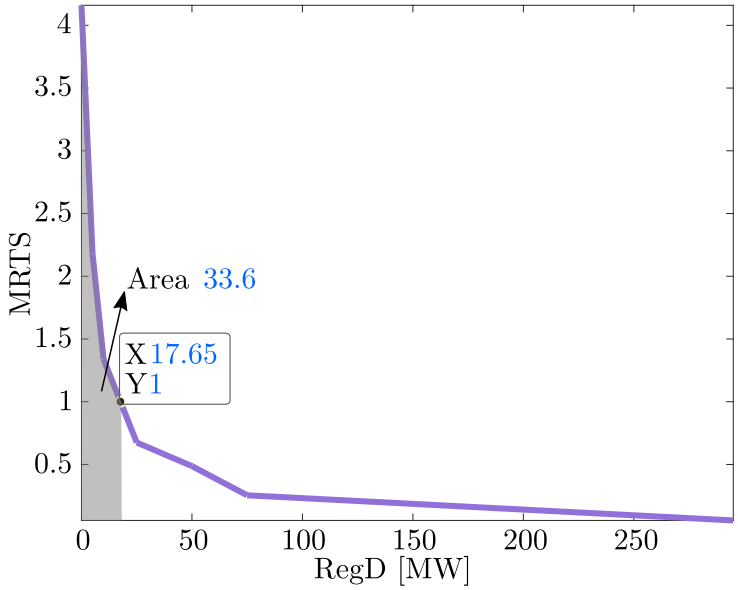

Figure 5.15: MRTS curve interpretation for Winter Morning ramp hours.

5.4 Summary

This chapter presented a detailed methodology to obtain heat maps and MRTS curves for a bulk power system. While the proposed methodology was demonstrated for the OPS, it is generic and could be applied to other ISOs with appropriate modifications. The heat maps, comparisons of MRTS curves, and parameters for the 80 MRTS curves, were discussed and are presented in Appendix A to Appendix C. The process and criteria used to obtain the 16 average optimized MRTS curves from the 80 cases, was also detailed. Finally, an example of how to use the average optimized MRTS curves was discussed. Heats maps and MRTS curves are proposed as analysis tools to allow ISOs to select the desired performance metric and the combination of *RegA* and *RegD* resources to achieve it, while still reducing the total required FR capacity.

Chapter 6

Conclusion

6.1 Summary and Conclusions

Fast FR resources can help address the issues of demand forecast errors and rapid fluctuations in frequency, arising from high penetration of RES in the bulk power systems. This thesis examined the feasibility of ESSs for FR in bulk power systems and proposed new models, taking into account CDs in signal transmission and the energy and power limitations of the ESSs.

The first part of the thesis focused on modelling of a bulk power system for FR studies from an ISO's perspective, using the OPS as a case study. The proposed model considered the bulk power system and ESSs, including the ACE calculation, ACE filtering, AGC, the aggregated model of TGs providing FR services, and the power system model. The latter model properly captured the system's primary frequency response, as well as the power on the tie-lines. The ESS models included the set-point calculation, which took into account their SoC. Similar models for BESS and FESS were developed with some distinctive features of each, because similar input and output signals were used for both facilities at the control center. The SoC was divided in operational bands to allow both charging and discharging, and a correction factor compensated for the different charging/discharging energy rates observed in the real data.

All the parameters included in the FR model were estimated using real data, re-sampled to 1 s resolution, and all the stages in the FR model were validated using a detailed dynamic transient stability model of the NAEI, as well as real system and ESS data for the OPS. The proposed FR model considered all the main stages of the FR control process, including

CDs and the SoC management model of the ESS facilities, thus ensuring a realistic closed-loop response. Therefore, these models were used to analyze the impact of CDs and the SoC model on the FR process, as well as assessing the computational efficiency of the proposed FR model.

The second part of this thesis focused on developing a filter design procedure to optimally split the FR signal between conventional and fast-regulating assets. The design approach comprised filtering the FR signal by producing a slowly-varying component ($RegA$) to be sent to the TGs, and a fast component ($RegD$) to be sent to the BESS and FESS facilities to take advantage of their fast response characteristic. The design of the filter was formulated as an optimal control problem, consisting of a GP that included weights associated with the disturbance inputs and the error outputs to be minimized. The GP was constructed from a simplified nonlinear version of the proposed FR model (Base Case FR Model). A detailed step-by-step process on how to obtain the GP was described. Various weighting filters penalized the disturbance inputs and error outputs, allowing to shape the closed-loop response. The GP was interconnected with the filter to be designed, which processed the available measurements to produce the control signals.

The optimal control problem, which was solved in an $\mathcal{H}_2$ framework, required the computation of a filter which minimized the norm of the transfer function from the disturbance inputs to the error outputs. The proposed Integrated Model comprised the Base Case FR Model, with a PSP calculation replacing the SP calculation, and substitution of the ACE filtered and AGC blocks by the designed $\mathcal{H}_2$ filter. The $RegA$ and $RegD$ signals, which were the outputs of the designed filter, were passed through a limiter block to account for the regulation capacity of TGs and ESSs. In addition, an anti-windup strategy was added to avoid saturation of the filter. Therefore, the proposed $\mathcal{H}_2$ filter sent $RegA$ and $RegD$ signals, which considered the SoC of ESSs and the capacity limits of ESSs and TGs, and depended on the conditions of the system, working in a coordinated manner.

Simulation results comparing the proposed Integrated Model and the Base Case FR Model for the OPS were presented. The impact of CDs and limited FR capacity from the ESSs, and the effect of PSP calculation and proposed anti-windup strategy were analyzed.

In the third part of this thesis, the MRTS curves for the IESO were generated, considering different ESSs and discharging times, scenarios, and seasons, for a total of 80 cases, and using one-year data from the OPS. The criteria agreed upon with the IESO for the generation of heat maps and MRTS curves were presented, as well as the procedure to select the representative typical days per season, and a detailed methodology to generate heat maps and MRTS curves.

Heat maps, which used the RMSE of ACE as performance metrics, were generated by

running simulations of the Integrated Model, considering CDs, with one ESS facility at a time and varying the FR capacity of fast and slow resources for each scenario and season. The heat maps obtained allowed evaluating how well the different combinations of $RegA$ and $RegD$ capacities impacted the RMSE of ACE. After these were generated, one isoquant was selected and a multi-segment approach was used to generate the MRTS curves. Each segment in the isoquants for all the 80 cases were approximated by a quadratic function.

Each MRTS curve was formed by the negative of the first derivative of the quadratic function approximating each interval of the isoquant for all the 80 cases studied. A criteria to reduce the number of curves was established through several comparisons of the MRTS curves, obtaining 16 average MRTS curves, which in turn were used to obtain 16 average optimized MRTS curves. Finally, an example of how to interpret the average optimized MRTS curves was presented.

The main conclusions of this thesis are as follows:

- The CDs and the SoC model of ESSs significantly impact the FR performance, measured in terms of the ACE, and thus must be included in FR studies, to obtain realistic results. Simulation studies demonstrated that in the FR control loop, the smaller the delay, the better is the ACE performance, and reducing the CDs had a similar effect on the ACE as increasing the ESS capacity with the original CDs. Thus, a combination of reduced CDs and increased fast FR capacity can realistically improve the FR performance. Finally, it is shown that ignoring the SoC of the ESS in the FR process yielded unrealistic ACE reductions, which could lead to under-procurement of ESS for FR provisions.

- Some stages in the proposed FR model are specific to the FR process of the IESO, while other stages can be partially modified for their use in other bulk power systems, and others can be directly used in any system after estimating the appropriate parameters.

- The main advantage of the Base Case FR Model and Integrated Model is that these allow long simulation periods, while still considering the main stages of the FR process under normal operating conditions in short execution times.

- The proposed $\mathcal{H}_2$ filter produces two different signals, $RegA$ and $RegD$, with similar characteristics to the current FR approach of PJM. However, the proposed filter has two main advantages over the PJM approach: First, the filtered $RegA$ and $RegD$ signals are the result of an optimal control design problem, which incorporates the aggregated dynamics of traditional FR resources, along with approximate CDs and

an aggregated model of the bulk power system. Second, the PJM neutrality condition that caused over-procuring of FR resources is avoided.

- The proposed filter design strategy to split the scheduled regulation signal, takes advantage of the high ramp rates of the ESSs; thus, the $\mathcal{H}_2$ filter, anti-windup method, and PSP calculation can be implemented by other ISOs, to exploit the fast resources that are currently part of their FR markets and to coordinate traditional and fast resources.

- The proposed approach to split the FR signal renders significantly better results in terms of reducing the ACE as compared to the existing FR process in Ontario. Indeed, when comparing the Integrated Model and the Base Case Model, under similar conditions, the former performed better in terms of ACE reduction for all the cases studied. By eliminating, or at least reducing the CDs, the ACE can be improved without adding extra FR capacity, which can be translated into economic savings for the system. Also, the Base Case Model with unlimited FR capacity is shown to have frequency oscillations leading to unstable operation, because the $RegA$ and $RegD$ signals are independent of each other. On the other hand, the proposed $\mathcal{H}_2$ filter produces FR signals that work in a coordinated manner, thus avoiding any instability in the system.

- Analyzing the maximum FR requirement using the Integrated Model allows for power capacity sizing of traditional and fast regulation requirements to achieve optimal ACE reduction.

- The addition of the PSP calculation and the anti-windup strategy allows taking full advantage of the coordinated control provided by the proposed $\mathcal{H}_2$ filter strategy.

- From the ISO's perspective, the participation of ESSs and the proposed $\mathcal{H}_2$ filtering strategy can improve the FR performance and reduce the overall capacity requirement for FR services.

- The MRTS curves allow finding the $RegA$ capacity that can be replaced by $RegD$ capacity to achieve the same performance while decreasing the total FR capacity used. Furthermore, increasing the share of $RegD$ capacity improved the FR performance for a given regulation capacity requirement. However, beyond a certain share of $RegD$, the FR performance deteriorates, which diminishes the returns from increased fast ESS resources.

6.2 Contributions

The most significant contributions of this thesis can be summarized as follows:

- A novel FR simulation model of a large interconnected power grid representing the main stages of the FR control process, operating under normal conditions, and from an ISO perspective was proposed. The model, which was validated for the OPS and whose parameters where estimated using real system information provided by the IESO, considers CDs in the signal transmission from/to the control center to/from the facilitates contracted for regulation, and SoC management of the ESS. Thus, the proposed model closely represents the frequency behaviour of a large interconnected power system, and it is able to run longer-horizon FR simulations in short periods of time.

- Empirically-based SoC models for FESS and BESS considering their charging and discharging characteristics, appropriate for FR simulation models and from an ISO's perspective, have been proposed for the first time. These models have been validated using data from actual FESS and BESS facilities currently providing FR in Ontario.

- A novel $\mathcal{H}_2$ filter design to optimally split the FR signal into fast and slow components, to improve the FR performance in terms of minimizing ACE variations, has been proposed. The proposed $\mathcal{H}_2$ filter is integrated with the validated FR simulation model of the OPS to form an Integrated Model of the FR process. This model, which includes CDs and ESSs considering their SoCs, accounts for the closed-loop feedback effects of filter outputs in the frequency control process, not considered in existing practical models thus far, and are based on open-loop system representations.

- The proposed Integrated Model is applied to the OPS to demonstrate the impact of fast response ESSs on the FR process, accounting for and evaluating the effect of CDs and limited regulation capacity, which have not been considered simultaneously in practical systems before.

- A detailed methodology is presented for the first time to generate heat maps and MRTS curves, which can be applied to any bulk power system with appropriate modifications. The methodology accounts for ESSs technologies with different discharging times, scenarios, and seasons. The proposed heat maps can help determine the benefit of adding fast resources to the FR process, and MRTS curves can help determine the $RegA$ capacity to be replaced by $RegD$ capacity, while maintaining the same FR performance, thus reducing the total FR capacity requirement.

The results reported in Chapter 3 has been submitted to the IEEE Transactions on Power Systems and is currently under revision [88], and the results discussed in Chapter 4 have been published in IEEE Transactions on Power Systems [89]. Finally, the heat map and MRTS work is being submitted for publication and presentation at the 2022 Power System Computation Conference (PSCC) [90].

6.3 Future Work

Based on the work presented in this thesis, the following issues may be undertaken for future research:

- Using the proposed FESS and BESS models, examine how changes in the parameters $\underline{U}_{off}$ and $\overline{L}_{off}$, which determine the upper and lower band of the SoC of the facilities, respectively, could affect the FR performance.
- Investigate the viability of distributed FR from fast response ESSs to address the issue of CDs in centrally generated FR signals, and evaluate their impact on the system frequency performance.
- Model and study the impact of synthetic inertia from BESS and FESS on FR for large interconnected power systems.
- Use MRTS curves together with market price forecast to determine the optimal combination of $RegD$ and $RegA$ resources that would yield the same FR performance at minimum cost. Furthermore, set up a methodology to appropriately use the MRTS curves through the different stages of IAMs, while ensuring a fair compensation for fast resources based on the actual benefit they provide to the FR process.

References

[1] J. P. Barton and D. G. Infield, "Energy storage and its use with intermittent renewable energy," *IEEE Transactions on Energy Conversion*, vol. 19, no. 2, pp. 441–448, Jun. 2004.

[2] B. P. Roberts and C. Sandberg, "The role of energy storage in development of smart grids," *Proceedings of the IEEE*, vol. 99, no. 6, pp. 1139–1144, June 2011.

[3] L. Meng, J. Zafar, S. K. Khadem, A. Collinson, K. C. Murchie, F. Coffele, and G. M. Burt, "Fast frequency response from energy storage systems—A review of grid standards, projects and technical issues," *IEEE Transactions on Smart Grid*, vol. 11, no. 2, pp. 1566–1581, Mar. 2020.

[4] A. Akhil, G. Huff, A. Currier, B. Kaun, D. Rastler, S. Chen, A. Cotter, D. Bradshaw, and W. Gauntlett, "DOE/EPRI electricity storage handbook in collaboration with NRECA," Sandia National Laboratories, Albuquerque, NM, USA, Tech. Rep., Jul. 2013.

[5] "Grid energy storage," US. Department of Energy, Tech. Rep., 2013.

[6] "Electricity storage and renewables; costs and markets to 2030," International Renewable Energy Agency, Tech. Rep., 2017.

[7] "IESO report: Energy storage," IESO, Toronto, ON, CA, Tech. Rep., Mar. 2016.

[8] "Electric storage participation in markets operated by regional transmission organizations and independent system operators," FERC, May 2019, Order No. 841–A, Docket Nos. RM16–23–001, AD16–20–001.

[9] "Removing obstacles for storage resources in Ontario," IESO, Toronto, ON, CA, Tech. Rep., Dec. 2018.

[10] C. Mu, Y. Zhang, H. Jia, and H. He, "Energy-storage-based intelligent frequency control of microgrid with stochastic model uncertainties," *IEEE Transactions on Smart Grid*, vol. 11, no. 2, pp. 1748–1758, Mar. 2020.

[11] "State of market report for PJM," Monitoring Analytics, Tech. Rep., Oct. 2016.

[12] "State of market report for PJM," Monitoring Analytics, Tech. Rep., Nov. 2021.

[13] "Order rejecting tariff revisions," FERC, Mar. 2018, dockets Nos. ER18-87-000, ER18-87-001, 162 FERC 61,295.

[14] "Frequency regulation compensation in the organized wholesale power markets," FERC, Order No. 755, Dockets RM11-7-000 AD10-11-000.

[15] M. Kintner-Meyer, "Regulatory policy and markets for energy storage in North America," *Proceedings of the IEEE*, vol. 102, no. 7, pp. 1065–1072, Jul. 2014.

[16] National Academies of Sciences, Engineering, and Medicine, *Enhancing the Resilience of the Nation's Electricity System*. Washington, D.C., USA: National Academies Press, 2017.

[17] Y. Chen, R. Leonard, M. Keyser, and J. Gardner, "Development of performance-based two-part regulating reserve compensation on MISO energy and ancillary service market," *IEEE Transactions on Power Systems*, vol. 30, no. 1, pp. 142–155, Jan. 2015.

[18] "Energy storage design project long-term design vision document," IESO, Tech. Rep., Sep. 2020.

[19] "Kermit study report to determine the effectiveness of the AGC in controlling fast and conventional resources in the PJM frequency regulation market," KEMA Inc., Chalfont, PN, USA, Tech. Rep., Dec. 2011.

[20] B. Xu, Y. Dvorkin, D. S. Kirschen, C. A. Silva-Monroy, and J. Watson, "A comparison of policies on the participation of storage in U.S. frequency regulation markets," in *IEEE Power and Energy Society General Meeting*, Boston, MA, USA, 2016, pp. 1–5.

[21] Energy storage procurement at the IESO. IESO.ca. (Accessed: October 31st, 2018). [Online]. Available: http://www.ieso.ca/en/Sector-Participants/Energy-Procurement-Programs-and-Contracts/Energy-Storage

[22] "O. Reg. 541/05: Net metering," Ontario Energy Board Act, 2018.

[23] Z. Zhou, T. Levin, and G. Conzelmann, "Survey of U.S. ancillary services markets," Argonne National Lab., Argonne, IL, USA, Tech. Rep., Jan. 2016.

[24] G. He, Q. Chen, C. Kang, Q. Xia, and K. Poolla, "Cooperation of wind power and battery storage to provide frequency regulation in power markets," *IEEE Transactions on Power Systems*, vol. 32, no. 5, pp. 3559–3568, Sep. 2017.

[25] H. S. Qazi, N. Liu, and A. Ali, "Power system frequency regulation using hybrid electrical energy storage system," in *IEEE 2nd International Electrical and Energy Conference*, 2018, pp. 377–381.

[26] E. Yao, V. W. S. Wong, and R. Schober, "Robust frequency regulation capacity scheduling algorithm for electric vehicles," *IEEE Transactions on Smart Grid*, vol. 8, no. 2, pp. 984–997, Mar. 2017.

[27] Y. Shi, B. Xu, D. Wang, and B. Zhang, "Using battery storage for peak shaving and frequency regulation: Joint optimization for superlinear gains," *IEEE Transactions on Power Systems*, vol. 33, no. 3, pp. 2882–2894, May 2018.

[28] B. Cheng and W. B. Powell, "Co-optimizing battery storage for the frequency regulation and energy arbitrage using multi-scale dynamic programming," *IEEE Transactions on Smart Grid*, vol. 9, no. 3, pp. 1997–2005, 2018.

[29] C. Jin, N. Lu, S. Lu, Y. V. Makarov, and R. A. Dougal, "A coordinating algorithm for dispatching regulation services between slow and fast power regulating resources," *IEEE Transactions on Smart Grid*, vol. 5, no. 2, Mar. 2014.

[30] G. Meng, Q. Chang, Y. Sun, Y. Rao, F. Zhang, Y. Wu, and L. Su, "Energy storage auxiliary frequency modulation control strategy considering ACE and SOC of energy storage," *IEEE Access*, vol. 9, pp. 26 271–26 277, Feb. 2021.

[31] K. Doenges, I. Egido, L. Sigrist, E. Lobato Miguélez, and L. Rouco, "Improving AGC performance in power systems with regulation response accuracy margins using battery energy storage system (BESS)," *IEEE Transactions on Power Systems*, vol. 35, no. 4, pp. 2816–2825, Jul. 2020.

[32] J. P. Lee and H. G. Kim, "Design of load frequency controller for flywheel energy storage system," in *International Conference on Electrical Machines and Systems (ICEMS), Busan, South Korea*, Oct 2013, pp. 381–384.

[33] T. Chakraborty, D. Watson, and M. Rodgers, "Automatic generation control using an energy storage system in a wind park," *IEEE Transactions on Power Systems*, vol. 33, no. 1, pp. 198–205, Jan. 2018.

[34] F. Calero, C. A. Cañizares, and K. Bhattacharya, "Dynamic modeling of battery energy storage and applications in transmission systems," *IEEE Transactions on Smart Grid*, vol. 12, no. 1, pp. 589–598, Jan. 2021.

[35] D. Peralta, C. Cañizares, and K. Bhattacharya, "Practical modeling of flywheel energy storage for primary frequency control in power grids," in *IEEE Power Energy Society General Meeting*, 2018, pp. 1–5.

[36] H. Zhao, M. Hong, W. Lin, and K. A. Loparo, "Voltage and frequency regulation of microgrid with battery energy storage systems," *IEEE Transactions on Smart Grid*, vol. 10, no. 1, pp. 414–424, Jan. 2019.

[37] M. Yoon, J. Lee, S. Song, Y. Yoo, G. Jang, S. Jung, and S. Hwang, "Utilization of energy storage system for frequency regulation in large-scale transmission system," *Energies*, vol. 12, no. 20, 2019.

[38] "Implementation and rationale for PJM's conditional neutrality regulation signals," PJM, Toronto, ON, CA, Tech. Rep., Jan. 2017.

[39] J. W. Shim, G. Verbič, N. Zhang, and K. Hur, "Harmonious integration of faster-acting energy storage systems into frequency control reserves in power grid with high renewable generation," *IEEE Transactions on Power Systems*, vol. 33, no. 6, pp. 6193–6205, Nov. 2018.

[40] Y. Cheng, M. Tabrizi, M. Sahni, A. Povedano, and D. Nichols, "Dynamic available AGC based approach for enhancing utility scale energy storage performance," *IEEE Transactions on Smart Grid*, vol. 5, no. 2, pp. 1070–1078, Mar. 2014.

[41] S. Pulendran and J. E. Tate, "Capacity scheduling of energy storage and conventional generation for frequency regulation based on CPS1," *IEEE Transactions on Power Systems*, vol. 35, no. 1, pp. 405–414, Jan. 2020.

[42] O. Leitermann, "Energy storage for frequency regulation on the electric grid," Ph.D. dissertation, MIT, Cambridge, MA, Jun. 2012.

[43] S. Prasad, S. Purwar, and N. Kishor, "H-infinity based non-linear sliding mode controller for frequency regulation in interconnected power systems with constant and

time-varying delays," *IET Generation, Transmission and Distribution*, vol. 10, no. 11, pp. 2771–2784, Aug. 2016.

[44] H. Bevrani and T. Hiyama, "On load–frequency regulation with time delays: Design and real-time implementation," *IEEE Transactions on Energy Conversion*, vol. 24, no. 1, pp. 292–300, Mar. 2009.

[45] X. Xie, Y. Guo, B. Wang, Y. Dong, L. Mou, and F. Xue, "Improving AGC performance of coal-fueled thermal generators using multi-MW scale BESS: A practical application," *IEEE Transactions on Smart Grid*, vol. 9, no. 3, pp. 1769–1777, May 2018.

[46] C. Goebel, D. S. Callaway, and H. Jacobsen, "The impact of state of charge management when providing regulation power with energy storage," *IEEE Transactions on Power Systems*, vol. 29, no. 3, pp. 1433–1434, May 2014.

[47] A. Gomez-Exposito, A. Conejo, and C. Canizares, *Electric energy systems analysis and operation*. Boca Raton, FL, USA: CRC Press, 2018.

[48] "Balancing and frequency control," NERC Resources Subcommittee, Princeton, NJ, USA, Tech. Rep., Jan. 2011.

[49] "Frequency instability problems in north american interconnections," National Energy Technology Laboratory, Tech. Rep., 2011.

[50] P. Kundur, *Power system stability and control*. McGraw Hill Education, 1994.

[51] "State of reliability 2018," NERC Resources Subcommittee, Tech. Rep., 2018.

[52] "Participant technical reference manual," IESO, Tech. Rep., 2018.

[53] "Frequency response standard whitepaper," NERC Resources Subcommittee, Tech. Rep., 2004.

[54] "18-month outlook - An assessment of the reliability and operability of the Ontario electricity system," IESO, Tech. Rep., 2018.

[55] D. Ganger, J. Zhang, and V. Vittal, "Forecast-based anticipatory frequency control in power systems," *IEEE Transactions on Power Systems*, vol. 33, no. 1, pp. 1004–1012, 2018.

[56] T. Lee, "Energy storage in PJM: Exploring frequency regulation market transformation," Kleinman Center for Energy Policy, Philadelphia, PA, USA, Tech. Rep., Jul. 2017.

[57] "RFP for Energy Storage Services Backgrounder," IESO, Tech. Rep., 2014.

[58] H. Chen, T. N. Cong, W. Yang, C. Tan, Y. Li, and Y. Ding, "Progress in electrical energy storage system: A critical review," *Progress in Natural Science*, vol. 19, no. 3, pp. 291 – 312, 2009.

[59] P. Nikolaidis and A. Poullikkas, "A comparative review of electrical energy storage systems for better sustainability," *Journal of Power Technologies*, vol. 97, no. 3, pp. 220–245, 2017.

[60] D. Peralta, "Primary frequency control with flywheel energy storage technologies," Ph.D. dissertation, University of Waterloo, Waterloo, ON, Canada, 2017.

[61] F. Nadeem, S. M. S. Hussain, P. K. Tiwari, A. K. Goswami, and T. S. Ustun, "Comparative review of energy storage systems, their roles, and impacts on future power systems," *IEEE Access*, vol. 7, pp. 4555–4585, Jan. 2019.

[62] F. Calero, "Impact of distributed battery energy storage on electric power transmission and distribution systems," Ph.D. dissertation, University of Waterloo, Waterloo, ON, Canada, 2021.

[63] Ancillary services market. IESO.ca. (Accessed: January 29$^{\text{th}}$, 2021). [Online]. Available: https://www.ieso.ca/ancillary-services

[64] "Market rules for the Ontario electricity market," IESO, Toronto, ON, CA, Tech. Rep., Jan. 2020.

[65] Increasing competition in ancillary services through regulation service procurement. IESO.ca. (Accessed: May 25$^{\text{th}}$, 2021). [Online]. Available: https://ieso.ca/-/media/Files/IESO/Document-Library/engage/esag/esag-20200915-long-term-design-vision.ashx

[66] "2016 IESO operability assessment - summary: Review of the operability of the IESO-controlled grid to 2020," IESO, Toronto, ON, CA, Tech. Rep., 2016.

[67] Energy procurement programs and contracts. IESO.ca. (Accessed: May 25$^{\text{th}}$, 2021). [Online]. Available: https://www.ieso.ca/en/Sector-Participants/Energy-Procurement-Programs-and-Contracts/Procurement-Archive

[68] Regulation service RFP. IESO.ca. (Accessed: October 23st, 2018). [Online]. Available: http://www.ieso.ca/sector-participants/market-operations/markets-and-related-programs/ancillary-services-market

[69] Storage design project (SDP). IESO.ca. (Accessed: May 25th, 2021). [Online]. Available: https://ieso.ca/-/media/Files/IESO/Document-Library/engage/esag/esag-20200520-sdp-long-term-design-proposals.ashx.

[70] Interim market rules and manuals for energy storage now posted and in effect. IESO.ca. (Accessed: May 25th, 2021). [Online]. Available: https://www.ieso.ca/en/Sector-Participants/IESO-News/2021/03/Interim-Market-Rules-and-Manuals-for-Energy-Storage-Now-Posted-and-in-Effect

[71] DSATools Overview. Dsatools.com. (Accessed: June 24th, 2020). [Online]. Available: https://www.dsatools.com/overview/

[72] "BAL-001-2– real power balancing control performance standard background document," NERC, Princeton, NJ, USA, Tech. Rep., Feb. 2013.

[73] Simulink. Mathworks.com. (Accessed: June 24th, 2020). [Online]. Available: https://www.mathworks.com/products/simulink.html

[74] F. Xiaodong, C. Changling, L. Changling, and S. Huihe, "An improved process data compression algorithm," in *Proceedings of the 4th World Congress on Intelligent Control and Automation, Shanghai, China*, vol. 3, June 2002, pp. 2190–2193.

[75] "Policy 1 - generation control and performance," NERC, Princeton, NJ, USA, Tech. Rep., Oct. 2002.

[76] "Attachment A, BAL-003-1 frequency response and frequency bias setting," NERC, Princeton, NJ, USA, Tech. Rep., 2012.

[77] M. Hannan, M. Lipu, A. Hussain, and A. Mohamed, "A review of lithium-ion battery state of charge estimation and management system in electric vehicle applications: Challenges and recommendations," *Renewable and Sustainable Energy Reviews*, vol. 78, pp. 834–854, Oct. 2017.

[78] 2020 year in review. IESO.ca. (Accessed: February 16th, 2021). [Online]. Available: https://www.ieso.ca/en/corporate-ieso/media/year-end-data

[79] Maps and diagram. ISO-NE.com. (Accessed: February 11th, 2021). [Online]. Available: https://www.iso-ne.com/about/key-stats/maps-and-diagrams/#system-diagram

[80] "Frequency Response Initiative Report," NERC Resources Subcommittee, Tech. Rep., 2012.

[81] "Industry advisory: Generator governor frequency response," NERC, Tech. Rep., 2015.

[82] Skogestad, S. and Postlethwaite, I., *Multivariable feedback control analysis and design*, 2nd ed. John Wiley and Sons, 2005.

[83] Matlab. Mathworks.com. (Accessed: August 26$^{\text{th}}$, 2020). [Online]. Available: https://www.mathworks.com/products/matlab.html

[84] N. S. Guzman, M. Arriaga, C. Cañizares, J. W. Simpson-Porco, D. Sohm, and K. Bhattacharya, "Regulation signal design and fast frequency control with energy storage systems: Generalized plant state-space matrices (with and without delays)," 2021. [Online]. Available: https://dx.doi.org/10.21227/g7m4-0z19

[85] "Market manual 7: System operations, part 7.1: IESO controlled grid operating procedures," IESO, Toronto, ON, CA, Tech. Rep., 2021.

[86] C. E. Ferguson and J. P. Gould, *Microeconomic theory*. Homewood, IL, USA: McGraw-Hill/Irwin, 1975.

[87] D. Besanko and R. Braeutigam, *Microeconomics*. Hoboken, NJ, USA: John Wiley & Sons, 2016.

[88] N. S. Guzman, C. A. Cañizares, K. Bhattacharya, and D. Sohm, "Frequency regulation model of bulk power systems with energy storage," *IEEE Transactions on Power Systems*, 2021, [Revised and resubmitted April 2021].

[89] N. S. Guzman, M. Arriaga, C. A. Cañizares, J. W. Simpson-Porco, D. Sohm, and K. Bhattacharya, "Regulation signal design and fast frequency control with energy storage systems," *IEEE Transactions on Power Systems*, 2021, [Accepted, available in IEEE Xplore Early Access].

[90] N. S. Guzman, C. A. Cañizares, K. Bhattacharya, and D. Sohm, "Marginal rate of technical substitution of traditional with dynamic regulation signals," in *Power System Computation Conference*, 2022, [Abstract submitted June 2021].

APPENDICES

Appendix A

Heat Maps

The heat maps presented in Fig. A.1 to Fig. A.20 correspond to all the 80 cases analyzed in Chapter 5, which consider combinations of the following features:

- Seasons: Spring, Summer, Fall, and Winter.
- Scenarios: Peak hours, Non-peak hours, Morning ramp hours, and Evening ramp hours.
- ESS technologies and discharging times: 15 min BESS, 1 h BESS, 2 h BESS, 4 h BESS, and 15 min FESS.

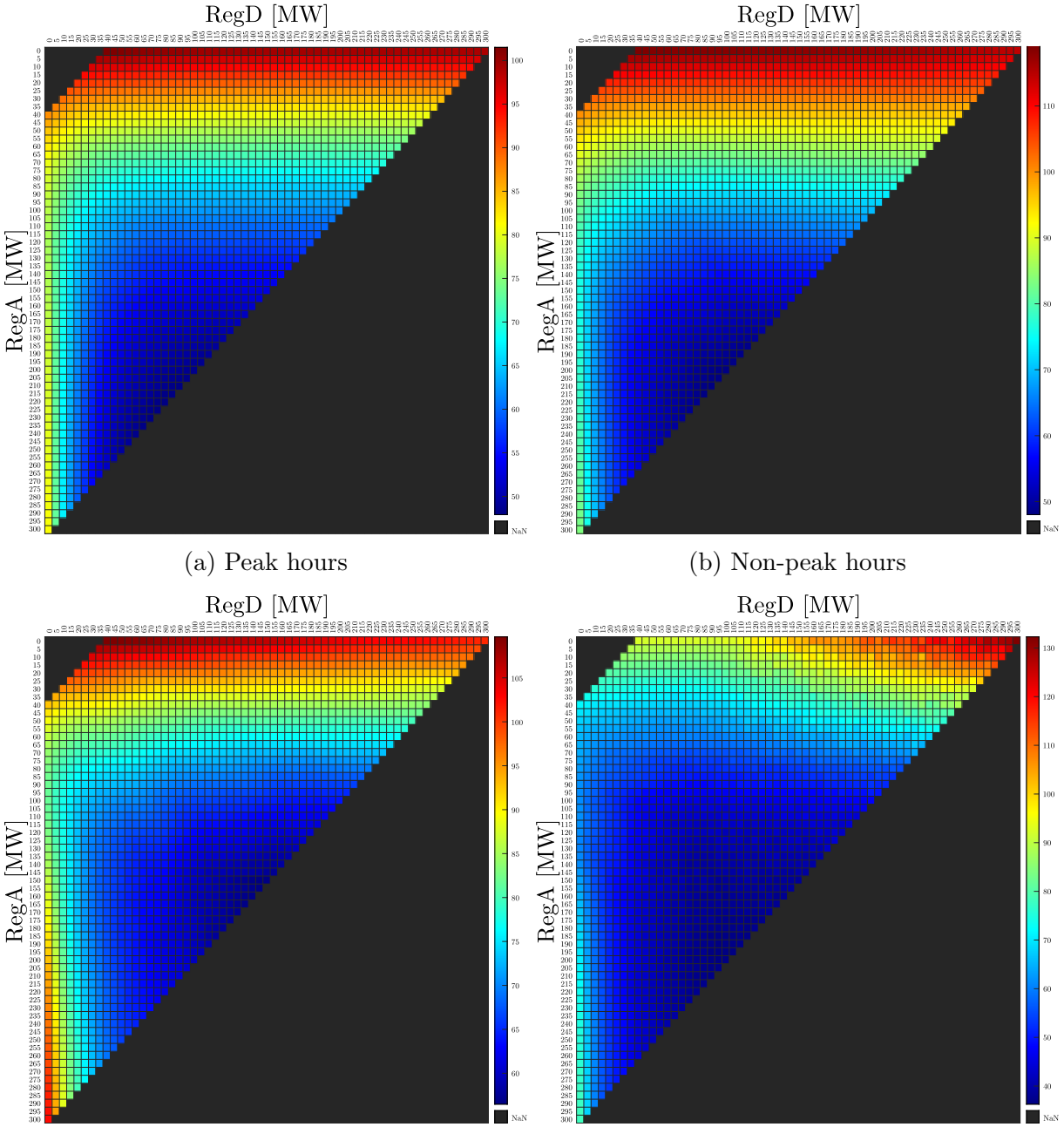

(a) Peak hours

(b) Non-peak hours

(c) Morning ramp hours

(d) Evening ramp hours

Figure A.1: Heat maps for Spring and 15 min BESS.

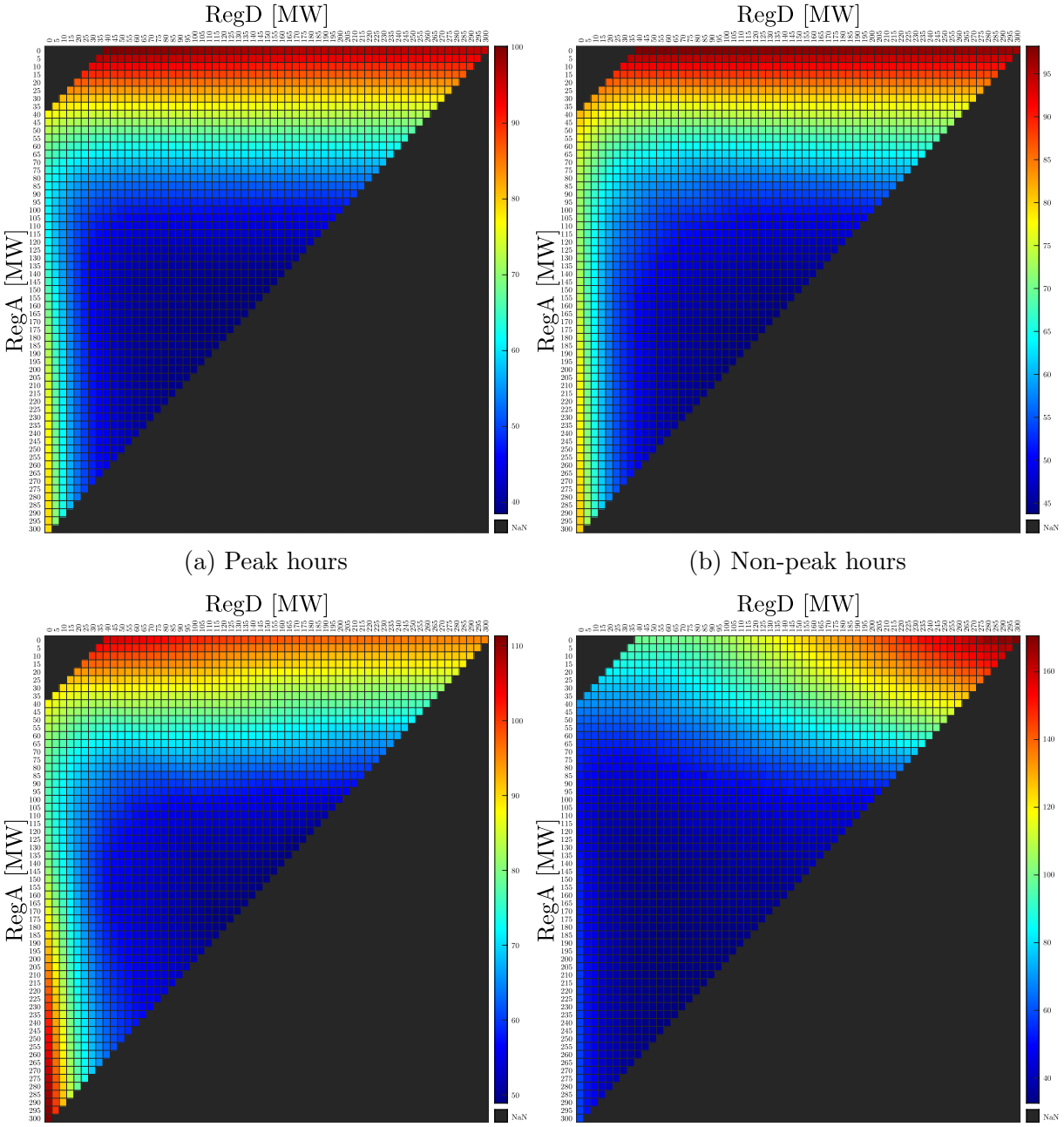

(a) Peak hours

(b) Non-peak hours

(c) Morning ramp hours

(d) Evening ramp hours

Figure A.2: Heat maps for Summer and 15 min BESS.

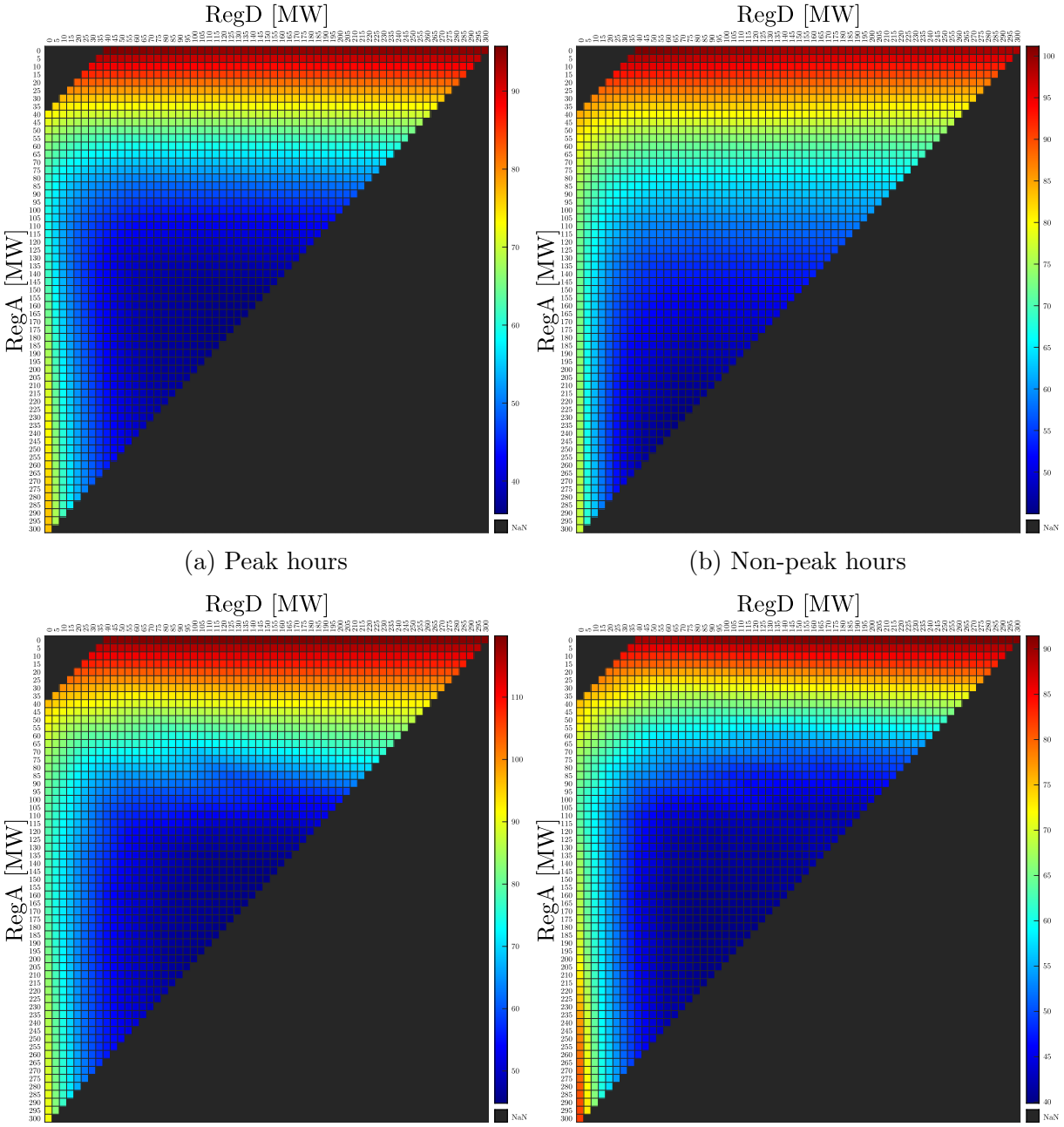

(a) Peak hours

(b) Non-peak hours

(c) Morning ramp hours

(d) Evening ramp hours

Figure A.3: Heat maps for Fall and 15 min BESS.

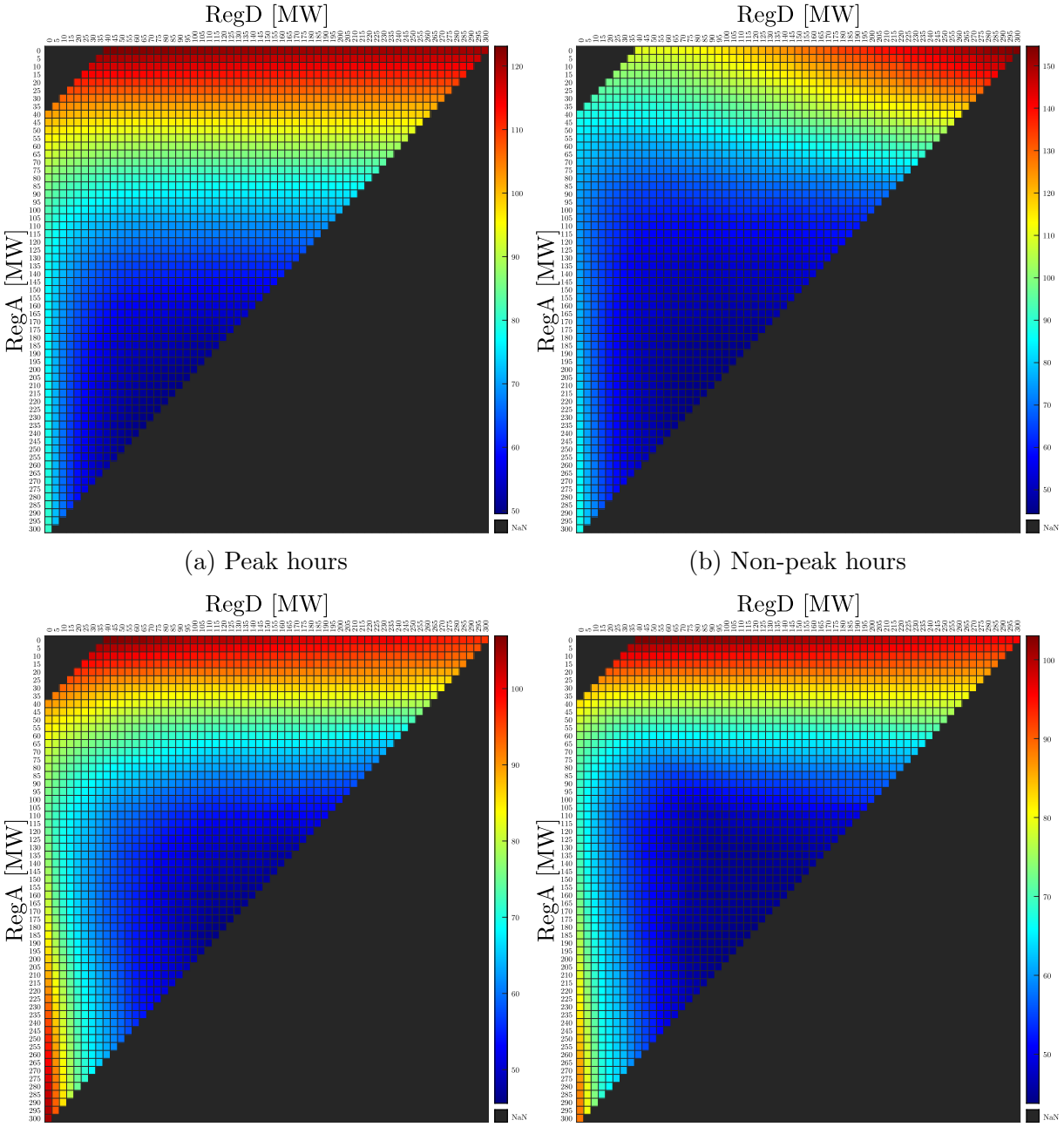

(a) Peak hours

(b) Non-peak hours

(c) Morning ramp hours

(d) Evening ramp hours

Figure A.4: Heat maps for Winter and 15 min BESS.

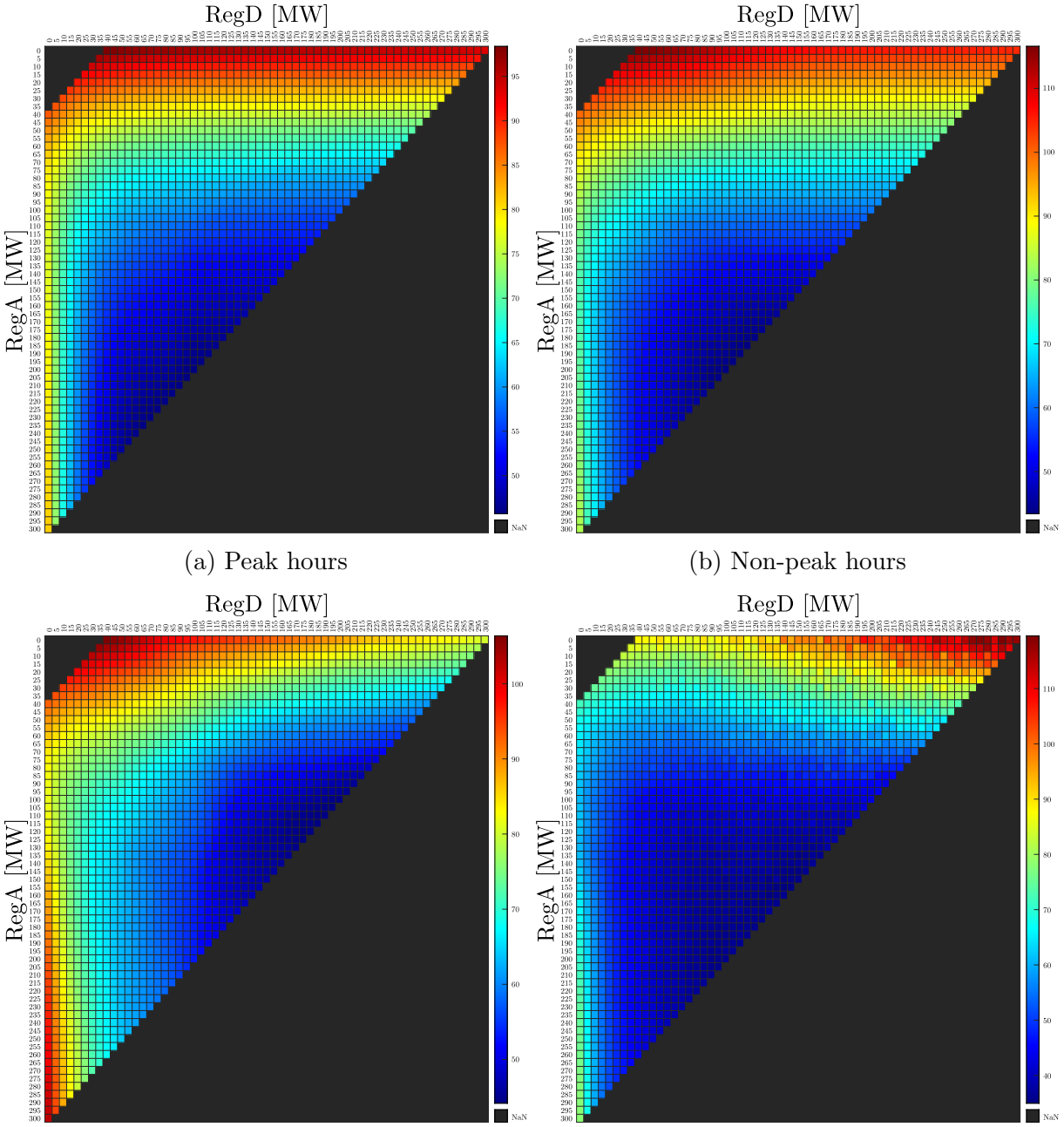

(a) Peak hours

(b) Non-peak hours

(c) Morning ramp hours

(d) Evening ramp hours

Figure A.5: Heat maps for Spring and 1 h BESS.

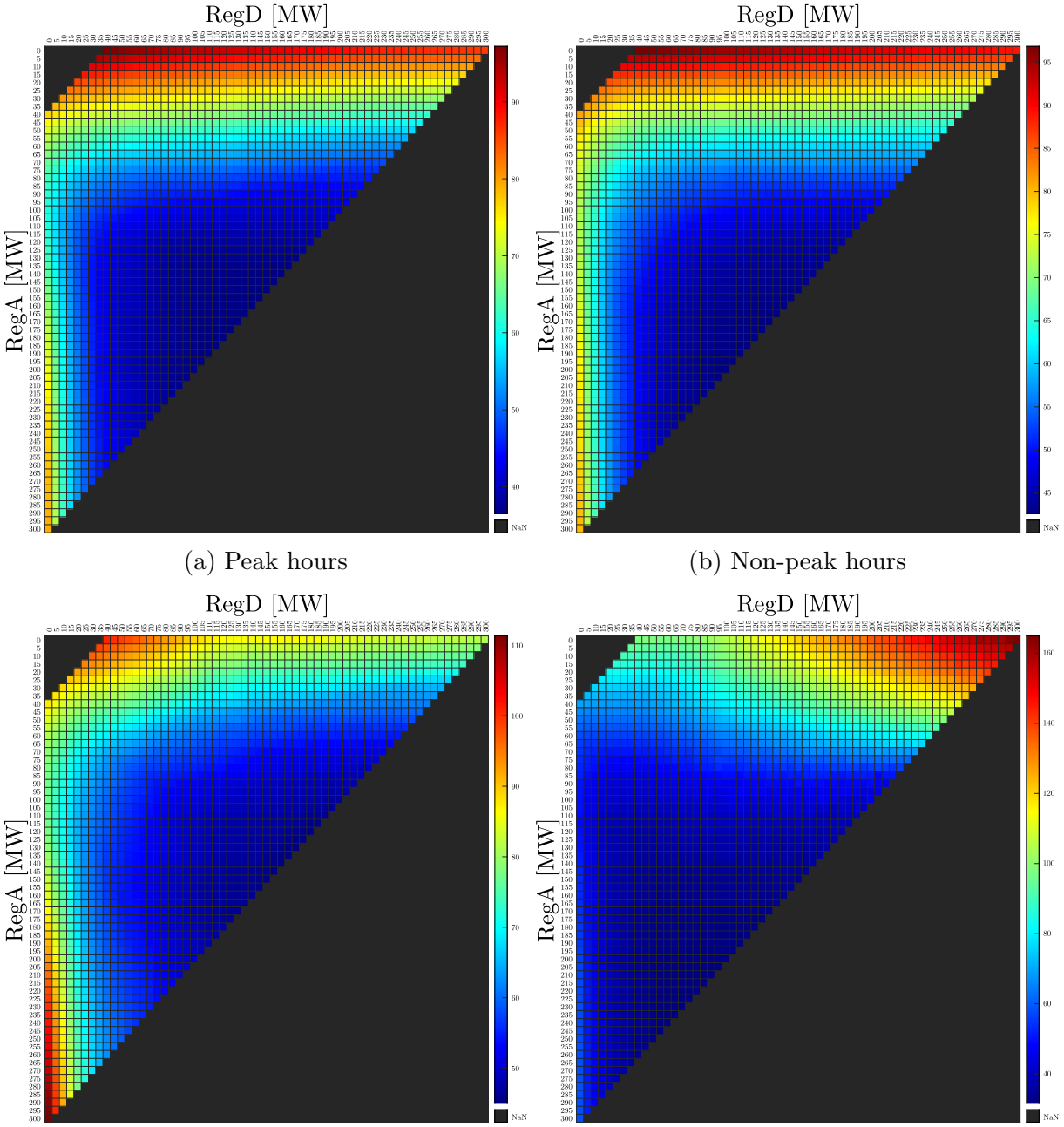

(a) Peak hours

(b) Non-peak hours

(c) Morning ramp hours

(d) Evening ramp hours

Figure A.6: Heat maps for Summer and 1 h BESS.

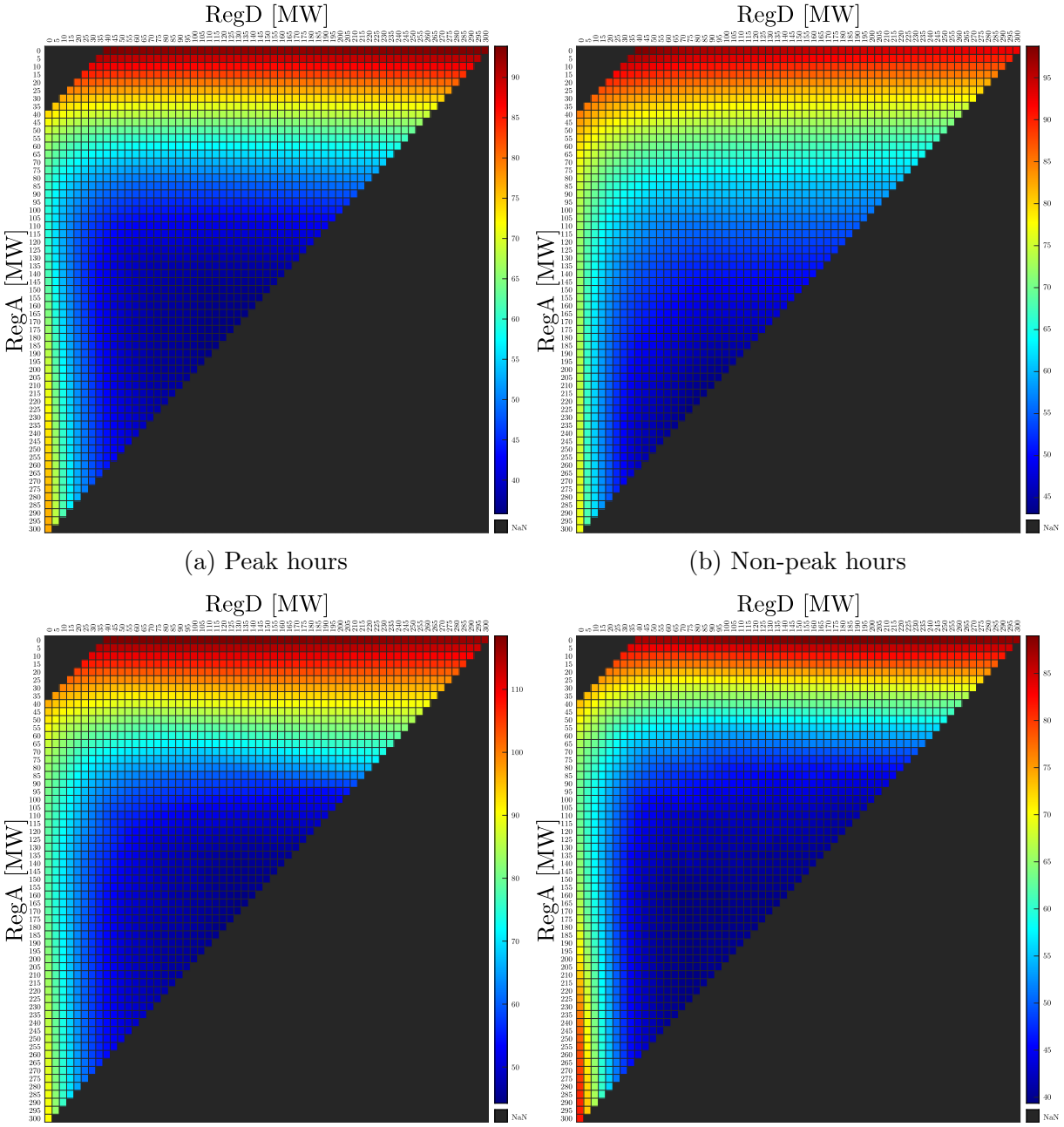

(a) Peak hours

(b) Non-peak hours

(c) Morning ramp hours

(d) Evening ramp hours

Figure A.7: Heat maps for Fall and 1 h BESS.

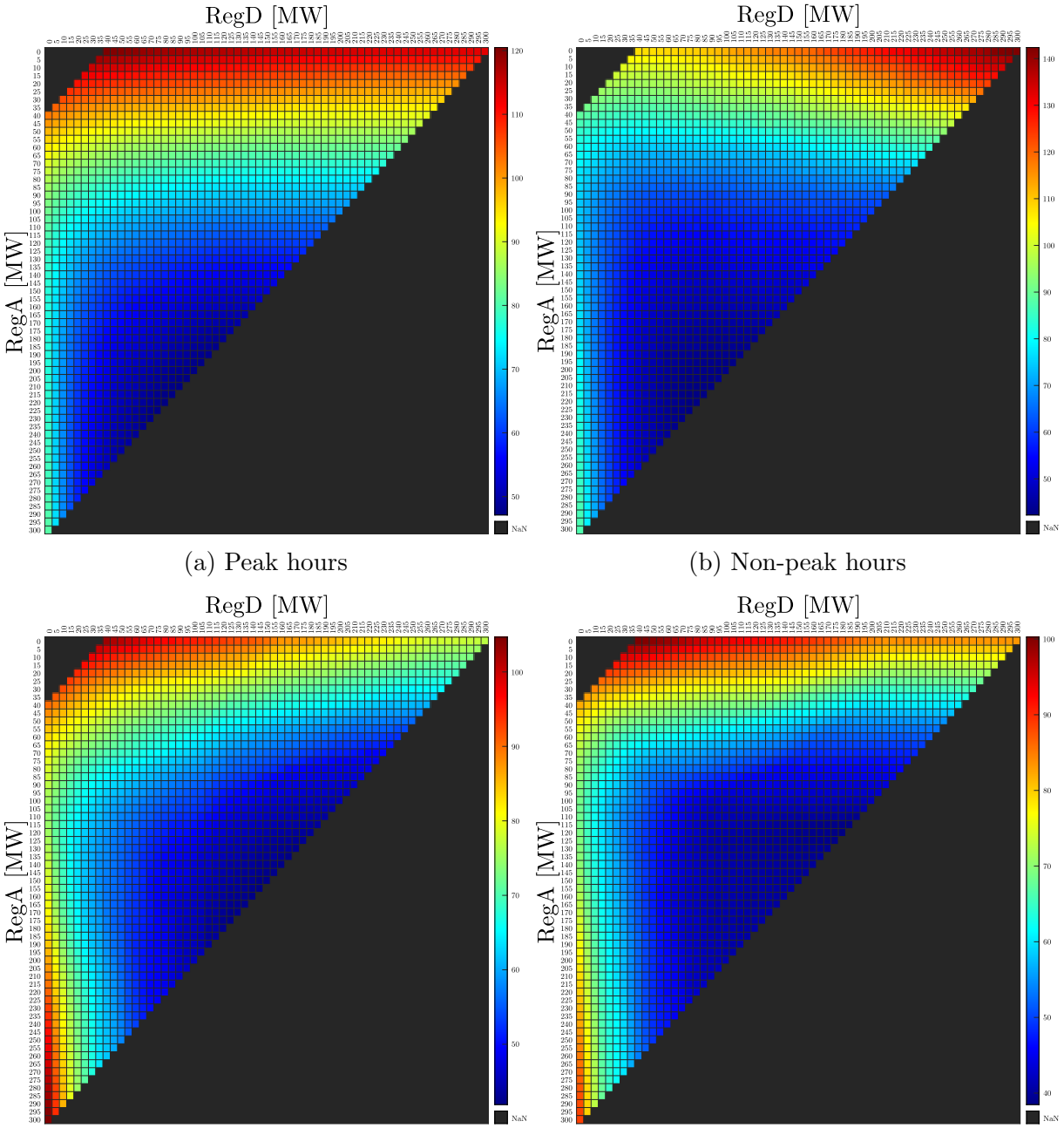

(a) Peak hours

(b) Non-peak hours

(c) Morning ramp hours

(d) Evening ramp hours

Figure A.8: Heat maps for Winter and 1 h BESS

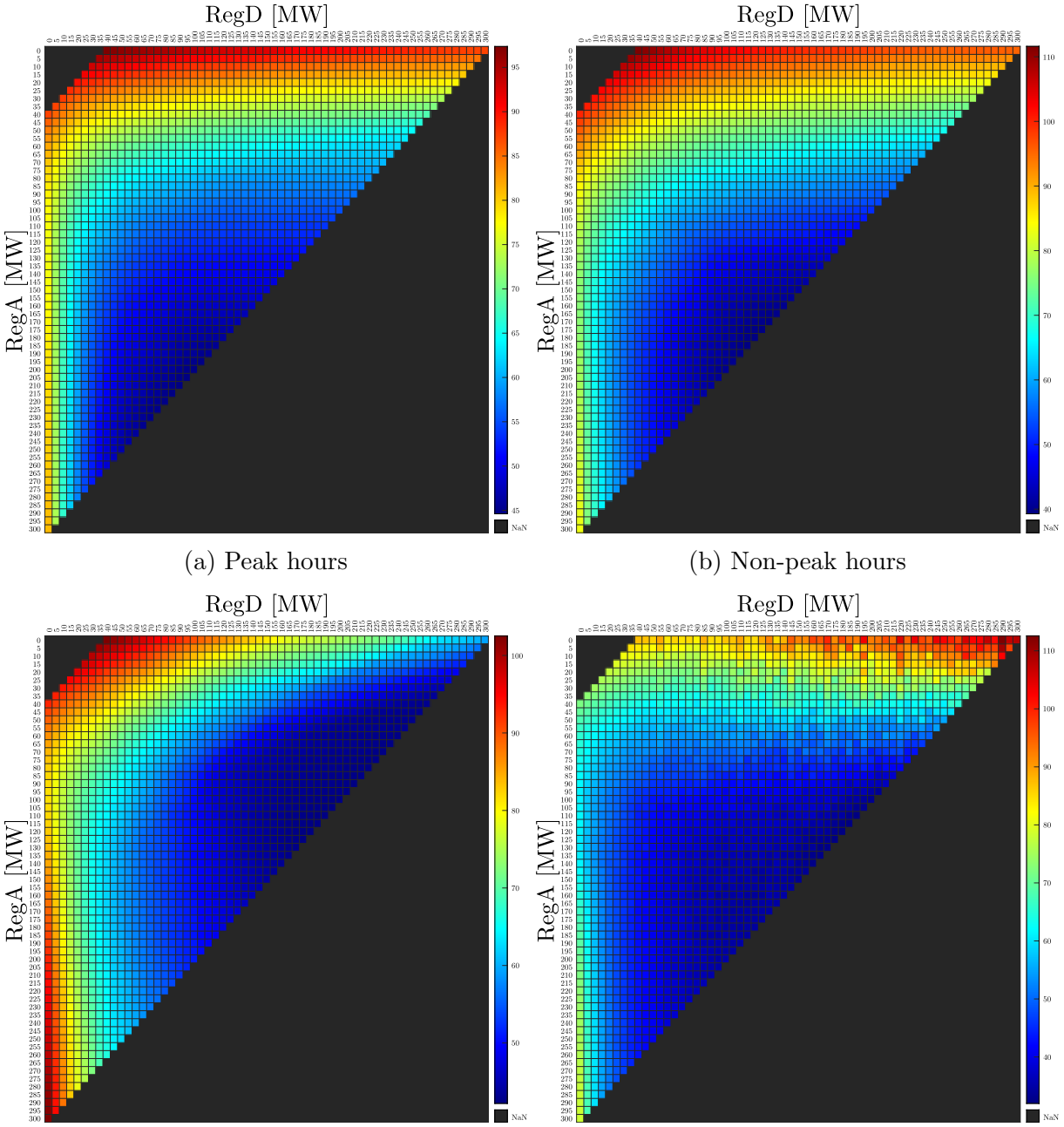

(a) Peak hours

(b) Non-peak hours

(c) Morning ramp hours

(d) Evening ramp hours

Figure A.9: Heat maps for Spring and 2 h BESS.

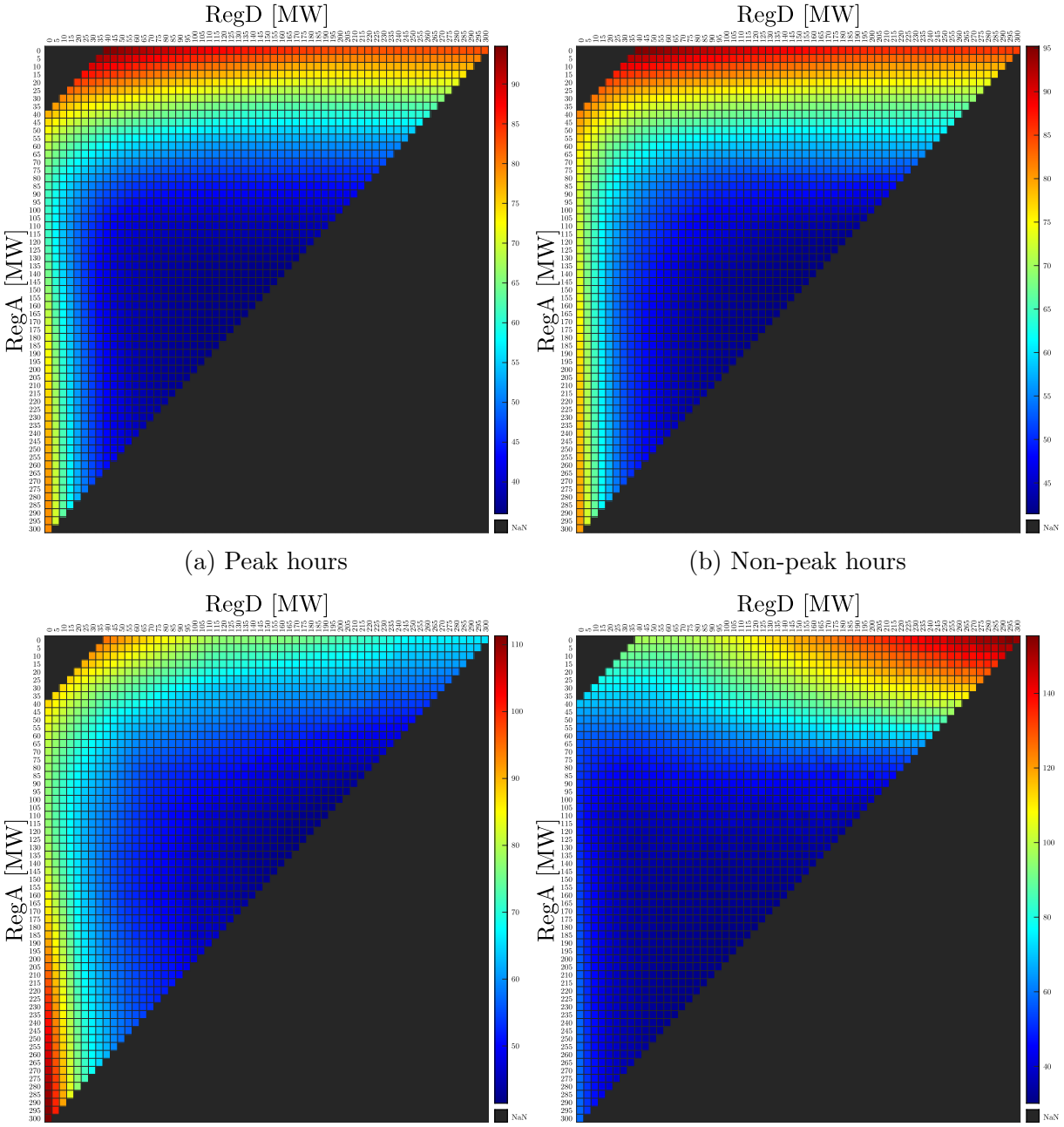

(a) Peak hours

(b) Non-peak hours

(c) Morning ramp hours

(d) Evening ramp hours

Figure A.10: Heat maps for Summer and 2 h BESS.

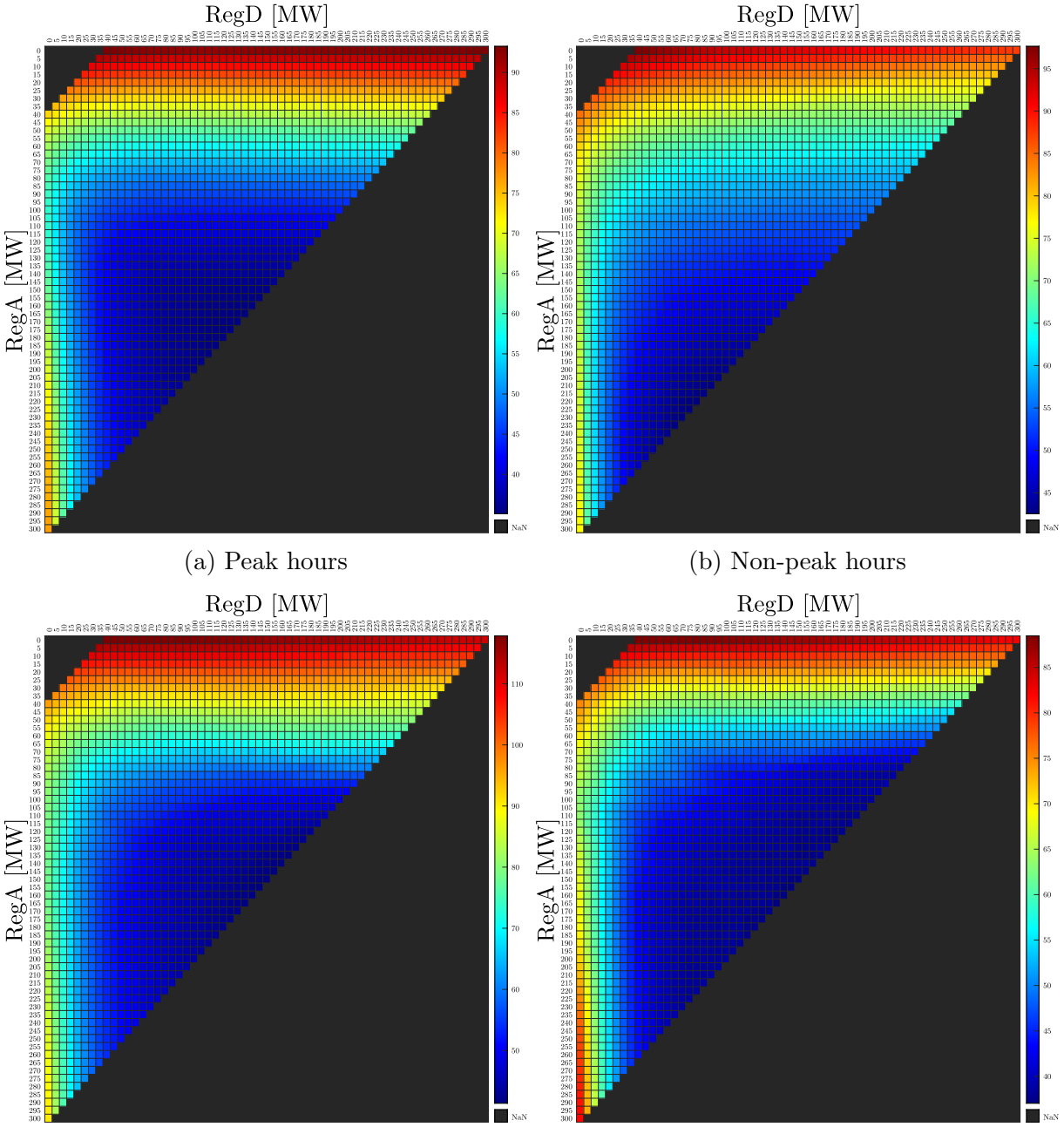

(a) Peak hours

(b) Non-peak hours

(c) Morning ramp hours

(d) Evening ramp hours

Figure A.11: Heat maps for Fall and 2 h BESS.

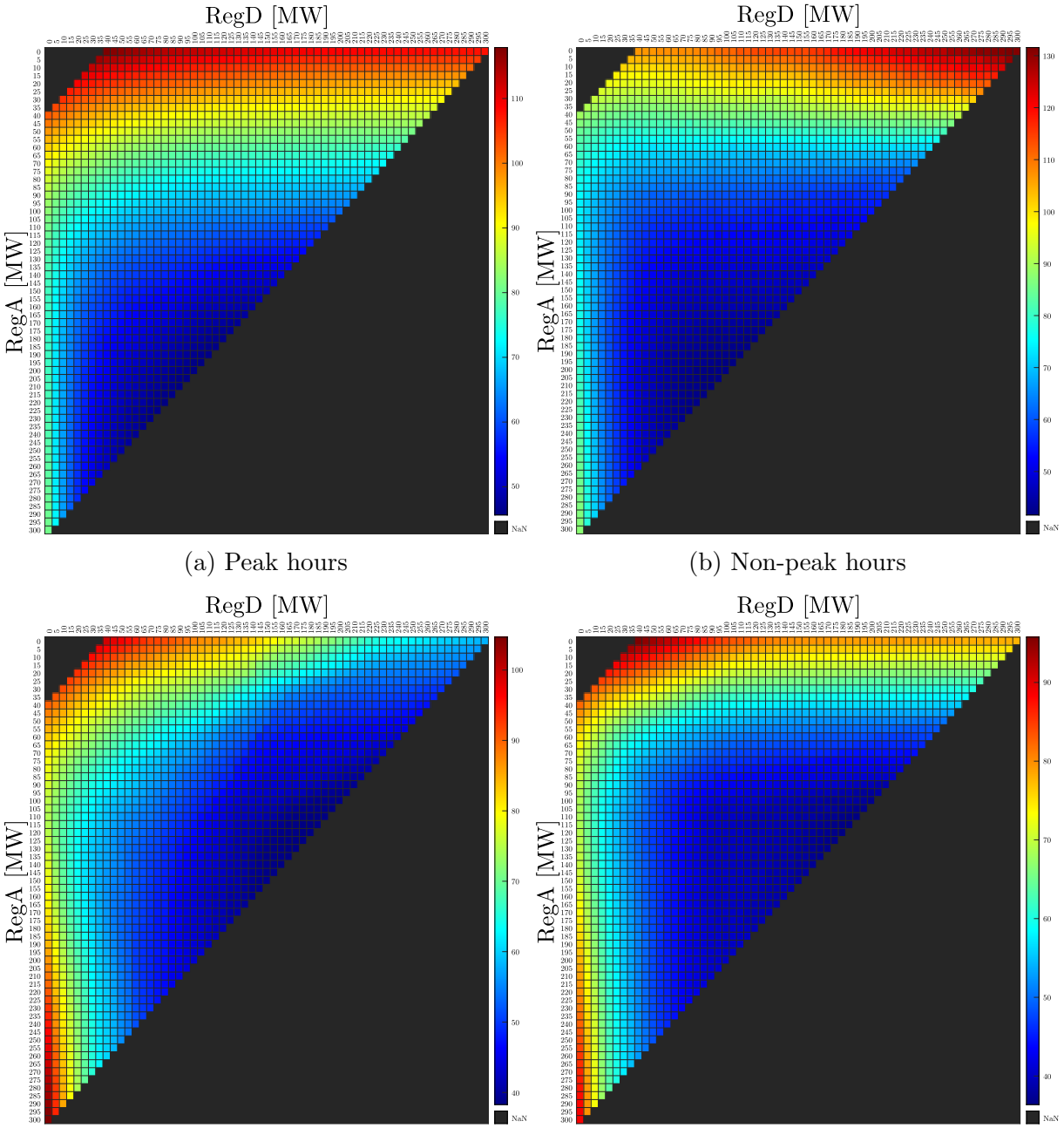

(a) Peak hours

(b) Non-peak hours

(c) Morning ramp hours

(d) Evening ramp hours

Figure A.12: Heat maps for Winter and 2 h BESS.

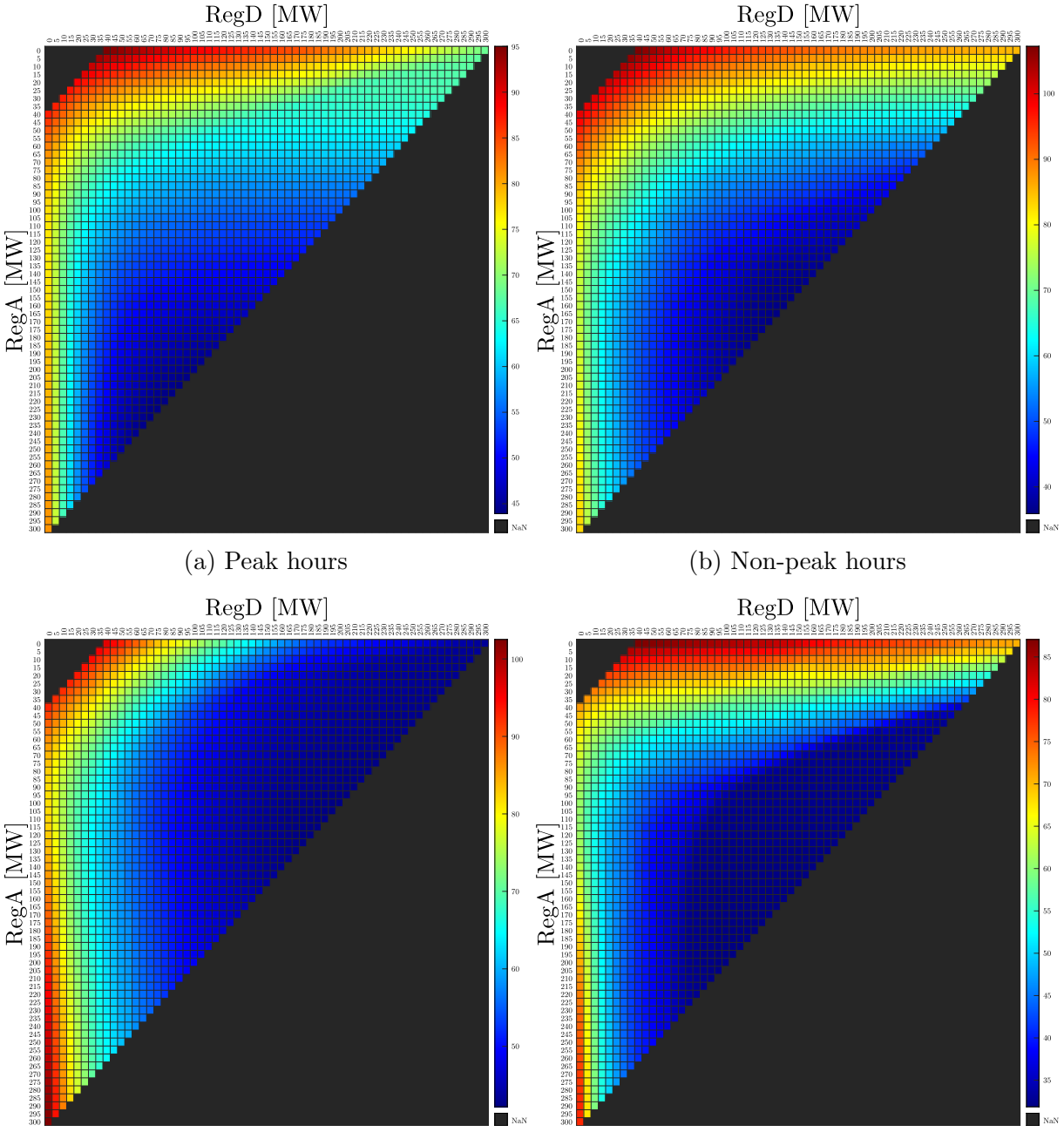

(a) Peak hours

(b) Non-peak hours

(c) Morning ramp hours

(d) Evening ramp hours

Figure A.13: Heat maps for Spring and 4 h BESS.

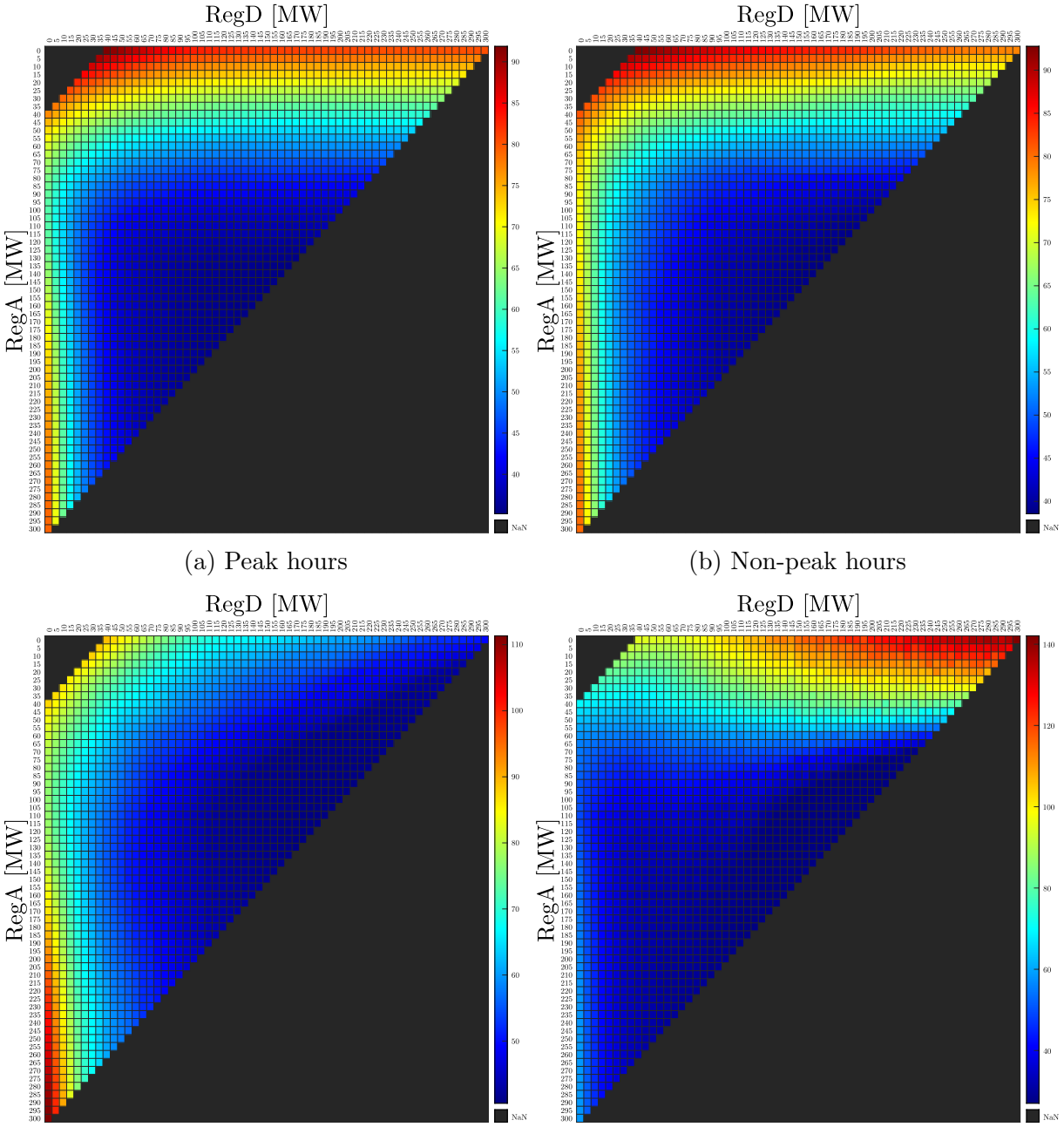

(a) Peak hours

(b) Non-peak hours

(c) Morning ramp hours

(d) Evening ramp hours

Figure A.14: Heat maps for Summer and 4 h BESS.

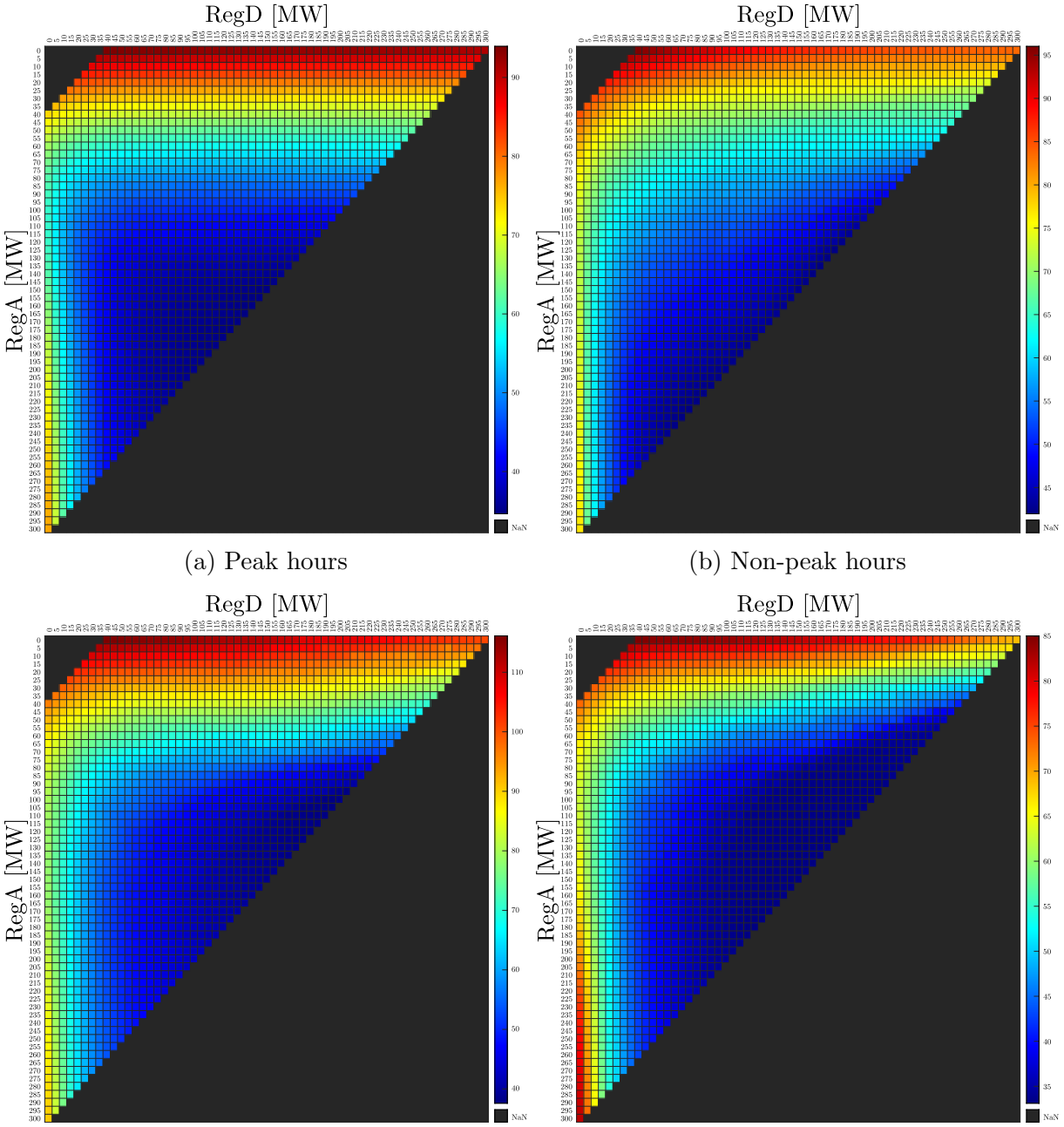

(a) Peak hours

(b) Non-peak hours

(c) Morning ramp hours

(d) Evening ramp hours

Figure A.15: Heat maps for Fall and 4 h BESS.

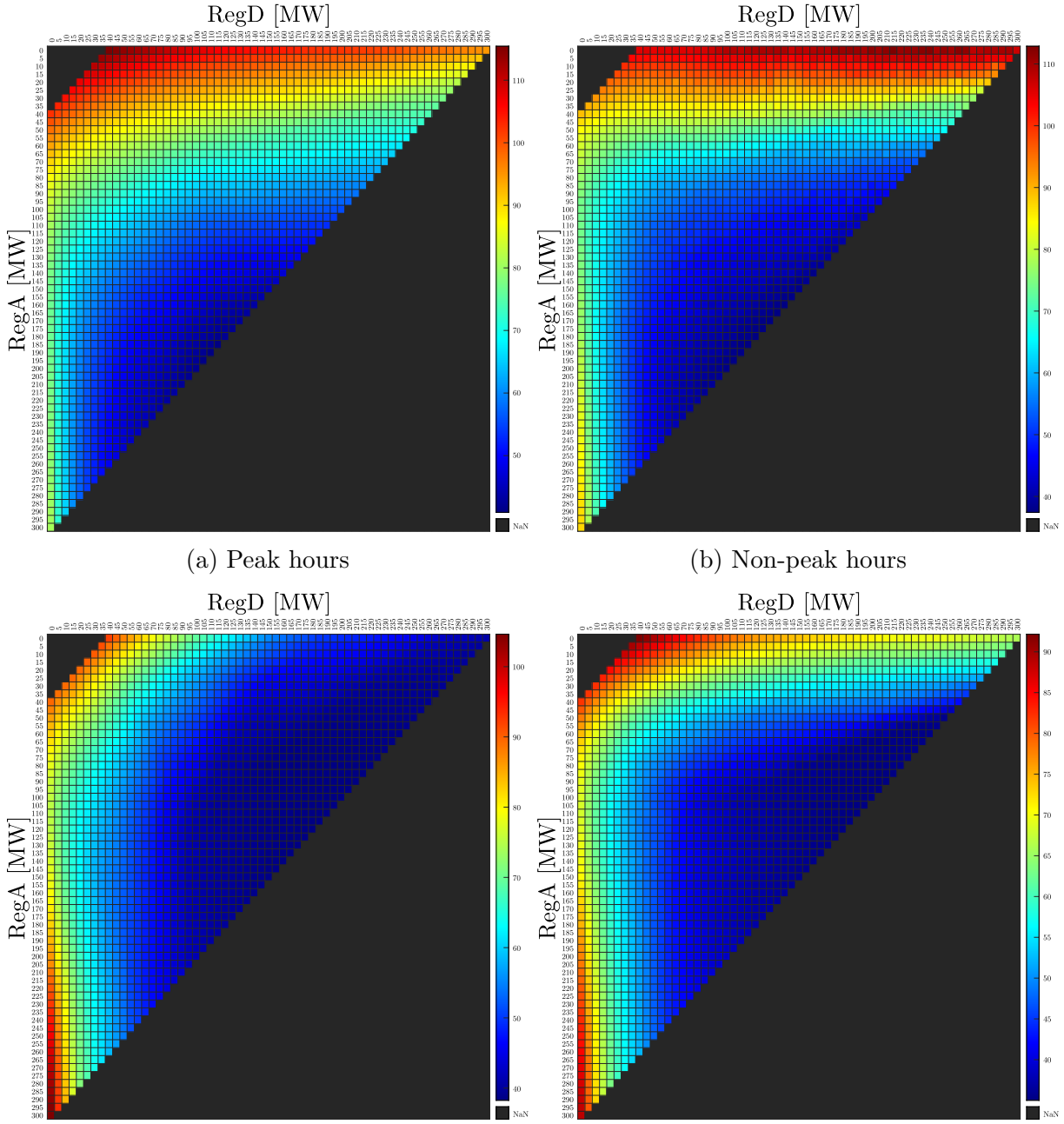

(a) Peak hours

(b) Non-peak hours

(c) Morning ramp hours

(d) Evening ramp hours

Figure A.16: Heat maps for Winter and 4 h BESS.

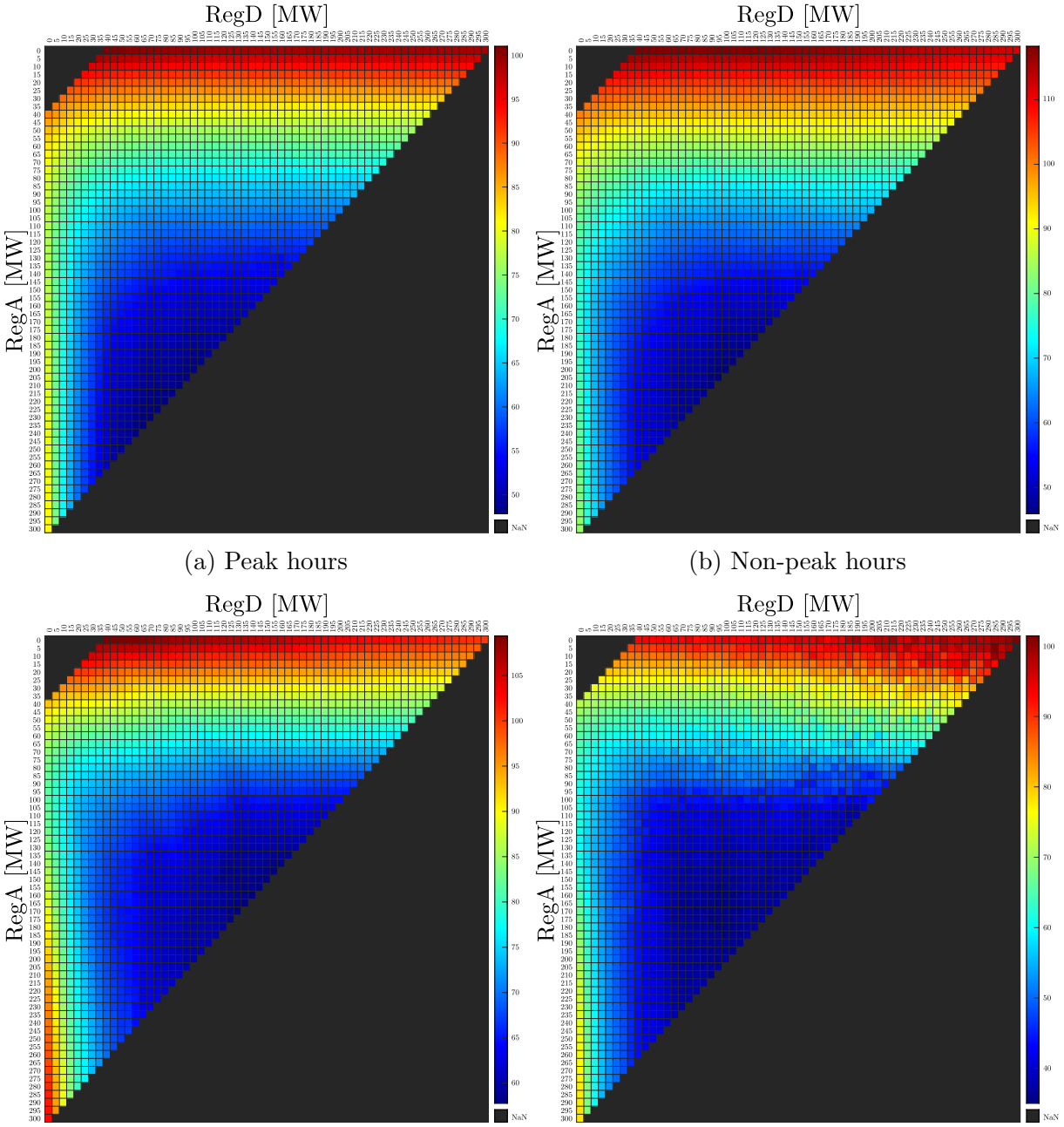

(a) Peak hours

(b) Non-peak hours

(c) Morning ramp hours

(d) Evening ramp hours

Figure A.17: Heat maps for Spring and 15 min FESS.

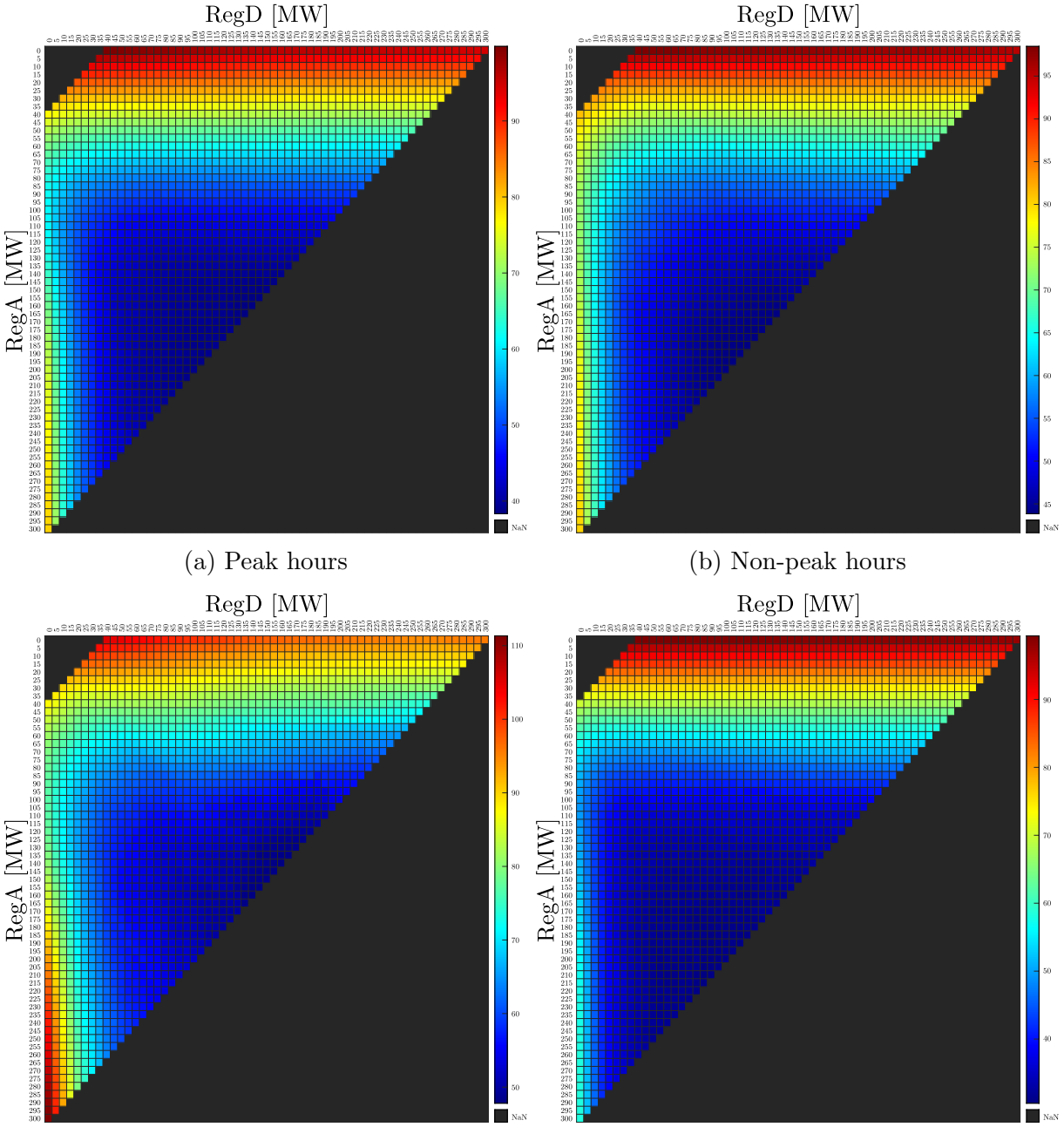

(a) Peak hours

(b) Non-peak hours

(c) Morning ramp hours

(d) Evening ramp hours

Figure A.18: Heat maps for Summer and 15 min FESS.

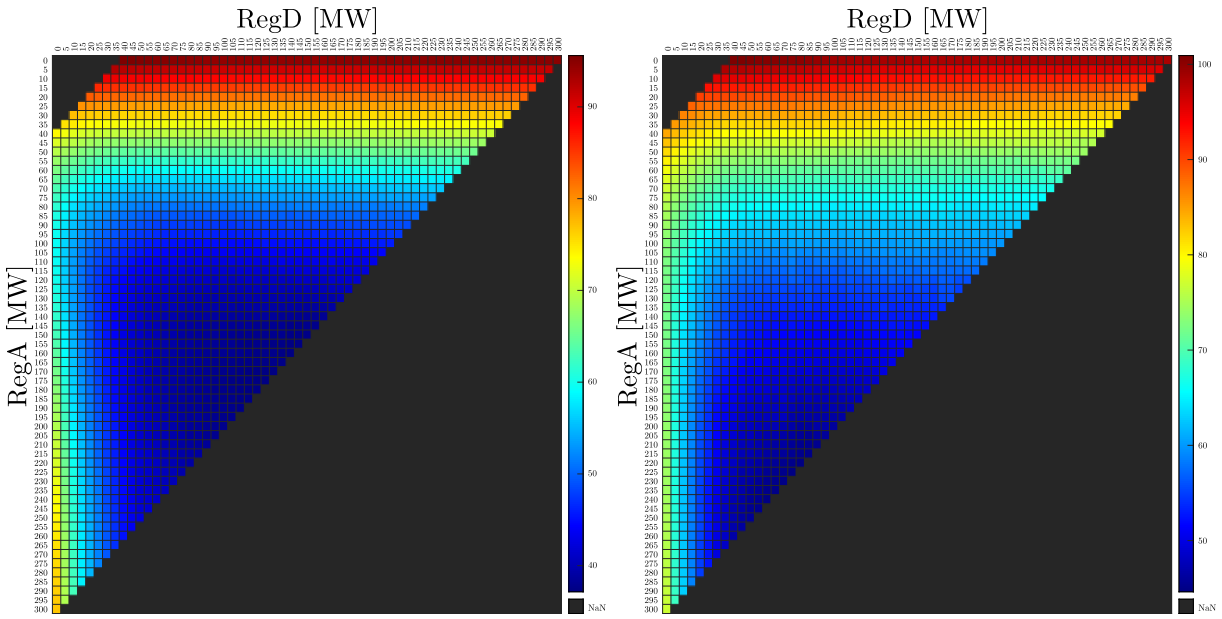

(a) Peak hours

(b) Non-peak hours

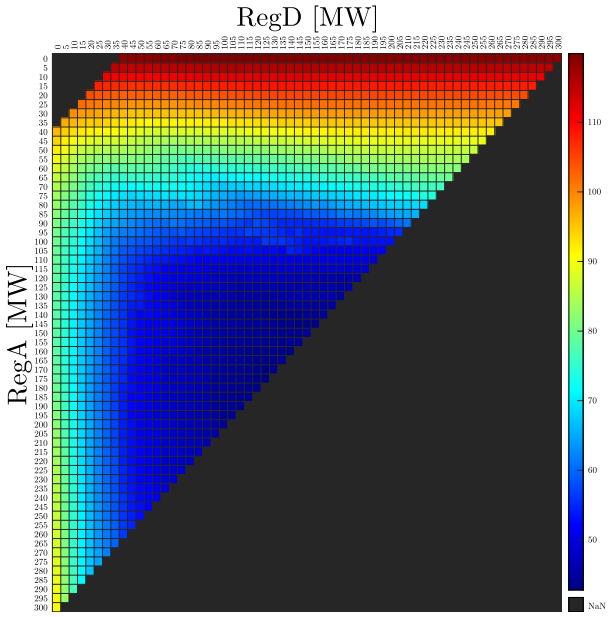

(c) Morning ramp hours

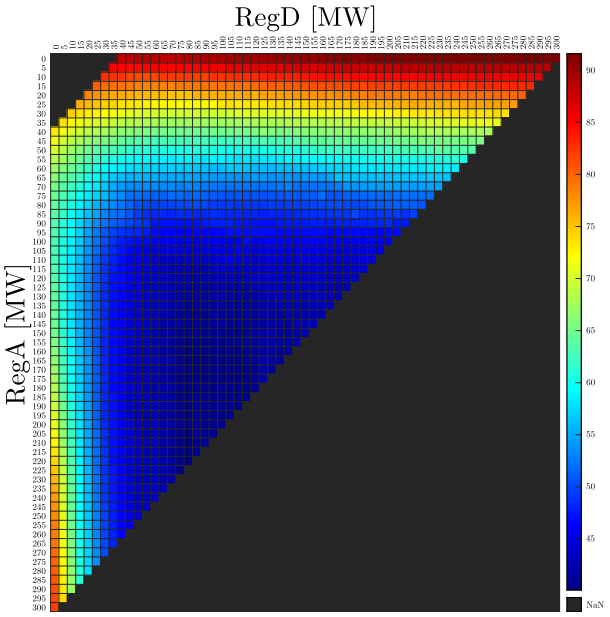

(d) Evening ramp hours

Figure A.19: Heat maps for Fall and 15 min FESS.

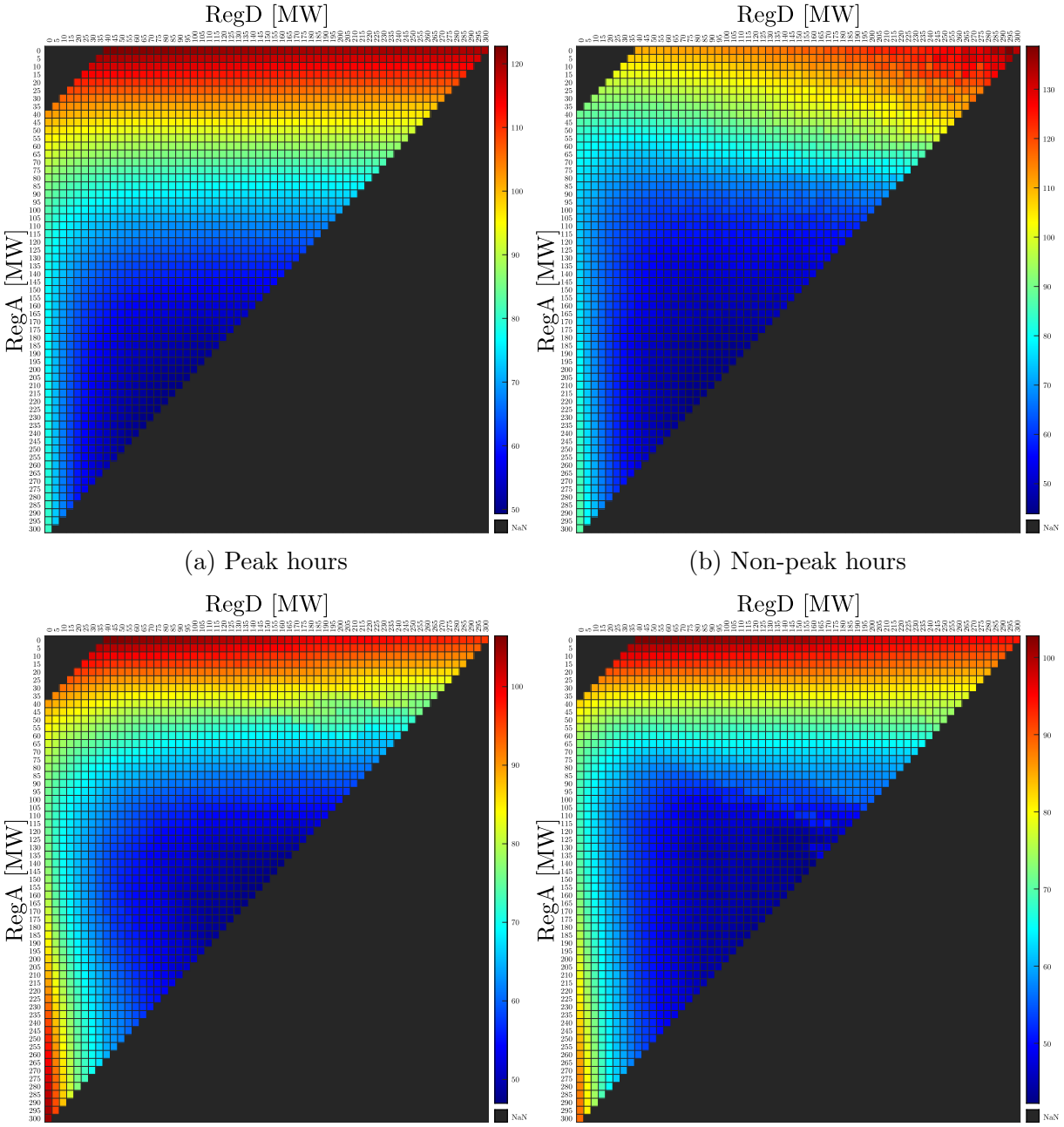

(a) Peak hours

(b) Non-peak hours

(c) Morning ramp hours

(d) Evening ramp hours

Figure A.20: Heat maps for Winter and 15 min FESS.

Appendix B

MRTS Curves' Parameters

The parameters presented in Table B.1 to Table B.5 correspond to the coefficients of each segment of the MRTS curves corresponding to all the 80 cases analyzed in Chapter 5, which consider combinations of the following features:

- Seasons: Spring, Summer, Fall, and Winter.
- Scenarios: Peak hours, Non-peak hours, Morning ramp hours, and Evening ramp hours.
- ESS technologies and discharging times: 15 min BESS, 1 h BESS, 2 h BESS, 4 h BESS, and 15 min FESS.

Table B.1: Parameters of MRTS curves for 15 min BESS.

Scenarios	Seg.	Spring		Summer		Fall		Winter	
	v	$2\tilde{a}$	$\tilde{b}$	$2\tilde{a}$	$\tilde{b}$	$2\tilde{a}$	$\tilde{b}$	$2\tilde{a}$	$\tilde{b}$
Peak hours	1	-0.90579	6.93091	-0.90972	6.185455	-1.08169	7.079888	-0.16754	1.965957
	2	-0.26822	3.743083	-0.16622	2.467967	-0.16891	2.515993	-0.10084	1.632468
	3	-0.04834	1.544279	-0.03679	1.173648	-0.03813	1.208208	-0.0239	0.863038
	4	-0.01021	0.590983	-0.00916	0.483014	-0.00868	0.471974	-0.00733	0.4488
	5	-0.00037	0.098879	-0.00069	0.059184	-0.00277	0.176306	-0.00217	0.190764
	6	-0.00059	0.11582	-1.27E-05	0.008665	-6.44E-05	4.14E-11	-0.00022	0.045037
Non-peak hours	1	-0.24267	2.514036	-1.35223	9.264273	-0.70383	5.598677	-0.59748	4.62024
	2	-0.11526	1.87696	-0.18984	3.452338	-0.18176	2.988314	-0.10618	2.163729
	3	-0.02029	0.927342	-0.08069	2.360776	-0.05512	1.721934	-0.05235	1.625465
	4	-0.01294	0.743506	-0.0097	0.586106	-0.01197	0.64322	-0.0165	0.729104
	5	-0.0014	0.166745	-0.00399	0.300459	-0.00033	0.0613	-0.00311	0.059683
	6	-0.00114	0.147041	-0.00016	0.013283	-0.00019	0.050808	-0.00227	0
Morning ramp hours	1	-1.44298	8.655111	-1.53094	9.492717	-0.37871	4.306615	-0.14594	2.642428
	2	-0.15068	2.193589	-0.15999	2.638006	-0.18465	3.336306	-0.18619	2.843666
	3	-0.03484	1.035215	-0.04913	1.529386	-0.07567	2.246524	-0.03268	1.308492
	4	-1.90E-12	0.164216	-0.0148	0.67119	-0.01255	0.668608	-0.00763	0.682452
	5	-4.34E-12	0.164216	-0.00138	9.84E-12	-1.18E-14	0.041069	-0.00737	0.669423
	6	-0.00139	0.268298	-0.00137	0	-0.00124	0.133929	-0.00089	0.183327
Evening ramp hours	1	-1.18812	7.322718	-0.45988	3.795849	-0.17881	2.650775	-0.89212	6.506176
	2	-0.08939	1.829082	-0.18207	2.406838	-0.20302	2.77179	-0.17709	2.93105
	3	-0.05559	1.491072	-0.05011	1.087202	-4.44E-16	0.741644	-0.04876	1.647713
	4	-5.04E-15	0.101396	-0.00662	4.18E-12	-0.02349	1.328979	-0.01672	0.846698
	5	-0.0033	0.266226	-0.00662	1.28E-11	-0.0034	0.324091	-0.00187	0.104262
	6	-0.00207	0.174268	-0.00662	0	-0.00092	0.138506	-0.00048	0

Table B.2: Parameters of MRTS curves for 1 h BESS.

Scenarios	Seg.	Spring		Summer		Fall		Winter	
	v	$2\tilde{a}$	$\tilde{b}$	$2\tilde{a}$	$\tilde{b}$	$2\tilde{a}$	$\tilde{b}$	$2\tilde{a}$	$\tilde{b}$
Peak hours	1	-1.08154	7.731113	-1.00753	6.677322	-1.07152	7.130538	-0.17255	2.180811
	2	-0.19599	3.303366	-0.12993	2.289311	-0.16463	2.596062	-0.10741	1.855106
	3	-0.05741	1.917559	-0.04072	1.397228	-0.04072	1.357017	-0.02847	1.065683
	4	-0.01261	0.79745	-0.0114	0.664277	-0.01135	0.62267	-0.00544	0.489858
	5	-0.00297	0.315419	-0.0001	0.099315	-0.00118	0.114358	-0.00395	0.415388
	6	-0.0005	0.130623	-0.00023	0.108779	-0.00047	0.060486	-0.00088	0.185226
Non-peak hours	1	-0.29239	2.903772	-1.47525	9.736662	-0.88391	6.382552	-0.43978	4.323309
	2	-0.11104	1.996984	-0.16101	3.165465	-0.13036	2.614807	-0.24538	3.351315
	3	-0.02215	1.108095	-0.07334	2.288826	-0.05623	1.873493	-0.03753	1.272823
	4	-0.01239	0.864056	-0.0136	0.795292	-0.01241	0.778012	-0.0118	0.629515
	5	-0.00315	0.402072	-0.00367	0.298561	-0.00208	0.261595	-0.00266	0.17262
	6	-0.00095	0.237048	-1.86E-16	0.045971	-0.00063	0.152651	-0.00065	0.02188
Morning ramp hours	1	-1.39669	8.830125	-1.57058	10	-0.3814	4.386852	-0.16992	3.439914
	2	-0.19016	2.797445	-0.14421	2.86816	-0.21505	3.555102	-0.2821	4.000791
	3	-0.03695	1.265341	-0.06533	2.079318	-0.06756	2.080194	-0.04275	1.607318
	4	-0.00028	0.348612	-0.00948	0.683093	-0.00956	0.630265	-0.00646	0.700029
	5	-0.0016	0.41475	-1.46E-12	0.20921	-0.00533	0.41862	-0.00386	0.569944
	6	-0.00101	0.370825	-0.00083	0.271477	-0.00071	0.072346	-0.00103	0.357854
Evening ramp hours	1	-1.27747	8.084507	-0.46111	4.07516	-1.17416	8.096931	-1.03682	7.352799
	2	-0.13947	2.394515	-0.07885	2.163818	-0.16822	3.067224	-0.19221	3.129762
	3	-0.04611	1.460976	-0.10246	2.399836	-0.06243	2.009258	-0.05677	1.775346
	4	-1.09E-12	0.308143	-0.00646	3.74E-12	-0.01268	0.76557	-0.00911	0.583751
	5	-0.02098	1.3571	-0.00646	6.31E-12	-0.00206	0.234495	-3.52E-14	0.128307
	6	-0.00281	0	-0.00646	0	-0.00085	0.143827	-0.00023	0.145452

Table B.3: Parameters of MRTS curves for 2 h BESS.

Scenarios	Seg.	Spring		Summer		Fall		Winter	
	v	$2\tilde{a}$	$\tilde{b}$	$2\tilde{a}$	$\tilde{b}$	$2\tilde{a}$	$\tilde{b}$	$2\tilde{a}$	$\tilde{b}$
Peak hours	1	-1.08246	7.855785	-0.97289	6.774502	-1.05631	7.08515	-0.20958	2.463558
	2	-0.20436	3.465304	-0.14365	2.628296	-0.16503	2.628741	-0.10823	1.956802
	3	-0.05908	2.012465	-0.04607	1.652502	-0.04213	1.399756	-0.03017	1.176201
	4	-0.01312	0.863502	-0.01335	0.834627	-0.01062	0.612022	-0.00532	0.554972
	5	-0.00253	0.333952	-0.00123	0.228531	-0.00305	0.233673	-0.00489	0.533114
	6	-0.00069	0.1957	-0.00099	0.210129	-0.00011	0.012942	-0.00115	0.253175
Non-peak hours	1	-0.30088	3.189891	-1.49321	10	-0.86407	6.45244	-0.38095	4.258444
	2	-0.10156	2.19332	-0.21891	3.628484	-0.15516	2.907893	-0.27521	3.729768
	3	-0.02703	1.447998	-0.05477	1.987121	-0.05137	1.869988	-0.0364	1.341618
	4	-0.01546	1.158692	-0.01911	1.09567	-0.01671	1.003335	-0.02025	0.937978
	5	-0.0055	0.660841	-0.00156	0.218171	-0.00264	0.300214	-0.00149	2.84E-14
	6	-0.00146	0.357604	-0.00051	0.139519	-0.00044	0.134651	-0.00139	0
Morning ramp hours	1	-1.46317	9.504323	-1.45961	10	-0.37831	4.417105	-0.1542	3.534785
	2	-0.18095	3.093248	-0.22025	3.803219	-0.21322	3.591647	-0.26954	4.111526
	3	-0.04607	1.744456	-0.04554	2.056094	-0.06963	2.155687	-0.03824	1.798513
	4	-0.00022	0.598146	-0.02416	1.521729	-0.00924	0.646091	-0.0104	1.10253
	5	-0.00654	0.914339	-4.46E-15	0.313574	-0.008	0.584053	-0.01356	1.260263
	6	-0.00238	0.602299	-0.00083	0.375504	-3.76E-05	4.05E-13	-1.34E-12	0.243359
Evening ramp hours	1	-1.22244	8.0441	-0.49914	4.151296	-0.17445	2.793356	-1.26334	8.333614
	2	-0.0862	2.362914	-0.078	2.045587	-0.1188	2.515121	-0.10249	2.529366
	3	-0.0743	2.243853	-0.08414	2.106929	-0.02146	1.541738	-0.06067	2.111117
	4	-1.28E-13	0.386474	-0.00809	0.205725	-0.03654	1.918768	-0.01185	0.890598
	5	-0.0124	1.006616	-0.00397	5.86E-11	-0.0023	0.206607	-4.47E-14	0.298344
	6	-0.00116	0.163613	-0.00397	1.78E-15	-8.94E-09	0.034094	-0.00219	0.462463

Table B.4: Parameters of MRTS curves for 4 h BESS.

Scenarios	Seg.	Spring		Summer		Fall		Winter	
	v	$2\tilde{a}$	$\tilde{b}$	$2\tilde{a}$	$\tilde{b}$	$2\tilde{a}$	$\tilde{b}$	$2\tilde{a}$	$\tilde{b}$
Peak hours	1	-1.07885	8.141602	-1.00576	6.973833	-0.99604	6.98219	-0.23979	2.630005
	2	-0.23027	3.898709	-0.16003	2.745143	-0.20416	3.022771	-0.09195	1.890795
	3	-0.06155	2.211466	-0.04144	1.559252	-0.0486	1.467167	-0.03027	1.274069
	4	-0.01524	1.05371	-0.01152	0.811334	-0.00651	0.414961	-0.00603	0.66796
	5	-0.00358	0.470847	-0.00324	0.397217	-0.00269	0.224057	-0.00474	0.603641
	6	-0.00037	0.230422	-0.00122	0.246127	-0.00014	0.032889	-0.0008	0.307747
Non-peak hours	1	-0.32431	3.5707	-1.40512	10	-0.89766	6.675633	-0.41907	4.718717
	2	-0.11528	2.525519	-0.2933	4.440927	-0.17477	3.061215	-0.25212	3.883982
	3	-0.02797	1.652402	-0.05357	2.043611	-0.04789	1.792376	-0.05677	1.930407
	4	-0.01645	1.364532	-0.02204	1.255256	-0.00991	0.842966	-0.01727	0.943053
	5	-0.00806	0.944949	-0.00097	0.201675	-0.00883	0.788621	-1.34E-08	0.07941
	6	-0.00206	0.495044	-0.00048	0.165166	-0.00054	0.167242	-1.86E-08	0.079409
Morning ramp hours	1	-1.43354	10	-1.38425	10	-0.34113	4.464424	-0.81679	6.290797
	2	-0.2649	4.15682	-0.25982	4.377841	-0.22591	3.888293	-0.04699	2.441832
	3	-0.03892	1.89704	-0.04291	2.208763	-0.07728	2.402013	-0.05718	2.54371
	4	-0.00737	1.108198	-0.01737	1.570056	-0.00877	0.689433	-0.00882	1.334585
	5	-0.00853	1.166375			-0.00811	0.655992	-0.01316	1.55186
	6	-0.00029	0.548083			-2.24E-09	0.048092	-1.88E-14	0.564717
Evening ramp hours	1	-1.03386	8.018112	-0.68052	4.743398	-1.24128	8.483822	-1.22251	8.459048
	2	-0.31051	4.401349	-0.02753	1.478447	-0.20942	3.324527	-0.14105	3.051765
	3	-0.05762	1.872487	-0.08088	2.01196	-0.05244	1.754725	-0.06608	2.302092
	4	-0.00999	0.681826	-0.0027	0.057472	-0.00899	0.668538	-0.01166	0.941472
	5	-1.51E-12	0.182122	-0.00155	2.01E-09	-0.00347	0.392324	-0.00164	0.440512
	6	-0.00062	0.22843	-0.00155	0	-0.00024	0.149887	-0.00208	0.473281

Table B.5: Parameters of MRTS curves for 15 min FESS.

Scenarios	Seg.	Spring		Summer		Fall		Winter	
	v	$2\tilde{a}$	$\tilde{b}$	$2\tilde{a}$	$\tilde{b}$	$2\tilde{a}$	$\tilde{b}$	$2\tilde{a}$	$\tilde{b}$
Peak hours	1	-0.82585	6.628104	-0.91476	6.04807	-1.03248	6.845974	-0.16111	1.934501
	2	-0.26393	3.818481	-0.10559	2.002224	-0.17211	2.544161	-0.09931	1.625455
	3	-0.05501	1.729369	-0.04587	1.405058	-0.03496	1.172601	-0.02276	0.859979
	4	-0.00833	0.562362	-0.00853	0.471554	-0.01036	0.557537	-0.00761	0.481285
	5	-0.00226	0.258542	-0.00301	0.195452	-0.00188	0.133502	-0.00245	0.223516
	6	-0.00078	0.147819	-0.00037	0	-0.00014	0.003518	-0.00015	0.050596
Non-peak hours	1	-0.23792	2.546453	-1.33285	9.037868	-0.63103	5.484795	-0.53047	4.124847
	2	-0.09589	1.836276	-0.18923	3.319786	-0.23981	3.528687	-0.15853	2.265159
	3	-0.01996	1.076973	-0.07166	2.144085	-0.04792	1.609729	-0.01422	0.82206
	4	-0.02155	1.116653	-0.01192	0.650525	-0.01446	0.77332	-0.02185	1.012729
	5	-1.42E-12	0.039337	-0.00184	0.146397	-0.00072	0.086188	-0.00159	3.45E-12
	6	-0.00034	0.065098	-0.00019	0.022576	-0.00024	0.049978	-0.00155	0
Morning ramp hours	1	-1.17846	7.904693	-1.44131	9.265348	-0.43342	4.764388	-0.69099	4.892373
	2	-0.27985	3.411643	-0.18536	2.985585	-0.24224	3.808483	-0.05872	1.731018
	3	-0.02663	0.879417	-0.05338	1.665883	-0.06973	2.083329	-0.05037	1.647523
	4	-0.00632	0.371773	-0.01618	0.735784	-0.01109	0.617422	-0.00431	0.496119
	5	-5.6E-15	0.055545	-0.00146	2.84E-14	-3.4E-13	0.062967	-0.00858	0.709319
	6	-0.00027	0.075769	-0.00145	0	-0.00182	0.199339	-0.00039	0.095186
Evening ramp hours	1	-1.09994	7.043494	-0.74961	5.209527	-0.83863	6.816869	-0.81431	6.364745
	2	1.29E-05	1.543709	-0.15262	2.22455	-0.29559	4.101688	-0.26009	3.59366
	3	-0.09891	2.532925	-0.04058	1.104179	-0.04588	1.604549	-0.04077	1.400414
	4	-3.64E-15	0.060208	-0.00453	0.202977	-0.01261	0.772981	-0.01477	0.750456
	5	-0.00365	0.242739	-0.00047	6.57E-14	-0.00563	0.423547	-0.00145	0.084568
	6	-0.00053	0.008693	-0.00047	5.33E-15	-0.00044	0.034654	-0.00032	0

Appendix C

MRTS Curves Comparisons

The MRTS curves comparisons discussed in Chapter 5 and presented in Fig. C.1 to Fig. C.14 intend to find similarities among the MRTS, and are based on the following criteria:

- Peak vs Non-peak scenarios per season for different ESS technologies and discharging times.
- Morning vs Evening ramp scenarios per season for different ESS technologies and discharging times.
- ESS technologies and discharging times per season for all the scenarios.

The seasons, scenarios, and different ESSs and discharging times considered are as follows:

- Seasons: Spring, Summer, Fall, and Winter.
- Scenarios: Peak hours, Non-peak hours, Morning ramp hours, and Evening ramp hours.
- ESS technologies and discharging times: 15 min BESS, 1 h BESS, 2 h BESS, 4 h BESS, and 15 min FESS.

C.1 Peak vs Non-peak Scenarios

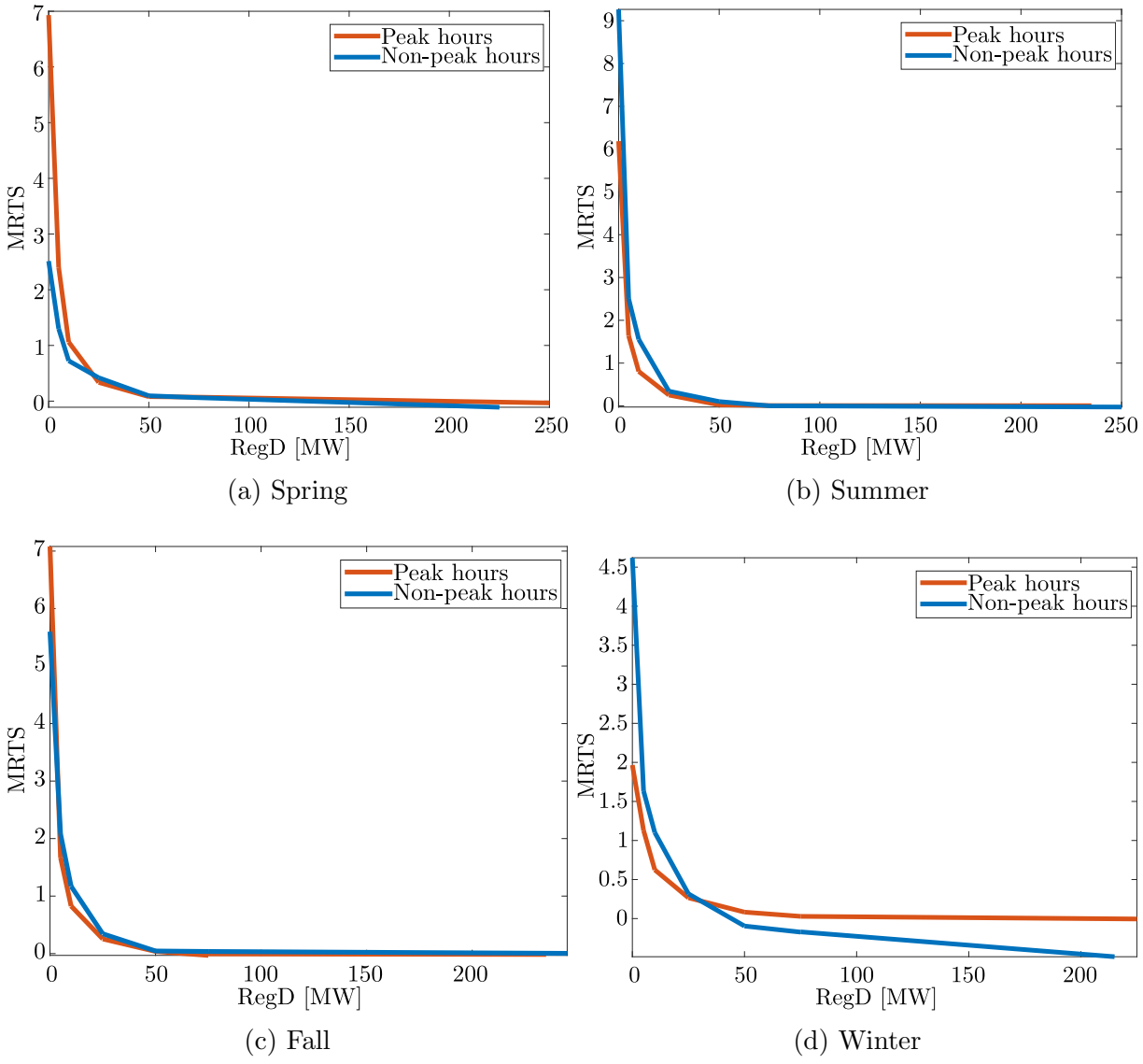

(a) Spring

(b) Summer

(c) Fall

(d) Winter

Figure C.1: Comparison of MRTS curves for Peak vs Non-peak scenarios per season for 15 min BESS.

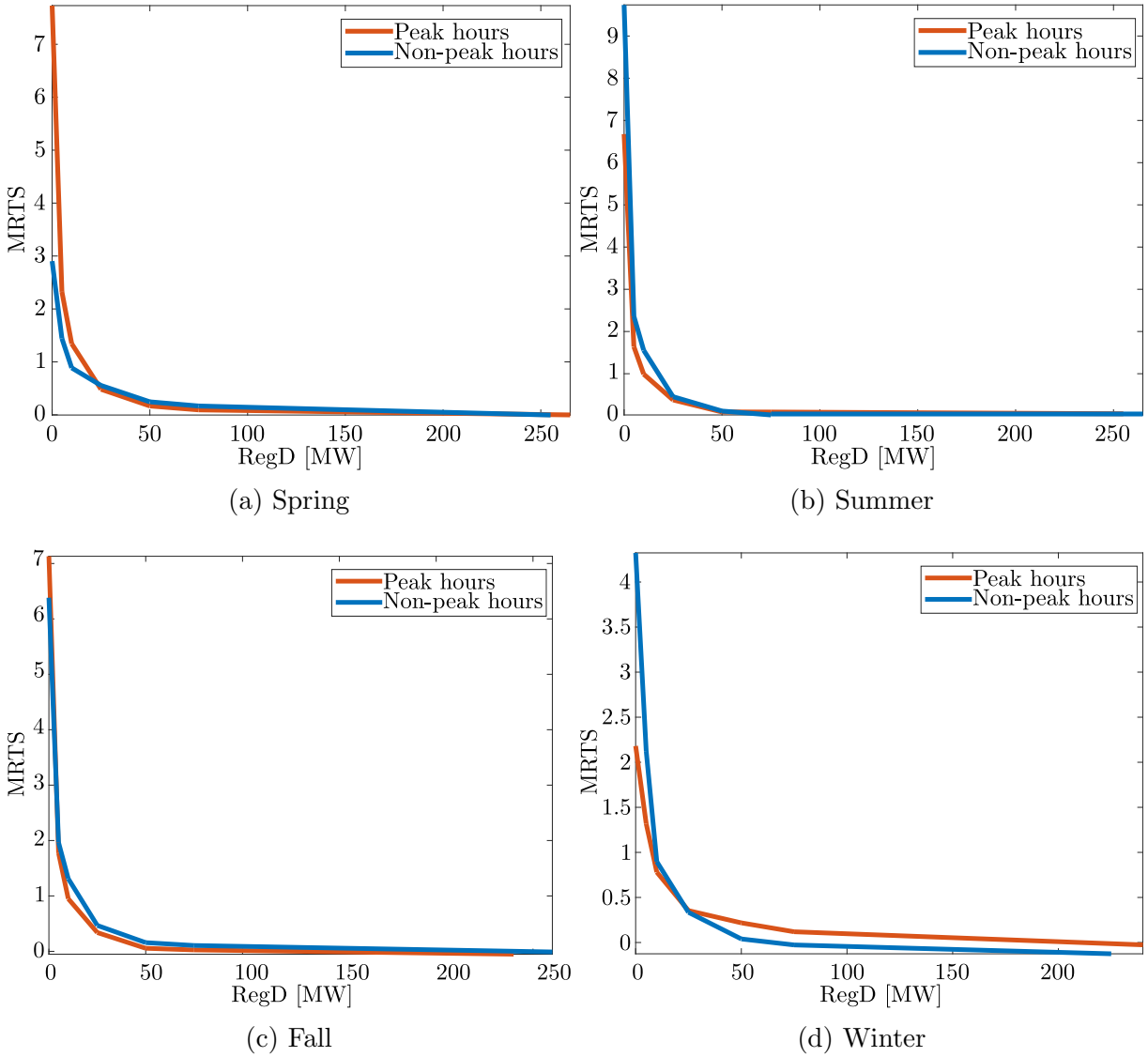

Figure C.2: Comparison of MRTS curves for Peak vs Non-peak scenarios per season for 1 h BESS.

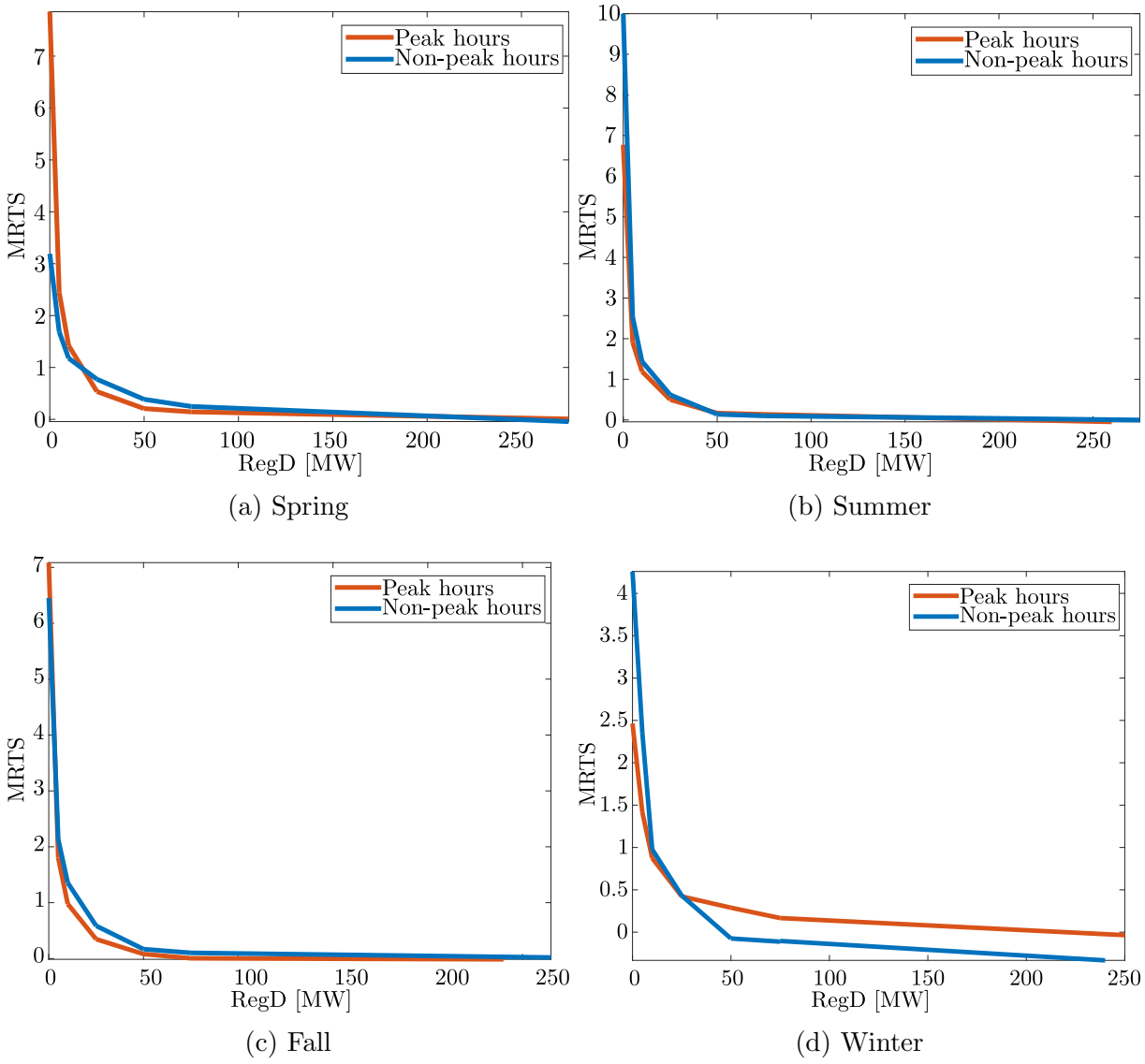

(a) Spring

(b) Summer

(c) Fall

(d) Winter

Figure C.3: Comparison of MRTS curves for Peak vs Non-peak scenarios per season for 2 h BESS.

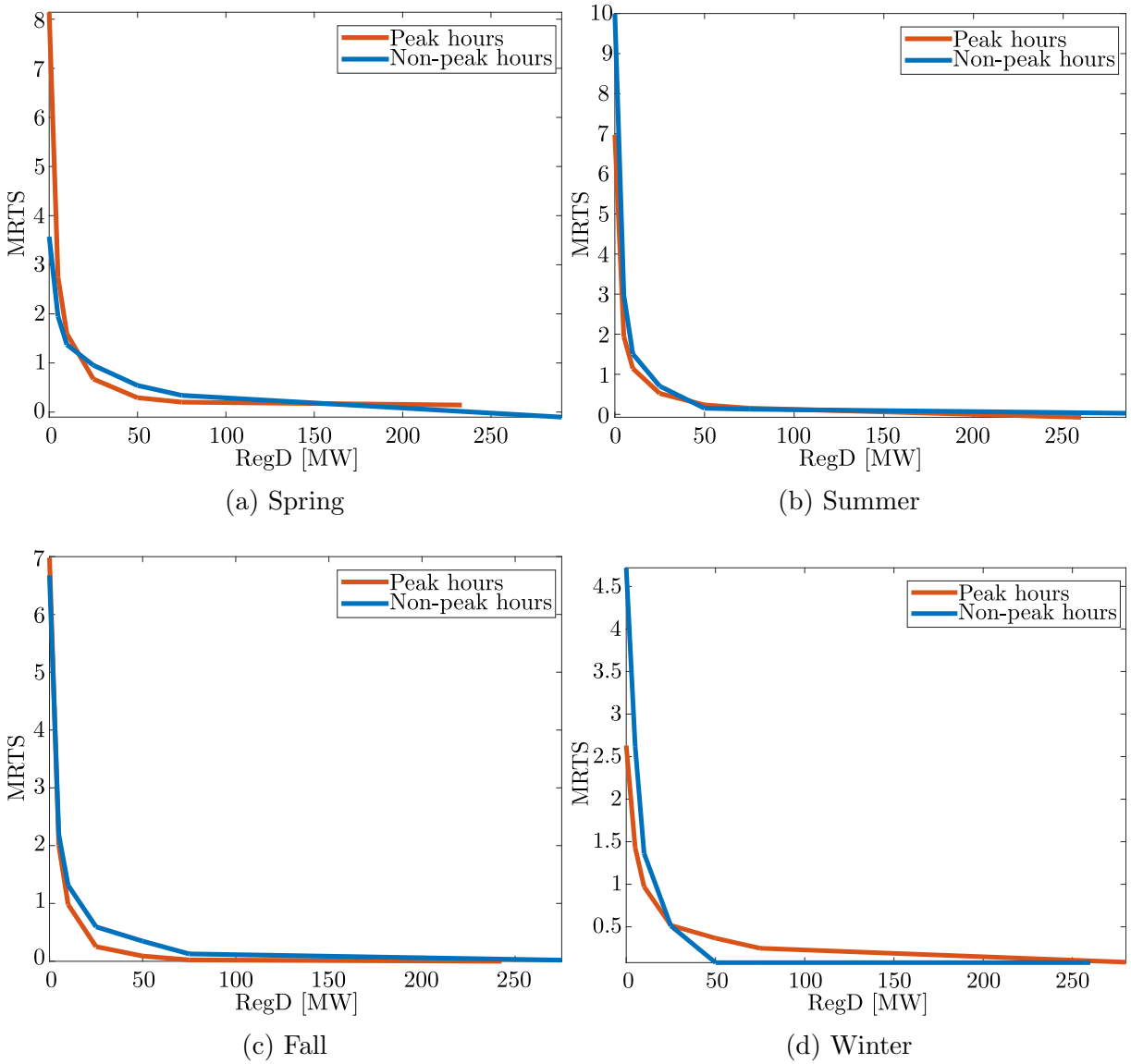

(a) Spring

(b) Summer

(c) Fall

(d) Winter

Figure C.4: Comparison of MRTS curves for Peak vs Non-peak scenarios per season for 4 h BESS.

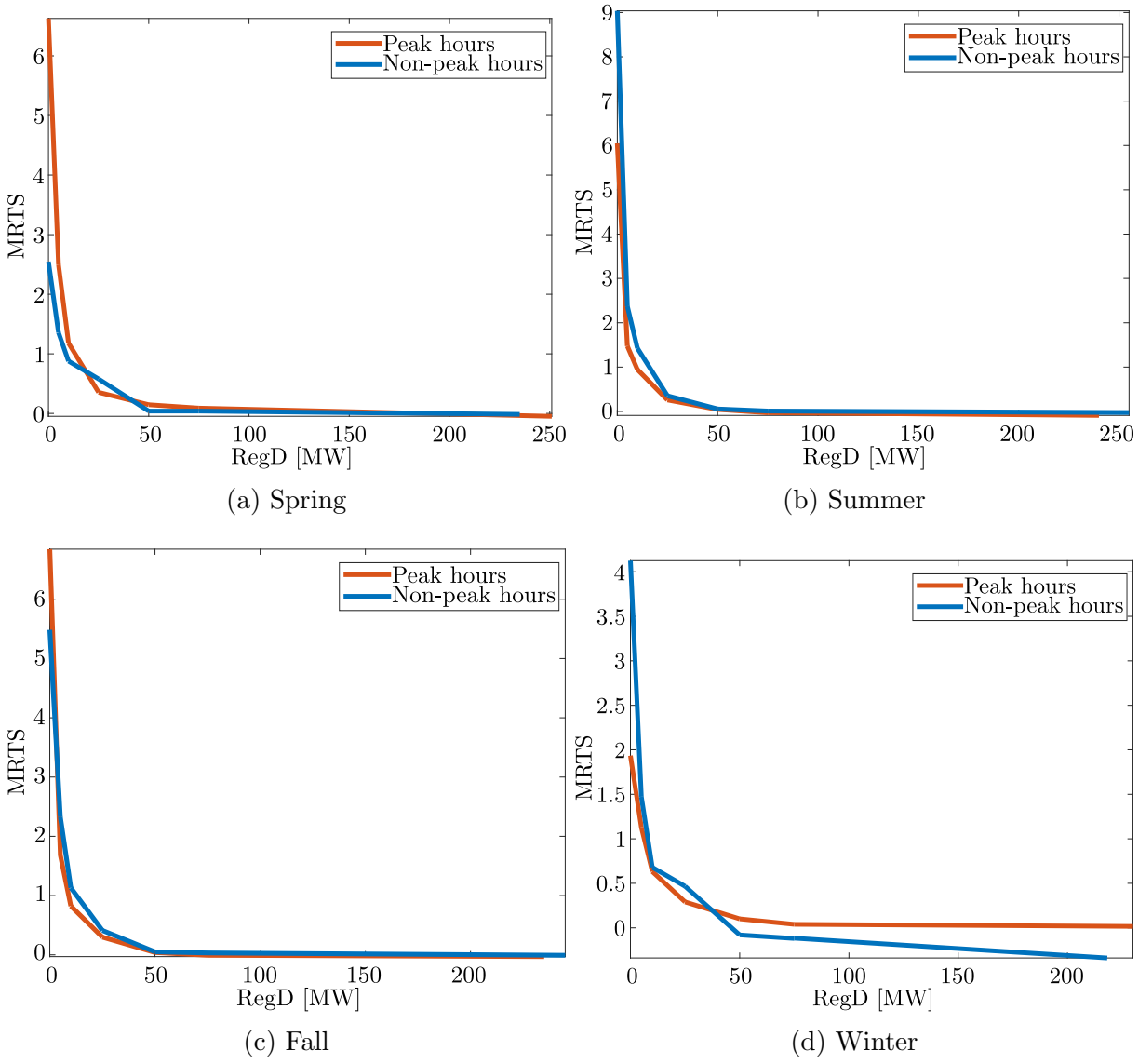

Figure C.5: Comparison of MRTS curves for Peak vs Non-peak scenarios per season for 15 min FESS.

C.2 Morning vs Evening Ramp Scenarios

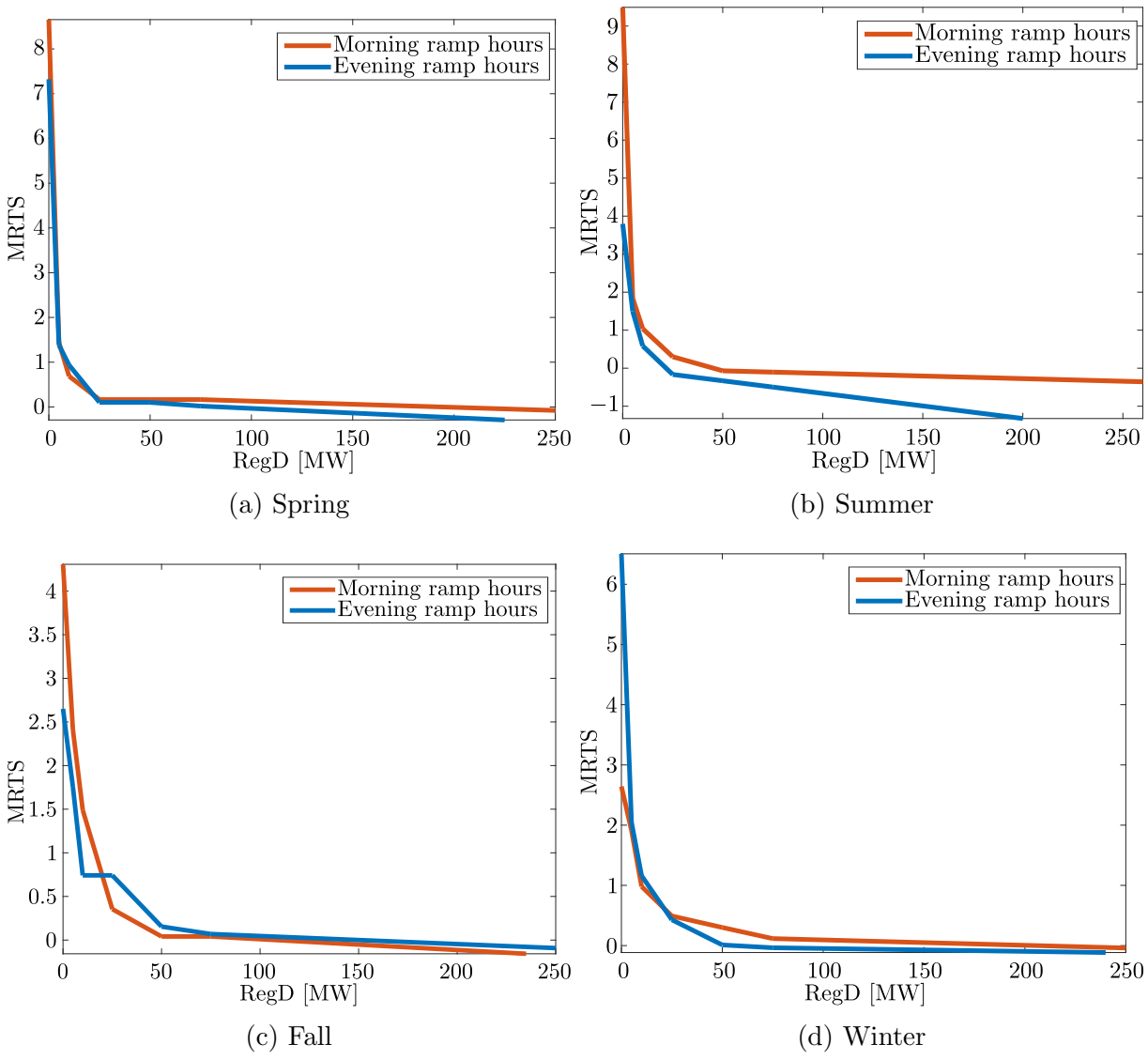

(a) Spring

(b) Summer

(c) Fall

(d) Winter

Figure C.6: Comparison of MRTS curves for Morning ramp vs Evening ramp scenarios per season for 15 min BESS.

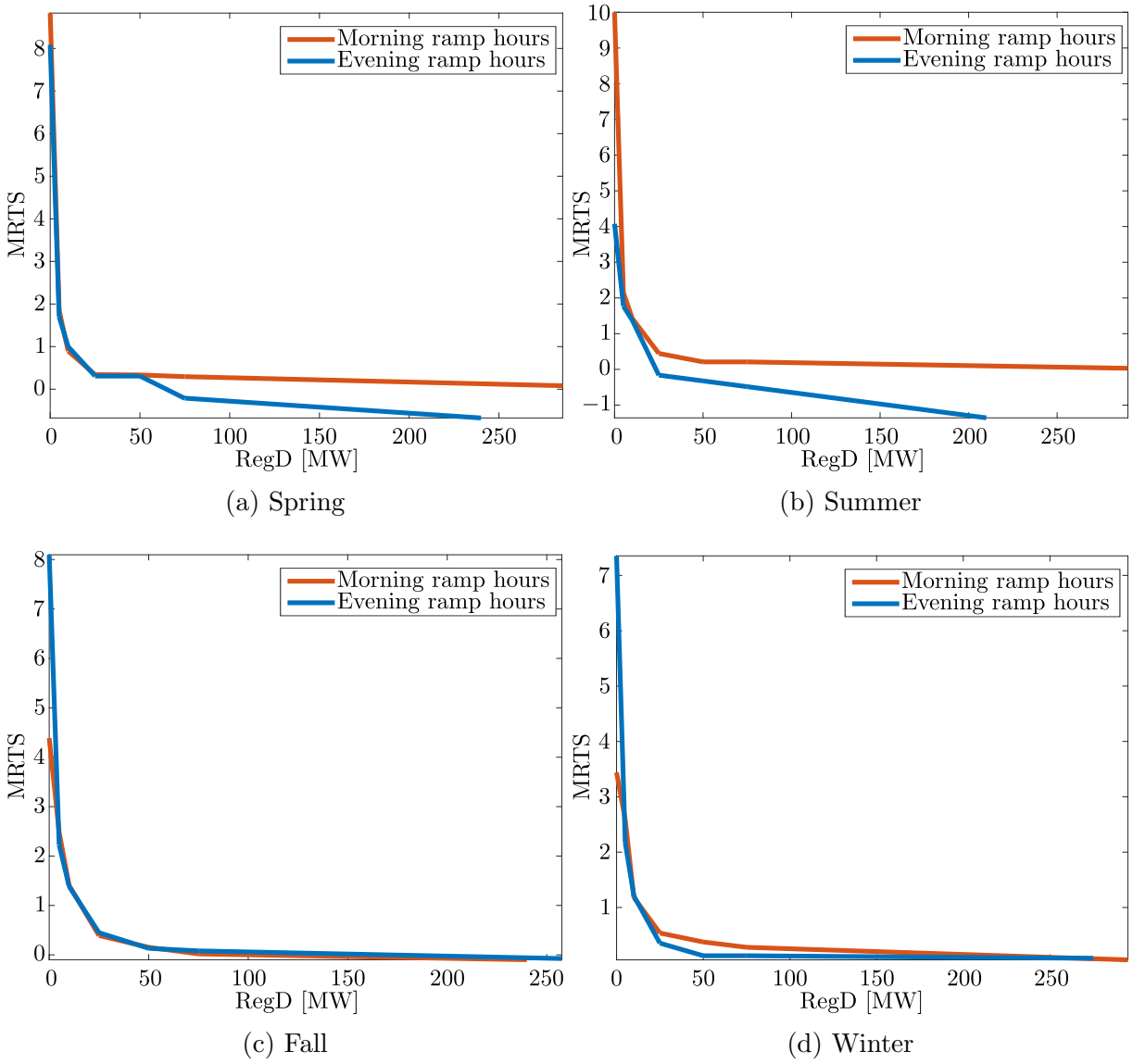

Figure C.7: Comparison of MRTS curves for Morning ramp vs Evening ramp scenarios per season for 1 h BESS.

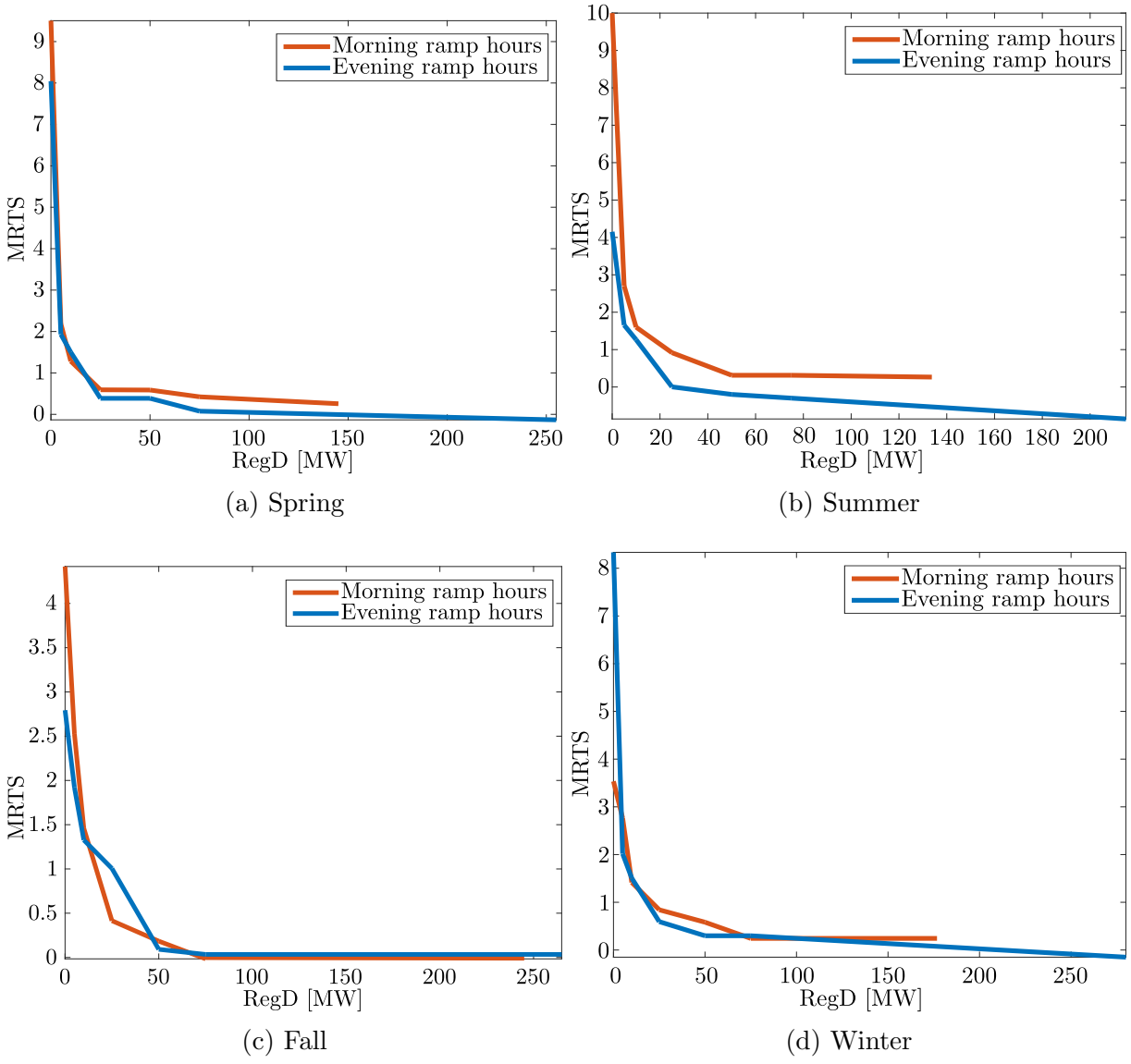

Figure C.8: Comparison of MRTS curves for Morning ramp vs Evening ramp scenarios per season for 2 h BESS.

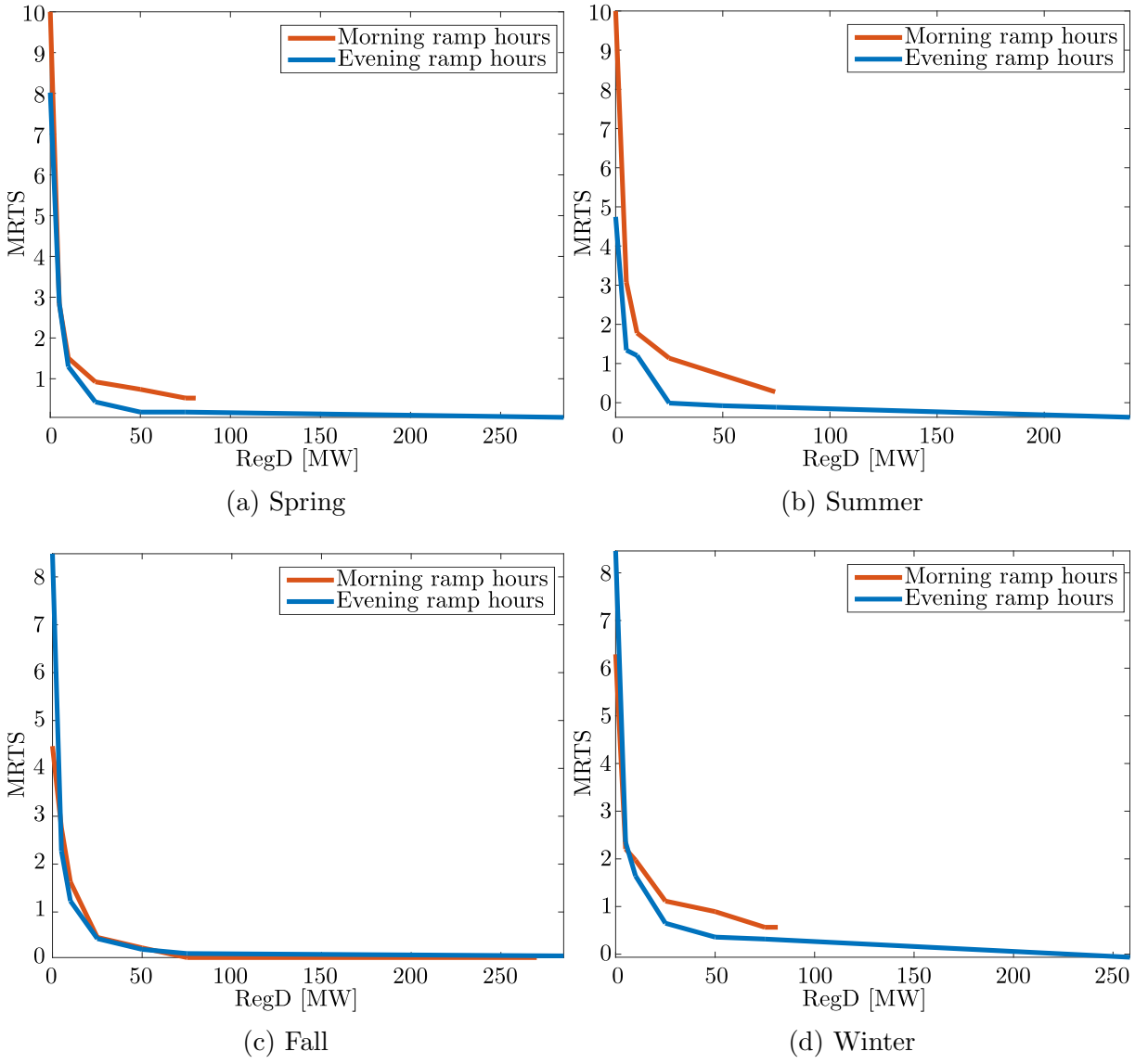

Figure C.9: Comparison of MRTS curves for Morning ramp vs Evening ramp scenarios per season for 4 h BESS.

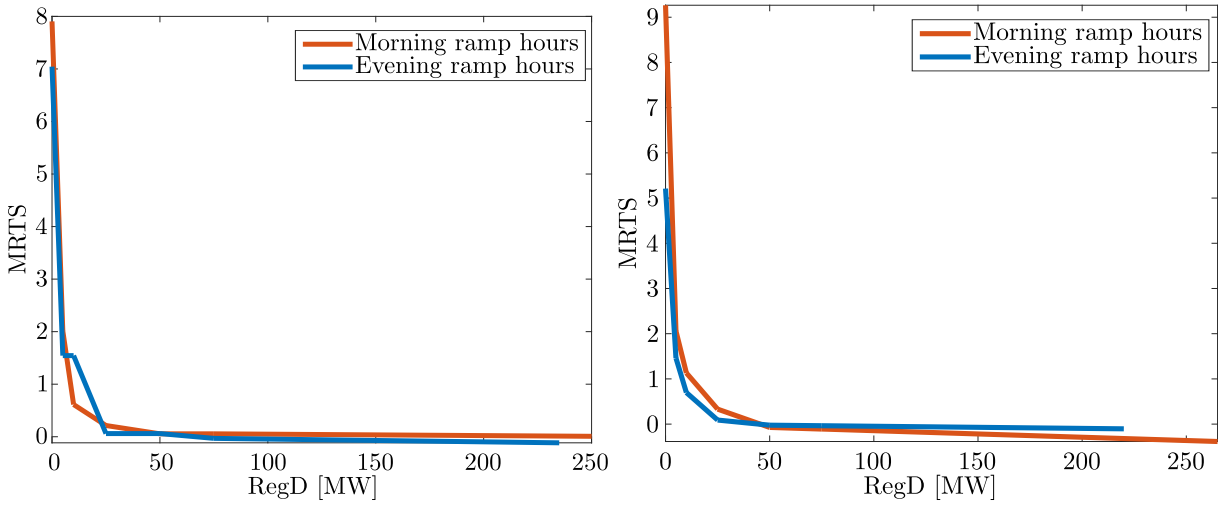

(a) Spring

(b) Summer

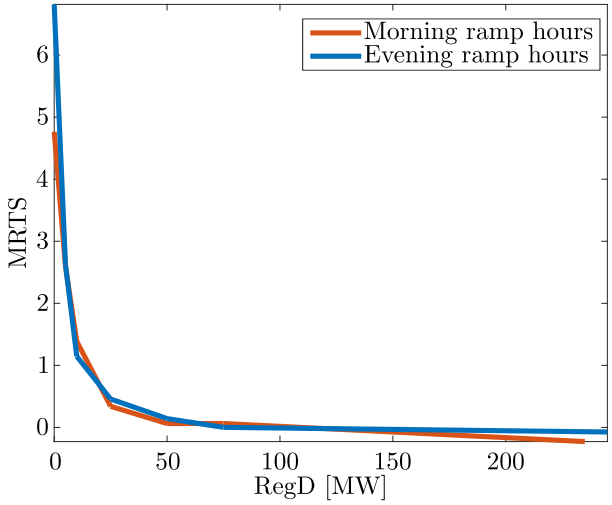

(c) Fall

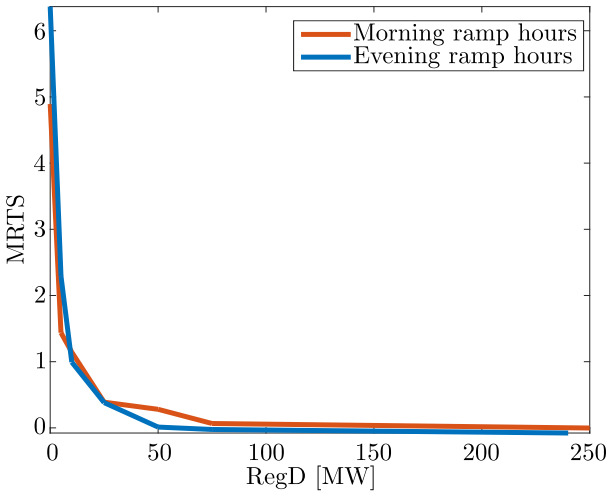

(d) Winter

Figure C.10: Comparison of MRTS curves for Morning ramp vs Evening ramp scenarios per season for 15 min FESS.

C.3 ESS Technologies and Discharging Times

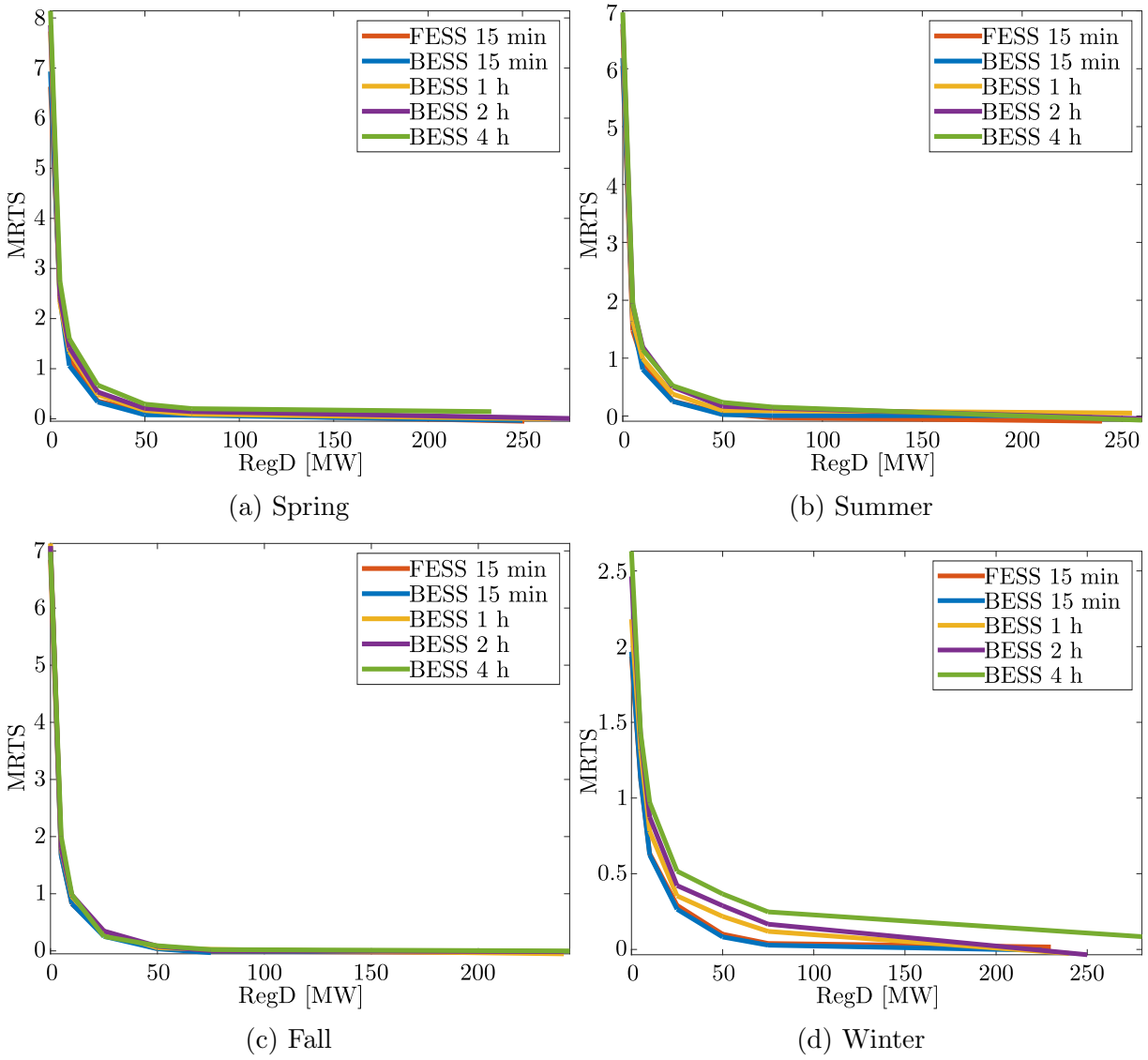

Figure C.11: Comparison of MRTS curves for different ESS technologies and discharging times per season for Peak hours.

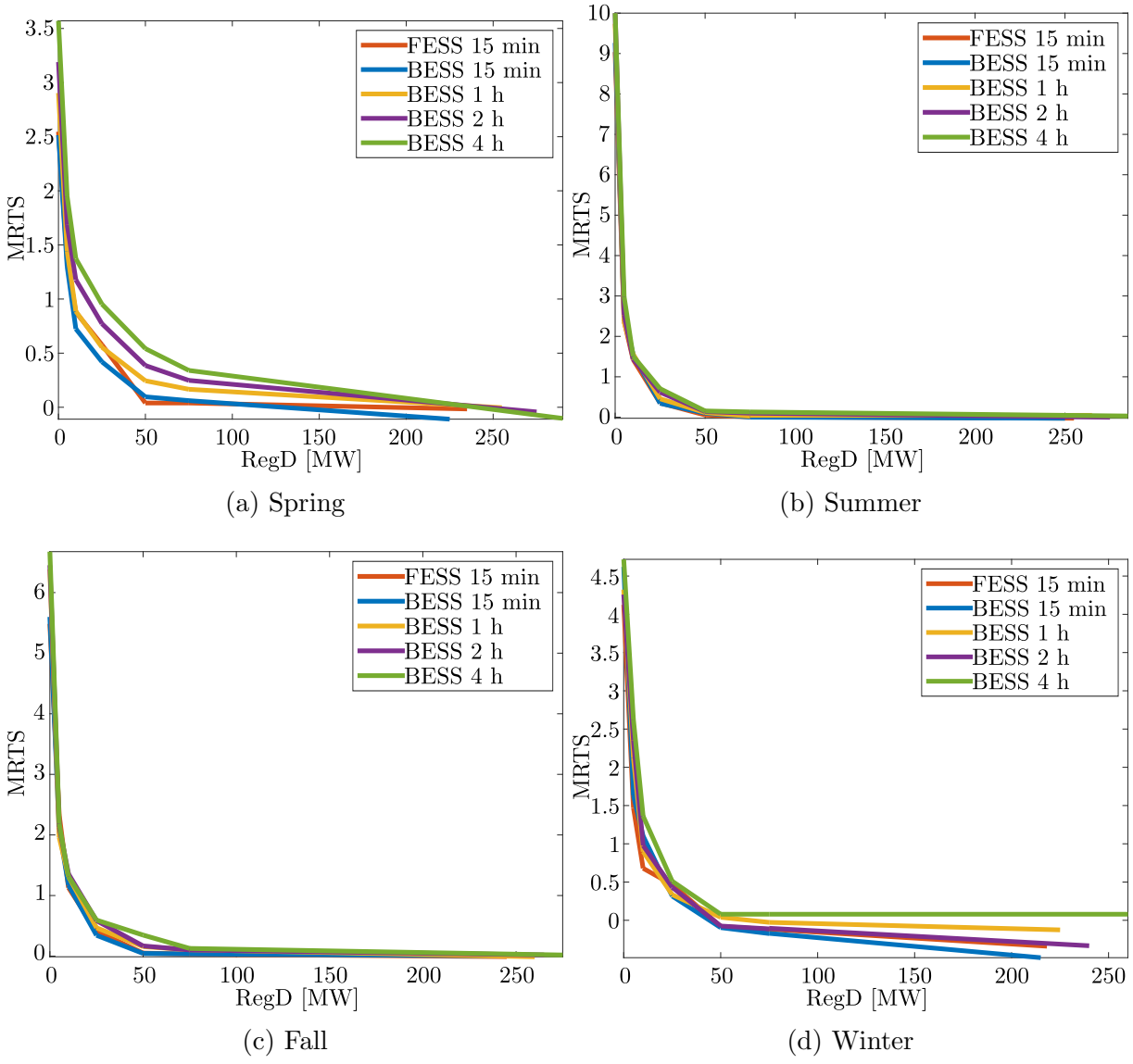

Figure C.12: Comparison of MRTS curves for different ESS technologies and discharging times per season for Non-peak hours.

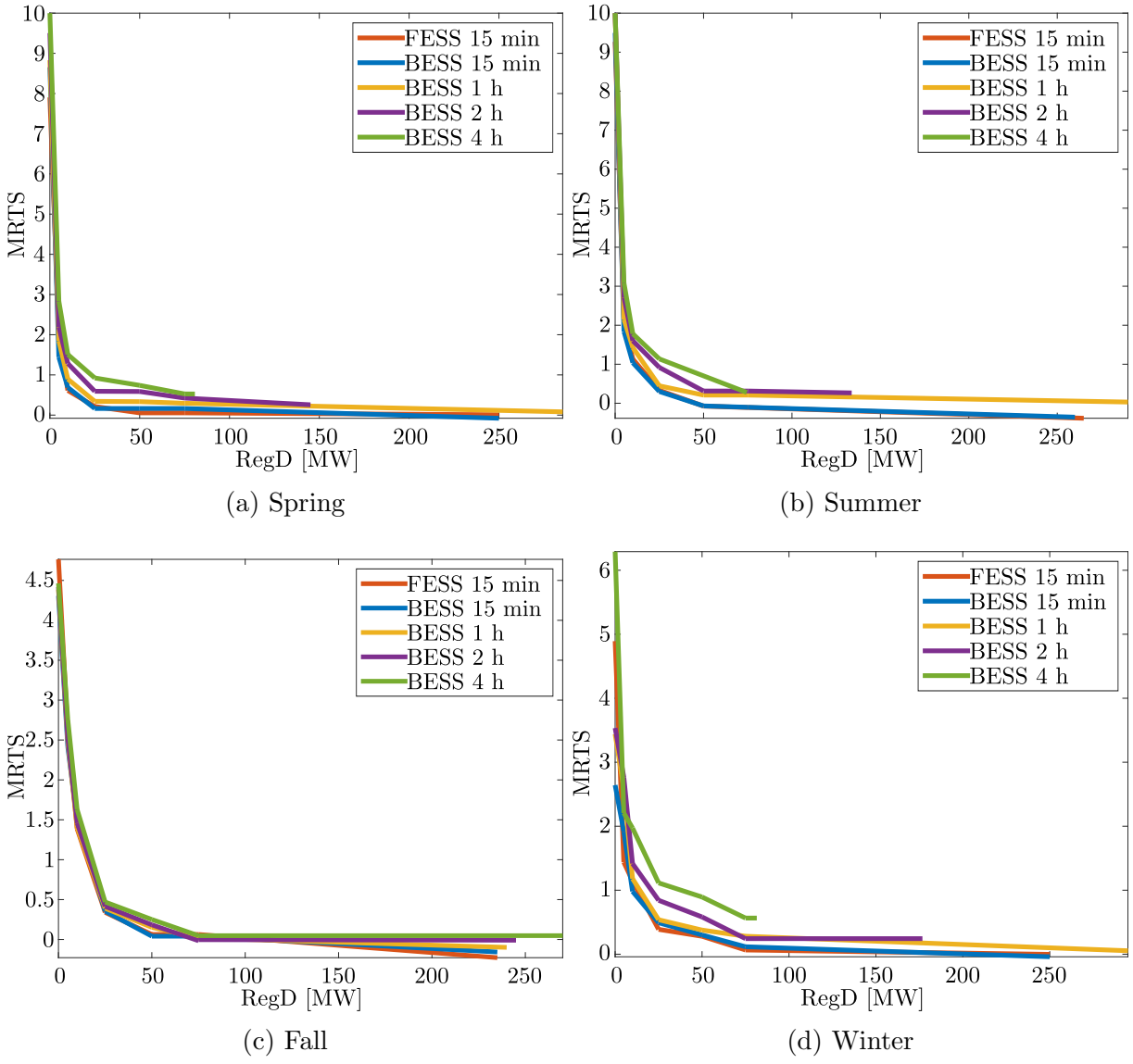

Figure C.13: Comparison of MRTS curves for different ESS technologies and discharging times per season for Morning ramp hours.

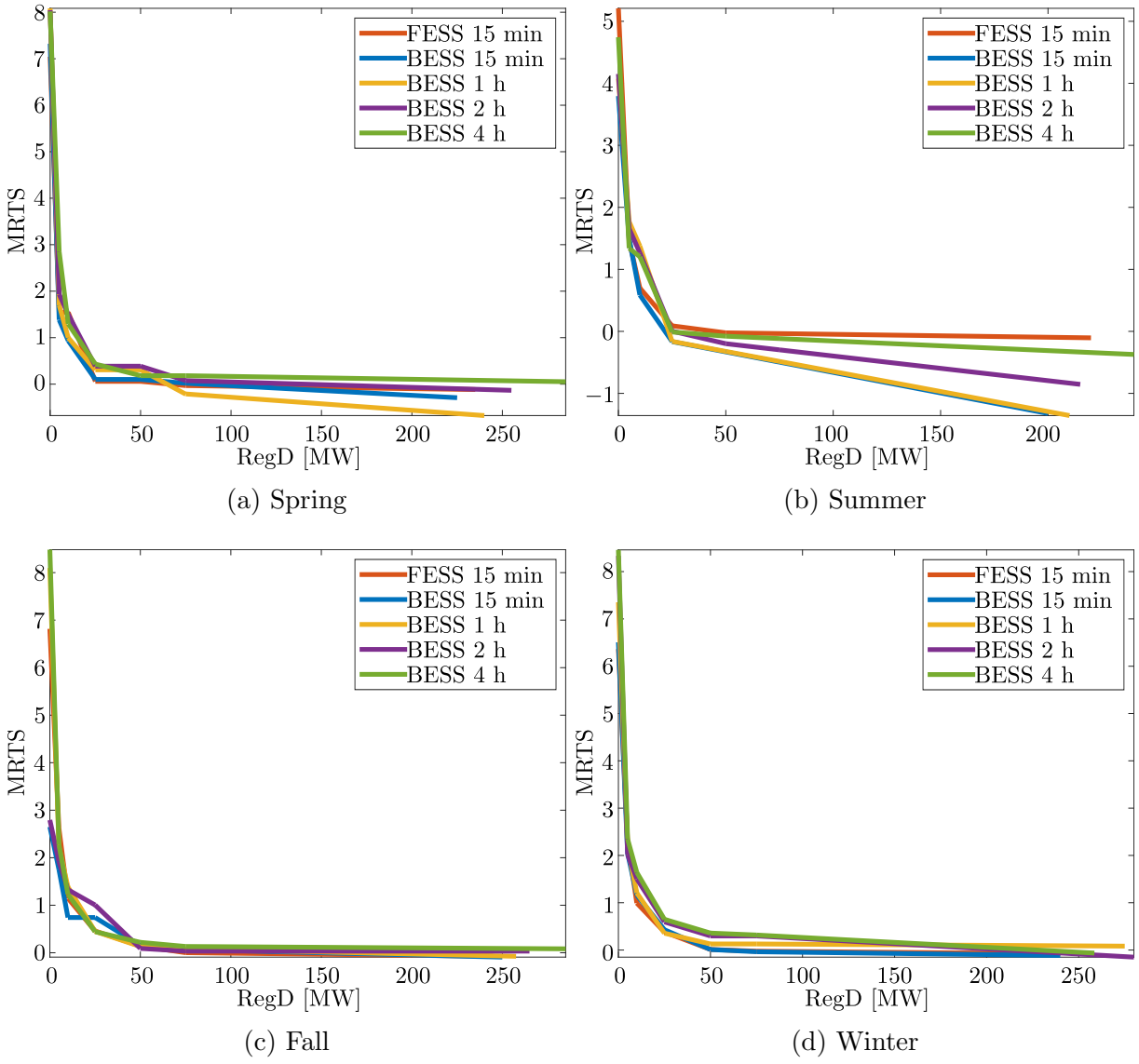

(a) Spring

(b) Summer

(c) Fall

(d) Winter

Figure C.14: Comparison of MRTS curves for different ESS technologies and discharging times per season for Evening ramp hours.